

1-1-2004

## Determination of the optimum base characteristics for pavements

Pavana Kumar Reddy Vennapusa  
*Iowa State University*

Follow this and additional works at: <https://lib.dr.iastate.edu/rtd>

---

### Recommended Citation

Vennapusa, Pavana Kumar Reddy, "Determination of the optimum base characteristics for pavements" (2004). *Retrospective Theses and Dissertations*. 20299.  
<https://lib.dr.iastate.edu/rtd/20299>

This Thesis is brought to you for free and open access by the Iowa State University Capstones, Theses and Dissertations at Iowa State University Digital Repository. It has been accepted for inclusion in Retrospective Theses and Dissertations by an authorized administrator of Iowa State University Digital Repository. For more information, please contact [digirep@iastate.edu](mailto:digirep@iastate.edu).

**Determination of the optimum base characteristics for pavements**

by

**Pavana Kumar Reddy Vennapusa**

A thesis submitted to the graduate faculty  
in partial fulfillment of the requirements for the degree of  
MASTER OF SCIENCE

Major: Civil Engineering (Geotechnical Engineering)

Program of Study Committee:  
David J. White, Major Professor  
Charles T. Jahren  
Jonathan A. Sandor

Iowa State University

Ames, Iowa

2004

Graduate College  
Iowa State University

This is to certify that the master's thesis of  
**Pavana Kumar Reddy Vennapusa**  
has met the thesis requirements of Iowa State University

Signatures have been redacted for privacy

---

**DEDICATION**

This thesis would be incomplete without a mention of the support given to me by my mother, father, sister, brother-in-law and my lovely friend, for whom this thesis is dedicated. I doubt it should ever have been completed without their unconditional love and inspiration through out this work. They knowingly or unknowingly led me to an understanding of some of the more subtle challenges and my ability to succeed.

**TABLE OF CONTENTS**

LIST OF FIGURES ..... viii

LIST OF TABLES ..... xiii

ABSTRACT ..... xv

INTRODUCTION ..... 1

    Research Objectives ..... 1

    Research Plan ..... 2

    Research Tasks ..... 2

    Significant Findings and Recommendations ..... 3

LITERATURE REVIEW ..... 4

    Effects of Stability and Permeability on Pavement Base ..... 4

    Influence of Aggregate Properties on Stability of Pavement Base ..... 12

        Effect of Aggregate Gradation ..... 12

        Effect of Particle Morphology ..... 20

        Effect of Type of Compaction ..... 22

    Influence of Aggregate Properties on Permeability of Pavement Bases ..... 25

        Effect of Gradation and Shape of Aggregate ..... 25

        Effect of Hydraulic Gradient ..... 32

        Effect of Porosity and Void Ratio ..... 33

        Effect of Viscosity of the Permeant ..... 33

        Effect of Degree of Saturation ..... 34

    Drainage Capacity of Pavement Bases ..... 34

        Surface Infiltration ..... 34

        Flow Analysis ..... 37

        Determination of Drainage Capacity and Thickness ..... 38

    Stability of Pavement Bases ..... 42

    Survey on Gradations by State DOT's ..... 47

    Stability and Permeability Measuring Techniques for Aggregates ..... 53

        Laboratory Measurement for Stability of Aggregates ..... 53

        In-Situ Measurement of Stability of Aggregate Base ..... 55

        Laboratory Permeability Testing ..... 57

        In-situ Hydraulic Conductivity Testing ..... 59

    Pavement Base Construction Practices ..... 65

    Key Findings from Literature Review ..... 66

LABORATORY INVESTIGATION ..... 68

    Test Methods ..... 68

    Aggregate Index Properties ..... 70

Test Results and Discussion.....	77
Influence of Fines Content on CBR.....	77
Influence of Fines Content on Hydraulic Conductivity.....	78
Influence of Gradation on Strength.....	80
Influence of Compaction Energy on Hydraulic Conductivity.....	82
Influence of Compaction Type on Dry Density: Vibration versus Impact.....	83
Key Observations from Lab Tests.....	84
PAVEMENT BASE CONSTRUCTION OPERATIONS.....	85
US 218 Base Construction Process.....	85
Placing the Aggregate.....	85
Spreading the Aggregate.....	87
Trimming Process.....	87
Final Compaction.....	88
Key Notes from the Construction Process.....	90
US151 Base Construction.....	91
Placing the Aggregate.....	92
Spreading the Aggregate.....	92
Trimming Process.....	93
Final Compaction.....	94
University-Guthrie Avenue Base Construction Process.....	95
Placing the Aggregate.....	95
Spreading the Aggregate.....	97
Final Compaction.....	97
Key Observations from Construction Operations.....	99
FIELD INVESTIGATION OF PAVEMENT BASES.....	100
Test Methods.....	100
Materials.....	101
Results from Field Testing.....	102
35 <sup>th</sup> Street Modified Subbase Construction.....	102
Knapp Street Granular Base Construction.....	105
IA218 Permeable Base Construction.....	107
US151 Permeable Base Construction.....	108
University-Guthrie Avenue, Permeable Base Construction.....	110
University-Guthrie Avenue Subbase Construction.....	111
I35 South Bound, Permeable Base Construction.....	112
Statistical Analysis of Test Results.....	114
Significance of the Test Results in Design.....	119
Feasibility of Various In-Situ Testing Methods.....	119
Key Observations from Field Testing.....	120
DESCRIPTION OF THE PAVEMENT DRAINAGE ESTIMATOR (PDE).....	122
What is PDE used for?.....	122

How is it used? .....	122
Sample Calculation .....	125
<b>FIELD INVESTIGATION OF PAVEMENT PATCHING PROJECTS .....</b>	<b>127</b>
I 235 East Bound, West Des Moines, Iowa .....	127
Materials .....	127
In-Situ Testing .....	130
US Hwy 30 East Bound, Boone, Iowa.....	132
Materials .....	133
In-Situ Testing .....	133
Key Observations from Patching Projects .....	136
<b>SUMMARY AND CONCLUSIONS .....</b>	<b>137</b>
Laboratory Investigation .....	137
Construction Operations .....	137
Field Investigations .....	138
Patching Projects.....	139
<b>RECOMMENDATIONS .....</b>	<b>140</b>
Optimal Range for In-Place Stability and Permeability .....	140
Field Quality Control/Quality Assurance .....	140
End-Results Specifications .....	141
Alternative Construction Practices .....	141
Future Research Needs .....	141
<b>BIBLIOGRAPHY .....</b>	<b>143</b>
<b>ACKNOWLEDGEMENTS .....</b>	<b>152</b>
<b>APPENDIX A. GRADATIONS USED BY VARIOUS STATE AND FEDERAL AGENCIES.....</b>	<b>153</b>
<b>APPENDIX B: TEST PROCEDURE FOR LABORATORY PERMEABILITY TESTING USING LARGE SCALE AGGREGATE COMPACTION MOLD PERMEAMETER (ACP) .....</b>	<b>164</b>
<b>APPENDIX C: RAW DATA FROM LABORATORY TESTING .....</b>	<b>170</b>
<b>APPENDIX D: DERIVATION AND VALIDATION FOR APT .....</b>	<b>172</b>
<b>APPENDIX E. METHOD OF TEST IN-SITU PERMEAMETER TEST (APT) FOR GRANULAR MATERIALS .....</b>	<b>189</b>

APPENDIX F CONTOUR GRAPHS .....195

APPENDIX G: RAW DATA FROM FIELD PROJECTS .....255

APPENDIX H: DCP PROFILES FROM PATCHING INVESTIGATION .....264



## LIST OF FIGURES

Figure 1. Possible failure in PCC Pavements (reproduced from Randolph et al. 2000).....	6
Figure 2. Possible failure in ACC Pavements (reproduced from Randolph et al. 2000).....	6
Figure 3. Schematic representation of failure in pavements due to freeze-thaw (a) Condensation of water during fall season creates ice rich soil near pavement base. (b) Excess water creates high pore pressure near pavement base. (c) High pore pressure trying to escape, bulges pavement, causes cracking. (d) High pore pressure reduces shear strength of soil and causes failure. (Reproduced from Eigenbrod and Knutsson, 1992) .....	8
Figure 4. Influence of fines on aggregate mix (Modified from <i>Aggregate Handbook</i> , 1996) .....	9
Figure 5. Void ratio vs. percent fines passing No. 200 sieve (modified from Ferguson 1972)....	10
Figure 6. Effect of fines on frost heave, VMA (density), drainage, and triaxial strength (modified from <i>Aggregate Handbook</i> , 1996) .....	11
Figure 7 Effect of fines content on axial strain after 100 deviator stress applications on Bedford crushed stone (Modified from Ferguson, 1972) .....	13
Figure 8. Effect of Fines on strength and density with change in lateral pressure (reproduced from <i>Aggregate Handbook</i> , 1996) .....	18
Figure 9 Effect of size of aggregate on strength (Reproduced from <i>Aggregate Handbook</i> , 1996) .....	23
Figure 10. Variation in CBR with density and change in compaction effort (Modified from <i>Aggregate Handbook</i> , 1996).....	24
Figure 11. Typical cross-section showing drainage system in a PCC pavement (Moulton, 1980) .....	35
Figure 12. Maximum 1-h duration/1-yr precipitation in the United States (After Cedergren et al. 1973) .....	36
Figure 13. Time-dependent drainage of saturated layer (After Barber and Sawyer, 1952).....	41
Figure 14. Correlation chart for estimating CBR and Modulus (psi) for bases (Reproduced from Van Til et al. 1972) .....	43
Figure 15. US Map showing gradations used by different state DOT's under PCC pavements (Courtesy of ACPA, 2001) .....	47
Figure 16. Gradations used by different state DOT's under PCC Pavements .....	48
Figure 17 Comparison of Iowa DOT middle gradation with mean upper and lower limits of gradations by other state and federal agencies.....	49
Figure 18. Comparison of Iowa DOT gradation with AASHTO 57 gradation .....	50
Figure 19 Comparison of Iowa DOT gradation with National Stone Association (NSA) specified gradation .....	50
Figure 20. Comparison of Iowa DOT gradation with Army Corps of Engineers specified Open-Graded (OG) material gradation .....	51
Figure 21 Comparison of Iowa DOT gradation with Army Corps of Engineers specified Rapid Draining (RD) material gradation .....	52
Figure 22. Comparison of Iowa DOT gradation with ASTM D 2940 gradation.....	52
Figure 23 Comparison of Iowa DOT gradation with ASTM D 1241 gradation.....	53
Figure 24. Schematic diagram of FPTD (Moulton et al. 1979).....	60

Figure 25 Sealed single-ring infiltrometer (SSRI) (Fenuik and Haug, 1990) .....	62
Figure 26. Sealed double ring infiltrometer (SDRI) (Fenuik and Haug, 1990).....	62
Figure 27 Air entry permeameter (Fenuik and Haug, 1990) .....	64
Figure 28. Schematic representation of soaked CBR test setup .....	69
Figure 29 Grain-size distribution curves of quarry samples comparing with Iowa DOT gradation according to section No. 4121 .....	72
Figure 30. Grain-size distribution curves of field samples compared to Iowa DOT gradation according to section No. 4121 .....	73
Figure 31 Influence of fines content on hydraulic conductivity of RPCC .....	80
Figure 32. Dense gradation chart for 0.75 in. maximum size aggregate .....	81
Figure 33 Laboratory hydraulic conductivity test results for field samples at high and low densities.....	83
Figure 34. Unstable shoulder under loaded trucks placing aggregate .....	86
Figure 35 Dumping of aggregate on subgrade.....	86
Figure 36. Spreading of aggregate piles using D6XL dozer.....	87
Figure 37 Initial Compaction using 563 CAT Roller .....	88
Figure 38. Final trimming using 9500 Gomaco.....	88
Figure 39 Final trimming of base, level indicator attached to trimmer, and aggregate pile formed after trimming.....	89
Figure 40. Placing trimmed aggregate back in to the haul trucks for re-use at other location .....	89
Figure 41 Final compaction using 563 CAT roller.....	90
Figure 42. Quarry aggregate sample on left side and aggregate from trimmer on right side .....	91
Figure 43. Dry sample on left from trimmer and wet sample on right from quarry.....	91
Figure 44. Haul way used by the trucks to transport the aggregate.....	92
Figure 45 Spreading of aggregates using a D6XL dozer.....	93
Figure 46. Final trimming process using TR 500 trimmer .....	93
Figure 47 Piling of trimmed aggregate on the side of trimmer.....	94
Figure 48. Roller used for final compaction .....	94
Figure 49 Trucks moving on base for placing the aggregate.....	95
Figure 50. Dumping of aggregates from the truck.....	96
Figure 51 Trucks using haul way on their way back to the quarry.....	96
Figure 52. Another method of dumping the aggregate .....	97
Figure 53. Spreading and trimming of aggregate .....	98
Figure 54. Bucket loader removing excess aggregate .....	98
Figure 55 Roller used for final compaction .....	99
Figure 56. Photograph of the modified subbase layer during construction at 35 <sup>th</sup> street test section .....	102
Figure 57 Photograph showing the process of measurements at grid points on US151 Test section .....	109
Figure 58. Picture showing segregation in fines on the final base layer.....	114
Figure 59 Relationship between hydraulic conductivity and fines content .....	117
Figure 60. Relationship between CIV and PI (mm/blow) .....	117
Figure 61 Relationship between CIV and GeoGauge Modulus (MPa) .....	118
Figure 62. Relationship between estimated CBR from DCP and GeoGauge Modulus (MPa) ...	118
Figure 63 Flow chart of PDE version 1.04 .....	123

Figure 64. Options in main menu of PDE version 1.04.....	124
Figure 65 Option in the program for PDE version 1.04 .....	124
Figure 66. Cross-section of pavement .....	125
Figure 67 Cross-section of the existing pavement on I-235, West Des Moines, Iowa.....	128
Figure 68. I-235 deteriorated PCC surface on the left, and excavation on the right .....	128
Figure 69 Recycled PCC aggregate placed over the existing subbase I-235.....	129
Figure 70. Grain-size distribution curves for subbase materials from patching projects compared to the Iowa DOT granular subbase gradation limits .....	129
Figure 71 Change in CBR with depth: I-235 patch project .....	132
Figure 72. Change in CBR with depth: US Hwy 30.....	134
Figure 73. Test section used for DCP testing to investigate the spatial variability US Hwy 30.....	134
Figure 74. Contour plot for variation in CBR for subbase layer (0 to 150 mm deep): US Hwy 30.....	135
Figure 75 Contour plot for variation in CBR for subgrade layer (150 to 450 mm deep): US Hwy 30.....	135
Figure B1 Cross-section of the large scale AC .....	165
Figure B2. Base mold placed on the concrete blocks .....	166
Figure B3 Aggregate compaction mold with screens placed over the base mold .....	166
Figure B4. Marshall impact hammer (left) and compaction procedure (right).....	167
Figure B5 Final setup ready for testing.....	167
Figure D1. Sample indicating pressure at inlet and outlet .....	174
Figure D2. Showing a three dimensional setup for Air Permeability Testing (Modified from Goggin et al. 1988) .....	175
Figure D3. Geometrical effect used by Evans and Kirkham (1949).....	176
Figure D4. Cross-section of the Air Permeability Testing (APT) Device developed at Iowa State University.....	177
Figure D5 Flowchart of the code written to calculate the geometric factor $G_0$ .....	180
Figure D6. Finite difference nodes and the dimensions of the sample used in the analysis.....	181
Figure D7 Showing Dimensionless Pseudo-Potential Contours for the case of $bd=2$ , $RD=LD=3$ , $a=1$ .....	182
Figure D8. Comparison of calculated $m \{ \phi \}$ values with values from Goggin et al. (1988). ....	183
Figure D9 $G_0$ curve showing the effect of sample size.....	183
Figure D10. Comparison of Laboratory vs. Field Hydraulic Conductivity Measurements.....	187
Figure D11 Comparing the Type of Measurement in Field (left) and Lab (right) .....	188
Figure F1 Aerial Photograph of the Test Location (Iowa DOT 2004) .....	197
Figure F2. Grid Setup for Testing at 35 <sup>th</sup> street Modified Subbase Construction Site .....	197
Figure F3. Spatial variation of GeoGauge Modulus (MPa) at 35 <sup>th</sup> Street, DSM, Pavement Subbase Test Section .....	198
Figure F4. Spatial variation of CBR% at 35 <sup>th</sup> Street, DSM, Pavement Subbase Test Section....	199
Figure F5 Spatial variation of Clegg Impact Value (CIV) at 35 <sup>th</sup> Street, DSM, Pavement Subbase Test Section .....	200
Figure F6. Spatial variation of Moisture Content (w %) at 35 <sup>th</sup> Street, DSM, Pavement Subbase Test Section .....	201
Figure F7 Spatial variation of Dry Density ( $\text{kg/m}^3$ ) at 35 <sup>th</sup> Street, DSM, Pavement Subbase	

Test Section.....	202
Figure F8. Aerial Photograph of the Test Location (IDNR, 2004).....	204
Figure F9 Grid Setup for Testing at Knapp Street Base Construction Site .....	204
Figure F10. Spatial variation of GeoGauge Modulus (MPa) at Knapp Street, Ames, Pavement Base Test Section .....	205
Figure F11. Spatial variation of CBR% at Knapp Street, Ames, Pavement Base Test Section ..	206
Figure F12. Spatial variation of Clegg Impact Value (CIV) at Knapp Street, Ames, Pavement Base Test Section .....	207
Figure F13. Spatial variation of Moisture Content (w%) at Knapp Street, Ames, Pavement Base Test Section .....	208
Figure F14. Spatial variation of Dry Density (kg/m <sup>3</sup> ) at Knapp Street, Ames, Pavement Base Test Section .....	209
Figure F15 Spatial variation of Saturated Hydraulic Conductivity (cm/sec) at Knapp Street, Ames, Pavement Base Test Section.....	210
Figure F16. Spatial variation of fines content (% passing No. 200) at Knapp Street, Ames, Pavement Base Test Section .....	211
Figure F17 Aerial Photograph of the Test Location (IDNR, 2004).....	213
Figure F18. Grid Setup for Testing on US 218 Base Construction Site .....	213
Figure F19 Spatial variation of GeoGauge Modulus (MPa) at US 218 South, Pavement Base Test Section .....	214
Figure F20. Spatial variation of CBR (%) at US 218 South, Pavement Base Test Section .....	215
Figure F21 Spatial variation of Clegg Impact Value (CIV) at US 218 South, Pavement Base Test Section .....	216
Figure F22. Spatial variation of Moisture Content (w %) at US 218 South, Pavement Base Test Section.....	217
Figure F23. Spatial variation of Dry Density (kg/m <sup>3</sup> ) at US 218 South, Pavement Base Test Section.....	218
Figure F24. Spatial variation of Saturated Hydraulic Conductivity at US 218 South, Pavement Base Test Section .....	219
Figure F25 Spatial variation of fines content (% passing No. 200) at US 218 South, Pavement Base Test Section .....	220
Figure F26. Aerial Photograph of the Test Location (IDNR, 2004).....	222
Figure F27 Grid Setup for Testing at US 151 Base Construction Site .....	222
Figure F28. Spatial variation of GeoGauge Modulus (MPa) at US151, Pavement Base Test Section.....	223
Figure F29 Spatial variation of CBR (%) at US151, Pavement Base Test Section.....	224
Figure F30. Spatial variation of Clegg Impact Value (CIV) at US151, Pavement Base Test Section.....	225
Figure F31 Spatial variation of Moisture Content (%) at US151, Pavement Base Test Section.....	226
Figure F32. Spatial Variation of Dry Density (kg/m <sup>3</sup> ) at US 151 Pavement Base Test Section.....	227
Figure F33. Spatial variation of Saturated Hydraulic Conductivity at US151, Pavement Base Test Section.....	228
Figure F34. Spatial variation of fines content (% fines passing No. 200) at US151,	

Pavement Base Test Section .....	229
Figure F35 Aerial Photograph of the Test Location (IDNR, 2004).....	231
Figure F36. Grid Setup for Testing at University-Guthrie Base Construction Site.....	231
Figure F37 Spatial variation of GeoGauge Modulus (MPa) at University-Guthrie Pavement Base Test Section.....	232
Figure F38. Spatial variation of CBR (%) at University-Guthrie Pavement Base Test Section.....	233
Figure F39 Spatial variation of Clegg Impact Value (CIV) at University-Guthrie Pavement Base Test Section.....	234
Figure F40. Spatial variation of Saturated Hydraulic Conductivity (cm/sec) at University- Guthrie Pavement Base Test Section.....	235
Figure F41 Spatial variation of fines content (% fines passing No. 200) at University- Guthrie Pavement Base Test Section.....	236
Figure F42. Aerial Photograph of the Test Location (IDNR, 2004).....	238
Figure F43. Grid Setup for Testing at University-Guthrie Base Construction Site.....	238
Figure F44. Spatial variation of GeoGauge Modulus (MPa) at University-Guthrie Special Backfill Test Section.....	239
Figure F45 Spatial variation of CBR (%) at University-Guthrie Special Backfill Test Section.....	240
Figure F46. Spatial variation of Clegg Impact Value (CIV) at University-Guthrie Special Backfill Test Section.....	241
Figure F47 Spatial variation of Moisture Content (w %) at University-Guthrie Special Backfill Test Section.....	242
Figure F48. Spatial variation of Dry Density ( $\text{kg/m}^3$ ) at University-Guthrie Special Backfill Test Section.....	243
Figure F49 Spatial variation of Saturated Hydraulic Conductivity at University-Guthrie Special Backfill Test Section.....	244
Figure F50. Spatial variation of fines content (% fines passing No.200) at University- Guthrie Special Backfill Test Section.....	245
Figure F51 Aerial Photograph of the Test Location (IDNR, 2004) .....	247
Figure F52. Grid Setup for Testing at I 35 South Bound Base Construction Site.....	247
Figure F53. Spatial variation of GeoGauge Modulus (MPa) at I35 South Bound Pavement Base Test Section.....	248
Figure F54. Spatial variation of CBR (%) at I35 South Bound Pavement Base Test Section.....	249
Figure F55 Spatial variation of Clegg Impact Value (CIV) at I35 South Bound Pavement Base Test Section.....	250
Figure F56. Spatial variation of Moisture Content (w %) at I35 South Bound Pavement Base Test Section.....	251
Figure F57 Spatial variation of Dry Density ( $\text{kg/m}^3$ ) at I35 South Bound Pavement Base Test Section.....	252
Figure F58. Spatial variation of Saturated Hydraulic Conductivity (cm/sec) at I35 South Bound Pavement Base Test Section .....	253
Figure F59 Spatial variation of fines content (% fines passing No. 200) at I35 South Bound Pavement Base Test Section.....	254

## LIST OF TABLES

Table 1 Effect of intrinsic and manufactured properties of aggregates as controlling factors on engineering properties of granular material in pavement layers (after Dawson et al. 2000) .....	12
Table 2. Summary of results (Ferguson, 1972).....	13
Table 3. CA-6 and CM-06 gradation (Thompson and Smith, 1990).....	15
Table 4. Summary of results (Thompson and Smith, 1990).....	15
Table 5 Gradations of material used for testing in Highlands and Hoffman, 1988 .....	16
Table 6. SB-2 gradation and the modified gradation (Thornton and Elliott, 1988).....	17
Table 7 Summary of results (Thornton and Elliott, 1988).....	17
Table 8. Summary of results (Cheung and Dawson, 2002).....	20
Table 9 Empirical relationships to determine hydraulic conductivity .....	27
Table 10. Summary of laboratory and In-situ hydraulic conductivity test results (Highlands and Hoffman, 1988).....	28
Table 11. Summary of in-situ hydraulic conductivity results (Miyagawa, 1991) .....	28
Table 12. Gradation and Constant Head Permeability Test results (Haiping et al. 1993).....	29
Table 13. Gradation and Constant Head Permeability Test results (Haiping et al. 1993).....	29
Table 14. Hydraulic conductivity results (Kazmierowski et al. 1994) .....	30
Table 15 Gradation of material used (Thornton and Leong, 1995) .....	31
Table 16. Summary of results (Thornton and Leong, 1995).....	31
Table 17 Gradations used by Richardson (1997).....	31
Table 18. Class 3 special gradation used by Minnesota DOT (Burnham, 1997).....	43
Table 19 Relationship between strength parameters and DCP Penetration Index (PI) value.....	45
Table 20. Performance rating based on GeoGauge results (Chen and Bilyeu, 1999) .....	46
Table 21 Aggregate samples obtained from quarry and field.....	71
Table 22. Grain-size distribution of quarry samples.....	72
Table 23 Grain-size distribution of field samples.....	73
Table 24. Grain-size distribution of field samples.....	74
Table 25 Summary of Engineering Properties for Quarry Samples .....	75
Table 26. Summary of Engineering Properties for Field Samples .....	76
Table 27 CBR at Optimum fines content.....	78
Table 28. Abrasion loss and performance rating of materials tested.....	78
Table 29 Falling head permeability test results for RPCC with variation in fines .....	79
Table 30. CBR% values for samples at dense and open gradation samples.....	81
Table 31 Hydraulic conductivity test results with variation in density .....	83
Table 32. Comparison of densities from static and vibratory compaction .....	84
Table 33. Statistical analysis of the data collected from each project .....	104
Table 34. Comparison of in-situ strength/stiffness to standard values .....	105
Table 35 Comparison of in-situ hydraulic conductivity to standard values .....	106
Table 36. Statistics of all field data.....	115
Table 37 Pearson s correlation coefficient (R) between various parameters measured .....	116
Table 38. R-Squared coefficients calculated from Pearson s Correlations .....	116
Table 39 Comparison between various in-situ testing methods .....	120

Table 40. Grain-size distribution data for samples from patching projects .....	130
Table 41 Summary of index properties of all samples from patching projects .....	131
Table 42. I-235 fines content and APT results in RPCC .....	132
Table C1 Summary of results from CBR testing .....	171
Table D1 Maximum and Minimum Hydraulic Conductivity values in Field and Lab.....	187
Table G1 Summary of results from testing on 35 <sup>th</sup> street Modified Subbase .....	257
Table G2. Summary of results from testing on Knapp Street pavement base .....	258
Table G3. Summary of results from testing on IA218 pavement base .....	259
Table G4. Summary of results from testing on US151 pavement base .....	260
Table G5 Summary of results from testing on University-Guthrie pavement base.....	261
Table G6. Summary of results from testing on University-Guthrie special backfill .....	262
Table G7 Summary of results from testing on I35 South Bound pavement base.....	263

## ABSTRACT

In recent years, it has become apparent that the design and maintenance of pavement drainage extends the service life of pavements. Most pavement structures now incorporate subsurface layers, part of whose function is to drain away excess water, which can be extremely deleterious to the life of the pavement. However, aggregate materials for pavement bases must be carefully selected and properly constructed to provide adequate permeability and stability as well. To assure the effectiveness of such drainage layers after they have been spread and compacted, simple, rapid, in-situ permeability and stability testing and end-result specification are needed.

This report includes conclusions and recommendations related to four main study objectives: (1) Determine the optimal range for in-place stability and in-place permeability based on Iowa aggregate sources; (2) Evaluate the feasibility of an air permeameter for determining the permeability of open and well-graded drainage layers in situ; (3) Develop reliable end-result quality control/quality assurance specifications for stability and permeability; (4) Refine aggregate placement and construction methods to optimize uniformity.

An Air Permeameter Test (APT) device was developed during this study for rapid measurement of in-place permeability of pavement bases. Dynamic Cone Penetrometer (DCP), Clegg Hammer, and GeoGauge vibration tests were performed for in-place stability measurements. Significant spatial variation of most parameters is observed over the final compacted base layer. To achieve the PCC pavement design assumptions and by considering the spatial variability occurring in field, a target CBR of 15% and target permeability of 4 cm/sec and 0.84 cm/sec to achieve 90% and 50% drainage respectively is recommended for QC/QA. A strong influence of fines content and aggregate type on strength, stiffness and permeability is observed. Construction operations are found to contribute to spatial variability in field. Alternate construction procedures and equipment are recommended to minimize this variation.



## INTRODUCTION

In recent years, it has become apparent that the design and maintenance of pavement drainage extends the service life of pavements. In new pavements, drainage issues are addressed by incorporating drainage layers into the design of the pavement. To achieve the desired benefits of these pavement designs, we must be able to accurately calculate the required permeability of the drainage layer and assess the true hydraulic conductivity of materials that will constitute the drainage system. This assessment requires a means to accurately measure the hydraulic conductivity of the drainage media, both in the laboratory for source approval and in the field, to determine whether the material and construction methods are producing the desired results.

Most pavement structures now incorporate subsurface layers. Part of the function of these subsurface layers is to drain away excess water, which can be extremely deleterious to the life of the pavement. However, aggregate materials for permeable bases must be carefully selected and properly constructed to provide not only permeability but uniform stability. Compaction of the drainage material can alter the gradation and create additional fines that may result in lower permeability than desired. Furthermore, construction activities to deposit and spread the aggregate can cause segregation and non-uniform permeability and stability. Spatial variability of both permeability and stability of bases and its degree and consequences are poorly understood.

To assure the effectiveness of such drainage layers after they have been spread and compacted, simple, rapid, in-situ permeability and stability testing and end-result specifications are needed.

### **Research Objectives**

The main objectives of this study were to:

- Determine the optimal range for in-place stability and in-place permeability based on Iowa aggregate sources;
- Evaluate the feasibility of an air permeameter for determining the permeability of open and well-graded drainage layers in situ;
- Develop reliable end-result QC/QA specifications for stability and permeability and

- Refine aggregate placement and construction methods to optimize uniformity

### **Research Plan**

This research project included in-situ testing of full-scale test sections of granular base materials on new construction projects using the described test methods. For stability testing, dynamic cone penetration (DCP), GeoGauge vibration tests, and Clegg Hammer impact tests were conducted side-by-side to develop comparisons and correlations. This equipment is viewed as being simple, rapid, and practical. For permeability testing, the Air Permeameter Test (APT) device was developed and used as the primary field tool to measure permeability.

Six projects with different aggregate sources and contractors were observed and tested. Prior to in-situ stability and permeability testing, construction operations were closely documented, aggregate source and gradation parameter values were determined, and laboratory permeability tests were conducted. Laboratory gradation and permeability tests served as the benchmark for tests conducted in-situ after base construction.

A wide range of Iowa aggregates were statistically analyzed to evaluate relationships of stability versus permeability as a function of pavement design parameter values, aggregate morphology and construction operations. As a result, guidelines for QC/QA specifications were developed for rapid in-situ field-testing.

### **Research Tasks**

The evaluation process consisted of the following tasks:

- Conduct a detailed literature search on information pertaining to aggregate stability and permeability and construction operations used to place and manipulate granular materials. A preliminary review indicates that extensive IHRB research was conducted by Iowa State University in the 1960's–1970s concerning aggregate stability as a function of gradation and morphology. Tests were mostly confined to the lab.
- Establish a database of permeability and stability characteristics for a wide range of drainage material used in Iowa.
- Derive relationships that optimize stability versus permeability for various pavement

design conditions and material.

- Conduct in situ permeability and stability tests on a range of drainage layers being constructed on county and state highway projects in Iowa.
- Develop a standardized air permeameter device and test procedure for conducting in situ permeability test measurements of granular drainage layers, including quantification of the influence of layer thickness.
- Demonstrate the feasibility of using the DCP, GeoGauge, and Clegg Hammer for stability measurements of the drainage layer.
- Develop standardized test procedures and equipment for laboratory permeability measurements and stability measurements of drainage material.
- Recommend construction operations and equipment to optimize aggregate placement by minimizing segregation, degradation and intrusion of soil fines.
- Prepare the final report incorporating field data, construction operations, laboratory studies, and developmental QC/QA specifications.

### **Significant Findings and Recommendations**

Some of significant findings from this research include the following:

- Documentation of the spatial variability of engineering properties of granular base materials;
- Development of a rapid QC/QA tool for determining in-place hydraulic conductivity (APT);
- Establishment of target QC/QA stability values using the DCP, Clegg Hammer and GeoGauge and target QC/QA hydraulic conductivity values using the APT
- Understanding the influence of fines content and aggregate type on the engineering properties of base materials (e.g. strength, stiffness, and hydraulic conductivity); and
- Recommending changes to construction operations to minimize segregation of fines.

## LITERATURE REVIEW

The purpose of this literature review was to summarize the key engineering properties affecting pavement base material performance and methods for characterizing properties of interest (i.e. permeability). More specifically the literature review includes a summary of (1) aggregate properties (e.g. gradation, morphology density etc.) affecting stability and permeability; (2) current practices/recommendations for minimum stability and permeability requirements; (3) construction practices and procedures to minimize aggregate segregation; and (4) methods for testing in-place stability and permeability

The optimization of structural contributions from high stability versus the need to provide adequate drainage for pavement base materials is still a point of debate at the national level. Currently two national level workshops are being organized to bring attention to the topic. Future research work is likely to follow especially with the movement to incorporate resilient modulus measurements of materials with the new AASHTO 200x pavement design guide.

A wide range of current practices have been identified from this literature review. Many researchers conclude that the use of treated permeable bases under PCC pavements significantly improves performance by adding more stability while maintaining adequate permeability. Others indicate that controlling the fines content is a more practical approach. The stability of pavement bases is often characterized using strength parameters such as CBR, but may not be of main concern in pavement design, as resilient properties of the aggregate and the tendency to develop plastic strains under repetitive loading are key. No field results of in-place permeability measurements on aggregate base layers were identified in this literature review.

### **Effects of Stability and Permeability on Pavement Base**

Pavement structures generally consist of three layers: (a) subgrade; (b) aggregate base/subbase course; and (c) wearing surface. The base course is the layer of aggregate material that lies immediately below the pavement layer and usually consists of crushed aggregate or gravel or recycled materials (e.g. recycled concrete or recycled asphalt). The pavement surface usually consists of Asphaltic cement concrete (ACC) or Portland cement

concrete (PCC). In Iowa, most new pavement construction is PCC followed several years later by an ACC overlay

According to Dawson (1995), the main roles of an aggregate base layer in pavements include providing (a) protection for subgrade from significant deformation due to traffic loading; (b) adequate support for the surface layer; (c) stable construction platform during pavement surfacing; (d) adequate drainage for the infiltration through cracks and joints particularly in PCC pavements; (e) subgrade protection against frost and environmental damage; and (f) waste disposal. Although construction joints are a major source of water infiltration, water penetrates and accumulates in the base and subbase for joint-less continuously reinforced concrete pavements and asphalt wearing surfaces as well (Randolph *et al.* 2000).

A considerable amount of research has been conducted to study the mechanisms of pavement deterioration, from which it is evident that undrained water in supporting layers is a major contributor to distress and premature failure in pavements. Huang (2004) summarized the detrimental effects of water, when trapped in a pavement's structure as follows:

- 1 It reduces the strength of unbound granular materials and subgrade soils.
2. It causes pumping of concrete pavements with subsequent faulting, cracking, and general shoulder deterioration.
3. With the high hydrodynamic pressure generated by moving traffic, pumping of fines in the base course of flexible pavements may also occur with resulting loss of support.
4. In northern climates with a depth of frost penetration greater than the pavement thickness, high water tables cause frost heave and the reduction of load-carrying capacity during the frost melting period.
- 5 Water causes differential heaving over swelling soils.
6. Continuous contact with water causes stripping of asphalt mixture and durability or "D" cracking of concrete (Huang 2004).

Sources of free water in pavement systems include (a) water infiltrated through cracks in the pavement; (b) water entering longitudinal pavement/shoulder joints; (c) seepage water

from ditches and medians; and (d) high ground water table (Baumgardner, 1992).

Repetitive traffic loading on saturated base materials cause temporary development of very high pore pressures which lead to loss in strength (Cedergren, 1974). Possible cases of failure in PCC and ACC pavements are shown in Figures 1 and 2, respectively. For PCC pavements, high pore pressures cause pumping of water and fine material out of the subsurface due to deflection at joints (Figure 1). For ACC pavements, water with fine material can also be pumped out causing enlargement of void spaces in the pavement base (Figure 2) (Randolph *et al.* 2000).

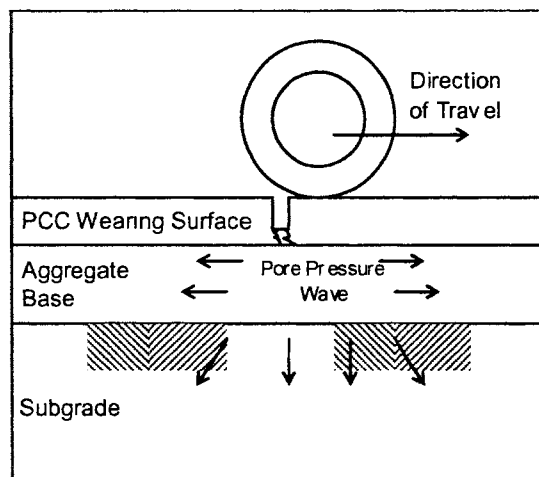


**Figure 1. Possible failure in PCC Pavements (reproduced from Randolph *et al.* 2000)**

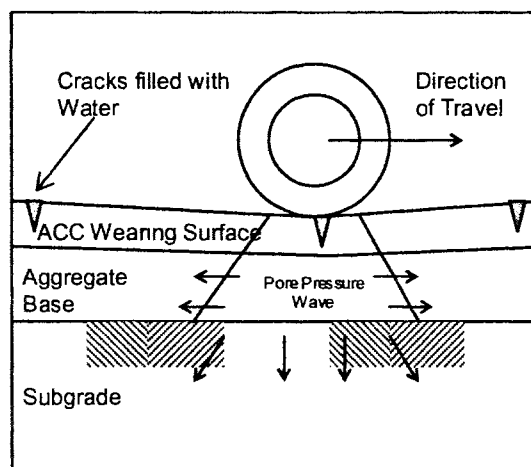


**Figure 2. Possible failure in ACC Pavements (reproduced from Randolph *et al.* 2000)**

Barenberg and Thompson (1970) investigated a pavement section at University of Illinois and concluded that ingress of free water into test pavements increased the rate of damage per traffic impact by 100 to 200 times. Investigations by Georgia DOT in 1969 (Adams, 1969) and the Federal Highway Administration in 1973 (FHWA, 1973) on 3 different interstate locations indicated that none of the causes for pavement failure were due to subgrade distress, but rather the main cause was water retained in the pavement base. Smith *et al.* (1990) conducted a nationwide performance study on 30 jointed concrete pavement test sections and concluded that (a) “The best bases in terms of pavement performance are those designed to be permeable” and (b) “An unexpected benefit of the use of permeable bases was the reduction in ‘D-cracking’ on pavements susceptible to that distress.”

Harrigan (2002) conducted an intensive study on 89 pavement sections to investigate the performance of pavement subsurface drainage on both flexible and rigid pavements. Findings from this study include: (a) using permeable base has a significant effect on reducing joint faulting in case of non-doweled jointed PCC pavements; (b) a significant reduction of D-cracking was identified for PCC pavement sections having permeable base as compared to dense-graded treated base; (c) permeable base use has a minimal effect on reducing joint faulting in case of doweled jointed PCC pavements; (d) both structural capacity and drainability are found to be important for the performance of flexible pavements; (e) conventional ACC pavements with dense-graded bases showed more fatigue when compared to ACC pavements with permeable bases. Hall and Correa (2003) observed that undrained PCC pavement sections with either granular base or lean concrete base may develop roughness, transverse cracking, and longitudinal cracking more rapidly than drained pavement sections with a permeable asphalt-treated base.

Cracks developed at the pavement surface from differential heave are a common problem in northern hemisphere climates. Harrigan (2002) also indicates that unbound dense-graded aggregate bases show significantly more rutting in colder areas when compared to warmer areas. This can be attributed to freeze-thaw action developed in the saturated aggregate base in colder regions. As shown in Figure 3, Eigenbrod and Knutsson (1992) illustrate the behavior of failure in flexible pavements due to freeze-thaw action in the

pavement base. Water condenses and forms ice lenses at the interface between ACC pavement and base as soon as the ground temperatures fall below freezing. These ice lenses start melting during thawing periods, and if the base does not allow adequate drainage, high pore water pressures can develop under the pavement, which results in loss of shear strength in the base and subgrade materials.

Kolisjo *et al.* (2002) examined the strength and deformation behavior of coarse aggregate with seasonal variation in Finland in terms of suction theory for a series of research projects from 1996 to 2000. Suction theory explains the function of effective stress between soil particles and the impact of water in the aggregate. This research shows that permanent deformation in an aggregate base is a significant problem, and originates from excess pore water pressures delivered by dynamic axle loads. The problem was increased from adsorbed water available during the freezing phase. Such excess pore water pressures decrease the effective stresses between particles, and lead to plastic deformations.

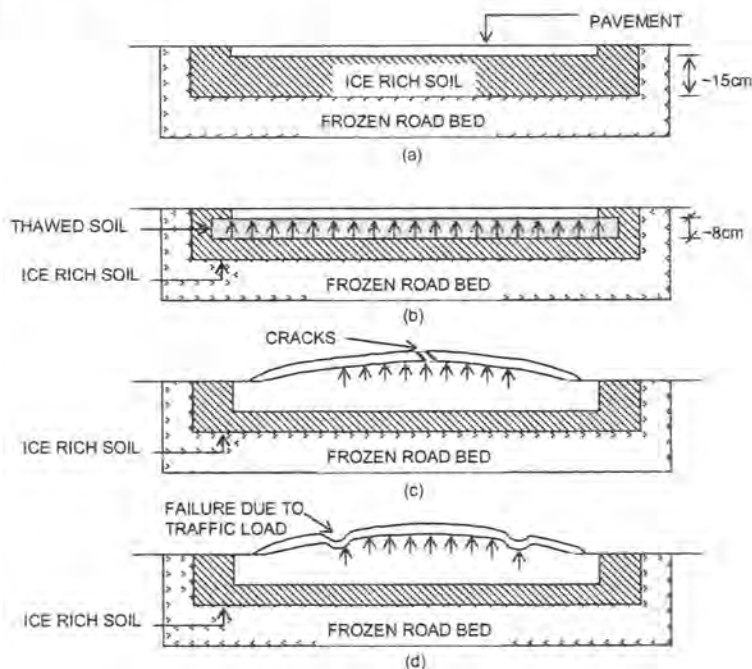


**Figure 3. Schematic representation of failure in pavements due to freeze-thaw\* (a) Condensation of water during fall season creates ice rich soil near pavement base. (b) Excess water creates high pore pressure near pavement base. (c) High pore pressure trying to escape, bulges pavement, causes cracking. (d) High pore pressure reduces shear strength of soil and causes failure. (Reproduced from Eigenbrod and Knuttsson, 1992)**



This literature review suggests that accumulated water in the base contributes to base instability and pavement distress. Thus, it is important to understand how water becomes trapped in the base layer. Gradation of the aggregate, particularly the fines content (passing No. 200 sieve), has been observed as a key factor. Figure 4 illustrates the influence of fines content on the large particle matrix. Aggregate base course containing no fines (Figure 4a), achieves stability through grain-to-grain interlock, which results in lower densities but higher permeability and less frost susceptibility. On the other hand, base course aggregate with void spaces filled with fines (Figure 4b) have higher density and higher stability but lower permeability. Gradations having excess fines (Figure 4c) cause aggregate particles to float in the matrix resulting in low permeability with low stability (Thornton and Elliott, 1988). This mechanism was demonstrated experimentally by Ferguson (1972) who investigated two crushed stone materials in Iowa. This work showed that increased fines content above a critical fines content, CF (Figure 5) causes separation of the coarse aggregate particles. This separation reduces the number of point contacts between larger particles thus allowing shear planes to develop within the matrix of fines. Figure 6 further illustrates the dependence of various engineering properties like frost heave, density, triaxial strength, and permeability with changes in fines content (Aggregate Handbook, 1996). Table 1 shows the effects of fines content on permanent deformation response, strength, stiffness, durability and permeability of aggregates. It can be seen that fines content exerts a significant influence on permeability of aggregates as well as important influences on the other properties.

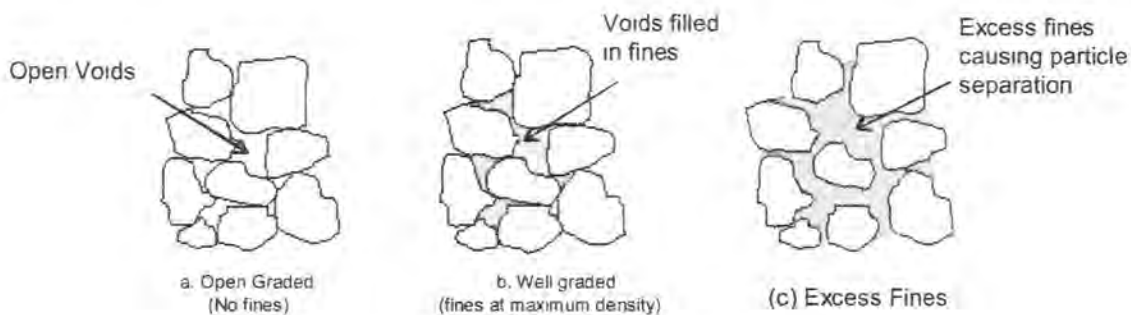


**Figure 4. Influence of fines on aggregate mix  
(Modified from *Aggregate Handbook*, 1996)**

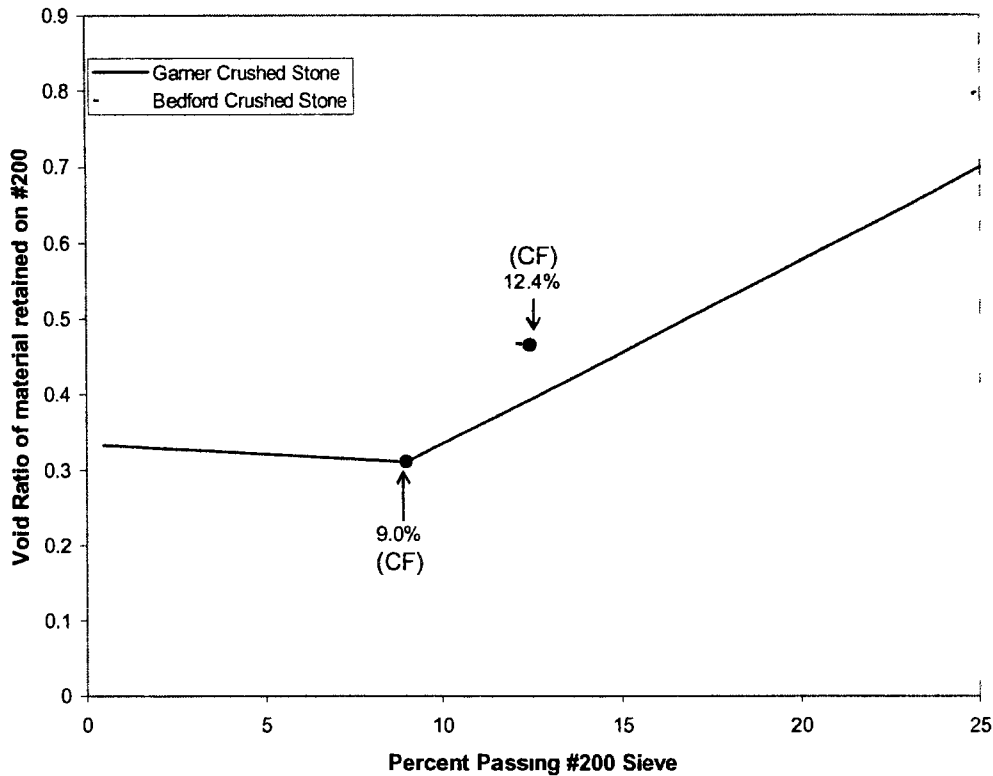


**Figure 5. Void ratio vs. percent fines passing No. 200 sieve (modified from Ferguson, 1972)**

Until the early 1970's, the emphasis in pavement design was on achieving high density and stability rather than on drainability. Likely this was because pavement designs were primarily based on the strength of the supporting layers. Furthermore, dynamic effects from wheel impacts on free water present in the structural supporting layers were not considered as a key design parameter. Premature failures in pavements were observed, however that suggested drainage problems. At that time, a typical remedy was to increase the percent cement or stabilizer to make the base more stable, to widen the base, or to increase the thickness of the wearing surface. No early attempts were made to improve the drainability of the base (Cedergren 1974). In 1973, a comprehensive study was undertaken by FHWA (FHWA 1973) to develop *Guidelines for the Design of Subsurface Drainage Systems for Highway Structural Sections*, and they concluded that poor drainage of heavy-duty pavements was a major contributing factor to premature failure of pavements. Based on this finding, drainable base layers were recommended. Later AASHTO also introduced drainability as an important factor in the 1986 *Guide for Design of Pavement Structures*.

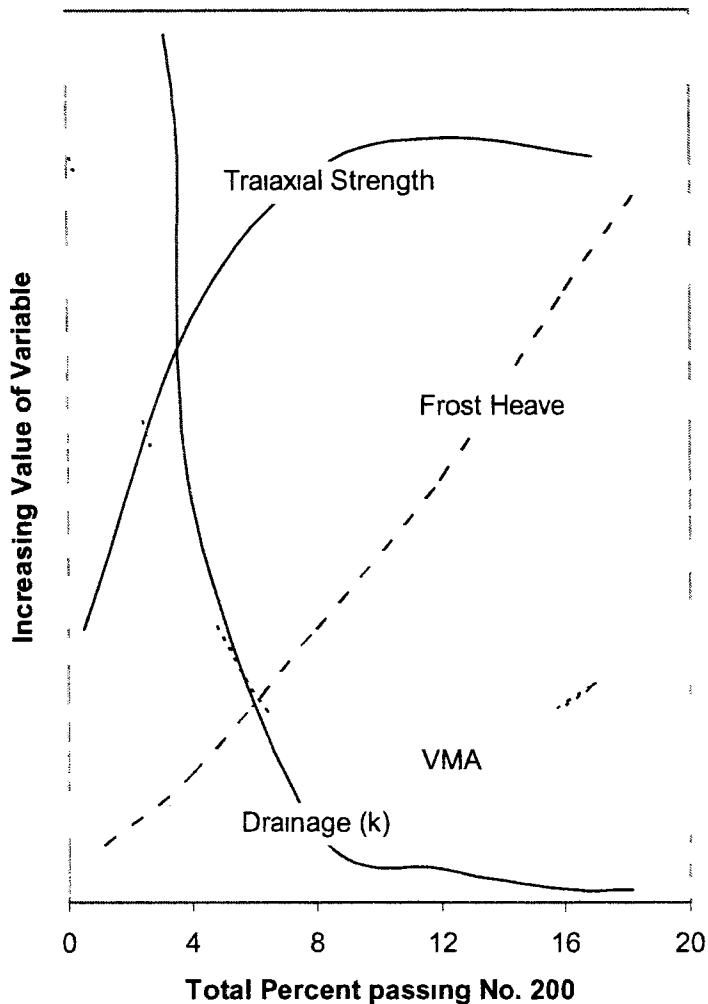


**Figure 6. Effect of fines on frost heave, VMA (density), drainage, and triaxial strength (modified from *Aggregate Handbook*, 1996)**

Subsequently, several researchers have worked to optimize gradations of aggregates for base construction by investigating a wide range of engineering properties (Table 1). Open-graded material with little or no fines has been compared for strength and drainability with well-graded materials. The influence of aggregate properties (gradation and particle morphology and compaction type/energy) on strength and drainability of pavement bases are reviewed in the following sections.

**Table 1. Effect of intrinsic and manufactured properties of aggregates as controlling factors on engineering properties of granular material in pavement layers (after Dawson et al. 2000)**

Controlling Factor	PROPERTY				
	Stiffness	Susceptibility to Permanent Deformation	Strength	Permeability	Durability
Fines content	↓?	↑	varies	major ↓	↓
Type Gravel instead of Crushed Rock	↑	↑	↑	none	usually ↑
Grading Well graded instead of Single-sized	minor ↑	↓	↑	major ↓	↓
Maximum size Large instead of small	↑	↓?	minor ↑	↑	↓?
Shape Angular/Rough instead of Rounded/Smooth	↑	↓	↑	minor	minor
Density	↑	↓	↑	↓	minor
Moisture Content	major ↓	major ↑	major ↓	major ↑	varies
Stress History	↑?	major ↓	minor ↓	none	?
Mean Stress Level	↑	↓	↑	minor ↓	↓

Notes:

↑ = Value of property increases with increase (or indicated change) in controlling factor

↓ = Value of property decreases with increase (or indicated change) in controlling factor

## **Influence of Aggregate Properties on Stability of Pavement Base**

### *Effect of Aggregate Gradation*

Ferguson (1972) examined the behavior of crushed limestone obtained from two sources in Iowa (Garner and Bedford) for different stress conditions and fines content. Results from this study are summarized in Table 2, and indicate that the fines content controls the permanent strain development under cyclic loading. Figure 7 shows the behavior of Bedford crushed stone at 100 deviator stress applications with variation in fines content. An increase in fines content above the critical fines content (CF) greatly increased the rate of permanent axial strain. This can be seen from the values of S2 (slope of line after CF) which are up to 200 times higher than the values of S1 (slope of line before CF). Values of S1 were independent of number of load cycles, whereas values of S2 were almost uniformly increasing with increased load applications.

**Table 2. Summary of results (Ferguson, 1972)**

Material	No. of load cycles	Deviator stress ( $\sigma_1 - \sigma_3$ ) (psi)	Critical Fines Content (CF) (%)	S1	S2	S2/S1
Garner	10	135	7.3	0.046	0.201	4.4
	100	135	8.8	0.059	0.078	1.3
	200	135	9	0.044	1.28	29.1
	500	135	8.6	0.019	2.18	114.7
	1000	135	9	0.035	7.47	213.4
Bedford	100	55.7	13.6	0.097	1.14	11.8
	200	55.7	15.5	0.116	2.2	19.0
	500	55.7	15.9	0.134	3.76	28.1
	1000	55.7	15.7	0.135	4.23	31.3

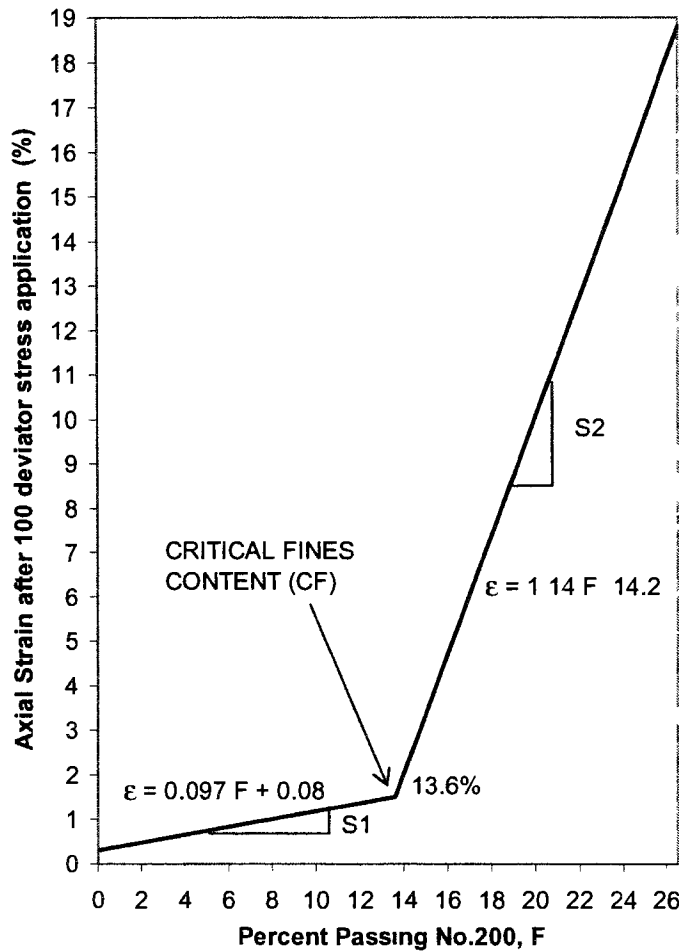


**Figure 7 Effect of fines content on axial strain after 100 deviator stress applications on Bedford crushed stone (Modified from Ferguson, 1972)**

Jones *et al.* (1972) investigated the effects of gradation on density and strength of a

crushed granite base. The aggregate gradations used in this study were varied within the specification band in ASTM D 2940, "Standard Specification for Graded Aggregate Material for Bases or Subbases for Highway or Airports." This study shows that the variation in shear strength of a graded aggregate mix is in the range of 68–123 psi within the specification band, and that the peak shear strength and maximum density are achieved for specimens near the middle gradation of the specification band. This study recommended limiting fines passing the No. 200 sieve to 10%.

Thompson and Smith (1990) studied the effect of fines on performance of granular base material used for pavements in Illinois. The study was performed to compare the performance of proposed open gradation CM-06 to the previous CA-6 dense-graded mix according to Illinois DOT standard specifications. CM-06 and CA-6 gradations are provided in Table 3. The only modification in the gradation from dense to open-graded mix is a reduction in percent fines passing the No. 200 sieve. Tests were conducted to determine pertinent strength properties such as resilient modulus, consolidation due to repetitive loading, and rapid shear strength characteristics of typical aggregates used in base construction. Rapid shear strength represents the measurement from triaxial compression tests where the specimen is rapidly loaded at 1.5 in/sec deformation rate to failure. Materials investigated include crushed limestone and crushed and uncrushed gravel meeting CA-6 and CM-06 gradations. Test results are summarized in Table 4 and show that there is no significant difference in rapid shear strength values with change in gradation, in both repetitive and non-repetitive loading cases. However, repetitive loading increased the strength and stiffness of samples compared to non-repetitive loading. Cohesion values were obtained which varied with changes in gradation for the crushed stone. There was little variability in friction angle and resilient modulus ( $M_r$ ) with change in gradation. Therefore, the authors recommended not using resilient modulus as a strength evaluating measure for granular materials. Finally the open-graded material (CM-06) was found to be satisfactory having sufficient stability with increased permeability

**Table 3. CA-6 and CM-06 gradation (Thompson and Smith, 1990)**

Sieve	% Passing	
	CA-6	CM-06
1.5"	100	100
1"	100-90	100-90
1/2"	90-60	90-60
#4	56-30	56-30
#16	40-10	40-10
#200	4-12	0-4

**Table 4. Summary of results (Thompson and Smith, 1990)**

Sieve Size	% Passing						
	Crushed Stone		Crushed Gravel		Gravel		Partially crushed gravel
	CA-6	CM-06	CA-6	CM-06	CA-6	CM-06	CA-6
1	100	100	100	100	95.1	100	99.1
3/4"	97.5	85.2	93.1	95.8	89.5	92.4	92
1/2"	90.2	67.9	72.3	77	81.8	78.4	78.1
#4	53.1	42	32.1	33.1	46.9	42.8	55.2
#16	25.4	12.7	15.8	14.1	20.3	15.7	23.8
#200	10.5	3.4	7.8	3.1	5	4.8	8.5
$\gamma_d$ max	143.6	122.5	134.1	128.4	134.4	135	133.4
Friction Angle	45.9	44.4	45.8	46.4	43.8	42.7	43.5
Cohesion (psi)	24.4	17.7	13.4	15.1	11.9	9.6	11.1
Resilient Modulus (ksi)	35.4	31.1	29.3	29.2	31	28.6	19.4
Rapid Shear Strength (Non-Repetitive) (psi)	194	171	164	175	127	109	116
Rapid Shear Strength (Repetitive) (psi)	354 <sup>1</sup>	354 <sup>1</sup>	220	354 <sup>1</sup>	354 <sup>1</sup>	346	211
Permanent Strain	0.087 <sup>2</sup>	0.114 <sup>2</sup>	0.145 <sup>3</sup>	0.076 <sup>2</sup>	0.067 <sup>3</sup>	0.130 <sup>3</sup>	0.337 <sup>3</sup>

<sup>1</sup> Maximum capacity of the test ram, <sup>2</sup> at stress rate ( $\sigma_1/\sigma_3$ ) 45/15, <sup>3</sup> at stress rate ( $\sigma_1/\sigma_3$ ) 30/15

Kazmierowski *et al.* (1994) investigated the performance of various open-graded drainage layers (OGDL) in field. The OGDL had a gradation of 90%–100% material retained on 4.75 mm sieve and a maximum of 2% passing No. 200. Falling Weight Deflectometer (FWD) testing was conducted on OGDL untreated, asphalt treated, and cement treated sections. The OGDL material treated with cement at the rate of 180 kg/m<sup>3</sup> resulted in small deflections of about 0.5 mm when compared to OGDL material treated with 1.8% of asphalt which exhibited deflections of 0.64 mm and untreated OGDL material with deflections of 0.74 mm. All three materials were in the range of acceptable deflection for performance

criteria according to Ministry of Transportation, Ontario.

Highlands and Hoffman (1988) also conducted FWD testing to measure deflection of pavement slabs constructed over various base and subbase layers. These base and subbase layers were prepared as test sections by the Pennsylvania DOT with a wide range of gradations, which are listed in Table 5. Cement treated base performed well by producing small deflections of about 0.13 mm, when compared to other base materials. The asphalt treated base, untreated open-graded base, and high permeable base exhibited slightly larger deflections of about 0.17 mm. A test section with dense-graded aggregate base showed significantly higher deflections of about 0.5 mm, when compared to all other materials.

**Table 5. Gradations of material used for testing in Highlands and Hoffman, 1988**

Sieve	Percent Passing %				
	CTB	ATB	OG	HP	DG
2"	100	100	100	100	100
1.5"		100	100	98	98
3/4"	75	85	66	72.5	80
#4	36	16	4	12	35
#10	17.5			7.5	25
#40	4			5	18
#200	3			4	4

The National Stone Association (Aggregate Handbook, 1996) undertook a laboratory investigation to evaluate the performance of dense-graded aggregate base materials. The Texas method of triaxial compression testing was used to simulate the capillary saturated base conditions in the field. Figure 8 shows the effect of fines content on strength and density with changes in confining pressure, for a 0.75 in. maximum size crushed stone. Results indicate that the optimum fines content for strength is about 9%. Based on these results, 5%–12% passing the No. 200 sieve was recommended as a proper practical range.

Thornton and Elliott (1988) studied the influence of fines content on the rapid shear strength of different types of aggregates including crushed stone, crushed gravel and uncrushed gravel available in Arkansas (in this case Rapid shear strength was measured using dynamic triaxial test). Materials tested were in accordance with the SB-2 gradation specified by Arkansas State DOT and a modified gradation to achieve a maximum density of



135 pcf (Table 6). Test results from this study are summarized in Table 7. Results show that the shear strength decreases with an increase in fines from about 8%–12%.

**Table 6. SB-2 gradation and the modified gradation (Thornton and Elliott, 1988)**

Sieve	Percent Passing	
	SB-2	Modified Gradation
1 1/2"	100	100
1	--	100
3/4"	50-90	100
3/8"	--	65.5
# 4	25-50	40
# 40	10-30	15
# 200	3-10	6

**Table 7 Summary of results (Thornton and Elliott, 1988)**

Property	Crushed Stone		Crushed Gravel		Uncrushed Gravel	
Dry Density (pcf)	135	135	135	135	135	135
Relative Density (%)	100	100	98	98	98	98
Moisture Content (%)	9	10.2	8.2	9.5	9	8.6
% fines (Pass No. 200)	6	12	6	12	6	8
Rapid Shear Strength (lbs)	3067	1881	1020	321	413	450

Kolisoja (1997) studied the factors affecting stability performance of aggregates used in road and railroad pavements in Finland. Resilient modulus was chosen to describe the deformation behavior with changes in density, moisture content, grain-size distribution, and aggregate type. In this study, a large variety of coarse-grained materials were tested using a large scale triaxial test with sample dimensions of 300 mm in diameter and 600 mm deep, in accordance with American SHRP protocol P46 testing procedure. The investigation shows that water content (i.e., degree of saturation) has a larger influence on resilient modulus for dense-graded aggregate than for open-graded aggregate. For dense-graded aggregate at lower moisture contents, resilient modulus increases due to suction. As saturation increases, excess pore water pressures can develop leading to a weakened response. The resilient modulus was also found to be stress and density dependent. An increase in density and applied stress showed an increase in resilient modulus.

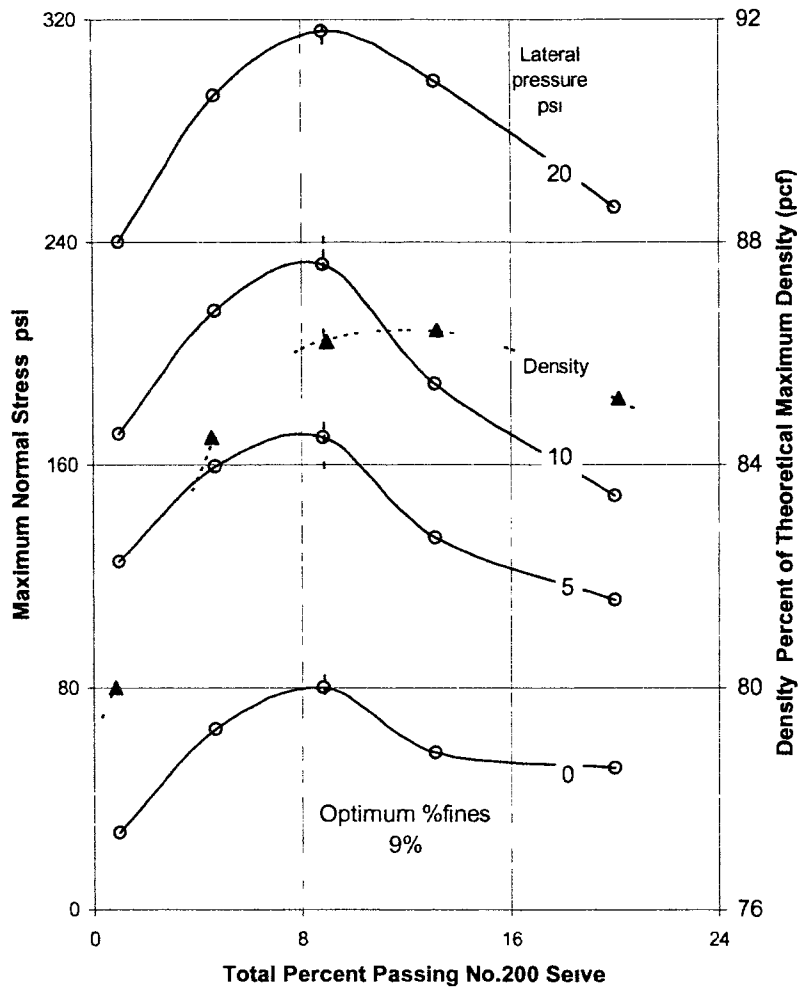


**Figure 8. Effect of Fines on strength and density with change in lateral pressure (reproduced from *Aggregate Handbook*, 1996)**

Cheung and Dawson (2002) investigated the effect of base aggregate gradation on pavement performance and other engineering properties. Crushed dolomitic limestone was tested for its strength characteristics at the upper limit, lower limit, and middle of the gradation band specified by the London Department of Transportation. The fines content was in the range of 0%-16.5%. Results summarized in Table 8 indicate a significant decrease in stiffness and an increase in axial strain for gradations towards the lower limit of the specification band (open-graded). Strength at the middle gradation was higher, evidenced by less axial strain under repetitive loading. Change in resilient modulus ( $M_r$ ) between different aggregates was not significant and suggests that  $M_r$  is not a good measure to evaluate the strength characteristics of base aggregates.

Ismail and Raymond (2002) investigated materials meeting a wide range of gradations for their strength and performance characteristics. Results indicate that dense-graded material exhibits less consolidation compared to open-graded material, in testing for  $5 \times 10^5$  cycles of  $140 \text{ kN/m}^2$  deviator stress followed by  $5 \times 10^5$  cycles of  $210 \text{ kN/m}^2$  deviator stress. The smallest particle size used for dense-graded material was material passing No. 50; hence this study is not indicative of the influence of fines passing No. 200.  $M_r$  results varied from  $94\text{--}112 \text{ MN/m}^2$  for different materials and gradations, which is not a significant change. An increase in  $M_r$  was observed with increased deviator stress.

Bowders *et al.* (2003), conducted a confined undrained (CU) cyclic loading test on a Type-5 base material, specified by the Missouri DOT to evaluate its strength and permanent deformation characteristics. The material had fines content in the range of 12%–19%. The CU stress-controlled test on this material showed that there is no significant change in deviator stress from 7% to 20% strain. This behavior is attributed to negative pore water pressures developed during loading. In contrast, strain-controlled tests up to 4% strain showed significant degradation and reduction of effective deviator stress to zero after the second load cycle due to build up of positive pore pressures. It was concluded that saturated bases with dense gradation are susceptible to strength loss during undrained cyclic loading within a few load cycles.

As discussed earlier, freeze-thaw effects in base material can be detrimental to pavement performance. Kolisoja *et al.* (2002) studied the effect of freeze-thaw action on base course aggregates as a function of fines content with an emphasis on suction, resilient deformation, and permanent deformation behavior for three aggregate materials in Finland. Results indicate that a significant increase in suction and frost heave action is observed with an increase in fines content above 5%. Adding bitumen to samples prevented frost heave at any fines content.  $M_r$  increased with increasing fines of 2.7%–10% for tests performed on dry samples. The  $M_r$  values for freeze-thaw samples were scattered and did not exhibit predictable behavior. However, permanent deformations increased significantly with increased fines from 3.9%–10.7%.

**Table 8. Summary of results (Cheung and Dawson, 2002)**

Property	Dolomitic Limestone				Granodiorite		Gravel	
	A	B	C	Field	Lab	Field	Lab	Field
Crushing strength	Low				Moderate		High	
Abrasion resistance	Low				Moderate		High	
Angularity	More				Moderate		Less (More Rounded)	
Surface texture	Coarse				Coarse		Fine	
Stiffness at 40kPa confining pressure	745	748	373	644	306	384	367	375
Axial strain	2077	619	1245	--	428	1160	1067	14055
Solid content %	72	83	78	80	87	79	88	78
Intercept "c" (kPa)	86	--	--	54	--	46	35	6
Friction angle ( $\phi$ )	46	--	--	62	--	53	63	48
Rutting performance in field				47mm at 220 truck passes		47mm at 100 truck passes		44mm at 4 truck passes
$M_r$ from FWD				52		41		41

\* A – upper limit of gradation band ( $D_{10} = 0.06$  mm,  $D_{30} = 0.19$  mm)

\* B – middle limit of gradation band ( $D_{10} = 0.085$  mm,  $D_{30} = 1.63$  mm)

\* C – lower limit of gradation band ( $D_{10} = 7.19$  mm,  $D_{30} = 19.3$  mm)

### *Effect of Particle Morphology*

Particle morphology is also a contributing factor for base performance as particle interlock, water absorption, degradation etc., are highly dependent on morphological properties of particles. Cheung and Dawson (2002) investigated the effect of particle morphology on engineering properties of different aggregates including dolomitic limestone, granodiorite, and river gravel (Table 8). Higher cohesion,  $c$ , was observed in the dolomitic limestone which has high angularity when compared to gravel and granodiorite. In this case, cohesion is achieved due to locked-in stresses and interparticle moisture causing negative pore pressures. Cohesion values reported by Thompson and Smith (1990) shown in Table 4 also indicate that crushed limestone attains higher cohesion when compared to gravel.

An investigation by the National Stone Association (*Aggregate Handbook*, 1996) on several aggregate types including river gravel, crushed gravel, crushed stone, and mixtures of these materials indicates that the shape of aggregate has a significant impact on strength characteristics. The 100% crushed limestone produced higher strength than all other mixtures. 100% river gravel has the lowest strength. Thornton and Elliott (1988) provided similar conclusions: crushed limestone is about three times stronger than both crushed and uncrushed gravel even at higher fines content. A study by Haiping *et al.* (1993) shows that an open-graded material with 100% fractured faces results in higher  $M_r$  than an open-graded material with 88% fractured faces.

Cheung and Dawson (2002) concluded that the consolidation behavior of aggregates depends on the particle angularity rather than on strength of individual particles. This is evidenced by higher friction angles, higher stiffness, and less axial strain in dolomitic limestone compared to gravel and granodiorite (Table 8). Ismail and Raymond (2002) also indicate that the deformation of material does not necessarily depend on the hardness of the material. When two materials, marble (soft) and granite (hard), are first loaded repeatedly then loaded to failure, a higher ultimate strength can be obtained for the softer material.

Thompson and Smith (1990) showed that the permanent deformation behavior varies significantly between different types of aggregates (Table 4). Gravel products could not survive the standard conditioning loading of 45 psi deviator stress and 15 psi confining pressure, while crushed aggregate performed well. A reduced stress of 30 psi deviator stress and 15 psi confining pressure was used to characterize gravel materials.

Cheung and Dawson (2002) compared the strength properties (Table 8) with a concept of solid content (%), which is defined as the dry density ( $\text{kg/m}^3$ ) divided by the specific gravity times 1000 ( $\text{kg/m}^3$ ). Results show that high solids content reduces plastic strains and increases strength. Cheung and Dawson (2002) also concluded that resilient modulus is an unrealistic parameter to evaluate the strength characteristics of aggregate base as similar resilient modulus values were achieved for different aggregates tested in this study (Table 8).

The National Stone Association (*Aggregate Handbook*, 1996) studied the effect of particle size on strength by performing triaxial tests on 3/8 in., 3/4 in., 1 in., and 1 1/2 in.

maximum size crushed aggregate. Figure 9 shows that a greater load carrying capacity is achieved for larger particle sizes. This behavior is believed to result from greater interlock between aggregates, particles acting as “obstacles” in the planes of failure, greater rigidity possessed by larger size aggregate, and particles experiencing less strain under a given normal and lateral pressure. Results from this study also show that percent fines to achieve maximum strength reduce with increasing particle size in a well-graded mix.

Ismail and Raymond (2002) measured the degradation of material on repetitive loading for different aggregates and concluded that for a given open-graded material, degradation increases with decrease in maximum particle size.

The Talbot equation (Equation 1) provides an estimate of maximum fines content required before coarse aggregates start floating in the fines (see Figure 4c) for well-graded mixtures. For an n-value of about 1/3, the optimum fines content is estimated at 9% for a 0.75 in. maximum size aggregate, and only 6% for a 2 in. maximum size aggregate.

$$P = (d/D)^n (100) \quad (1)$$

Where:

P = percent passing sieve size “d” in inches,

d = sieve size opening in inches for which the percent passing (P) is applicable,

D = maximum aggregate size in inches,

n = an empirical gradation exponent (usually 0.45 for well graded mix).

#### *Effect of Type of Compaction*

Charles (1977) illustrated the importance of compaction on pavement base and subbase materials which can significantly impact performance of pavements. Compaction is defined as “the act or process of compacting; the state of being compacted; to closely unite or pack, to concentrate in a limited area or small space.” Compaction is a process of particles being forced together to contact one another at as many points as physically possible with the material. Density is defined as “the quality or state of being dense; the quantity per unit volume,” as the weight of solids per cubic foot of material. Density is simply a measure of amount of solids in unit volume of material. Thus, density and degree of compaction differ.

Two aggregate bases may have the same density but different degrees of compaction. Thus, an aggregate base can exhibit good performance with good compaction, but it may or may not exhibit good performance at its maximum density. And the maximum density that is achievable is calculated based on standard lab procedures at a certain level of degree of compaction, which is true only when (a) the material tested in the laboratory is identical to the field material in all respects of engineering parameters, which is not usual and (b) the same compactive effort is utilized to achieve compaction. Change in such factors can significantly change the density and render the calculated percent compaction meaningless. Laboratory compaction testing performed on base course aggregates in accordance with AASHTO T-180 (modified Proctor energy) shows a significant change in density and optimum water content with change in gradation in similar aggregates types. Therefore, use of reference density values correlated to gradation for compaction control of aggregate materials in field to avoid inadequate compaction is recommended.

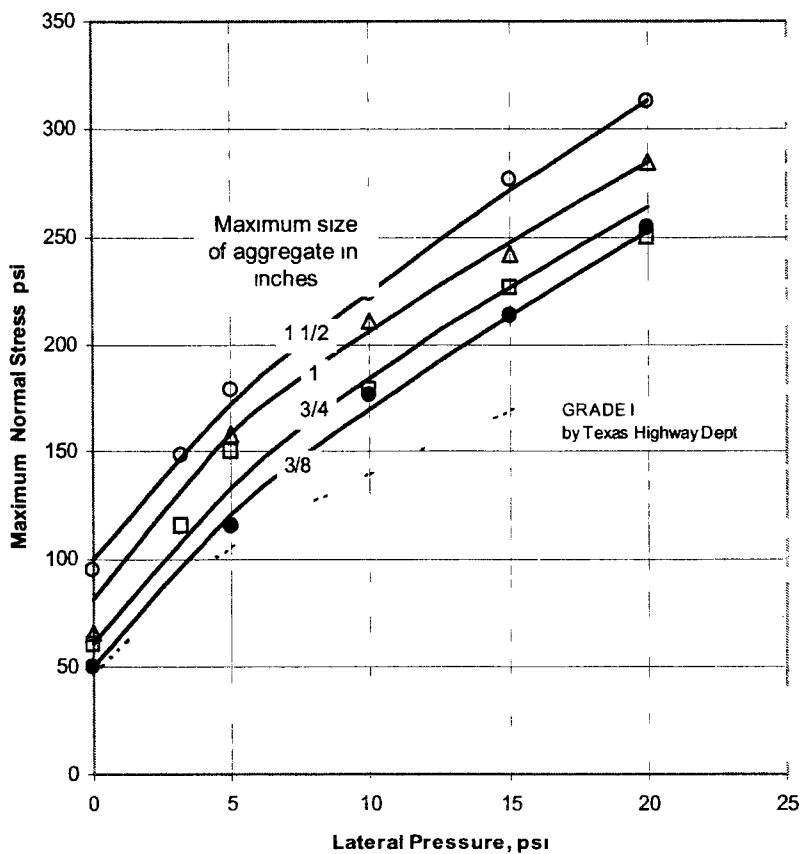


**Figure 9 Effect of size of aggregate on strength  
(Reproduced from *Aggregate Handbook*, 1996)**

Jones *et al.* (1972) studied the effect of compaction energy on the strength of an aggregate mix. Results show that change in compaction energy from AASHTO T-99 to AASHTO T 180 almost doubled the CBR strength. A similar trend of variation was shown from a study conducted by the National Stone Association, as shown in Figure 10. Figure 10 shows that the variation in CBR is significant when examined along with the change in compaction energy. High quality dense-graded aggregates can even show a CBR value above 100, and well-graded gravel (GW) typically have a CBR value of 30–80 and less well-graded gravel (GP, GM, GC) typically develop lower CBR values from about 20–60 (*Aggregate Handbook*, 1996).

Hoover (1967) conducted a laboratory investigation to ascertain a standard laboratory compaction procedure for aggregate base materials. Comparison between AASHTO-ASTM, static compaction, vibratory compaction, and drop hammer compaction concluded that vibratory compaction is the best method for producing a uniform mix, controllable density minimizing degradation and aggregate segregation. A combination of 3600 cycle/min frequency, 35 lb surcharge weight, 0.368 mm of amplitude, and 2 minutes of vibration was adopted.

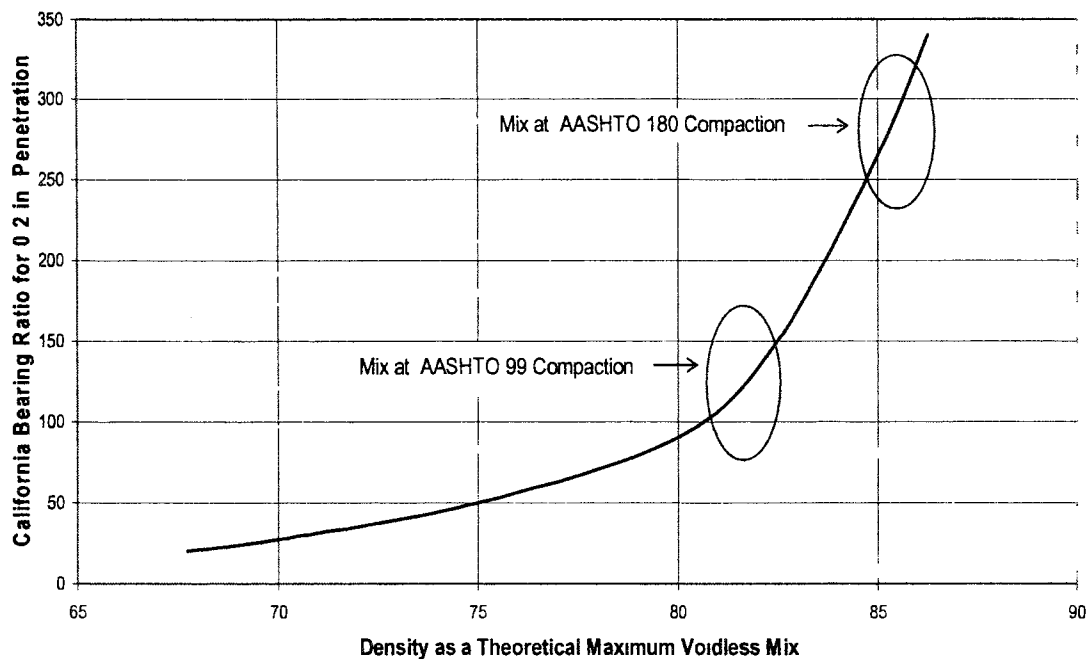


**Figure 10. Variation in CBR with density and change in compaction effort (Modified from *Aggregate Handbook*, 1996)**



## **Influence of Aggregate Properties on Permeability of Pavement Bases**

As discussed earlier, the subject of drainage has been an integral part of pavement design. The drainability of a pavement base is measured using the coefficient of permeability (K), which defines the quantity of water that flows through a material for a given set of conditions (*Aggregate Handbook*, 1996). The quantity of flow through a given medium increases as the coefficient of permeability increases.

K is defined as “the rate of discharge of water at 20°C under conditions of laminar flow through a unit cross sectional area of a soil medium under a unit hydraulic gradient” (Thornton and Leong, 1995). K measured in pavement bases is denoted as hydraulic conductivity, which has the same units as velocity and is expressed in units of length per time (cm/sec or ft/day) (note: 1 cm/s = 2835 ft/day). Various properties that influence hydraulic conductivity of a pavement base include the (a) gradation and shape of aggregate; (b) hydraulic gradient; (c) viscosity of the permeant; (d) porosity and void ratio of the mix; and (e) degree of saturation (Das, 1990).

### *Effect of Gradation and Shape of Aggregate*

According to Cedergren (1994), the life of a poorly-drained pavement is reduced to 1/3 or less of the life of a well-drained pavement. The hydraulic conductivity increases up to 40,000 times if the base material is composed of coarse open-graded aggregate of 0.5–1.0 in. size compared to sand. The range of hydraulic conductivity is recommended to be 10,000 ft/day–100,000 ft/day for an open-graded aggregate base (Cedergren, 1994).

A significant amount of research has been conducted on hydraulic conductivity of pavement bases with a wide range of material types and gradations. There are many empirical relationships available to estimate the hydraulic conductivity of a given material based on grain-size distribution. Some of these are summarized in Table 9. For uniform sand, Hazen (1930) proposed an empirical relationship to measure the hydraulic conductivity as shown in No. 1 of Table 9. Cedergren (1974) proposed two relationships to differentiate between crushed and rounded texture of aggregate, as shown in Nos. 7 and 8 of Table 9. Kenny *et al.* (1984) conducted several laboratory tests under laminar flow conditions on granular soils in which particle sizes varied from 0.074 mm to 25.4 mm and

proposed an equation to determine the hydraulic conductivity as shown in No. 2 of Table 9. Based on several experimental verifications, Shahabi *et al.* (1984) proposed a relationship to estimate the hydraulic conductivity considering grain size distribution and coefficient of uniformity of the material, as shown in No. 3 of Table 9. Moulton (1980) proposed an equation shown in No. 4 of Table 9 depending on porosity of the mix, particle size and percent passing a No. 200 sieve. This equation has been used since 1980 in estimating the hydraulic conductivity of pavement bases and has served well for dense-graded mixtures. But increasing use of more quantitative methods of base design necessitates more accurate and realistic models (Richardson, 1997).

Richardson (1997) performed multi-regression analysis on various parameters influencing hydraulic conductivity including particle sizes, and effective porosity of the mix and developed equations shown in No. 10 through 13 of Table 9. Equations were developed using results reported for a wide variety of materials, and gradations by various researchers.

Highlands and Hoffman (1988) conducted in-situ hydraulic conductivity tests on pavement bases at five different sections. These test sections were prepared by the Pennsylvania DOT meeting the gradations listed in Table 5. Hydraulic conductivity test results are shown in Table 10. Results indicate that the cement treated bases (CTB) and dense-graded (GD) bases are denser and less permeable. Asphalt treated base (ATB), open-graded (OG) base, and highly permeable (HP) base are more permeable and have a hydraulic conductivity rating several orders of magnitude higher than cement treated and dense-graded mixes. Based on the results of this study, it was recommended to use OG drainage layer (see Table 5) between the wearing surface and a dense subbase to meet Pennsylvania permeability and stability requirements.

**Table 9 Empirical relationships to determine hydraulic conductivity**

No.	K (units)	Equation	Proposed By	Suitability
1	K (cm/sec)	$K = cD_{10}^2$ (c varies from 1 to 1.5)	Hazen (1930)	loose sand and clean filter sands
2	K (mm <sup>2</sup> )	$K = cD_5^2$ (c varies from 0.05 to 1)	Kenny <i>et al.</i> (1984)	Coarse sand
3	K (cm/sec)	$K = 1.2C_u^{0.735}D_{10}^{0.89} \left( \frac{e^3}{1+e} \right)$	Shahabi <i>et al.</i> (1984)	Medium to fine sands
4	K (ft/day)	$K = \frac{6.214 \times 10^5 D_{10}^{1.478} n^{6.654}}{P_{200}^{0.597}}$	Moulton (1980)	Aggregates
5	K (cm/sec)	$K = \frac{D_s^2 \gamma^3 C}{\mu(1+e)}$	Taylor (1948)	Soils
6	K (cm/sec)	$K = \frac{\gamma^3}{k_o S^2 \mu(1+e)}$	Kozeny-Carman Eq.	Soils
7	K (m/sec)	$K = 0.001(d_{100})^{1.4}$	Cedergren (1974)	Crushed aggregate
8	K (m/sec)	$K = 0.001(d_{100})^{1.5}$	Cedergren (1974)	Round Aggregate
9	K (cm/sec)	$K = 1.4e^2 k_{0.85}$	Casagrande	Fine-medium clean sand
10	K (cm/sec)	$\log K = 3.062 + 6.4 \log \eta + 1.905 \log D_{10}$	Richardson (1997)	For $k = 10^{-5}$ to $10^1$ cm/sec
11	K (cm/sec)	$K = -2.873 + 23.923\eta + 1.005D_{10} - 0.107P_{3/8} - 0.214P_{50} + 0.218P_{16}$	Richardson (1997)	For $k > 0.1$ cm/sec open-graded materials
12	K (cm/sec)	$K = -0.024 + 5.573\eta - 0.024P_{3/8} + 0.004P_8$	Richardson (1997)	For $k = 0.1$ to $1$ cm/sec
13	K (cm/sec)	$k = 7.137 + 12.521\eta + 0.411D_{10} - 0.192P_{3/8}$	Richardson (1997)	For $k > 1$ cm/sec

**Note:**

$K$  = hydraulic conductivity or coefficient of permeability,

$k_{0.85}$  = hydraulic conductivity at a void ratio of 0.85,

$D_{10}$  = particle diameter at 10% passing (mm),

$c$  &  $C$  = constants,

$C_u$  = coefficient of uniformity,

$e$  = void ratio,

$\gamma$  = unit weight of permeant,

$\eta$  = effective porosity,

$n$  = porosity,

$\mu$  = viscosity of Water,

$S$  = specific surface area,

$k_o$  = factor depending on pore shape and ratio of length of actual flow path to soil bed thickness,

$D_s$  = effective particle diameter,

$P_{200}$  = % passing #200 sieve,

$P_{3/8}$  = % passing 3/8" sieve,

- $P_8$  = % passing #8 sieve,  
 $P_{16}$  = % passing #16 sieve,  
 $d_{100}$  = nominal size of aggregate in mm.

**Table 10. Summary of laboratory and In-situ hydraulic conductivity test results (Highlands and Hoffman, 1988)**

Base type	Laboratory hydraulic conductivity (ft/day)	In-situ hydraulic conductivity (ft/day)	
		K1	K2
CTB	$2.83 \times 10^{-4}$	NR	NR
ATB	$6.519 \times 10^3$	$5.39 \times 10^3$	$6.07 \times 10^4$
OG	$2.15 \times 10^4$	$7.74 \times 10^3$	$2.39 \times 10^4$
HP	$1.81 \times 10^4$	$1.73 \times 10^4$	$1.78 \times 10^4$
DG	1.22	$3.97 \times 10^1$	$1.79 \times 10^1$

Note: K1 and K2 = hydraulic conductivities measured in orthogonal directions; NR = No Results

Miyagawa (1991) conducted both laboratory and in-situ hydraulic conductivity tests on a wide range of pavement bases in Iowa. Laboratory test results indicate that crushed limestone has a higher hydraulic conductivity with a range of 7,000–36,900 ft/day compared to crushed concrete with a range of about 340–12,780 ft/day. Later, in-situ hydraulic conductivity tests were conducted to validate the results obtained from laboratory testing. A procedure was developed to obtain a relative measure of in-situ hydraulic conductivity tests. The procedures consisted of coring out an approximately 4 in. diameter hole to a depth of 4–5 in, filling the hole with one liter of water, and measuring the time taken to drain water from the hole. Compared to laboratory test results, in-situ tests produced lower measured hydraulic conductivities on the order of 20–1000 ft/day (Table 11). This reduction was believed to be a result of changes in gradation during compaction of the base material.

**Table 11. Summary of in-situ hydraulic conductivity results (Miyagawa, 1991)**

Location	Material	Average K (ft/day)	Reduction in K <sup>1</sup>
Pottawattamie	Crushed Concrete	41	8-310
Cass Co.	Crushed Concrete	70	5-180
Hardin Co	Crushed Concrete	516	1-25
Poweshiek Co.	Crushed Concrete	126	3-100
Johnson Co.	Crushed Stone	1004	7-1000
Cedar Co.	Crushed Concrete	89	4-140
Cedar Co.	Crushed Concrete	20	17-640
Cedar Co.	Crushed Concrete	390	1-33

<sup>1</sup>Calculated as the reduction of K from the obtained values in laboratory

Haiping *et al.* (1993) conducted laboratory hydraulic conductivity tests on a wide range of aggregate base materials in Oregon. Gradations of materials reported in this investigation are provided in Tables 12 and 13. Both constant head and falling head permeability tests were conducted. Results show that the lower bound of gradation (see Table 12) exhibits the highest hydraulic conductivity of about 3000 ft/day. A significantly higher hydraulic conductivity is observed in 100% crushed faces compared to 88% crushed faces with similar New Jersey gradation (2376 ft/day to 770 ft/day respectively). The 100% fractured faces New Jersey gradation and proposed open gradation (see Table 13) resulted in similar hydraulic conductivities at around 2400 ft/day.

**Table 12. Gradation and Constant Head Permeability Test results (Haiping et al. 1993)**

Aggregate with 88% fractured faces					
Sieve Size	Existing Open Graded	New Jersey	Proposed Upper Bound	Proposed Lower Bound	Existing Dense Graded
1 1/2"	100	100	100	100	97.5
1"	97.5	97.5	100	100	80
3/4"	67.5	86	98	80	64
1/2"	56.5	70	85	60	54
1/4"	37.5	54	60	45	42
#10	7.5	12.5	20	5	23
#40	4	3	6	0	12
#200	1	1.5	5	0	5
k (ft/day)	971	770	226	3018	140
Standard Deviation	322	138	42	370	64

**Table 13. Gradation and Constant Head Permeability Test results (Haiping et al. 1993)**

Aggregate with 100% fractured faces			
Sieve Size	New Jersey	Proposed Open Graded	Existing Dense Graded
1 1/2"	100	100	97.5
1"	97.5	100	80
3/4"	86	89	64
1/2"	70	68	54
1/4"	54	53	42
#10	12.5	13	23
#40	3	3	12
#200	1.5	2.5	5
k (ft/day)	2376	2489	475
Standard Deviation	338	309	150

Kazmierowski *et al.* (1994) investigated the drainability characteristics of an open-graded drainage layer (OGDL) in the field. The gradation specification of OGDL was in accordance with the Ontario Ministry of Transportation (90% to 100% material retained on 4.75 mm sieve and a maximum of 2% passing No. 200). Hydraulic conductivity tests were conducted on OGDL untreated, cement treated, and asphalt treated test sections. Cores were obtained from test sections by wrapping in a paraffin wax and then tested in a constant head permeameter according to ASTM D2434, "Standard Test Method for Permeability of Granular Soils." The average hydraulic conductivity values obtained are summarized in Table 14. This study concluded that all core samples met the standard requirement of  $10^{-2}$  cm/sec. The asphalt treated OGDL has slightly higher hydraulic conductivity than the other materials.

**Table 14. Hydraulic conductivity results (Kazmierowski et al. 1994)**

Material	Average Hydraulic Conductivity (cm/sec)
Untreated OGDL	$7.5 \times 10^{-2}$
Asphalt Treated OGDL (1.8%)	$8.6 \times 10^{-2}$
Cement Treated OGDL	$5.9 \times 10^{-2}$

Thornton and Leong (1995) investigated hydraulic conductivity for various aggregates used for pavement bases in Arkansas. Materials tested included limestone, sandstone, igneous rock, and Razorrock chert. Table 15 lists the gradation requirements according to standard specifications by the Arkansas DOT. The influence of fines content at 3%, 6.5%, and 10% were investigated. Hydraulic conductivity tests were conducted according to the U.S. Bureau of Reclamation standard for falling head test procedures, in a 19 in. diameter by 9 in. thick falling head permeameter. Final results were compared with the DRAINIT program developed at the University of Illinois, which is based on the equation proposed by Moulton (1980) shown in No. 4 of Table 9. It was found that the results obtained from the DRAINIT program are approximately 100 times less than the laboratory test results summarized in Table 16. It is clearly seen that an increase in fines content from 3% to 10% reduced the hydraulic conductivity significantly in case of sandstone and igneous rock.

**Table 15. Gradation of material used (Thornton and Leong, 1995)**

Sieve Size	Percent Passing
1 1/2"	100
3/4"	50-90
#4	25-55
#40	10-30
#200	3-10

**Table 16. Summary of results (Thornton and Leong, 1995)**

Type of Aggregate	Percent Fines Used		
	3%	6.5%	10%
	K (cm/sec)	K (cm/sec)	K (cm/sec)
Limestone	5.52 E-03	3.48 E-03	2.49 E-03
Sandstone	4.34 E-03	1.66 E-03	1.86 E-04
Igneous Rock	4.53 E-03	1.57 E-03	8.36 E-04
Razzorrock Chert	2.91 E-03	1.76 E-03	1.05 E-03

Richardson (1997) reports hydraulic conductivity measurements on various aggregates in Missouri. Table 17 lists the aggregate gradations and results. Hydraulic conductivity tests for open-graded material (according to New Jersey DOT (NJ DOT) and Pennsylvania OGS (PA OGS gradation) and dense-graded material (according to Missouri DOT (MO DOT) gradation) were conducted in a rigid wall permeameter and a flexible wall permeameter, respectively. Results are reported in Table 17. Material with PA OGS resulted in a higher hydraulic conductivity of about 990 ft/day compared to NJ DOT gradation at 790 ft/day. MO DOT dense graded mix resulted in a low hydraulic conductivity of about 1 ft/day compared to other gradations. Comparison of observed values with estimated values by Moulton's equation (No. 4 of Table 9) showed that the estimated values are always under predicted up to one order of magnitude, for both dense and open-graded material.

**Table 17 Gradations used by Richardson (1997)**

Sieve	Percent Passing %		
	MODOT	NJ DOT	PAOGS
1"	100	100	100
1/2"	75	68	60
#4	50	47	30
#16	33	5	8
#40	25	3	5
#200	8	2	2
Average K (ft/day)	1	794	992

Bowders *et al.* (2003) investigated the drainability performance on a wide range of aggregate materials used for pavement bases in Missouri with MO DOT Type-5 gradation both in laboratory and field. The materials tested had fines content in the range of 12%–19%. In-situ testing was conducted using a double ring infiltrometer. For comparison, laboratory tests were also performed using a flexible wall permeameter and constant head method according to ASTM D 5084, “Standard Test Methods for Measurement of Hydraulic Conductivity of Saturated Porous Materials using Flexible Wall Permeameter.” Laboratory measurements ranged from 0.0008 ft/day to 8 ft/day. In-situ results were 1 to 2 orders of magnitude lower values than the laboratory results. The variation in results is attributed to (a) the variation in compaction from lab and field and (b) piping of fine particles in the laboratory testing. It was concluded that materials tested are highly impermeable, and when subjected to undrained loading can lead to deterioration in a few load cycles.

#### *Effect of Hydraulic Gradient*

Hydraulic gradient is an important factor that affects the measurement of hydraulic conductivity and is also a key parameter in Darcy’s equation. Head loss in a flow system is used to calculate the hydraulic gradient  $i = \Delta h/L$ . In most soils where the flow is laminar, velocity is directly proportional to hydraulic gradient which is given as  $v \propto i$ . But non-laminar flow conditions can exist in open-graded pavement base materials even at relatively low gradients (Moulton, 1980). Croveti and Dempsey (1993) reported an interesting conclusion from the constant head permeability test conducted on an open-graded material. They found that there is a significant drop in hydraulic conductivity (up to approximately 50%) as the hydraulic gradient is increased. This finding is contradictory with Darcy’s assumption  $v \propto i$ , thus indicating turbulent flow conditions. Excessive hydraulic gradients can be detected by plotting discharge velocity ( $v$ ) vs. gradient ( $i$ ). Darcy’s law says that these two variables are directly proportional and that hydraulic conductivity is the slope of the line plotted. If at some point the slope begins to decrease with increasing gradient, then a change in flow from laminar to non-laminar can be identified (Richardson, 1997).

Several researchers have provided modifications to Darcy’s equation to describe more closely the non-laminar flow conditions in granular materials. Fwa *et al.* 1998, provides a



general relationship to determine hydraulic conductivity under turbulent flow conditions as  $v = k i^n$  where “n” is equivalent to 1 for laminar flow conditions. Factor “n” is defined as the slope of the plot between  $\log v$  and  $\log i$ . However, there is a potential problem of movement of fines if the material is tested under turbulent flow conditions (Richardson, 1997).

#### *Effect of Porosity and Void Ratio*

Porosity is the ratio of volume of voids to total volume for a given material. This is a function of relative density, and indirectly particle shape. In general, an increase in porosity of an aggregate mix increases the hydraulic conductivity. However, the degree of connectivity of these pores (i.e. effective pores and measured as effective porosity), dictates the hydraulic conductivity of a material. Porosity can be greater in a mix with excess fines, as shown in Figure 5 but due to lack of interconnectivity of pores the mix is relatively impermeable. Usually for open-graded materials the effective porosity is the same as total porosity. Moulton (1980) and Richardson (1997) have developed some empirical relationships with porosity as a key parameter to determine hydraulic conductivity shown in No. 4 and No. 10 through 13 of Table 9 respectively.

Void ratio is defined as the ratio of volume of voids to volume of solids present in a given material. There are many empirical relationships developed by researchers to determine hydraulic conductivity based on void ratio of the material. One of those is the Kozeny-Carman equation shown in No. 6 of Table 9 which yields a directly proportional relationship between void ratio and hydraulic conductivity (see Lambe and Whitman, 1979). Das (1990) states that in general an increase in void ratio increases the hydraulic conductivity. However, this statement could be contradictory because Figure 5 shows that after a limiting fines content (CF) void ratio increases causing volume change, but reduces the hydraulic conductivity significantly. Casagrande proposed a simple relation for the hydraulic conductivity of fine-medium-clean sand as shown in No. 9 of Table 9, based on the void ratio of material (see Das, 1990).

#### *Effect of Viscosity of the Permeant*

An equation reflecting the influence of the properties of permeant was developed, known as the Kozeny-Carman equation, shown in No. 6 of Table 9, to determine the

hydraulic conductivity of porous media. As a simplification for the Kozeny-Carman equation, Taylor (1948) proposed an equation as shown in No. 5 of Table 9 using Poiseuille's law. Both equations indicate that permeability is directly proportional to the unit weight of permeant ( $\gamma$ ), and inversely proportional to the viscosity of permeant ( $\mu$ ) (see Lambe and Whitman, 1979).

#### *Effect of Degree of Saturation*

The degree of saturation is defined as the ratio of volume of water to the volume of voids. A decrease in degree of saturation of soil tends to decrease the hydraulic conductivity. The hydraulic conductivity is significantly reduced if the degree of saturation is less than 85% because the air bubbles block some of the pores (Thornton and Leong, 1995). Richardson (1997) also found that during flow through, partially saturated specimen air bubbles are created due to voids. They tend to block the flow of water, reducing the hydraulic conductivity.

#### **Drainage Capacity of Pavement Bases**

##### *Surface Infiltration*

The major sources of water in pavement systems are surface infiltration, ground water seepage, and melting of ice lenses. The drainage requirements determined in this section will account only for the infiltration caused due to rainfall. In locations where other sources of water are significant, adjustments to the drainage requirements may be warranted. A complete pavement drainage system is typically composed of an aggregate base layer, longitudinal drains, and transverse outlet systems daylighted to surface drainage channels as shown in Figure 11. A positive drainage system should transport water from the point of infiltration to the final exit (transverse drains) through material having high hydraulic conductivity and should eliminate any conditions that would restrict the flow (Moulton, 1980).

Infiltration of water into the pavement system is a complicated phenomenon. Theoretical transient flow studies in uniform porous pavements provided insight into this problem (see Jackson and Ragan, 1974). However, estimating infiltration rates is still

difficult due to the non-uniformity of the surface. Methods for estimating surface infiltration rates in highway pavements are presented in the *FHWA Highway Subdrainage Design Manual* (Moulton, 1980). One method recommended by Cedergren *et al.* (1973) proposes calculating the infiltration rate based on precipitation rates (inches/hour) (Figure 12) and a coefficient depending on pavement type. The coefficient varies from 0.33 to 0.50 for ACC pavements and 0.50 to 0.67 for PCC pavements. For Iowa, which has a precipitation rate of about 1.3 in. and using the coefficient suggested for PCC pavements, the infiltration rates would result in the range of 1.3 to 1.7 ft<sup>3</sup>/day/ft<sup>2</sup>. Ridgeway (1976) found that the ingress channel condition (whether sealed or unsealed, or wide or narrow cracks/joints), and the type of aggregate base layer (whether open-graded or dense-graded) are key factors in defining the infiltration capacity of a joint/crack. For high capacity joints/cracks, high intensity and short duration storms are critical. Whereas for low capacity joints/cracks, storm duration is more important than intensity

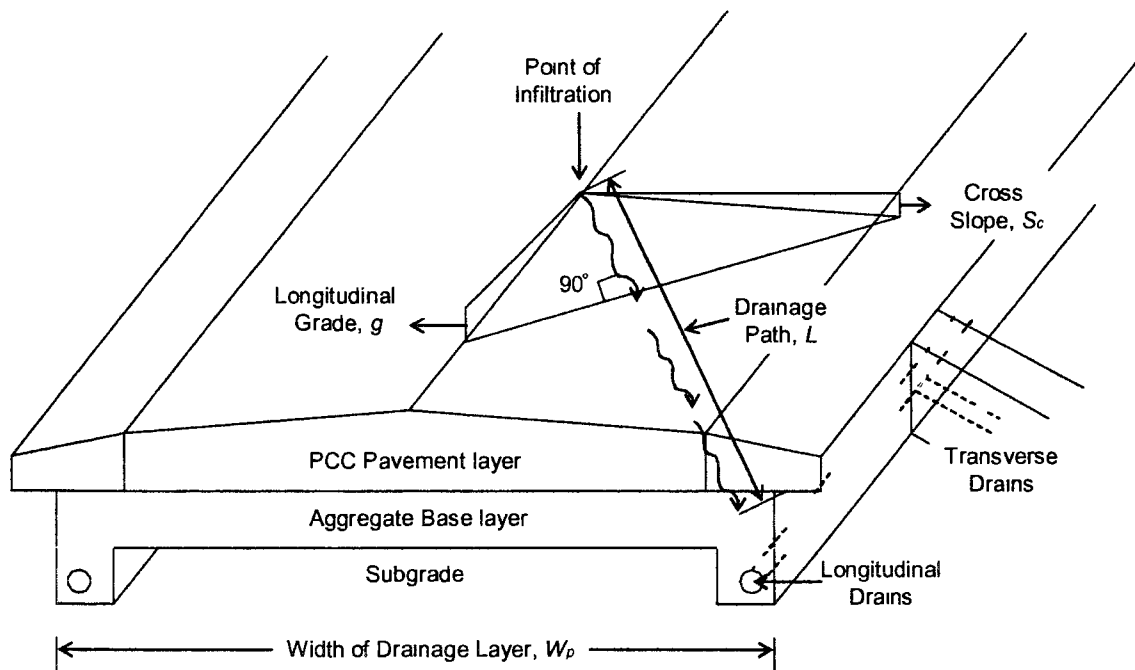


**Figure 11. Typical cross-section showing drainage system in a PCC pavement (Moulton, 1980)**

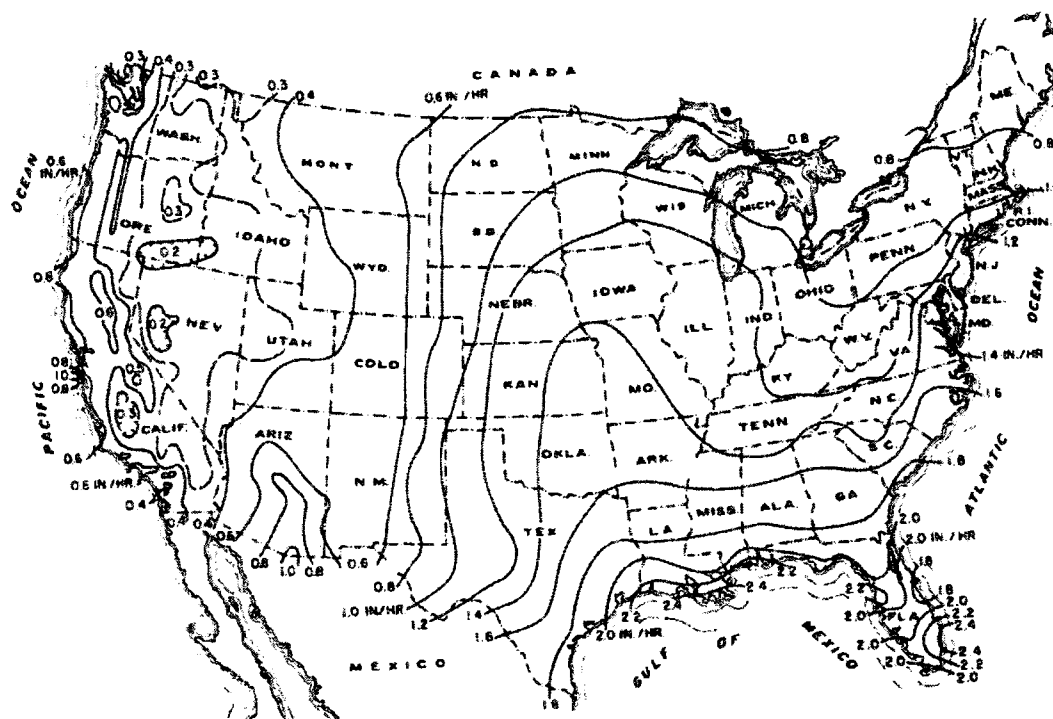


**Figure 12. Maximum 1-h duration/1-yr precipitation in the United States (After Cedergren et al. 1973)**

Ridgeway (1976) recommended a method (summarized in the FHWA design manual) for estimating the surface infiltration based on total length of joints/cracks per unit area of pavement surface and the infiltration capacity of joints/cracks. For normal conditions, it is assumed that (a) the pavement surface layer is impermeable in uncracked locations; (b) continuous longitudinal joints separate at least two individual driving lanes and separate outer driving lanes and shoulders; and (c) transverse joints or cracks are regularly spaced. Based on these assumptions, Equation 2 is suggested for calculating the surface infiltration rates per unit area of crack in highway pavements. An infiltration rate of a joint/crack,  $I_c$ , of  $0.22 \text{ m}^3/\text{day}/\text{m}$  ( $2.4 \text{ ft}^3/\text{day}/\text{ft}$ ) is suggested for design.

$$q_i = I_c \left( \frac{N+1}{W_p} + \frac{W_c}{W_p C_s} \right) \quad (2)$$

Where:

- $q_i$  = infiltration rate per unit area ( $\text{m}^3/\text{day}/\text{m}^2$ ),
- $I_c$  = infiltration rate of crack ( $\text{m}^3/\text{day}/\text{m}$ ),
- $W_c$  = length of transverse cracks/joints (m),
- $W_p$  = width of the drainage layer (m),
- $N$  = number of traffic lanes, and
- $C_s$  = spacing of transverse cracks or joints (m).

Although these two methods are based on empirical relationships, Ridgeway's approach is considered to be more appropriate because it is based on field measurements. Therefore, it is recommended that a uniform design infiltration rate be estimated using Equation 2 (Moulton, 1980). Croveti and Dempsey (1993) also state that the suggested  $I_c$  value is a reasonably conservative value for pavements with open-graded bases. However, Cedergren's method is seen to be better correlated with western states where there is less precipitation compared to eastern states (Moulton, 1980).

### *Flow Analysis*

Key factors that control the time to effectively drain the water include flow-path gradient, flow-path length, and hydraulic conductivity of the material. Based on the geometry of typical pavement bases, the flow of water is primarily horizontal. The flow-path gradient,  $S$ , is a key for horizontal flow analysis, which is a function of pavement geometry and may be obtained using Equation 3. Flow-path length,  $L$ , is defined as the path of water flow from the point of ingress to the outlet. This length is a function of the cross slope, longitudinal gradient, and width of the drainage layer, and can be calculated using Equation 4. Using these relationships, it is seen that increasing the pavement cross slope increases the flow-path gradient and decreases the flow-path length at any given longitudinal gradient. Thus, the end result will be a reduction in drainage times (Croveti and Dempsey, 1993). Therefore, it is important to consider pavement geometry in an effective and economical design of a drainage layer.

$$S = \sqrt{S_c^2 + g^2} \quad (3)$$

$$L = \frac{W_p}{2} \sqrt{1 + \left(\frac{g}{S_c}\right)^2} \quad (4)$$

Where:

$S$  = flow-path gradient (m/m),

$L$  = flow-path length (m),

$W$  = width of the drainage layer (m),

$S_c$  = cross slope (m/m), and

$g$  = longitudinal gradient (m/m).

#### *Determination of Drainage Capacity and Thickness*

After the design infiltration rate,  $q_i$ , is computed, the aggregate base must be designed to an optimal combination of thickness ( $H$ ) and hydraulic conductivity ( $k$ ). Barber and Sawyer (1952) suggest determining the capacity of a drainage layer under steady state flow conditions based on geometry of the drainage layer, using Equation 5. This equation is an enhancement of Darcy's law by including the flow path gradient,  $S$ . This permits the determination of required hydraulic conductivity of a drainage layer when values of the infiltration rate per unit area of crack,  $q_i$ , thickness of drainage layer,  $H$ , flow-path length,  $L$ , and flow-path gradient,  $S$ , are known (Moulton, 1980).

$$q = q_i \times W_c = kH \left( S + \frac{H}{2L} \right) \quad (5)$$

Where:

$q$  = discharge capacity of the drainage layer ( $\text{m}^3/\text{day}/\text{m}$ ),

$k$  = permeability of the drainage layer (m/day),

$S$  = flow-path gradient (m/m),

$H$  = thickness of the base layer (m), and

$L$  = flow-path length (m).

Equation 5 is based on the assumption that the inflow is uniformly distributed across the surface of pavement. To avoid any moisture retention in the base layer, proper drainage

conditions should be maintained by increasing its transmissibility (transmissibility is defined as the product of hydraulic conductivity and thickness of base). This can be achieved by increasing the thickness of base. However, sometimes increasing the thickness of base may not be economically feasible (Moulton, 1980).

Casagrande and Shannon (1952) suggested a relationship for unsteady-state flow conditions (Equation 6) based on degree of drainage. The degree of drainage,  $U$  is defined as the ratio of volume of water drained once the rain stops to the total storage capacity of the drainage layer. During the 1950's, a value of  $t_{50} = 10$  days (50% degree of drainage) was used in the design of base layers. If the time taken to drain 50% of the water is 10 days, it may take several months to drain the remaining water. According to AASHTO (1993), drainage layers that take more than a month to drain water are rated as "VERY POOR" For excellent drainage, AASHTO (1993) recommended that the water is drained within 2 hours. There is no guidance provided on whether the drainage required is 50% removal or complete removal. Ridgeway (1982) suggested that the time for complete or 95% drainage should be less than 1 hour. Carpenter (1990) indicated that the longer the material remains above 85% saturation, the worse it will perform under traffic. Barber and Sawyer (1952) presented a chart (Figure 13), to determine the time factor,  $T_f$ , for any degree of drainage,  $U$  for a given slope condition,  $S$ , based on Equations 7 and 8. A time factor that is determined at any degree of drainage may be used to determine the required hydraulic conductivity using equations shown in Figure 13.

$$t_{50} = \frac{n_e L^2}{2k(H + SL)} \quad (6)$$

For  $U > 0.5$

$$T_f = (c/2) \left[ S + S * \ln \left( \frac{2S - 2US + 1}{(2 - 2U)(S + 1)} \right) - S'^2 * \ln \left( \frac{S + 1}{S} \right) \right] \quad (7)$$

For  $U \leq 0.5$

$$T_f = (c/2) \left[ 2US - S'^2 * \ln \left( \frac{S + 2U}{S'} \right) \right] \quad (8)$$

Where:

$n_e$  = effective porosity of aggregate base material,

$U$  = degree of drainage or percent of drainage that has occurred which is given by the area drained divided by the area that can be drained,

$S$  = slope index =  $H/(L \tan S)$ ,

$T$  = time factor,

$t$  = time for drainage,  $U$ , to be reached (days),

$c$  = geometrical coefficient =  $2.4 - 0.8/S^{1/3}$

Therefore, it is important to note that the required hydraulic conductivity of a pavement base layer required to effectively drain the infiltration is not a fixed value. The required hydraulic conductivity is a function of several factors, including:

- infiltration rate,
- spacing of cracks on surface layer,
- width of pavement,
- number of lanes,
- longitudinal gradient of pavement,
- cross slope,
- gradation of aggregate in the base layer,
- thickness of base, and
- degree of drainage required.

A computer program entitled “*Pavement Drainage Estimator (PDE Version 1 0)*” was developed during this study to estimate the required hydraulic conductivity of an aggregate base layer as a factor of the various factors listed above. A detailed discussion of this program is provided later in this report.



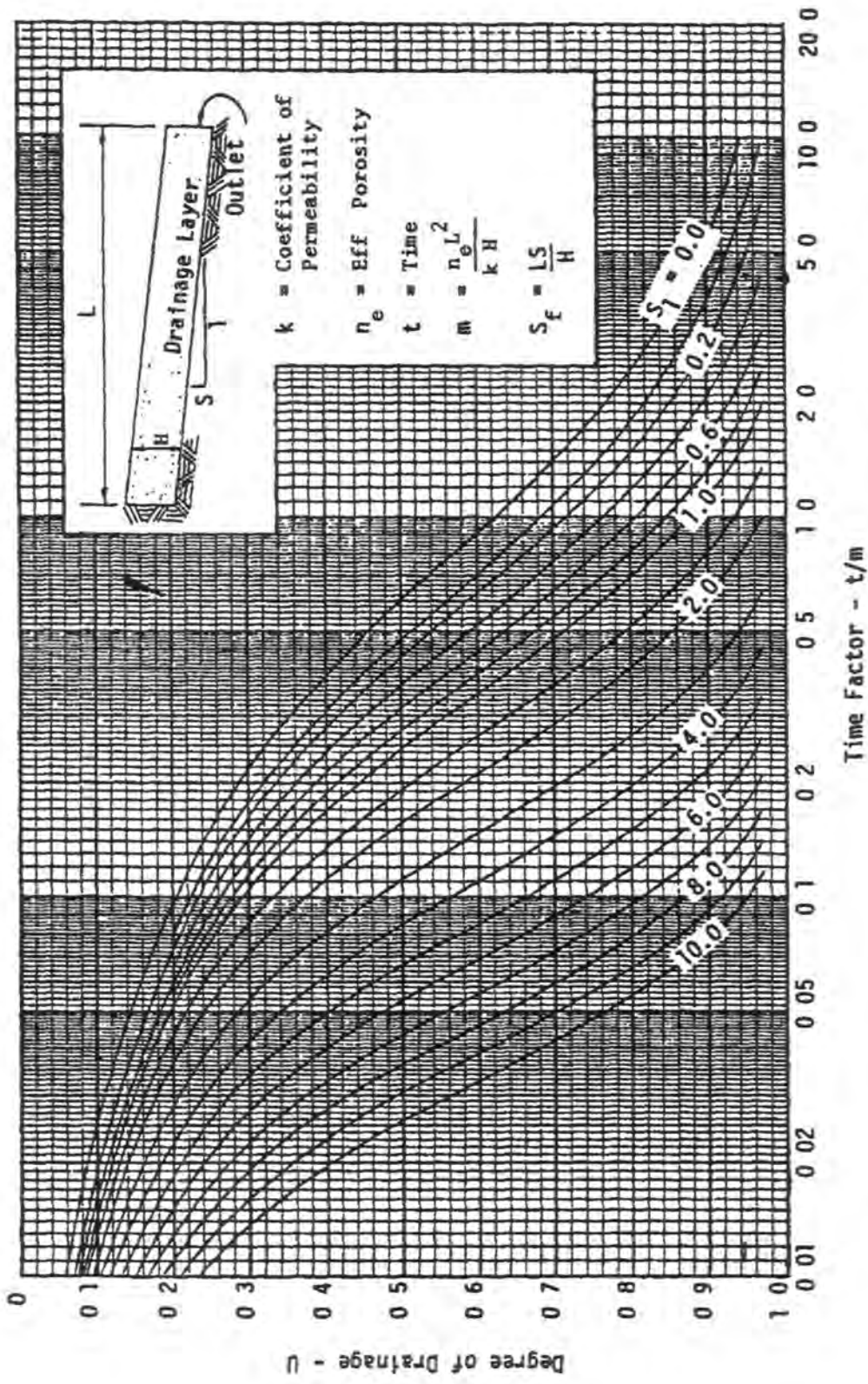


Figure 13 Time-dependent drainage of saturated layer (After Barber and Sawyer, 1952)

## Stability of Pavement Bases

An aggregate base layer should possess high resistance to consolidation under repetitive traffic loading. At the same time, it should meet the minimum drainage requirements discussed in the previous section. Thus, it is important to consider the relationship between strength or stability and permeability

In 1985, a Transportation Research Board committee distributed a questionnaire to all state agencies in United States, in order to better understand the structural contribution being assigned to permeable aggregate base (PAB) layers. It was noted that 47% of the responses to the questionnaire indicated that a layer coefficient of 0.14 (as specified by AASHTO) was being used in the design of a permeable aggregate base layers. The remaining 53% of the responses indicated a layer coefficient value in the range of 0.08 to 0.18. Similarly NAPA distributed a questionnaire in 1990 which indicated that 11 states assigned no structural value for PAB layers while 10 states assigned a layer coefficient of 0.10 to 0.14. For an asphalt-stabilized aggregate base, 6 states assigned a value equal to 0.2 to 0.3 (Minnesota DOT 1994). Using Figure 14, an AASHTO layer coefficient of 0.14 is approximately equivalent to a CBR% value of about 100%.

In lieu of layer coefficient values, Burnham (1997) suggests using Penetration Index (PI) determined from Dynamic Cone Penetrometer (DCP) testing as a rapid quality control measure to characterize pavement bases in the field. It was recommended that DCP tests be conducted to ensure that the PI is less than 19 mm per blow (0.75 inches per blow) on a pavement base immediately after compaction. Further, it was found that the PI value dramatically decreases under traffic loading and as the material's set-up time increases. 700 DCP tests were conducted on base/subbase and subgrade layers, to find a limiting PI value with regard to the pavement performance. A limiting PI value of 5 mm/blow was recommended for Class 3 special gradation (Table 18) used in pavement bases in Minnesota. Using the CBR-PI relationship proposed by the Army Corps of Engineers (No. 4 of Table 19) the limiting CBR value of an aggregate base with Class 3 gradation would be approximately 50%.

Table 18. Class 3 special gradation used by Minnesota DOT (Burnham, 1997)

Total Percent Passing Sieve Size	Class 3
75 mm (3")	--
50 mm (2")	100
37.5 mm (1.5")	--
25.0 mm (1")	--
19.0 mm (3/4")	--
9.5 mm (3/8")	--
4.75 mm (#4)	35-100
2.00 mm (#10)	20-100
425 $\mu$ m (#40)	5-50
75 $\mu$ m (#200)	5-10

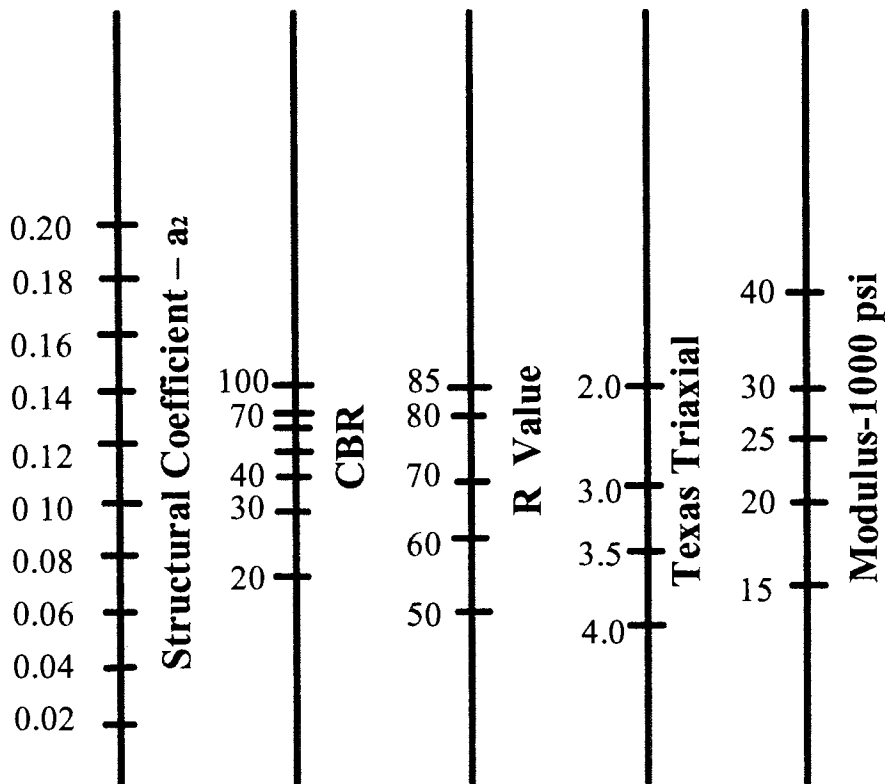


Figure 14. Correlation chart for estimating CBR and Modulus (psi) for bases (Reproduced from Van Til et al. 1972)

Ese *et al.* (1994), observed the deterioration of pavements with respect to different pavement and material strength properties in Norway DCP tests conducted during thawing periods provided a good correlation with the existing pavement conditions. A PI value of 2.6

mm/blow was found to be “critical” for the stability of a pavement base. This PI value is approximately equal to 100% CBR (Equation No. 4 of Table 19). Bases having a PI value higher than 2.6 mm/blow were rated “POOR.” However, all the base materials tested during this research were well-graded materials.

Based on the general agreement between PI and percent compaction, the Minnesota DOT has revised the limiting penetration rates for a 12” thick aggregate base layer as follows (Siekmeir *et al.* 1998):

- a) 15 mm/blow in the upper 75 mm (3.0 in),
- b) 10 mm/blow at depths between 75 and 150 mm (3 and 6 in), and
- c) 5 mm/blow at depths below 150 mm (6 in).

Amini (2003) concludes that the use of DCP for materials with a maximum aggregate size larger than 2 in. is questionable. And all the published relationships between PI and strength parameters are only applicable to certain material types and conditions, but not to all cases. Various strength parameters that can be determined from measured PI value. Their relationships are listed in Table 19

Another approach to characterizing pavement bases in-situ is Falling Weight Deflectometer (FWD) testing. Kazmierowski *et al.* (1994) conducted FWD testing on untreated, asphalt treated, and cement treated open graded drainage layer (OGDL) sections. The OGDL material treated with cement at the rate of 180 kg/m<sup>3</sup> resulted in deflections of about 0.5 mm whereas OGDL material treated with 1.8% of asphalt exhibited deflections of 0.64 mm. Untreated OGDL material resulted in deflections of 0.74 mm. Highlands and Hoffman (1988) also concluded that cement treated base (CTB) performed well by producing small deflections of about 0.13 mm, when compared to other base materials (for gradation see Table 5). The asphalt treated base (ATB), untreated open-graded (OG) base, and high permeable (HP) base exhibited similar deflections of about 0.17 mm. Interestingly a test section with dense-graded (DG) aggregate base showed significantly higher deflections of about 0.5 mm, when compared to all other materials.

Table 19 Relationship between strength parameters and DCP Penetration Index (PI) value

No	Relationship	Suitability	A°, B mm	C(kg)	Proposed by
1	$\log(\text{CBR}) = 2.20 - 0.71 \log(\text{PI})^{1.5}$	Granular and Cohesive soils	30, NI	NI	Livneh (1987)
2	$\log(\text{CBR}) = 2.81 - 1.32 \log(\text{PI})$	Granular and Cohesive soils	60, 20	NI	Harrison (1987)
3	$\log(\text{CBR}) = 2.45 - 1.12 \log(\text{PI})$	Granular and Cohesive soils	NI	NI	Livneh <i>et al.</i> (1992)
4	$\text{CBR} = \frac{292}{\text{PI}^{1.12}}$	All soils except CL below CBR 10% and CH soils	60 20	8 or 4 6 <sup>1</sup>	Webster <i>et al.</i> (1992)
5	$\text{CBR} = \frac{1}{(0.017019 \times \text{PI})^2}$	CL soils CBR < 10%	60 20	8 or 4 6 <sup>1</sup>	Webster <i>et al.</i> (1994)
6	$\text{CBR} = \frac{1}{0.002871 \times \text{PI}}$	CH soils	60 20	8 or 4 6 <sup>1</sup>	Webster <i>et al.</i> (1994)
7	$\log(\text{CBR}) = 2.44 - 1.065 \log(\text{PI})$	Aggregate Base Course	60, 20	8	Ese <i>et al.</i> (1994)
8	$\log(\text{CBR}) = 2.60 - 1.07 \log(\text{PI})$	Aggregate base course and cohesive soils	NI	NI	NC DOT (Pavement 1998)
9	$\log(\text{CBR}) = 2.53 - 1.14 \log(\text{PI})$	Piedmont residual soil	NI	NI	Coonse (1999)
10	$M(\text{psi}) = 7013.065 - 2040.783 \ln(\text{DCPI})$	Soils only at optimum moisture content	60 20	8 or 4 6 <sup>1</sup>	Hassan (1996)
11	$E(\text{MN/m}^2) = 17.6 (269/\text{PI})^{0.64}$	In situ subgrade modulus	NI	NI	Chai and Roslie (1998)
12	$M(\text{psi}) = 532.1 (\text{PI})^{0.492}$	Fine grained soils	NI	NI	George and Uddin (2000)
13	$M(\text{psi}) = 235.3 (\text{PI})^{0.475}$	Coarse grained soils	NI	NI	George and Uddin (2000)
14	$\log(\text{UCS}) = 3.56 - 0.807 \log(\text{DCPI})$	Lime stabilized subgrade (50% probability of under estimation)	60 20	8	McElvaney and Djatnika (1991)
15	$\log(\text{UCS}) = 3.29 - 0.809 \log(\text{DCPI})$	Lime stabilized subgrade (95% probability of under estimation will not exceed 15%)	60 20	8	McElvaney and Djatnika (1991)
16	$\log(\text{UCS}) = 3.21 - 0.809 \log(\text{DCPI})$	Lime stabilized subgrade (99% probability of under estimation will not exceed 15%)	60 20	8	McElvaney and Djatnika (1991)

## Notes for Table 19

- A° the angle of cone in degrees,  
 B the diameter of the cone in mm,  
 C the weight of the hammer in kg,  
 CBR California Bearing Ratio (%),  
 PI Penetration Index from DCP (mm/blow),  
 PI' Penetration Index at 300 mm/blow,  
 DCPI Dynamic Cone Penetration Index (inches/blow),  
 E Modulus (MN/m<sup>2</sup>),  
 M<sub>r</sub> Resilient Modulus (psi),  
 UCS Unconfined Compression Strength (KPa).  
<sup>1</sup>If 4.6 kg mass is used the PI is multiplied by 2.

Chen and Bilyeu (1999) conducted a case study during the evaluation of the GeoGauge for compaction control in the field. This study proposed a performance rating for pavement bases depending on the stiffness (K) and modulus (E) obtained from GeoGauge as shown in Table 20.

**Table 20. Performance rating based on GeoGauge results (Chen and Bilyeu, 1999)**

Base quality	Stiffness (MN/m)	Modulus (MPa)
Weak	<10	<87
Good	18-24	156-208
Excellent	>30	>260

The American Concrete Paving Association (ACPA) provided survey results summarizing the gradations used by different state agencies for base materials under PCC pavements (Figure 15). Twenty-four states use permeable (treated/untreated) bases considering the importance of both stability and permeability in pavement performance. Thirteen states use granular bases (dense-graded), five states use asphalt-treated bases, and six states use cement-treated or lean concrete bases to increase stability

Brown (1997) suggests that for the design of pavements, knowledge of resilient properties of a material and their tendency to develop plastic strains under repetitive loading is a key parameter. Further, Brown (1997) notes that it is surprising that CBR, which is an indirect measure of undrained shear strength, has been used in characterizing the base/subbase and subgrade materials by most pavement engineers. It is important to recognize that the shear strength of material is not of direct interest in design, but rather the elastic modulus of the material and the behavior under repeated loading is of main concern.

A detailed study by Hight and Stevens (1982) shows that CBR does not relate to stiffness of soils at low strains, which is of primary interest in pavement design. Dawson and Plaistow (1996) further showed that it is important to consider resilient characteristics of the granular base layer as well as the subgrade.

The literature review clearly indicates that the requirements of both stability and permeability are still a point of debate.

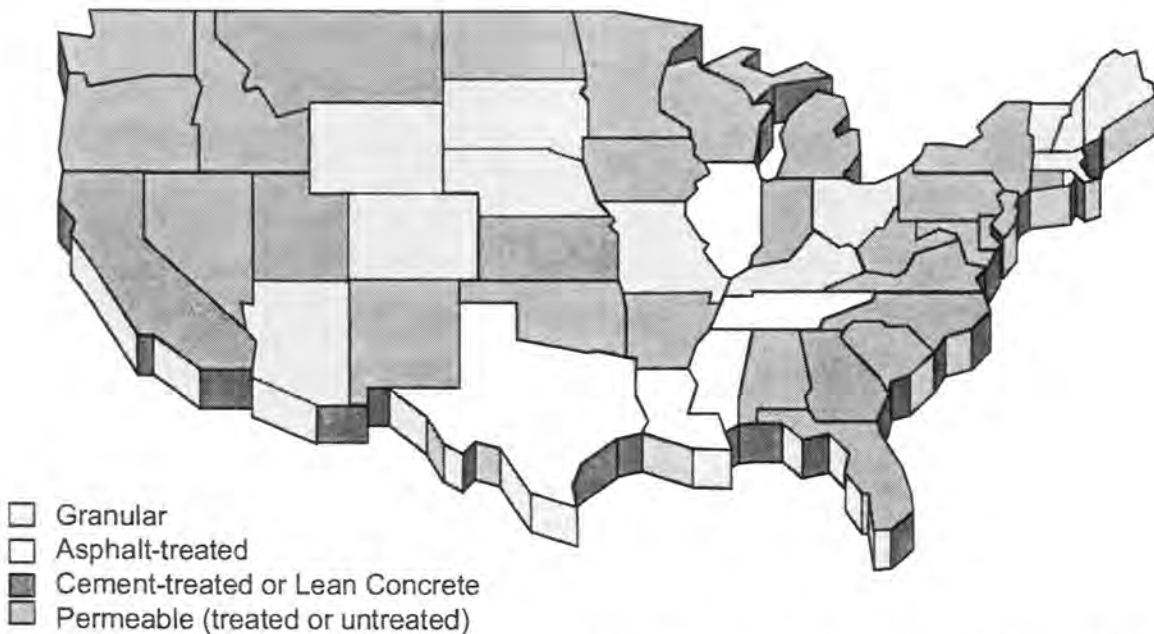


**Figure 15. US Map showing gradations used by different state DOT's under PCC pavements (Courtesy of ACPA, 2001)**

### Survey on Gradations by State DOT's

A detailed survey on gradations suggested by various state and federal agencies for aggregate bases is documented in this section (see Appendix A for values). Data obtained is provided in Figures 17 through 23 with comparison to the Iowa DOT gradation for permeable bases (Gradation No. 4121). The Iowa DOT middle gradation line plotted in all figures refers to the middle values of the specified gradation band. Vertical bars in the figures show the upper and lower limits of the gradation.

Figure 16 shows the gradations used by various state DOT's. Few states had more than one gradation specified for aggregate bases under PCC pavements. Hence, it is divided

into three groups: (a) only permeable bases; (b) only dense-graded bases; and (c) both permeable and dense-graded bases. This figure shows that 6 states use only permeable bases, 11 states use only dense-graded bases, and 29 states use both dense-graded and permeable bases.

Representatives from 8 states (including Iowa) attended the 5<sup>th</sup> Midwestern Pavement Design Workshop held in Iowa, where they discussed base type and thickness requirements under PCC pavements. At the workshop, 4 states use an open-graded base on top of a dense-graded subbase, 2 states suggested using only dense-graded base with no compromise on stability, while 1 state suggested using cement-treated or asphalt-treated permeable base to improve stability while maintaining high permeability. Iowa suggested using only permeable bases (untreated) under PCC pavements.

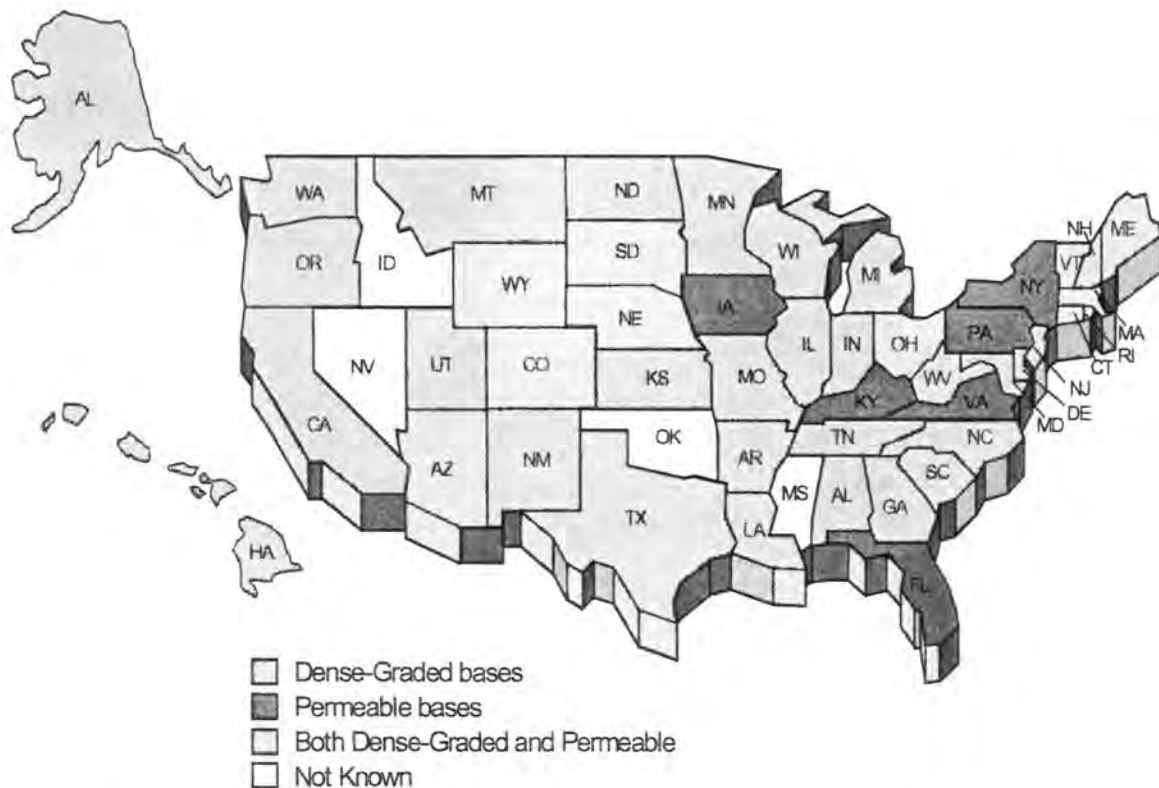


**Figure 16. Gradations used by different state DOT's under PCC Pavements**

From the above discussion and Figure 16, it is clear that different state agencies have different opinions on why, when, and where a permeable base or a dense-graded base should



be used.

Figure 17 compares the Iowa DOT gradation with the mean upper and lower limits of gradations specified by various state and federal agencies. Iowa DOT gradation falls within the mean upper and lower limits. The lower limits of Iowa DOT gradation are very low compared to the mean values, whereas the upper limits are within the range.

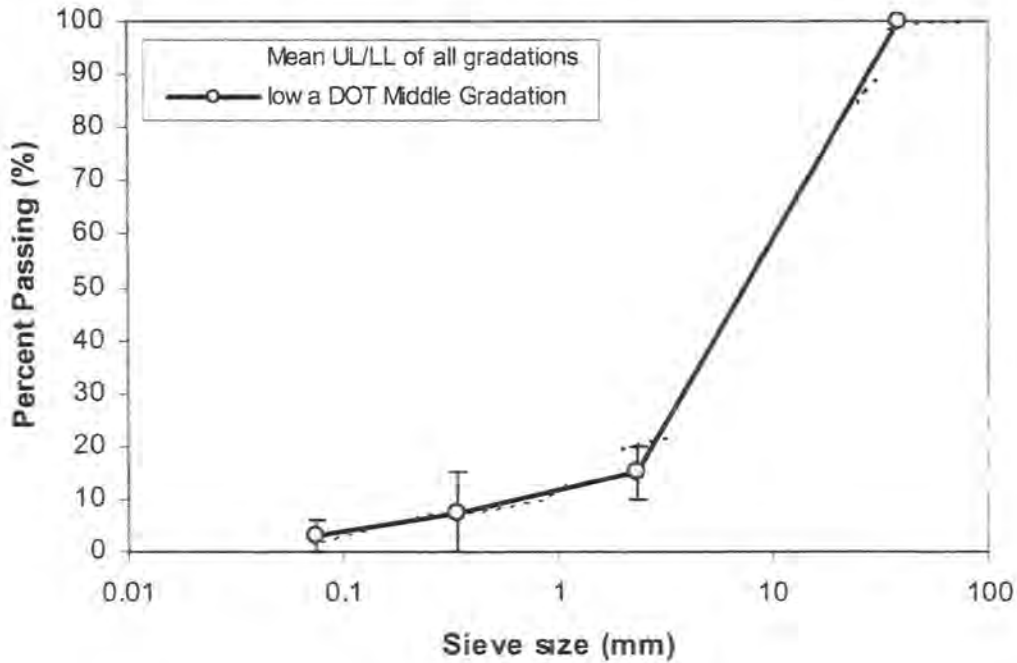


**Figure 17 Comparison of Iowa DOT middle gradation with mean upper and lower limits of gradations by other state and federal agencies**

Figure 18 compares the Iowa DOT gradation with AASHTO No. 57 gradation. This shows that the AASHTO No. 57 is more open-graded. AASHTO No. 57 gradation does not specify the amount of fines passing No. 200 sieve. FHWA recommended AASHTO No. 57 gradation in constructing many permeable aggregate bases in United States (Freeman and Aderton, 1994).

Figure 19 shows the comparison between the Iowa DOT gradation and the gradation specified by National Stone Association (NSA) (Aggregate Handbook, 1996). This indicates that the Iowa DOT gradation is very similar except with particles passing No. 50 sieve (0.3 mm). NSA does not specify the amount of fines passing No. 200 sieve.

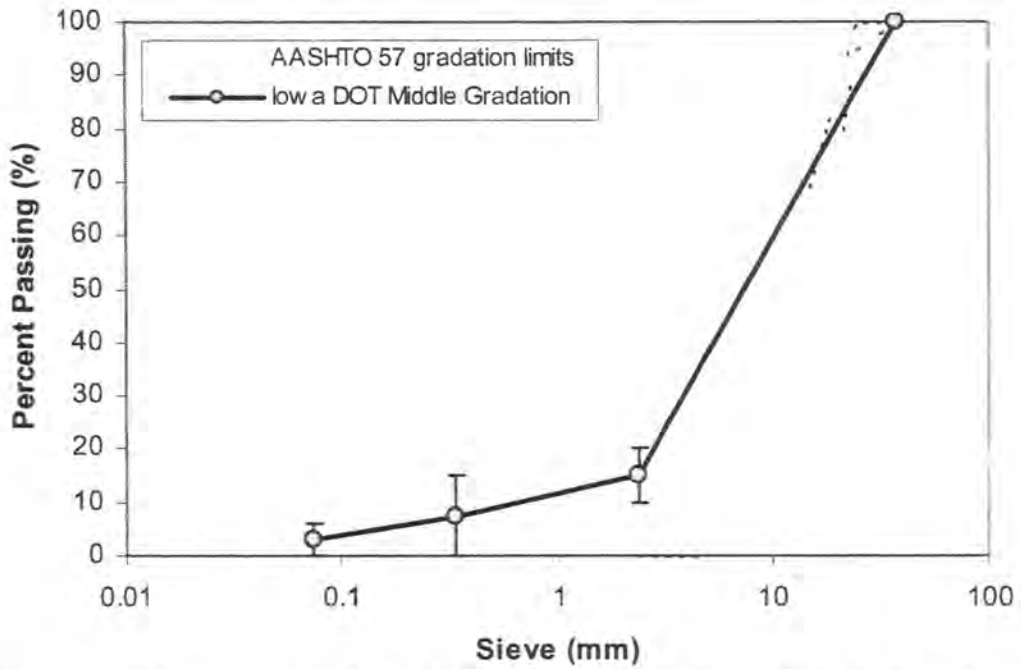


Figure 18. Comparison of Iowa DOT gradation with AASHTO 57 gradation

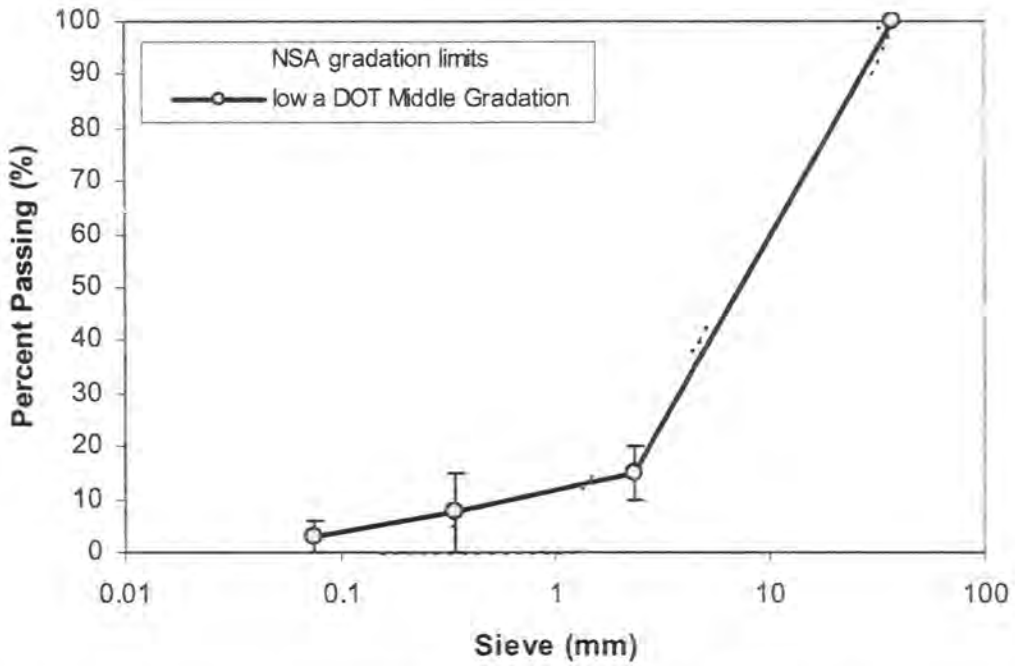
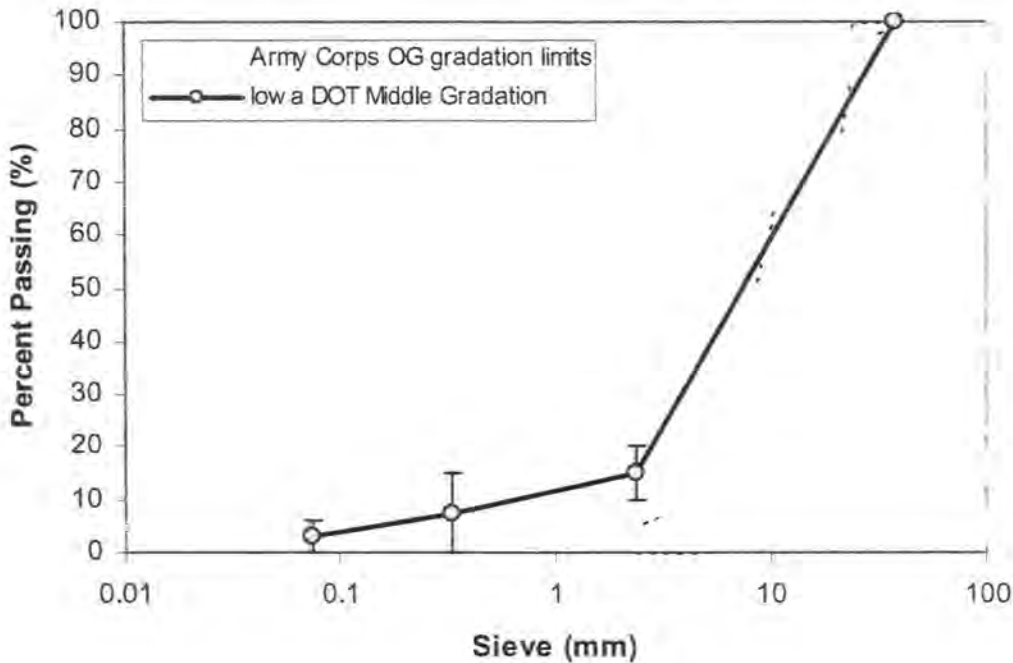


Figure 19 Comparison of Iowa DOT gradation with National Stone Association (NSA) specified gradation

Figures 20 and 21 compare the Iowa DOT gradation with the gradations specified by Army Corps of Engineers for open-graded (OG) material and rapid draining (RD) material, respectively. Gradation for OG material is similar to AASHTO No. 57 gradation. RD material is less open-graded compared to OG material, and is proposed with a purpose of promoting stability while sacrificing permeability (Army Corps, 1992). Figure 20 indicates that the Iowa DOT gradation does not fall within the limits of OG material, whereas it is well compared to RG material (Figure 21), except for the material passing No. 50 sieve.



**Figure 20. Comparison of Iowa DOT gradation with Army Corps of Engineers specified Open-Graded (OG) material gradation**

Figures 22 and 23 compare the Iowa DOT gradation with ASTM D2940, "Standard specification for graded aggregate material for bases or subbases for highways and airports," and ASTM D1241, "Standard specification for materials for soil-aggregate subbase, base, and surface courses," gradations respectively. These figures indicate that the Iowa DOT gradation is more open-graded than ASTM D2940 gradation, while the percent fines passing No. 200 is similar. The Iowa DOT middle gradation line lies within the gradation band of ASTM D1241.

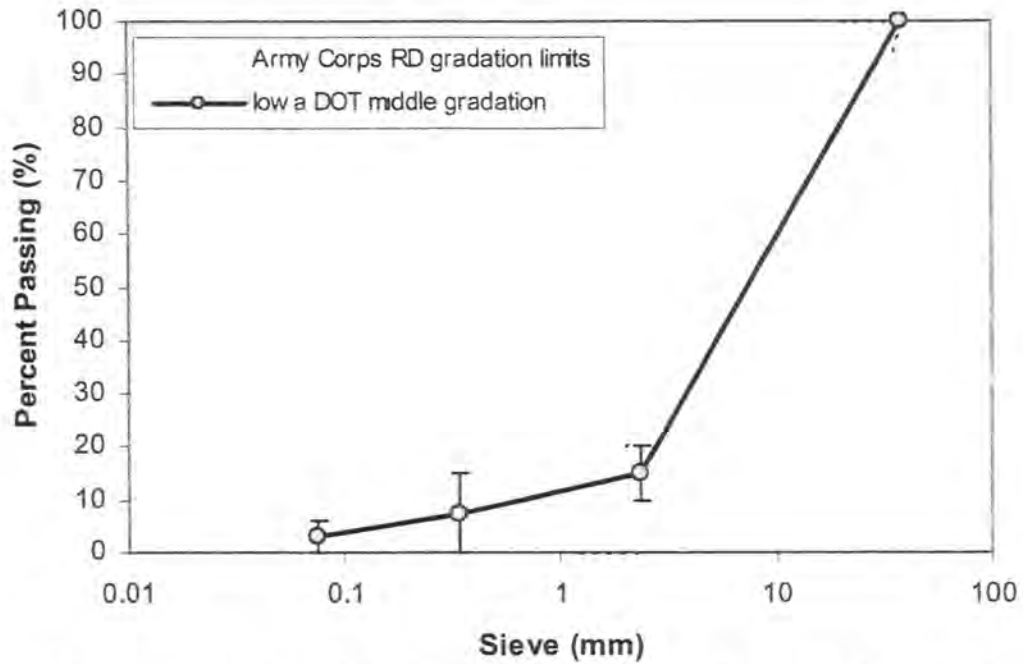


Figure 21. Comparison of Iowa DOT gradation with Army Corps of Engineers specified Rapid Draining (RD) material gradation

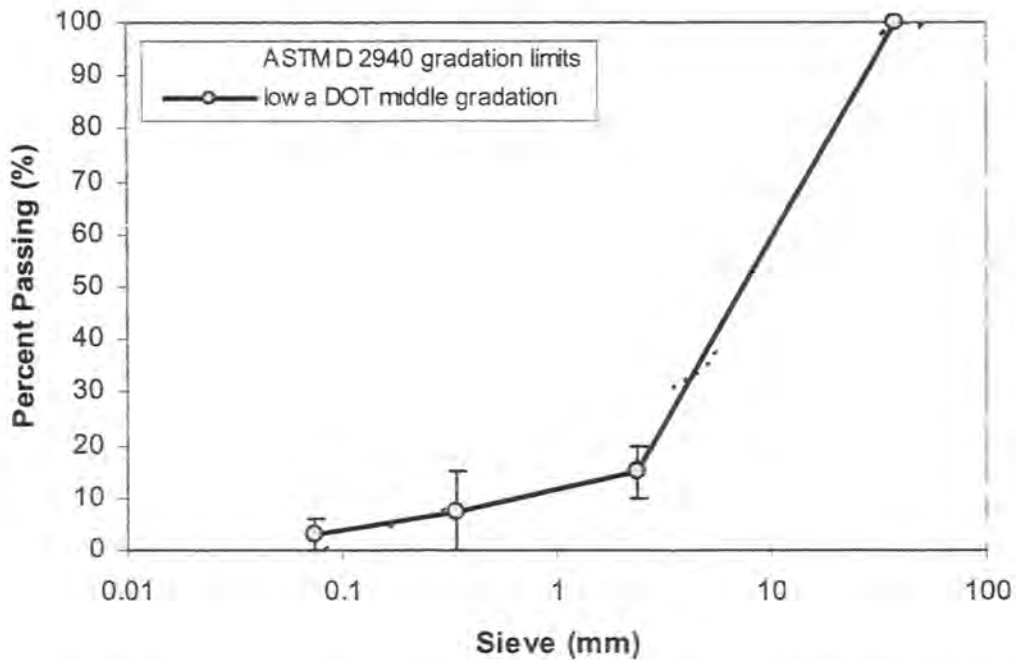
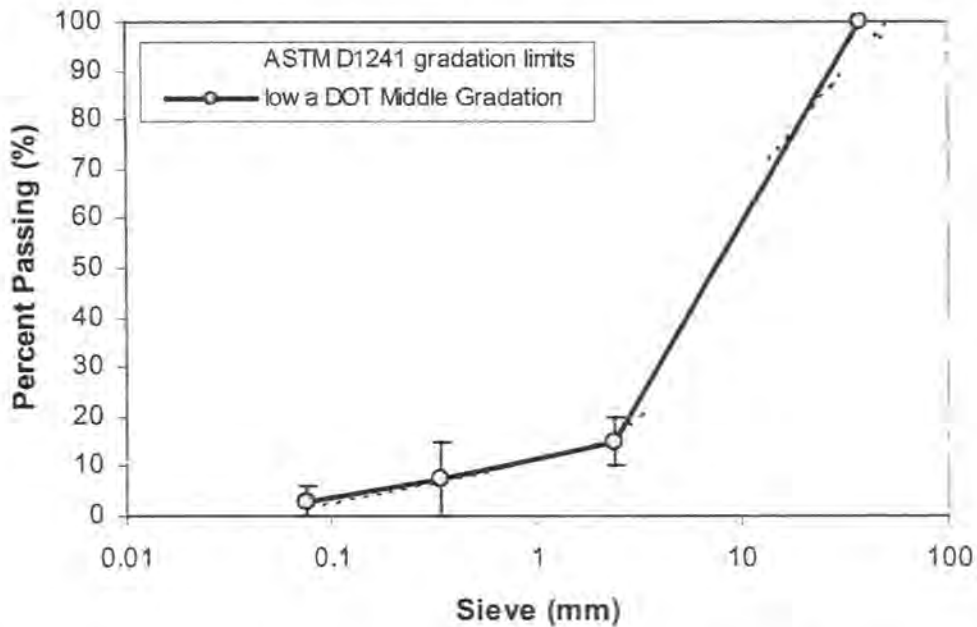


Figure 22. Comparison of Iowa DOT gradation with ASTM D 2940 gradation



**Figure 23. Comparison of Iowa DOT gradation with ASTM D 1241 gradation**

## Stability and Permeability Measuring Techniques for Aggregates

### *Laboratory Measurement for Stability of Aggregates*

#### Repeated Load Triaxial Testing

Repeated load triaxial testing provides the material response measurements that simulate dynamic traffic loading conditions, which can be used in pavement design. Resilient modulus can be determined from this test, which provides a basic constitutive relationship between stress and deformation of material under repeated dynamic axial stress. This test is superior to static tests such as the CBR or the Texas Triaxial test. This test was standardized as AASHTO T 274, but was withdrawn in 1990 (*Aggregate Handbook*, 1996).

Later in 1996, FHWA developed a standard test procedure, LTPP Protocol P46, to determine the resilient modulus of unbound granular base/subbase materials and subgrade soils. Tests can be conducted to simulate stress states under repetitive pavement traffic loadings. Stress levels used on specimens are based on the location of the specimen within the pavement structure. A repeated axial cyclic stress of fixed magnitude, load duration (0.1 second), and cycle duration (1 second) is applied to a cylindrical test specimen. During

testing, the specimen is subjected to a dynamic axial cyclic stress and a static confining stress provided by means of a triaxial pressure chamber. The total resilient (recoverable) axial deformation of the specimen is measured and used to calculate the resilient modulus (LTTP 1996).

### Triaxial Shear Test

Triaxial testing is a fundamental test to characterize soils and aggregates. The *Aggregate Handbook* (1996) summarizes the procedure for the slow triaxial shear test. A specimen prepared at the target density and moisture content is encased in a membrane, and subjected to a constant all-round confining pressure,  $\sigma_3$ . The specimen is then loaded with increasing axial stress until failure at a slow axial strain rate in the range of 0.5 to 2 in/in/min. Axial strain is determined by dividing axial deformation with the distance over which the deformation is measured. Deviator stress ( $\sigma_1 - \sigma_3$ ) and axial strain data is measured during testing to calculate the shear strength of the specimen. Typical confining pressures used during this test vary in between 3 and 40 psi.

If the applied axial strain ranges from 10–17 in/in/sec, it is considered a rapid shear test. Rapid loading is believed to be more representative of loading conditions that exist in field, compared to the conventional slow triaxial shear test. This test is commonly referred to as the “Illinois rapid shear test” (*Aggregate Handbook*, 1996).

### Texas Triaxial Test

The Texas Triaxial Test was developed by Texas Department of Highways and Transportation to evaluate the performance of soil and soil-aggregate mixtures. This test is similar to the conventional triaxial test but varies in the sample dimensions. A specimen of 6 in. diameter and 8.5 in. high is compacted in four lifts in a metal mold at the target moisture content and density. The specimen is carefully finished with hand tools, placed on a porous stone, and then extruded from the mold. The specimen, with a porous stone on each end, is then placed into a steel triaxial testing cell of 6.75 in. diameter and 12 in. high. Next, the cell is lowered into a pan of water to increase the degree of saturation in the sample by capillary absorption and left overnight. Later, a constant confining pressure,  $\sigma_3$ , is applied by inducing

air pressure between the membrane and cell wall. Axial loading at the rate of about 0.15 in/min is applied on the specimen until failure occurs. Tests are performed at different lateral confining pressures. Mohr circles with failure envelopes are then prepared to determine the shear strength of sample (*Aggregate Handbook*, 1996).

#### Laboratory California Bearing Ratio (CBR) Test

The California Bearing Ratio (CBR) is an indirect measure of undrained shear strength and is one of the commonly used parameters in characterizing the stability of aggregates in pavement bases. The CBR test measures the resistance of material to a punching shear failure. This test is performed in accordance with ASTM D1883, "Standard Test Method for California Bearing Ratio of Laboratory-Compacted Soils." The maximum aggregate size used in this test is 0.75 in. The test specimen is compacted in a 6 in. diameter proctor mold to its target density and moisture content. After three or more representative samples are prepared, a cylindrical piston of 2 in. diameter is pushed into each specimen at a constant rate of 0.05 in. per minute. The CBR value is calculated by dividing the force on the piston with a standard reference load at respective penetrations (ASTM D1883).

An advantage of the CBR test is that it is a relatively rapid test method compared to all other laboratory tests used to evaluate the strength properties of aggregates. However, CBR testing has its own limitation in that relating CBR values to stiffness is difficult.

#### *In-Situ Measurement of Stability of Aggregate Base*

##### In-situ CBR Testing

In-situ CBR tests are occasionally used for evaluation of pavement bases. This test method is described in ASTM D4429 "Standard Test Method for California Bearing Ratio of soils in place," but was withdrawn in 2002. This test method is applicable only when (1) the degree of saturation of the material is 80% or greater; (2) the material is coarse grained and cohesionless; and (3) the material has not been modified by construction activities during the 2 years before the test. Subsequent treating, disturbing, handling, compaction or change in water content of the material invalidates the results (*Aggregate Handbook*, 1996).

### Dynamic Cone Penetrometer (DCP) Test

DCP is an instrument designed for rapid in-situ measurement of the structural properties of existing pavements with unbound granular materials (Ese *et al.* 1994). The cone penetration is inversely related to the strength of the material. DCP test is conducted in accordance with ASTM D6951, "Standard Test Method for Use of Dynamic Cone Penetrometer in Shallow Pavement Applications," which was first released in 2003. This test involves measurement of penetration rate per each blow of a standard 8 kg (17.6 lb) hammer, through undisturbed and/or compacted materials. Measured penetration is usually expressed as Penetration Index (PI), which has units of length of penetration per blow (mm/blow or in/blow). Numerous DCP tests have been conducted by researchers on different materials, and various equations have been proposed to correlate PI with strength properties such as CBR, resilient modulus ( $M_r$ ), unconfined compressive strength (UCS), as shown in Table 19. The primary advantages of this test are its availability at lower costs and ease in collecting and analyzing the data rapidly.

### Clegg Impact Hammer Test

The Clegg Hammer was developed by Clegg during the late 1970's. This test was standardized in 1995 as ASTM D5874, "Standard Test Method for Determination of the Impact Value (IV) of a Soil." This is a simple and rapid in-situ test that can be performed on base/subbase and subgrade materials. Clegg Impact Value (IV) is measured as the rebound for 4 blows of a standard 4.5 kg hammer. IV is correlated to CBR using various empirical relationships developed by researchers depending on the type of soil. Clegg (1986) proposed the relationship:  $CBR = (0.24 IV + 1)^2$ . This test method is suitable for evaluating the strength characteristics of soils because soil-aggregates have a maximum particle size less than 1.5 in. (ASTM D5874).

### GeoGauge Vibration Test

The GeoGauge is a 22 lb electro-mechanical instrument invented by Frank Berkman and developed by Humboldt Mfg Co. The GeoGauge provides a direct measure of in-situ stiffness (MN/m) and modulus (MPa). This test is a simple non-nuclear test for soils and



granular materials that can be performed without penetrating into the ground. A Poisson's ratio of 0.35 is set as a standard in this instrument to calculate Young's modulus from stiffness. FHWA is administering a pooled funded study to validate use of the GeoGauge for compaction control in field. The modulus and stiffness values obtained from GeoGauge have been compared to a plate load modulus at 57 sites, which shows a linear regression line with an  $R^2$  value of 0.824 (Briaud, 2003).

#### Falling Weight Deflectometer (FWD) Test

The FWD test is a simple and rapid non-destructive test performed according to ASTM WK2080, "Standard Guide for General Pavement Deflection Measurements." This test does not entail removal of pavement materials, and is therefore often preferred over destructive methods. In addition, the testing apparatus is easily transportable. Layer moduli can be "back-calculated" from the observed dynamic response of the pavement surface to an impulse load. FWD results are often dependent on factors including the particular model of the test device, the specific testing procedure, and the method of back-calculation (FAA, 2003).

#### *Laboratory Permeability Testing*

Investigating the hydraulic conductivity properties of aggregates is essential in performing drainage analysis prior to construction of a base. There are two standard methods used to determine the hydraulic conductivity: (a) constant head permeability tests; and (b) falling head permeability tests. Considering the limitations of typical lab-scale permeameters, various researchers have proposed new large scale permeameters as discussed below

#### Constant Head/Falling Head Permeability Testing

Constant head testing is performed according to ASTM D2434, "Standard Method for Permeability of Granular Soils (Constant Head)," to determine the hydraulic conductivity under laminar flow conditions of water through granular soils. The mold used for testing should have a diameter approximately 8 to 12 times the maximum particle size. The porous disk used in testing should have a greater permeability than that of the soil specimen with openings no larger than 10% finer size, to prevent movement of finer particles (ASTM

D2434). The quantity of flow at the outflow end at a particular constant head is measured to determine the hydraulic conductivity using Darcy's equation. In order to limit consolidation influences during testing, this procedure is limited to disturbed granular soils containing not more than 10% fines passing a No. 200 sieve. Falling head permeability tests need a similar setup as constant head test. But methods for performing the test vary. While testing under falling head, the sample is saturated and water is allowed to flow through the sample, and change in time with head is observed. Hydraulic gradient versus velocity of flow is plotted to calculate the hydraulic conductivity.

### Large Scale Permeameters

Various large scale laboratory permeameters have been developed within the last few decades to determine the hydraulic conductivity of aggregate base materials. Head (1982) developed a large scale permeameter with dimensions of 16 in. diameter and 34 in. long. This permeameter was used for aggregates with gradation having 3 in. maximum size. The material is compacted or vibrated in the cell, and a water supply tank of 900 liters capacity with several outflow levels is connected to the permeameter. This test is similar in principle to the standard laboratory permeability test, but represents more realistic conditions by allowing larger aggregates.

Jones and Jones (1989) introduced a horizontal permeameter to measure the hydraulic conductivity of aggregates used in drainage layers. This permeameter works for material having  $D_{50}$  up to 1.2 in. The permeameter cell is of dimension 39.37 in. x 11.8 in. x 11.8 in. where the sample is compacted using a vibrating hammer. A lid with bar stiffeners and neoprene foam placed on top of the aggregate surface is used to seal the top of the compaction mold. After the specimen is saturated, tests are conducted at various hydraulic gradients. Test results show a satisfactory basis for the measurement of hydraulic conductivity. However, further investigation was suggested to develop a repeatable and reproducible test method.

Similarly, Chapuis *et al.* (1989) developed a horizontal permeameter to measure the hydraulic conductivity of granular and sandy soils. Dimensions of the permeameter were 5.9 in. x 5.9 in. x 11.8 in. The design details were compatible with those of the vertical permeameter recommended by ASTM D2434, except a flexible rubber membrane was used

on the top of compaction mold, to provide a good seal against leakage. After the sample is saturated using de-aired water, tests are conducted at various hydraulic gradients.

Randolph *et al.* (2000) also developed a horizontal permeameter to measure the hydraulic conductivity of granular materials. A sample is compacted vertically and the measurement of hydraulic conductivity is done horizontally representing field conditions of vertical compaction and horizontal movement of water in bases. The cross sectional dimensions of the permeameter mould are 12 in. x 12 in. x 18 in. long. This permeameter cell has a perforated plate with 0.35 in. diameter holes both at the inlet and outlet end of the flow. Flexible closed-cell polypropylene foam sheets are glued to all sides of the sample cell to ensure no leakage in the system. Water chambers are attached with piezometers at the outflow and inflow end to measure the head loss during flow. Using the measured head loss and the quantity of water flowing through sample, hydraulic conductivity of the material is determined using Darcy's equation.

#### *In-situ Hydraulic Conductivity Testing*

Construction operations may significantly alter the material properties from that which is tested in the laboratory. Hence, in-situ hydraulic conductivity testing provides better in-sights to evaluate the performance of pavement bases. There are a few in-situ hydraulic conductivity test methods that were developed and evaluated.

Moulton and Seals (1979) developed a Field Permeability Test Device (FPTD), which uses a velocity measurement technique principle. A schematic diagram of the measurement system is shown in Figure 24. The FPTD device consists of three major subsystems: (a) the reservoir and pressure subsystem; (b) the control and measurement subsystem; (c) the plate and probe subsystem. Water is supplied from the reservoir and the difference in head between two probes,  $\Delta h$ , for a distance of travel  $L$ , in time,  $t$  seconds is recorded. If porosity of the material,  $n$ , is known, Equation 9 may be used to determine the hydraulic conductivity  $k$ .

$$k = \frac{L^2 n}{t \Delta h} \quad (9)$$

Where:

$L$  = Probe Spacing (cm),

$\Delta h$  = Head Loss (cm),

$t$  = time of flow between probes (sec), and

$n$  = porosity

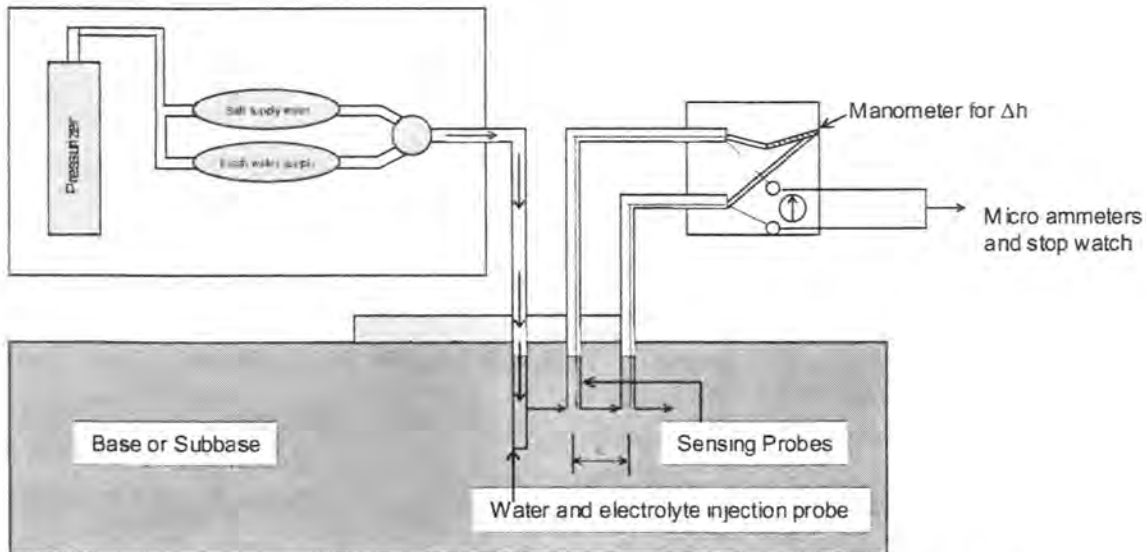


**Figure 24. Schematic diagram of FPTD (Moulton et al. 1979)**

Fernuik and Haug (1990) describe in-situ hydraulic conductivity test methods for clay fill liners, which included (a) the sealed single-ring infiltrometer (SSRI) test; (b) the sealed double-ring infiltrometer (SDRI) test; and (c) the air entry permeameter (AEP) test.

SSRI is a device used to measure the rate of infiltration (Figure 25), which can later be used to determine the hydraulic conductivity. SSRI does not have standard dimensions. Fernuik and Haug (1990) used two different SSRI's of 10.25 in. and 24 in. diameters by 8.25 in. and 6 in. high, respectively. SSRI is installed by jacking the steel ring smoothly into the soil or by setting it into a pre-excavated circular trench. The narrow zone immediately adjacent to the inside of the ring is filled with bentonitic grout. This prevents escape of water down along the sides and under the ring. Loose sand and a steel plate are placed over the test area to prevent erosion of the liner. After the test setup is ready, water is filled rapidly up to a head of approximately 24–28 in. and the quantity of water infiltrating the soil from the

graduated cylinder is measured. The depth of infiltration  $L_f$  is determined using the volume of permeant, porosity dry density, degree of saturation, and the area of soil. Thus, hydraulic gradient can be calculated using Equation 10 and substituted in the Darcy's equation (Equation 11) to determine the hydraulic conductivity. However, this test assumes that the suction pressures developed during flow of water in unsaturated regions of soils is negligible (Fenuik and Haug 1990).

$$i = \frac{(H + L_f)}{L_f} \quad (10)$$

$$Q = k_i A \quad (11)$$

Where:

$i$  = hydraulic gradient (cm/cm),

$H$  = height of water in the infiltrometer (cm),

$L_f$  = depth of infiltration (cm),

$A$  = area of soil being tested ( $\text{cm}^2$ ), and

$Q$  = flow rate ( $\text{cm}^3/\text{sec}$ ).

The SDRI test may be performed in accordance with ASTM D5093, "Standard Test Method for Field Measurement of Infiltration Rate Using a Double-Ring Infiltrometer with a Sealed-Inner Ring." Test setup for SDRI is shown in Figure 26. Full penetration of water through the liner eliminates sources of error associated with soil suction and unsaturated hydraulic conductivity that persist in SSRI tests. The hydraulic gradient in this test is given by Equation 12, and substituting it in Darcy's Equation (Equation 11) determines the hydraulic conductivity. The SDRI typically has inner and outer rings of 72 in. and 144 in. diameter and a height of 6 in. and 38 in. respectively. A modified SDRI with bigger dimensions is also available. Test setup for SDRI is similar to the SSRI in most aspects, except that the SDRI has two rings. The area adjacent to the outer ring is sealed with bentonitic grout to ensure that no leakage occurs. A uniform water level in the graduated cylinder is maintained during the test, and the flow rate within the inner ring is determined by

measuring the quantity of water required to keep the level constant (Fenuik *et al.* 1990). However, as per ASTM D5093 SDRI is limited to soil with a hydraulic conductivity in the range of  $10^{-7}$  to  $10^{-10}$  cm/sec.

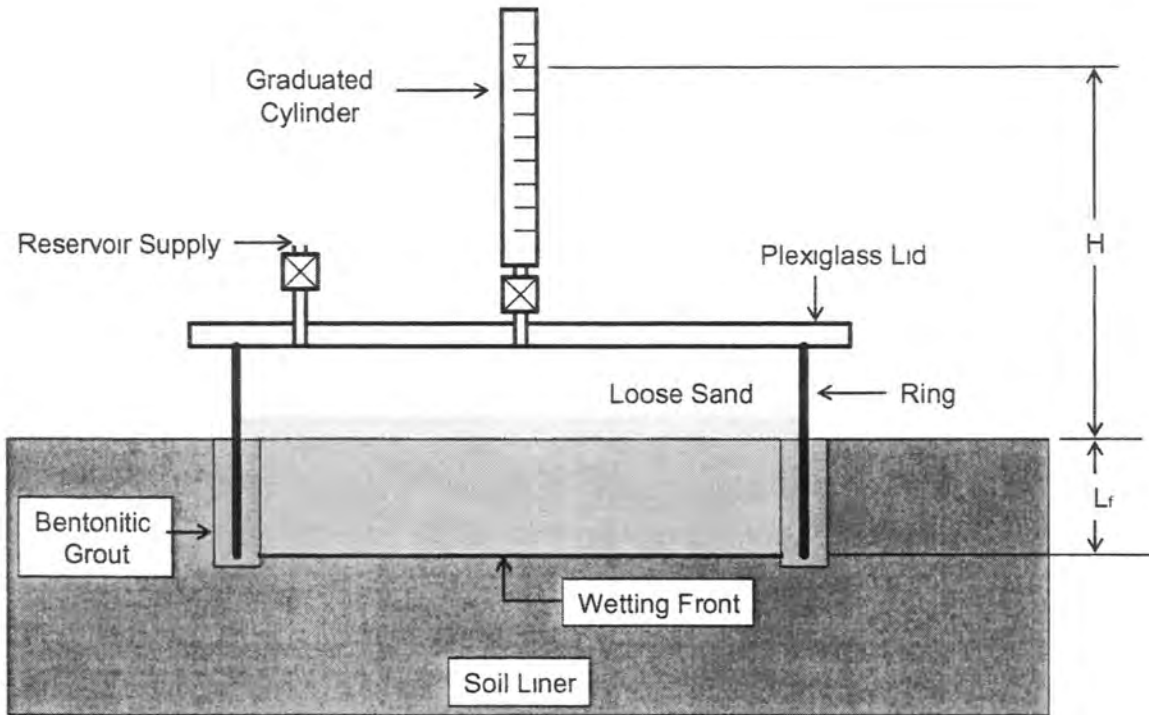


Figure 25. Sealed single-ring infiltrometer (SSRI) (Fenuik and Haug, 1990)

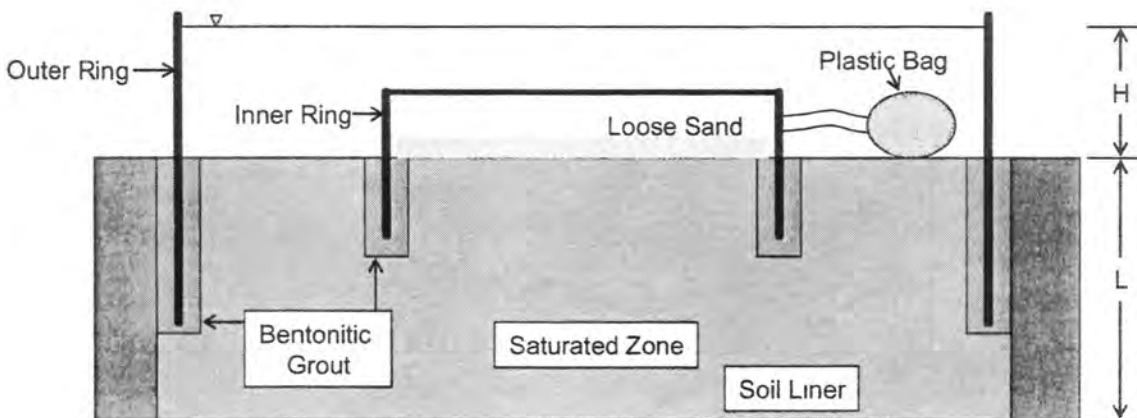


Figure 26. Sealed double ring infiltrometer (SDRI) (Fenuik and Haug, 1990)

Bouwer (1966) proposed using an Air Entry Permeameter (AEP) to measure the in-situ hydraulic conductivity of clay fill liners (Figure 21). The AEP is similar to SSRI in design and operation in that the volumetric flux of water entering the soil is used to calculate the saturated hydraulic conductivity in the unsaturated zone. Tests using the AEP are performed in two stages. During the first stage, the water is introduced into the permeameter through a stand pipe over which a graduated cylinder and mercury manometer are attached. Water is allowed into the soil within the permeameter ring, and the flow rate is measured by observing the decline of the water level within the reservoir. The second stage of the test starts after the flow rate during infiltration becomes constant. At this point, the flow of water into the permeameter is stopped, and the wetted zone is allowed to drain. This causes a pressure drop within the permeameter as water in the wetted zone reacts to the suction pressures in the underlying unsaturated soil. As the water drains, tension in the water within the ring increases until the point where air-entry pressure ( $P_a$ ) or bubbling pressure is reached and bubbles migrate upward through the soil into the ring. The minimum pressure value ( $P_{min}$ ) attained during this stage is used to calculate  $P_a$  using Equation 12. The hydraulic gradient may be calculated using Equation 13. Once the minimum pressure is achieved, the permeameter is removed and the depth to the wetting front,  $L_f$ , is measured. Then, by substituting the hydraulic gradient value in Equation 11, the hydraulic conductivity may be determined.

$$P_a = P_{min} + G + L_f \quad (12)$$

$$i = (H + L_f - 0.5 P_a) / L_f \quad (13)$$

Where

$P_a$  = air-entry pressure or bubbling pressure (cm),

$P_{min}$  = minimum pressure attained in the water above ground (cm),

$G$  = height of the vacuum gauge above the surface of the liner (cm).

The AEP is most suitable for sand, silt, and clayey soils having hydraulic conductivity in the range of  $10^{-9}$  cm/sec to  $10^{-4}$  cm/sec (Stephens and Associates, 2004).

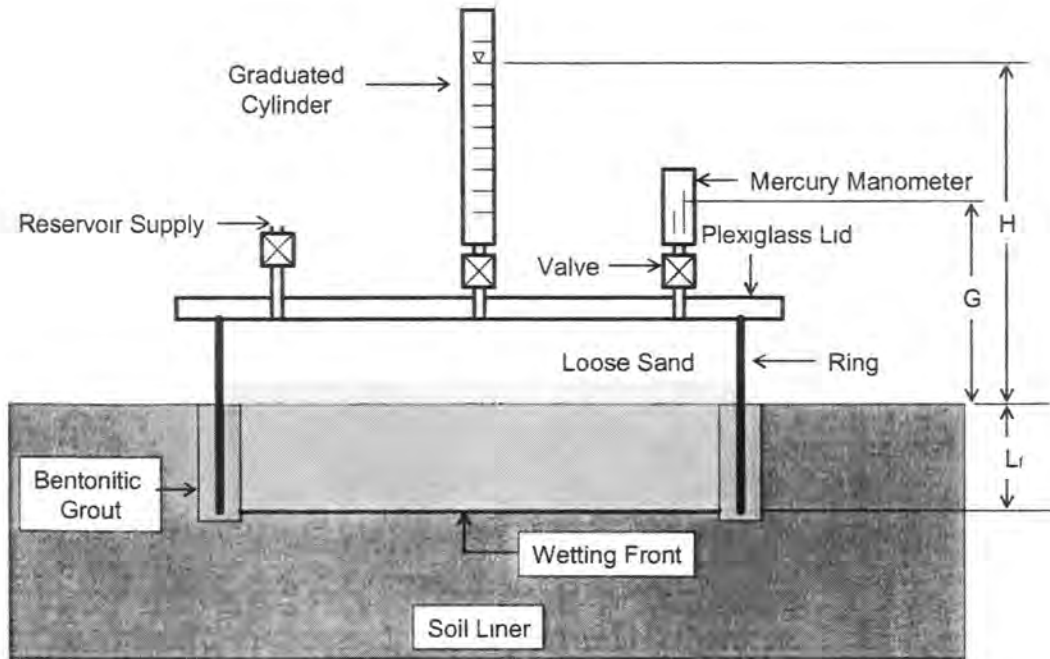


**Figure 27 Air entry permeameter (Fernuik and Haug, 1990)**

The double ring infiltrometer (DRI) test is also used in determining the infiltration rate of water into soils. The DRI test may be performed in accordance with ASTM D3385, "Infiltration Rate of Soils in Field Using Double-Ring Infiltrometers." Infiltration rates have the same units as hydraulic conductivity (cm/sec), but it should be noted that they are distinctly different. This instrument has outer and inner ring dimensions of 12 in. and 24 in. diameter, respectively and is 20 in. high. The test method involves driving the outer and inner rings into the ground, partially filling the rings with water and then maintaining it at a constant level. The volume of water added to the inner ring to maintain the constant level, is noted to determine the infiltration rate. This test is suitable only for soils with hydraulic conductivity in the range of  $10^{-2}$  to  $10^{-6}$  cm/sec (ASTM D3385).



## Pavement Base Construction Practices

The benefits of using an open-graded permeable base layer are widely accepted throughout the world. But working with open-graded material in the field and obtaining a workable platform for the overlying surface are not yet well defined. Many researchers (Reed 1995, Kazmierowski *et al.* 1994) summarized their experiences in construction of an OGDL during their study and suggested a method of construction meeting the today's construction standards.

Kazmierowski *et al.* (1994) provided the following recommendations for open-graded base construction, which is in implementation by the Ontario Ministry of Transportation.

- Construction traffic should not be permitted on the Open-Graded Drainage Layer (OGDL) for the paving train during placement of the overlying pavement. Haul trucks should not be allowed on the OGDL except to discharge material directly on to the paver.
- The OGDL should be covered with the concrete pavement within 30 days of placement to prevent contaminations resulting from prolonged exposure. The OGDL should be protected from dust during construction.
- Compaction of Asphalt Treated Permeable Bases (APTB) should consist of three to five passes of a class S2 roller weighing 9 to 11 tons. Final compaction should be such that the OGDL can support the weight of the paving equipment. Pneumatic tires or vibratory rollers should not be used.

Reed (1995) summarizes the Illinois DOT's experiences in stabilized OGDL construction during the mid 1980's through 1993. The Illinois DOT concluded that the open-graded drainage material, which met Illinois DOT CA-7 gradation and was stabilized with Portland cement of  $142 \text{ kg/m}^3$  and w/c ratio of 0.5, produced a fairly uniform mix with good workability and results in a stable OGDL. This mix was compacted using vibratory pans attached to the subgrade planer. They also concluded that no curing is required for this mix, as there was no significant difference in strength between cured and non-cured sections. Further they recommended using a subgrade planer (e.g. motor grader) or similar equipment that has the ability to spread the harsh mix for laying a Portland cement stabilized OGDL.

## Key Findings from Literature Review

The major finds determined from this literature review are summarized as follows:

- Undrained PCC pavement sections with granular or lean concrete bases may develop roughness, transverse cracking, and longitudinal cracking more rapidly than drained pavement sections with permeable asphalt-treated base (Hall and Correa, 2003).
- Incorporating permeable bases reduces joint faulting and D-cracking in the case of non-doweled jointed PCC pavements (Harrigan, 2002).
- An increase in fines content above the critical fines content, CF greatly increases the rate of permanent strain for some Iowa aggregates (Ferguson, 1972).
- The strength of the aggregate material decreases significantly with increased fines content over the optimum fines content (Aggregate Handbook, 1996).
- Cement-treated open-graded materials result in smaller deflections as compared to material treated with asphalt and untreated material (Kazmierowski *et al.* 1994, Highlands and Hoffman, 1988).
- Increasing the fines content above 5% increases the suction and frost heave action. Adding bitumen helps prevent frost heave at any fines content (Kolisoja *et al.* 2002).
- Higher stiffness, higher friction angle, higher cohesion due to interparticle water tension, and less axial strain is observed in crushed limestone, compared to uncrushed or crushed gravel (Cheung and Dawson, 2002).
- The life of a poorly drained pavement is reduced by 1/3 or less of the life than a well-drained pavement (Cedergren, 1974).
- Recycled concrete materials result in lower hydraulic conductivity compared to crushed limestone, both in lab and field (Miyagawa, 1991).
- Aggregate material with 100% crushed faces exhibit greater hydraulic conductivity compared to 88% crushed faces with similar gradation (Haiping *et al.* 1993).
- The minimum required hydraulic conductivity of a pavement base layer and/or the time to achieve a given percent drainage is dependent on various factors, including properties of aggregates, dimensions of the pavement, rainfall intensity and the amount of drainage required.

- Requirements on the minimum stability required for an aggregate base are not well established. Structural contributions being assigned in design continues to be a point of debate.
- State DOT gradation surveys indicate that six states use only permeable bases, eleven states use only dense-graded bases, and twenty-nine states use both dense-graded and permeable bases.
- Surprisingly CBR, which is an indirect measure of undrained shear strength, has been used in characterizing the base/subbase and subgrade materials by most pavement engineers, but is not of direct interest in the pavement design. The knowledge of resilient properties of a material and their tendency to develop plastic strains under repetitive loading may be the key parameter for design (Brown, 1997).

## LABORATORY INVESTIGATION

This section summarizes laboratory hydraulic conductivity and strength measurements on several Iowa aggregates (limestone, gravel and recycled concrete) used for pavement base construction. Table 21 lists the aggregate materials and the sample locations. To study the influence of fines content on hydraulic conductivity and strength, constant/falling head permeability and CBR tests were performed. The results show that hydraulic conductivity exponentially decreases as fines content increases and that maximum strength is achieved for fines contents between 6% and 14%. The measured hydraulic conductivity and CBR values were also found to vary significantly as a function of aggregate type, gradation, and density. Particle degradation of recycled concrete aggregates is higher than crushed limestone and gravel, which leads to lower hydraulic conductivity values. Target hydraulic conductivity values for granular subbase aggregates were established based on criteria of achieving 50% or 90% drainage in less than 2 hours for a typical two lane pavement. The results for various aggregates were then compared to the established drainage criteria.

### Test Methods

Grain-size analyses were conducted in accordance with ASTM C136, "Standard Test Method for Sieve Analysis of Fine and Coarse Aggregates." Particle-size distribution curves were determined using an air-dried sample of about 2000 g and sieving over the 1.5, 1, 0.75, 0.5, 0.375 mm, Nos. 4, 8, 10, 30, 50, and No. 200 sieve sizes.

Atterberg limits were determined in accordance with ASTM D4318-93, "Liquid Limit, Plastic Limit, and Plasticity Index of Soils." Liquid limit tests were performed according to Method A (multi-point liquid limit) by estimating the water content until the sample required 25 blows to close the groove. Three representative air-dried samples of about 200 g each passing No. 40 sieve were used to determine the liquid and plastic limits.

Specific gravity was determined using a helium-pycnometer. Tests were conducted using a Density-Multipycnometer manufactured by Quantachrome Instruments and in accordance with the standard test procedures provided by the manufacturer. Sample mass used for testing varied between 35 to 50 g passing the No. 10 (2 mm) sieve.

Micro-Deval tests were conducted on three different aggregate materials (crushed limestone, gravel and recycled concrete) to determine the abrasion loss. Tests were performed in accordance with the standard test procedures recommended by the Ontario Ministry of Transportation (MTO 1997). This test entails abrading a graded sample in a small rotating drum with steel charges in the presence of water. This process can simulate degradation of aggregate under repetitive traffic loading during saturated base conditions.

CBR tests were conducted to investigate the influence of fines content (passing No. 200 sieve) on strength. Tests were performed in accordance with ASTM D1883, "Standard Test Method for CBR (California Bearing Ratio) of Laboratory-Compacted soils." Variations in fines content ranged from 0 to 14%. Aggregate gradations with particles retained on the 0.75 in. sieve were modified by adding an equal amount of material passing through the 0.75 in sieve and retained on the No. 4 sieve, according to ASTM D1883 Standard Proctor compaction energy was used to produce the CBR test specimens. As shown in Figure 28, tests were performed by placing the sample in a container filled with water. This approach represents loading under saturated base conditions. A surcharge weight of 2.2 kg (5 lb) was applied to the top of the sample to prevent bulging during loading.

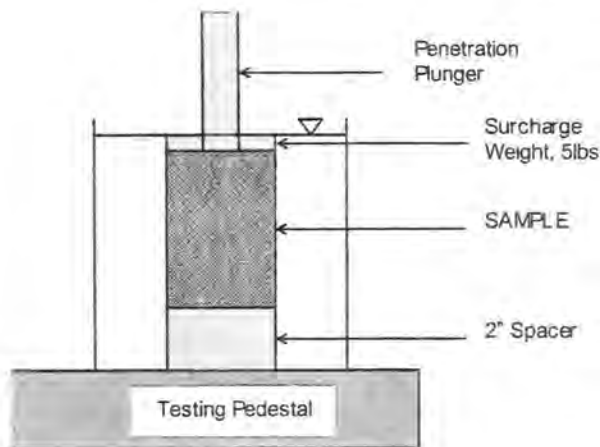


**Figure 28. Schematic representation of soaked CBR test setup**

Relative density compaction tests were conducted on oven-dried samples in accordance with Test Method A of ASTM D4254, "Standard Test Method for Minimum Index Density and Unit Weight of Soils and Calculation of Relative Density" and Test

Method 1A of ASTM D4253, "Standard Test Method for Maximum Index Density and Unit Weight of Soils using a Vibratory Table" to determine minimum and maximum dry densities of the aggregates, respectively. To accommodate materials having a maximum particle size up to 1.5 in, a 0.0142 cu m. (0.5 cu ft.) volume compaction mold was used.

Constant/falling head permeability tests were conducted using a large-scale aggregate compaction-mold permeameter (ACP) fabricated for this study. Tests were conducted in accordance with the standard test procedures developed during this study and provided in Appendix B. Test specimens were compacted by striking the sides of the mold with a rubber hammer and/or using a Marshall compaction hammer.

### **Aggregate Index Properties**

Aggregate materials were obtained in bulk from the quarry or from base construction projects in the field. Information on the aggregate type, source and sampling location is summarized in Table 21.

Grain-size distribution curves for all samples are shown in Figures 29 and 30. The Iowa DOT gradation specification according to No. 12 section 4121 (granular subbase) is provided for comparison. A summary of the gradation test results is provided in Table 22 for the quarry samples and Tables 23 and 24 for the field samples. The coefficient of uniformity  $C_u$ , coefficient of curvature,  $C_c$ , and percent fractions of gravel, sand, and silt/clay are listed in Tables 25 and 26. All materials were classified according to AASHTO and the Unified Soils Classification System (USCS).

It can be seen that, with the exception of CLS151 and RPCC35, none of the quarry or field samples specified as granular subbase meet all of the Iowa DOT gradation requirements (see Tables 22 and 23). Aggregates used for special backfill (RAUG), modified subbase (MSB) and porous backfill (CLSD) did meet the Iowa gradation requirements (see Table 24). The AALS and sand samples are considered well-graded materials and were included in this study for purposes of comparison with engineering properties of open-graded materials.

**Table 21. Aggregate samples obtained from quarry and field**

<b>Material</b>	<b>Iowa Aggregate Gradation</b>	<b>Text Designation</b>	<b>Source</b>	<b>Sampling Location</b>
Crushed Limestone	Granular Subbase (4121)	CLS	Martin Marietta, Cedar Rapids, Iowa	Quarry
Crushed Limestone	Granular Subbase (4121)	ALS	Martin Marietta, Ames, Iowa	Quarry
Recycled PCC	Granular Subbase (4121)	RPCC	Mannats Materials, Ames, Iowa	Quarry
Crushed Limestone	ACC (0.5")	AALS	Martin Marietta, Ames, Iowa	Quarry
Uncrushed Gravel	Granular Subbase (4121)	AG	Hallet Materials, Iowa	Quarry
Sand	Granular Backfill (4133)	Sand	Hallet Materials, Iowa	Quarry
Crushed Limestone	Granular Subbase (4121)	CLS218	IA218 Pavement base construction site, South-East Iowa	Field
Crushed Limestone	Granular Subbase (4121)	CLS151	US151 Pavement base construction site, Cedar Rapids, Iowa	Field
Recycled PCC	Granular Subbase (4121)	RPCCAmes	Knapp Street Pavement base construction site, Ames, Iowa	Field
Crushed Limestone	Granular Subbase (4121)	CLSUG	University-Guthrie Pavement base construction site, Des Moines, Iowa	Field
Recycled PCC	Granular Subbase (4121)	RPCC35	I-35 North Bound Pavement Base Construction, Story Co., Iowa	Field
Crushed Limestone	Modified Subbase (4123)	MSB	35th Street Pavement subbase construction site, Des Moines, Iowa	Field
Crushed Limestone	Porous Backfill (4131)	CLSD	University-Guthrie drainage trench construction site, Des Moines, Iowa	Field
Recycled Asphalt	Special Backfill (4132.02)	RAUG	University-Guthrie Pavement sub-base construction site, Des Moines, Iowa	Field

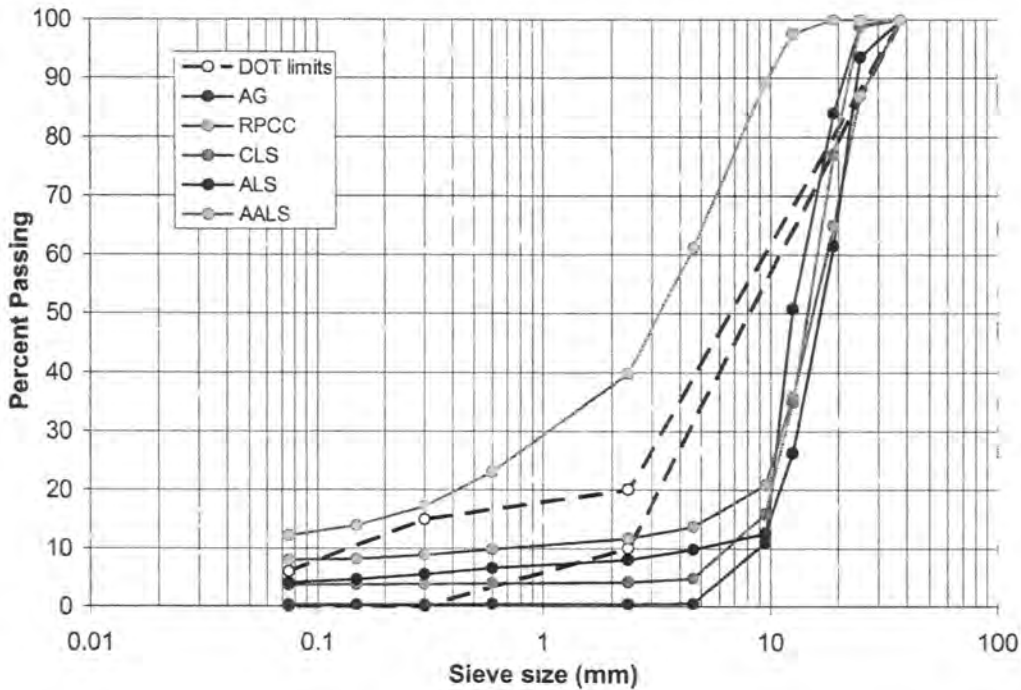


Figure 29 Grain-size distribution curves of quarry samples comparing with Iowa DOT gradation according to section No. 4121

Table 22. Grain-size distribution of quarry samples

Sieve		% Passing								
Sieve No.	Size (mm)	AG	RPCC	CLS	ALS	Iowa DOT <sup>1</sup>	Sand	Iowa DOT <sup>2</sup>	AALS	Iowa DOT <sup>3</sup>
1.5"	37.5	100.0	100.0	100.0	100.0	100	100.0	—	100.0	—
1"	25	99.0	86.9	98.7	96.5	—	100.0	—	100.0	—
0.75"	19	84.0	64.9	77.0	65.2	—	100.0	—	100.0	100.0
0.5"	12.5	50.8	35.7	34.9	27.5	—	99.8	—	97.6	92-100
0.375"	9.5	11.0	20.8	15.9	9.8	—	99.6	—	89.3	70-91
No. 4	4.75	0.5	13.7	4.8	2.4	—	98.0	—	61.2	50-72
No. 8	2.36	<b>0.4</b>	11.6	<b>4.1</b>	<b>2.3</b>	10-20	91.5	20-100	39.8	36-57
No. 30	0.6	0.3	9.8	3.9	2.2	—	12.3	—	23.0	16-34
No. 50	0.3	0.3	8.8	3.8	2.2	0-15	4.0	—	17.2	—
No. 100	0.15	0.3	8.1	3.7	2.1	—	2.0	—	13.9	—
No. 200	0.075	0.3	<b>7.9</b>	3.6	1.9	0-6	1.6	0-10	<b>12.7</b>	3-7

<sup>1</sup> Iowa DOT specified gradation according to section No. 4121 – granular subbase

<sup>2</sup> Iowa DOT specified gradation according to section No. 4121 – granular backfill

<sup>3</sup> Iowa DOT specified gradation according to section No. 4121 – ACC (0.5 m.)

Not required

Does not meet Iowa DOT specification



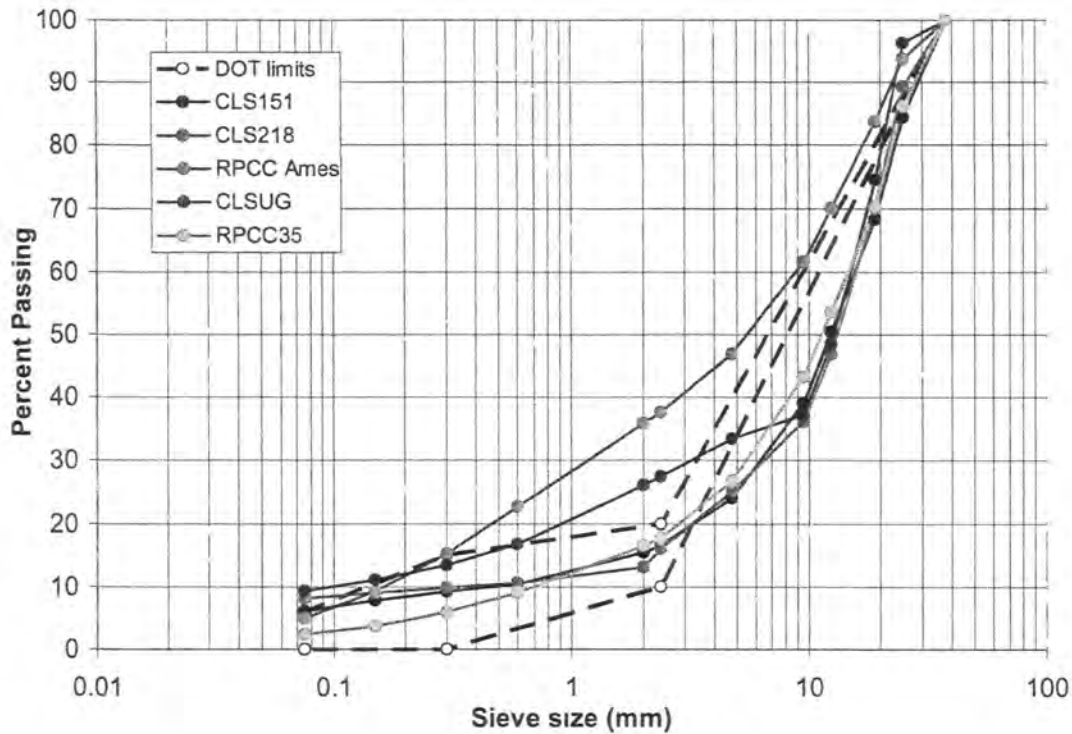


Figure 30. Grain-size distribution curves of field samples compared to Iowa DOT gradation according to section No. 4121

Table 23. Grain-size distribution of field samples

Sieve		% Passing					
Sieve No.	Size (mm)	CLS218	CLS151	RPCCAmes	CLSUG	RPCC35	Iowa DOT*
1.5"	37.5	100	100	100	100	100	100
I	25	89.2	84.4	93.7	96.3	86.1	—**
0.75"	19	70.2	68.3	83.7	74.5	70.2	—
0.5"	12.5	46.8	50.4	70	48.4	53.6	—
0.375"	9.5	36.1	39.1	61.5	37.2	43.2	—
No. 4	4.75	25.1	24	46.9	33.5	26.7	—
No. 8	2.36	15.9	16.6	<b>37.6</b>	<b>27.5</b>	17.7	10-20
No. 10	2	13.1	15.4	35.9	26.1	16.5	—
No. 30	0.6	10.6	10.4	22.7	16.8	9	—
No. 50	0.3	9.8	9.2	15.3	13.4	5.9	0-15
No. 100	0.15	9	7.8	9.2	11	3.6	—
No. 200	0.075	<b>8.2</b>	6.1	4.9	<b>9.3</b>	2.4	0-6

\* Iowa DOT specified gradation according to section No. 4121 – granular subbase

\*\* Not required

Does not meet DOT specification

**Table 24. Grain-size distribution of field samples**

Sieve		% Passing					
Sieve No.	Size (mm)	RAUG	Iowa DOT <sup>1</sup>	CLSD	Iowa DOT <sup>2</sup>	MSB	Iowa DOT <sup>3</sup>
1.5"	37.5	100.0	100	100.0	—	100.0	100.0
1	25	94.0	—	100.0	—	89.9	—
0.75"	19	86.1	—	100.0	100	71.0	70-90
0.5"	12.5	76.3	—	100.0	95-100	57.0	—
0.375"	9.5	68.4	—	84.3	50-100	45.2	—
No. 4	4.75	52.2	—	17.7	10-50	30.0	—
No. 8	2.36	37.8	15-45	6.2	0-8	22.6	10-40
No. 10	2	34.3	—	6.1	—	21.4	—
No. 30	0.6	8.8	—	5.7	—	14.4	—
No. 50	0.3	2.6	—	5.3	—	12.4	—
No. 100	0.15	1.1	—	4.8	—	11.0	—
No. 200	0.075	0.7	0-10	4.4	—	10.0	3-10

<sup>1</sup> Iowa DOT specified gradation according to section No. 4132.02 special backfill

<sup>2</sup> Iowa DOT specified gradation according to section No. 4131 porous backfill

<sup>3</sup> Iowa DOT specified gradation according to section No. 4123 modified subbase

A summary of Atterberg limits are provided in Tables 25 and 26 for the quarry and field samples, respectively. Of all the materials, only CLS218, RPCCAmes and MSB exhibit plasticity with PI values ranging between 3 and 8. The granular subbase materials are classified as A-1-a according to AASHTO and from GP to GW according to USCS. The well-graded crushed limestone (AALS) is classified as A-1-a and SM and the Sand as A-1-b and SP-SM. Specific gravity values ranged from 2.4 for recycled asphalt to 2.8 for gravel.  $C_u$  and  $C_c$  values varied widely as a function of gradation. The minimum and maximum dry densities determined from the vibratory compaction method yield relatively low values (i.e. 1400 to 1600 kg/m<sup>3</sup>) for the granular subbase materials and higher values (e.g. 2000 kg/m<sup>3</sup>) for the more well-graded materials.

Table 25 Summary of Engineering Properties for Quarry Samples

Material (see Table 21)	% material gravel > #4 sand < #4 > #200 silt/clay < #200	LL	PI	C <sub>u</sub>	C	D <sub>10</sub>	AASHTO	Unified soils classification	Dry density (kg/m <sup>3</sup> )	Specific gravity, G <sub>s</sub>	Abrasion loss %
CLS	gravel = 84.1% sand = 12.1% silt/clay = 3.7%		NP	2.2	1.2	7.50	A 1 a	GP	$\gamma_d$ Min = 1374.3 $\gamma_d$ Max = 1450.5	2.77	15.3
ALS	gravel = 87.4% sand = 8.0% silt/clay = 4.6%		NP	3.8	1.9	5.00	A 1 a	GP	$\gamma_d$ Min = 1390.7 $\gamma_d$ Max = 1467.2	2.64	—
RPCC	gravel = 79.2% sand = 12.7% silt/clay = 8.1%	27	NP	30.0	12.2	0.60	A 1 a	GP GM	$\gamma_d$ Min = 1344.4 $\gamma_d$ Max = 1411.4	2.54	22.5
AALS	gravel = 10.7% sand = 75.4% silt/clay = 13.9%		NP	90.0	6.4	0.05	A 1 a	SM	$\gamma_d$ Min = 1682.1 $\gamma_d$ Max = 2016.2	2.74	—
AG	gravel = 99.5% sand = 0.2% silt/clay = 0.3%	29	NP	1.5	1.0	9.20	A 1 a	GP	$\gamma_d$ Min = 1575.4 $\gamma_d$ Max = 1641.6	2.86	9.8
Sand	gravel = 2.0% sand = 96.4% silt/clay = 1.6%		NP	2.7	0.9	0.55	A 1 b	SP SM	$\gamma_d$ Min = 1502.2 $\gamma_d$ Max = 1610.7	2.64	*

Notes:

\* Tests not performed

LL – Liquid Limit

PI – Plasticity Index

NP – Non Plastic

C – Coefficient of Uniformity

C – Coefficient of Curvature

D<sub>10</sub> – Particle diameter at 10% passing (mm)

Table 26 Summary of Engineering Properties for Field Samples

Material (see Table 21)	% material gravel > #4 sand < #4 > #200 silt/clay < #200	LL	PI	C	C	D <sub>10</sub>	AASHTO	Unified soils classification	Dry density (kg/m <sup>3</sup> )	Specific gravity G <sub>s</sub>
CLS218	gravel = 74.9% sand = 17.0% silt/clay = 8.2%	20	8	53.3	10.2	0.30	A 1 a	GP GC	$\gamma_d$ Min = 1534.0 $\gamma_d$ Max = 1635.1	2.73
CLS151	gravel = 76% sand = 17.9% silt/clay = 6.1%		NP	33.3	5.5	0.50	A 1 a	GP GM	$\gamma_d$ Min = 1530.9 $\gamma_d$ Max = 1626.1	2.84
RPCCAmes	gravel = 53.1% sand = 42.0% silt/clay = 4.9%	29	3	56.3	4.3	0.20	A 1 a	GW GM	$\gamma_d$ Min = 1554.8 $\gamma_d$ Max = 1651.1	2.53
CLSUG	gravel = 66.5% sand = 24.2% silt/clay = 9.3%		NP	150.0	6.0	0.10	A 1 a	GP GM	$\gamma_d$ Min = 1532.6 $\gamma_d$ Max = 1627.9	2.73
MSB	gravel = 70.0% sand = 20.0% silt/clay = 10.0%	22	5	156.3	18.3	0.10	A 1 a	GP GM	—	—
CLSD	gravel = 82.3% sand = 13.3% silt/clay = 4.4%		NP	2.2	1.2	3.50	A 1 a	GP	—	2.73
RAUG	gravel = 47.8% sand = 51.5% silt/clay = 0.7%	18	NP	8.8	0.6	0.80	A 1 a	GP GM	$\gamma_d$ Min = 1434.5 $\gamma_d$ Max = 1513.7	2.43
RPCC35	gravel = 73.3% sand = 24.3% silt/clay = 2.4%		NP	21.4	3.1	0.70	A 1 a	GP	$\gamma_d$ Min = 1423.6 $\gamma_d$ Max = 1498.5	2.54

Notes:

\* Tests not performed

LL – Liquid Limit PI – Plasticity Index NP – Non Plastic

C – Coefficient of Uniformity

C – Coefficient of Curvature

D<sub>10</sub> – Particle diameter at 10% passing (mm)

## Test Results and Discussion

### *Influence of Fines Content on CBR*

The influence of fines content on strength was investigated by performing laboratory CBR tests on aggregate gradations with fines content varied from 0%–14%. For this study, test materials included CLS, ALS, RPCC, AALS, AG, and RPCCAmes. Table 27 shows the maximum CBR (%) achieved at 0.4 in. penetration and the corresponding optimum fines content. Optimum fines content was determined as the fines content that produced the maximum CBR value. Typically 0.1 or 0.2 inch penetration values are used to determine CBR for aggregates. However, for our tests, the best correlation between CBR and fines content was observed at 0.4 in. penetration. Lower penetration depths produced erratic values. A summary CBR measurements at all penetration depths is provided in Appendix C.

For 0.4 inch penetration, the optimum fines content necessary to achieve maximum CR is between 6% and 14%. Results show that the RPCC materials exhibit the lowest CBR at 22 to 31 with optimum fines content of 8% and 14%. CLS exhibits the highest CBR at about 52 with an optimum fines content of about 8%. All limestone aggregates (CLS, ALS, and AALS) exhibit higher CBR values than the recycled concrete aggregates (RPCC, RPCCAmes), which is believed to be a result of significant particle breakage/degradation observed during testing of the RPCC materials. To verify this observation, Micro-Deval degradation tests were performed on the recycled concrete (RPCC) with comparisons to limestone (CLS) and gravel (AG). A summary of the test results is provided in Table 28. As expected, RPCC exhibits poor performance with higher abrasion loss when compared to CLS and AG.

CBR test results for AG did not exhibit predictable behavior with varying fines content at any penetration level. The behavior may be attributed to a lack of interlock between the gravel particles. It was further observed that (1) fines segregated during the saturation process prior to testing; and (2) during loading it was difficult to maintain a constant increase in load because the load piston was carried by just a few individual gravel particles, thus concentrating the load. As particles fractured during loading, the rate of loading would abruptly decrease. Hence, the CBR values obtained for AG are highly

variable.

**Table 27 CBR at Optimum fines content**

Material	Optimum % fines <sup>1</sup>	CBR(%) at 0.4 in penetration
CLS	8	52
ALS	10	45
RPCC	8	22
AALS	6	51
AG	~ 8	~ 43
RPCCAmes	14	31

Notes:

<sup>1</sup>Fines passing No. 200 sieve,  
Highly variable results

**Table 28. Abrasion loss and performance rating of materials tested**

Material	% Abrasion loss	Performance Rating
AG	9.8	Good
CLS	15.3	Fair
RPCC	22.5	Poor

Note: Rating according to Cooley *et al.* (2002)

### *Influence of Fines Content on Hydraulic Conductivity*

To investigate the influence of fines content on hydraulic conductivity falling head permeability tests were conducted on RPCC with fines contents ranging from 0% to 15% in increments of 3%. A summary of the results is shown in Table 29 Results show that hydraulic conductivity decreases from about 1.6 cm/s to 0.6 cm/s with an increase in fines from 0% to 3%, then decreases exponentially with further increases in fines to 0.07 cm/s at 15% fines content. The drainage times for achieving 50% and 90% drainage of this material were estimated using PDE 1.0. In order to calculate the drainage times using PDE 1.0, assumptions of a two-lane highway with 150mm thick base material having effective porosity of 30%, a cross-slope of 2% and 0% longitudinal gradient were used. At the specified upper limit of 6% fines content, 50% and 90% drainage time varies from less than 1 hour to 3.5 hours. At a fines content of 15%, the hydraulic conductivity is reduced over 20 times and the drainage times increase about 21 times.

**Table 29 Falling head permeability test results for RPCC with variation in fines**

% fines	Dry density (kg/m <sup>3</sup> )	K (cm/sec)	$K_0/K_x$ *	Time for 50% drainage (h)**	Time for 90% drainage (h)**
0	1556	1.55	—	< 1.0	1.4
3	1604	0.56	2.8	< 1.0	3.8
6	1619	0.53	2.9	< 1.0	4.0
9	1675	0.37	4.2	1.1	5.7
12	1722	0.13	11.9	3.2	16.1
15	1778	0.07	22.1	5.9	29.9

Notes

\*  $K_x$  indicates K at designated fines content $K_0$  indicates K at 0% fines\*\* Estimated using *PDE 1.04*

Figure 31 shows the variation in hydraulic conductivity and drainage time for 50% and 90% drainage on the y-axis with increase in fines content on the x-axis. An exponential decay relationship exists between K and fines content with an  $R^2$  value of 0.95. Conversely exponential growth is observed for drainage time versus fines content. To achieve the drainage time recommended by AASHTO (< 2 hrs) at the 50% and 90% drainage levels, the hydraulic conductivity should be greater than 0.22 cm/sec and 0.97 cm/sec, respectively. 50% drainage can be achieved with less than 10% fines content, while 90% can only be achieved with fines content less than about 2%. For RPCC having a maximum CBR of 22 with 8% fines content, 50% and 90% drainage would take about 1 hour and 5 hrs, respectively. At 2% fines content, the CBR is reduced to 18.

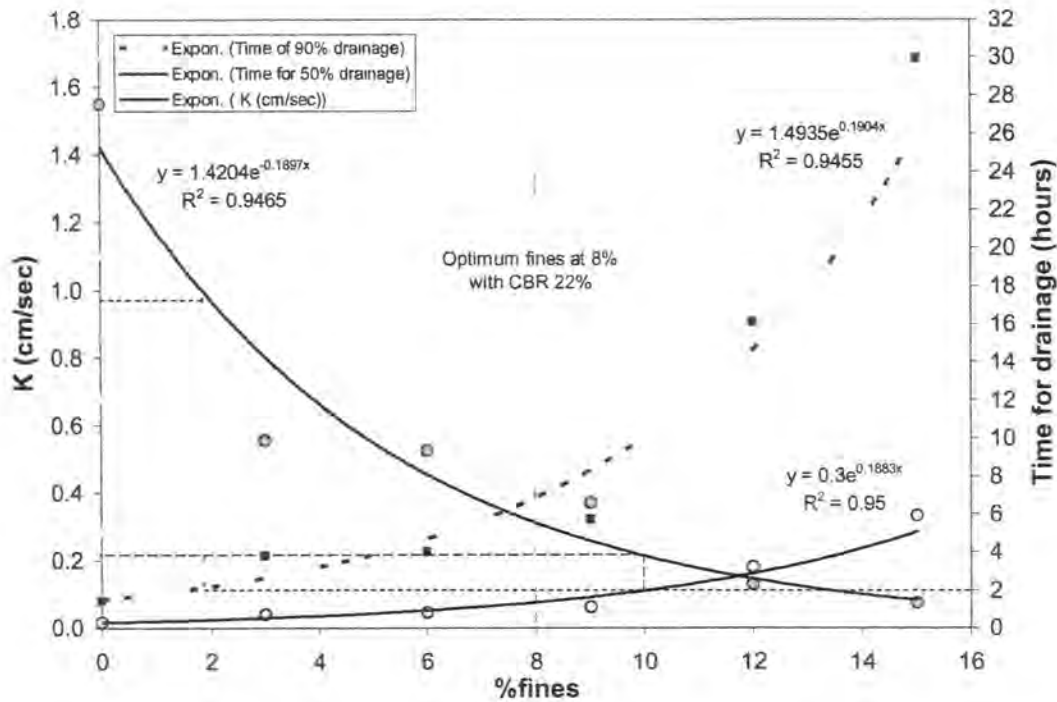


Figure 31. Influence of fines content on hydraulic conductivity of RPCC

### *Influence of Gradation on Strength*

To investigate the influence of gradation on strength, CBR tests were performed on aggregate samples that were re-graded to form both open-graded and dense-graded mixtures of the sample material. Comparative tests were performed for RPCC, CLS, and AG aggregates. Particles passing the 0.75 in. sieve and retained on 0.5 in. sieve constituted the open gradation whereas the dense gradation was determined from the 0.45 power gradation curve for a 0.75 in. maximum particle size. Figure 32 shows the open and dense gradation curves. Test results are summarized in Table 30.

In summary results show that CBR values increase 1.1 to 2.8 times from open-graded to dense-graded mixtures. This is an indication of the sensitivity of strength on gradation. RPCC again exhibited significantly lower CBR values compared to CLS for both open and dense gradations, but less reduction going from dense to open gradation. AG showed fairly uniform results for both gradations and at all penetration depths.



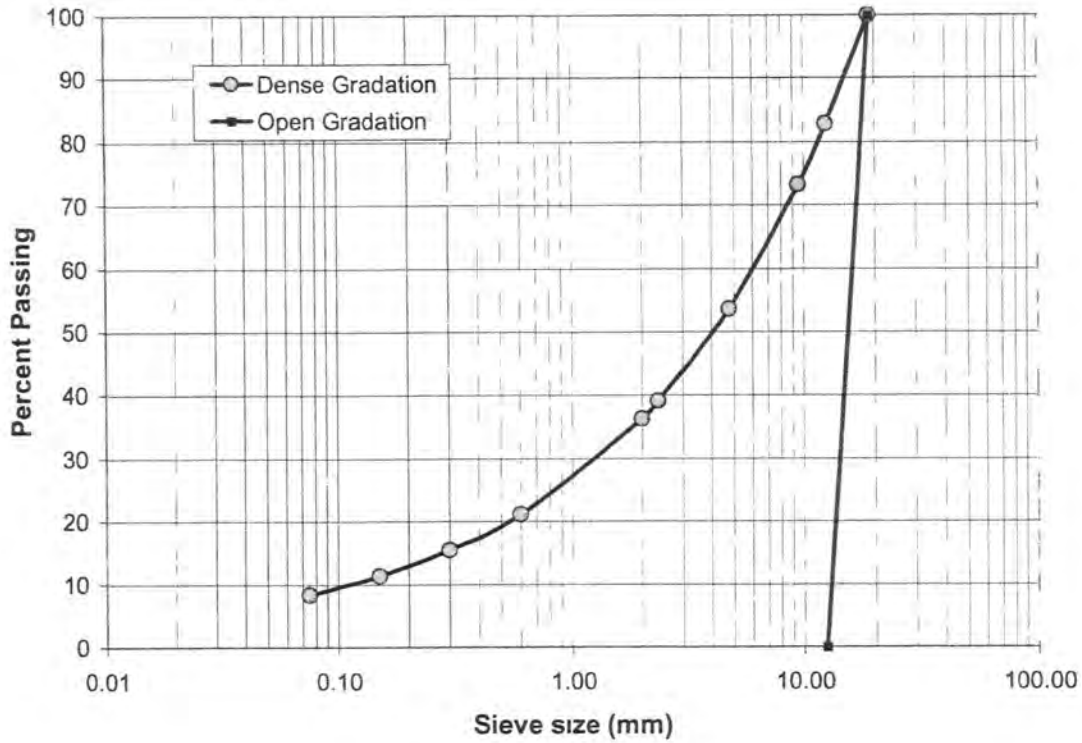


Figure 32. Dense gradation chart for 0.75 in. maximum size aggregate

Table 30. CBR% values for samples at dense and open gradation samples

Material	Penetration (inch)	CBR (%)		CBR <sub>D</sub> /CBR <sub>O</sub>
		Dense Gradation	Open Gradation	
RPCC	0.5	18	13	1.4
	0.4	17	10	1.7
	0.3	17	10	1.7
	0.2	16	8	2.0
	0.1	11	7	2.8
CLS	0.5	38	35	1.1
	0.4	63	32	2.0
	0.3	51	27	1.9
	0.2	44	27	1.6
	0.1	31	18	1.7
AG	0.5	39	36	1.1
	0.4	41	38	1.1
	0.3	43	39	1.1
	0.2	49	38	1.3
	0.1	49	38	1.3

Note:

CBR<sub>D</sub> – CBR at dense gradation, CBR<sub>O</sub> – CBR at open gradation

### *Influence of Compaction Energy on Hydraulic Conductivity*

To investigate the influence of increased compaction energy of (i.e. increased number of roller passes in the field) on density and hydraulic conductivity falling head tests were conducted on field samples that were compacted to the minimum and maximum dry densities measured in situ. Results are summarized in Table 31. Figure 33 compares the hydraulic conductivities at minimum and maximum dry densities for all samples. The drainage times required to achieve 50% and 90% drainage were again estimated using PDE 1.0 for a two-lane highway.

Results show that the hydraulic conductivity can be significantly affected by compaction energy (e.g. density), but depends on the material type. RAUG special backfill exhibited the lowest hydraulic conductivity of about 0.02 to 0.09 cm/sec (60 to 250 ft/day) at its high and low densities, respectively. This material is dense-graded (see Table 24). CLS218, CLS151, and RPCC35 granular subbase materials exhibited higher hydraulic conductivities than CLSUG. RPCC35 exhibited the largest decrease in hydraulic conductivity from 3.2 cm/s to 0.2 cm/s (16 times less) with increased compaction effort. This was not unexpected given the potential for RPCC particle degradation discussed previously.

CLS218 and CLS151 meet the recommended drainage time for 50% and 90% drainage even at the higher densities, whereas RPCC35 meets this criterion only at its lower density. CLSUG and RAUG do not meet the threshold limit at both the high and low densities. Thus, it can be determined that the crushed limestone granular subbase materials still meet the drainage requirements at the higher compaction effort. A benefit of increased density should be improved strength/stability. A relationship between compaction density, resilient modulus, and permanent strain should be investigated in the future for Iowa aggregates.

Table 31. Hydraulic conductivity test results with variation in density

Material	Dry density, $\gamma_d$ (kg/m <sup>3</sup> )	Change in $\gamma_d$ (kg/m <sup>3</sup> )	K (cm/sec)	$K_{low}/K_{high}$	Time for 50% drainage (hours)	Time for 90% drainage (hours)
CLS218	1676.8	—	2.83	—	< 1.0	< 1.0
	1857.4	180.6	1.39	2.0	< 1.0	1.5
CLS151	1683.4	—	3.22	—	< 1.0	< 1.0
	1863.4	180.0	1.22	2.6	< 1.0	1.7
RPCC35	1334.7	—	3.24	—	< 1.0	< 1.0
	1689.0	354.3	0.20	16.2	2.0	10.3
CLSUG	1574.7	—	0.21	—	2.0	10.0
	1891.5	316.8	0.06	3.5	6.9	34.9
RAUG	1595.2	—	0.09	—	4.7	23.8
	1691.5	96.3	0.02	4.5	19.6	99.6

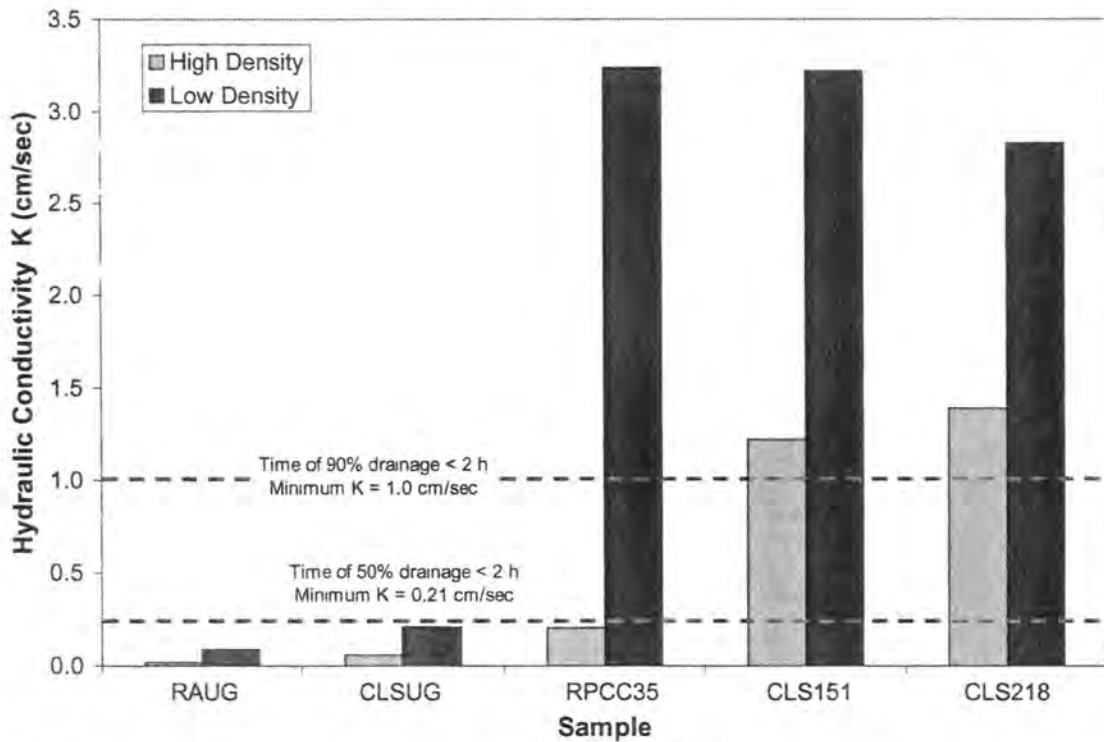


Figure 33. Laboratory hydraulic conductivity test results for field samples at high and low densities

#### *Influence of Compaction Type on Dry Density: Vibration versus Impact*

Maximum dry densities obtained from standard Proctor (impact) compaction energy were compared to the dry densities obtained from vibratory compaction tests. The results are

summarized in Table 32. All materials except sand show higher dry densities (about 260 kg/m<sup>3</sup> or 10% to 15%) with impact compaction compared to vibratory compaction.

**Table 32. Comparison of densities from static and vibratory compaction**

Material	Dry Density (kg/m <sup>3</sup> )		
	Vibratory compaction <sup>1</sup>	Impact compaction <sup>2</sup>	Change in density
SAND	1611	1608	3
RPCC	1411	1672	261
ALS	1467	1723	256
CLS	1451	1712	261
AG	1641.6	1758.7	6.7
AALS	2016.2	2369.6	14.9

Notes

<sup>1</sup>Dry density from vibratory compaction test

<sup>2</sup>Dry density determined during hydraulic conductivity testing

### Key Observations from Lab Tests

- None of the aggregates obtained from the quarry and only a two from the field meet the specified Iowa DOT gradation requirements for granular subbase.
- Maximum CBR is achieved at fines contents between 6% and 14% for granular subbase materials. All crushed limestone materials (CLS, ALS, and AALS) exhibit higher CBR values than recycled concrete materials (RPCC, RPCCAmes).
- The degradation/abrasion loss is higher for recycled concrete than crushed limestone and gravel.
- Hydraulic conductivity decreases exponentially with increasing fines content.
- The fines content of RPCC must be 2% or less to meet the drainage requirement of 90% in < 2h or less than 10% to achieve 50% drainage in < 2h.
- CBR decreases from dense to open gradations.
- Hydraulic conductivity can significantly decrease with increasing compaction energy (i.e. density), but depends on the aggregate type. RPCC exhibited a 16 times decrease in hydraulic conductivity with increased compaction energy. The crushed limestone granular subbase materials achieved adequate hydraulic conductivity even at high compaction energies.

## PAVEMENT BASE CONSTRUCTION OPERATIONS

Operations from new construction of aggregate bases under PCC pavements in Iowa are documented in this section. Construction operations varied significantly between each project and contractor. The spreading and trimming processes was found to significantly influence segregation and localized increases in fines in the base layer. Moisture content present during trimming also influenced segregation as finer particles can be easily separated from larger particles at lower moisture contents.

### **US 218 Base Construction Process**

This site is located on US 218 South Bound about 15 miles south to Mount Pleasant, Iowa. A crushed limestone granular subbase (CLS218) of about 6 in. thick at the edges and 10 in. thick at the center (cross-slope of about 2%) was constructed at this location and overlaid with a PCC pavement. Various stages of the construction process are described in the following section.

#### *Placing the Aggregate*

Aggregate haul trucks used the shoulder as shown in Figure 34, to transport the aggregate to the prepared subgrade. Trucks then dumped and drove back out on the subgrade. No construction traffic except the trimmer was allowed to move on the base layer. Figure 35 shows dumping of the aggregate. The shoulder areas became unstable and rutted during the hauling operations.



**Figure 34. Unstable shoulder under loaded trucks placing aggregate**



**Figure 35. Dumping of aggregate on subgrade**

### *Spreading the Aggregate*

The aggregate piles were spread to the full width of the prepared subgrade using a D6XL dozer as shown in Figure 36. The process involved spreading the aggregate longitudinally up and down the subgrade. The dozer blade left about 1 to 1.5 inches of extra material over the full width of the pavement. Initial compaction was performed on the leveled base layer using a 563 CAT steel drum roller of 5 ton capacity for one roller pass with no vibration (Figure 37).

### *Trimming Process*

After initial compaction, final trimming was performed to remove excess base material and meet the required thickness for paving. The trimming process was performed using a 9500 Gomaco trimmer shown in Figure 38. The trimmer used a level indicator as shown in Figure 39, to control the depth. Excess material trimmed during the process was placed in a pile longitudinally on the base as shown in Figure 39. The excess aggregate was later removed and placed back into the haul trucks as shown in Figure 40, for use on other parts of the base construction.



**Figure 36. Spreading of aggregate piles using D6XL dozer**



**Figure 37 Initial Compaction using 563 CAT Roller**



**Figure 38. Final trimming using 9500 Gomaco**

### *Final Compaction*

After the base layer was trimmed to the desired thickness and elevation, final compaction was performed using a C563 CAT steel drum roller of 5 ton capacity as shown in Figure 41. Compaction was again performed with no vibration for 2 roller passes over the



full width of the pavement (note that one pass forward and one pass backward account for one full roller pass of compaction).



**Figure 39 Final trimming of base, level indicator attached to trimmer, and aggregate pile formed after trimming**



**Figure 40. Placing trimmed aggregate back in to the haul trucks for re-use at other location**



**Figure 41. Final compaction using 563 CAT roller**

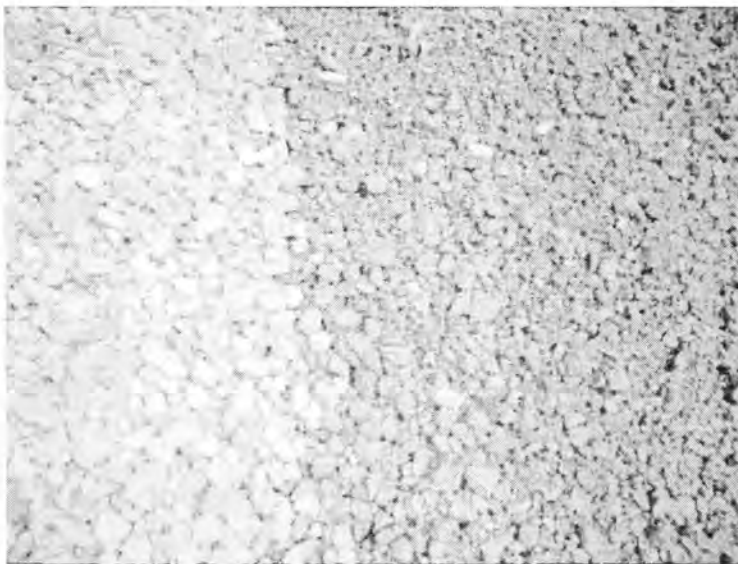
*Key Notes from the Construction Process*

Figure 42 shows a picture of sampled aggregate used during the base construction. The bucket on the left contains material collected from the truck which carried aggregate directly from the quarry whereas the bucket on the right contains aggregate collected from the trimmed material. As mentioned before, the aggregate collected from the trimmer was also used in other parts of the base construction. From the picture it can be seen that the aggregate collected from the trimmer contains more open-graded material and less fines than the quarry sample.

Figure 43 shows the difference between the aggregate from the quarry (right) and trimmer (left). It can be seen that the aggregate from the quarry is wet; whereas the trimmed sample on the right is dry. Effective mixing of these materials was not possible in the field. A consequence of dry granular subbase in the field is that fines will segregate more readily. Test results on the final base layer indicating significant segregation and increase in fines. Further discussions on segregation are provided in later sections of this report.



**Figure 42. Quarry aggregate sample on left side and aggregate from trimmer on right side**



**Figure 43. Dry sample on left from trimmer and wet sample on right from quarry**

### **US151 Base Construction**

This site is located on US 151 East bound near Springville and Cedar Rapids, Iowa. A crushed limestone granular subbase (CLS151) about 8 in. thick on the edges and 10 in. thick near the center (cross-slope of about 1%) was constructed at this location and then overlaid with PCC pavement. Various stages involved during the construction process are described

in this section.

### *Placing the Aggregate*

Aggregate haul trucks were using the shoulder, as shown in Figure 44, to transport the aggregate base material to the prepared subgrade. Trucks backed onto the subgrade to place the aggregates. After dumping, the empty trucks returned to the shoulder. No construction traffic, except the dozer, trimmer, and roller, was allowed to operate on the base layer.



**Figure 44. Haul way used by the trucks to transport the aggregate**

### *Spreading the Aggregate*

The aggregate piles were spread to full width of the prepared subgrade using a D6XL dozer as shown in Figure 45. The process was carried out by spreading the aggregate longitudinally along the pavement. The dozer blade was then set to a level of about 1 to 2 inches greater than the desired thickness of the final base layer, and is approximately leveled over the full width of the pavement.



**Figure 45. Spreading of aggregates using a D6XL dozer**

### *Trimming Process*

After spreading the aggregate, trimming was performed to remove the excess base material and meet the required thickness and elevation. The trimming process was performed using a TR 500 trimmer as shown in Figure 46. The trimmer has a precise level indicator as shown in Figure 46, to control the trimming process. The trimmed aggregate was deposited on the side of the trimmer as shown in Figure 47



**Figure 46. Final trimming process using TR 500 trimmer**

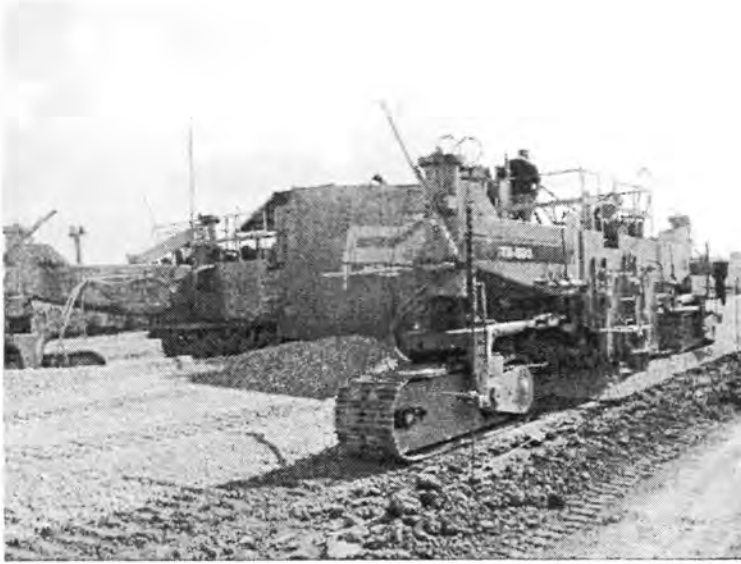


**Figure 47 Piling of trimmed aggregate on the side of trimmer**

### *Final Compaction*

After the base layer was trimmed to the desired thickness and elevation, final compaction was achieved using a C563 CAT steel drum roller of 5 ton capacity as shown in Figure 48. Uniform compaction was performed with no vibration for 2 roller passes over full width of the pavement. No significant variation or segregation in fines was observed at this location.



**Figure 48. Roller used for final compaction**

### **University-Guthrie Avenue Base Construction Process**

This site is located at the exit of University Avenue from I235 West bound in Des Moines, Iowa. A crushed limestone granular subbase (CLSUG) of about 6 in. thickness was constructed at this location and overlaid with PCC pavement.

#### *Placing the Aggregate*

At this site, the aggregate haul trucks used the pavement base as a haul way to place the aggregate on the prepared subgrade. Figures 49 and 50 show the truck traffic and placement of the aggregate. All construction traffic was allowed onto the base without restriction. Figure 52 shows the haul way being used by a truck to return after dumping. Figure 53 shows another method that was used at this site for dumping the aggregate on the subgrade. A side dump truck used the existing concrete pavement to dump the aggregate on to the subgrade.



**Figure 49. Trucks moving on base for placing the aggregate**



**Figure 50. Dumping of aggregates from the truck**



**Figure 51. Trucks using haul way on their way back to the quarry**





**Figure 52. Another method of dumping the aggregate**

### *Spreading the Aggregate*

The aggregate piles were spread on the full width of the prepared subgrade using a CAT 140H grader as shown in Figure 53. The process was carried out by spreading the aggregate longitudinally and transversely along the pavement. The grader blade was initially set to a level of about 1 to 2 in. greater than the desired base thickness. After spreading the aggregate, the level in the grader blade was changed to meet the desired thickness. Thus, excess aggregate was trimmed and placed as a pile on the edge of the pavement as shown in Figure 54. The trimmed aggregate pile was cleaned by a bucket loader as shown in Figure 54.

### *Final Compaction*

After the base layer was trimmed to the desired thickness and elevation and the trimmed excess aggregate piles were removed, compaction was performed using a C 563 CAT steel drum roller of 5 ton capacity as shown in Figure 55. Compaction was performed with no vibration for 2 roller passes over the full width of the pavement.

Significant segregation and increase in fines was observed at this location, which is indicated in the test results described in later sections of this report.



**Figure 53. Spreading and trimming of aggregate**



**Figure 54. Bucket loader removing excess aggregate**



**Figure 55. Roller used for final compaction**

### **Key Observations from Construction Operations**

- The construction equipment and procedures varied between projects.
- Trimming aggregate with the Gomaco type trimmers leads to segregation, especially for dry base materials.
- There was no moisture control during placement or compaction of final base layer.
- Low moisture content is believed to contribute to increased segregation as there is poor adhesion between finer and larger particles.
- Significant segregation and an increase in fines content was observed in two of the three projects visited.
- Only one of the three projects visited did not restrict construction traffic. Although segregation was observed, it can not be solely linked to increased construction track, as other projects with no construction traffic showed similar segregation problems.

## FIELD INVESTIGATION OF PAVEMENT BASES

In-situ stability and permeability measurements on several sections of newly constructed pavement base are summarized in this section. Modulus of subgrade reaction (k) values were estimated from DCP test results correlated to in-situ CBR and are compared to the current Iowa DOT pavement design value of 150 pci. GeoGauge values are also compared to the minimum modulus values proposed by Chen and Bilyeu (1999) for base materials. Drainage times for 50% and 90% drainage were estimated from the in-situ hydraulic conductivity values determined from the APT measurements. Considering variations in density, water content, degree of saturation, and fines content, results show that fines content accounts for more variation in strength/stiffness than any other parameter. Further, the strongest correlation between any two measured parameters is between fines content and hydraulic conductivity. Significant spatial variability of most parameters is also observed in each project. Considering all projects with granular subbase, the calculated coefficient of variations are as follows: 9% for density, 41% for modulus, 53% for water content, 64% for fines, 83% for CBR, and 97% for hydraulic conductivity. Spatial variations of these parameters from in situ measurements have not been previously documented.

### Test Methods

Dynamic Cone Penetrometer (DCP) tests were conducted in accordance with ASTM D6951, "Standard Test Method for Use of Dynamic Cone Penetrometer in Shallow Pavement Applications." Penetration Index (PI) (mm/bow) was measured and used to estimate CBR using Equation No. 4 of Table 19

Clegg Impact Hammer tests were conducted in accordance with ASTM D5874, "Standard Test Method for Determination of the Impact Value (IV) of a Soil." CBR was estimated from the measured Clegg impact value (CIV) using the following equation:  $CBR = (0.24 CIV + 1)^2$  (Clegg 1986).

GeoGauge vibration tests were conducted in accordance with the standard test procedures provided by the manufacturer (Humboldt Co.). Material properties including Young's modulus (MPa) and stiffness (MN/m) were determined. A Poisson's ratio of 0.35 was assumed in order to calculate Young's modulus from stiffness.

Nuclear density gauge tests were performed to determine in-place density and moisture content. Tests were performed using the back scattering method in accordance with ASTM WK218, "Test Method for In-Place Density and Water (Moisture) Content of Soil and Soil-Aggregate by Nuclear Methods (Shallow Depth)."

In-situ hydraulic conductivity was determined from Air Permeameter Tests (APTs). Saturated hydraulic conductivity was calculated from APT measurements and Equation 21 of Appendix D. Tests were performed according to the standard test procedures provided in Appendix E.

To document segregation of fines on the final compacted base layer, fines content was determined from bag samples collected at each test point location. About 1000 g of sample was washed over a No. 200 sieve and oven dried to determine percent fines.

## **Materials**

Samples from several new base construction projects were obtained in bulk for laboratory characterization. The base construction projects investigated during this study and material designations are as follows:

- 1 35<sup>th</sup> Street, Des Moines, Iowa, modified subbase construction for North side ramp (MSB),
2. Knapp Street, Ames, Iowa, Recycled PCC granular subbase construction (RPCCAmes),
- 3 IA 218 South Bound, Mount Pleasant, granular subbase construction (CLS218),
4. US 151 East Bound, Cedar Rapids, granular subbase construction (CLS151),
- 5 University-Guthrie Avenue, Des Moines, granular subbase construction (CLSUG),
6. University-Guthrie Avenue, Des Moines, special backfill construction (RAUG) and
- 7 I 35 South Bound, Story Co., granular subbase construction (RPCC35).

Grain-size distribution curves for the aggregates are summarized in Tables 22 and 23 and shown in Figure 30. A summary of index properties including atterberg limits, percent gravel, sand, and silt/cay the coefficient of uniformity,  $C_u$ , coefficient of curvature,  $C_c$ , specific gravity and maximum and minimum dry densities is provided in Table 25

## Results from Field Testing

The in-situ tests were conducted side by side on a grid pattern of 24 to 30 test points with spacing of about 6 to 10 ft directly on the compacted final base layer. Contours graphs showing the spatial variation of all parameters are provided in Appendix F. The contour graphs were plotted using geostatistical analysis and Kriging approach. A summary of test results for individual projects is provided in Tables G1 through G7. Mean, standard deviation, and coefficient of variation for all test parameters are summarized in Table 33. In the following, results from each individual project are described in detail.

### *35<sup>th</sup> Street Modified Subbase Construction*

This test site is located on the North 35<sup>th</sup> street ramp at I235 West Bound in West Des Moines, Iowa. An aerial photograph of the test location is shown in Figure F1. The grid test pattern included the full width of the pavement as shown in Figure F2. A crushed limestone modified subbase material 12 inches in thickness was constructed at this location and overlaid with ACC pavement. The final subbase layer was compacted using a 5 ton steel drum roller with vibration for 8 to 16 roller passes. A photograph of the modified subbase layer during construction is shown in Figure 56.



**Figure 56. Photograph of the modified subbase layer during construction at 35<sup>th</sup> street test section**

Results from GeoGauge tests show a mean modulus (MOD) of about 51 MPa with coefficient of variation at 30% (Table 33). The contour plot (Figure F3) shows that the modulus varies from about 30 and 80 MPa with lower modulus values on the southern half of the test section. This base is considered weak according to the criteria established by Chen and Bilyeu (1999) (see Table 34).

DCP test results show a mean Penetration Index (PI) of about 13 mm/blow with a coefficient to variation at 57% (Table 33). Mean CBR estimated from the PI is about 20 with a coefficient of variation at 40% (Table 33). The contour plot (Figure F4) indicates significant spatial variation in CBR ranging from about 5 to 30. Similar to the variation in modulus, CBR is lowest on the southern half of the test section. The modulus of subgrade reaction value (k) estimated from the mean CBR is about 250 pci.

Results from Clegg Impact Hammer tests show a mean CIV of about 21 with a coefficient of variation at 27% (Table 33). The contour plot (Figure F5) shows the variation in CIV, which is similar to the variation in CBR and modulus with comparatively lower values on the southern half of the test section.

The mean value for moisture content is about 8.5% with a coefficient of variation at 16% (Table 33). The contour plot (Figure F6) shows the variation in moisture content, having higher values on the southern half of the test section. Comparing the variation in moisture content with the variation in modulus, CBR, and CIV it can be seen that the strength and stiffness are lower at locations with high moisture contents. Dry densities were in the range of about 1600 to 2000 kg/m<sup>3</sup>, with a coefficient of variation of 6%. There is no predictable relationship between the variation in dry density and strength/stiffness (CBR, modulus, and CIV). This gives an indication that the strength of the base material does not solely depend on the dry density of the material.

Table 33 Statistical analysis of the data collected from each project

Project	Number of Tests	Statistics	GeoGauge Test			DCP Test		K (cm/sec)	% fines	w%	$\gamma_d$ (kg/m <sup>3</sup> )
			S (MN/m)	MOD (MPa)	PI (mm/blow)	CBR %	CIV				
MSB	24	M	5.9	51.0	13.5	20	20.7	—	—	8.5	1814.7
		SD	1.8	15.4	7.8	8	5.7			1.3	120.4
		CV	30.3	30.3	57.6	41	27.5			15.8	6.6
RPCCAs	24	M	9.5	82.8	10.0	23	23.5	3.8	7.9	10.4	1668.9
		SD	1.5	13.4	1.8	5	3.1	3.9	1.9	0.9	68.3
		CV	16.2	16.2	18.1	20	13.3	102.9	23.8	8.3	4.1
CLS 218	30	M	8.4	72.8	30.4	8	13.4	1.8	9.0	3.8	1743.6
		SD	1.2	10.4	12.3	3	3.5	1.4	1.6	0.7	45.6
		CV	14.2	14.2	40.4	44	26.0	78.8	18.1	17.9	2.6
CLS 151	30	M	8.0	69.0	27.3	9	13.8	5.6	4.3	3.8	1713.0
		SD	1.4	11.8	14.1	4	2.3	3.2	0.8	0.7	101.8
		CV	17.1	17.1	51.6	45	16.3	57.4	18.2	17.9	5.9
CLSUG	30	M	13.2	114.2	4.7	53	25.3	2.6	8.5	—	—
		SD	1.9	16.1	0.8	11	6.1	4.2	3.1	—	—
		CV	14.1	14.1	17.0	21	24.1	158.2	36.2	—	—
RAUG	30	M	15.7	136.4	8.9	12	29.3	4.9	0.3	6.7	1640.3
		SD	3.4	29.5	8.0	16	11.7	4.0	0.1	3.1	81.2
		CV	21.7	21.7	89.9	139	40.0	81.4	42.4	46.9	5.0
RPCC35	24	M	5.5	48.0	24.2	10	12.9	6.0	6.1	11.2	1474.0
		SD	0.7	6.3	12.1	4	2.5	6.5	2.3	1.7	83.8
		CV	13.2	13.2	50.2	38	19.8	107.5	36.8	15.5	5.7

Notes

\* Test not performed

S Stiffness measured from GeoGauge Test

MOD Modulus measured from GeoGauge Test

CBR California Bearing Ratio estimated from PI (mm/blow) using Equation 4 of Table 19

K Saturated Hydraulic Conductivity

M - Mean SD - Standard Deviation CV - Coefficient of Variation



**Table 34. Comparison of in-situ strength/stiffness to standard values**

Project	Mean MOD (MPa)	RATING <sup>1</sup>	Mean CBR %	k* (pci)	k*/k**
MSB	51.0	Weak	20	250	1.7
RPCCAmes	82.8	Weak	23	260	1.7
CLS 218	72.8	Weak	8	180	1.2
CLS 151	69.0	Weak	9	190	1.3
CLSUG	114.2	Weak/Good	53	500	3.3
RPCC35	48.0	Weak	10	200	1.3
RAUG	136.4	—	12	230	1.5

Notes

<sup>1</sup>Ratings are according to Chen and Bilyeu (1999), see Table 18

k\*Modulus of Subgrade Reaction estimated according to Middlebrooks and Bertram (1942)

k\*\* = 150 pci, Modulus of Subgrade Reaction assuming a loss of support value  $\approx 0.0$ , being used in the PCC pavement design by Iowa DOT

### *Knapp Street Granular Base Construction*

This site is located on the west end of Knapp Street in Ames, Iowa. An aerial photograph of the test location is shown in Figure F8, and the grid test pattern used for testing the full width of pavement is shown in Figure F9. A granular recycled concrete base (RPCCAmes) of about 8 inches thickness with a cross-slope of about 2% was constructed, and then overlaid with PCC pavement. No information was available on the number of roller passes used during compaction of the base.

Results from GeoGauge tests show a mean modulus (MOD) of about 83 MPa with a coefficient of variation at 16%. Contour plots (Figure F10) show that there is relatively low spatial variation in modulus with most area from about 70 to 80 MPa. Although relatively uniform, this base is rated as weak according to Chen and Bilyeu (1999).

DCP test results show a mean penetration index (PI) of about 10 mm/blow with a coefficient of variation of 18%. Mean CBR estimated from the PI is about 23% with a coefficient of variation at 20%. Figure F11 shows the spatial variation in CBR over the test section. The modulus of subgrade reaction value estimated from CBR is about 260 pci.

Results from Clegg Impact Hammer test show a mean CIV of about 23 with a coefficient of variation of 13%. The contour plots (Figure F12) show the variation in CIV and indicates similar variation as CBR on the west edge of the test section. A few locations of higher CIV coincide with higher modulus values.

The mean value for moisture content is about 10% with a low coefficient of variation

at 8%. Figure F13 shows the variation in moisture content over the test section. Dry densities were in the range of 1550 to 1750 kg/m<sup>3</sup>, with a low coefficient of variation at 4%. The variation in moisture content (Figure F13) is similar to dry density (Figure F14) with locations of higher moisture contents having lower dry densities and vice-versa. There is no predictable relationship between the variation in dry density and strength/stiffness (CBR, modulus, and CIV).

Results from the APT show a mean saturated hydraulic conductivity (K) of about 4 cm/sec, with a high coefficient of variation at 100%. The values obtained were in the range of about 1 to 30 cm/sec (see Table G2). However there are only a few locations with hydraulic conductivities greater than 8 cm/sec as shown in Figure F15. The mean fines content (passing No. 200 sieve) is about 8% with a coefficient of variation at 24%. By comparing the contour plots for variation in fines content (Figure F16) and hydraulic conductivity (Figure F15), it can be seen that locations of high fines contents exhibit low hydraulic conductivities. No relationship was identified between the variation in dry density and hydraulic conductivity.

The laboratory gradation analysis on RPCCAmes shows a fines content of about 5% (see Table 22), which is within the Iowa specification. However, analyses on field collected samples shows that fines content varies from 4% to 11% (Figure F16). This gives an indication of segregation and possibly particle crushing during the construction process.

**Table 35. Comparison of in-situ hydraulic conductivity to standard values**

Project	Mean K (cm/sec)	Time <sup>1</sup> for 90% drainage (h)	Time <sup>2</sup> for 50% drainage (h)	Quality of drainage <sup>2</sup>	Drainage coefficient <sup>3</sup> C <sub>d</sub>
RPCCAmes	3.8	< 1	< 1	Excellent	1.10 to 1.25
CLS 218	1.8	< 2	< 1	Excellent	1.10 to 1.25
CLS 151	5.6	< 1	< 1	Excellent	1.10 to 1.25
CLSUG	2.6	< 1	< 1	Excellent	1.10 to 1.25
RPCC35	6.0	< 1	< 1	Excellent	1.10 to 1.25
RAUG	4.9	< 1	< 1	Excellent	1.10 to 1.25

Note

<sup>1</sup>Time of drainage estimated from PDE 1.0

<sup>2</sup>Quality of drainage rating according to AASHTO recommendation of 2 h maximum drainage time

<sup>3</sup>Drainage Coefficient estimated using the Quality of Drainage, according to AASHTO (1986)

Using the mean hydraulic conductivity value and assuming a 0% longitudinal gradient of the base, cross slope of 2%, 8 in thickness of base, and 30% effective porosity the time of drainage was estimated using the PDE 1.0 program. The estimate 50% and 90% degree of drainage is < 1 hour and is rated “Excellent” (Table 35).

#### *IA218 Permeable Base Construction*

This site is located on IA 218 South Bound about 15 miles south to Mount Pleasant, Iowa. An aerial photograph of the test location is shown in Figure F17, and the grid test pattern is shown in Figure F18. A crushed limestone granular subbase (CLS218) was constructed to be 6 in. thick at the edges and 10 in. thick at the center (cross-slope of about 2%). The base was overlaid with PCC pavement. The final base layer was compacted using a 5 ton steel drum roller with no vibration for 2 roller passes (see Figure 37).

Results from GeoGauge tests show a mean modulus of about 73 MPa with a relatively low coefficient of variation at 14%. The contour plots (Figure F19) show the variation in modulus, which is comparatively lower at the edges than the center. According to Chen and Bilyeu (1999), a modulus value of 73 MPa is rated weak.

DCP test results show a mean Penetration Index (PI) of about 30 mm/blow with a coefficient of variation at 40%. Mean CBR estimated from PI is about 8 with a coefficient of variation at 44%. The contour plots show variation in CBR (Figure F20) which is similar to modulus with lower values at the edges compared to the center. The modulus of subgrade reaction value estimated from CBR is about 180 pci.

Clegg Impact Hammer tests show a mean CIV of about 13 with a coefficient of variation at 26%. The contour plots show the variation in CIV, indicating similar variation to CBR and modulus with lower values on the east edge of the test section (Figure F21).

The mean value for moisture content is about 4% with a coefficient of variation of variation at 18%. Dry Densities were from about 1650 and 1800 kg/m<sup>3</sup>, with a low coefficient of variation at 3%. Similar to the variation in moisture content (Figure F22), there is no significant variation in dry density (Figure F23). There is no relationship between the variation in dry density and strength/stiffness (CBR, modulus, and CIV).

Results from the APT show a mean hydraulic conductivity of about 2 cm/sec, with a

high coefficient of variation at 80%. Hydraulic conductivities varied between 0.25 cm/sec and 7.5 cm/sec (see Table G3) over the test section. Contour plot (Figure F24) indicates a significant spatial variation in hydraulic conductivity. The mean fines content is about 9% with a coefficient of variation at 18%. By comparing the contour plots for variation in fines content (Figure F25) and hydraulic conductivity (Figure F24), it can be seen that locations of high fines contents exhibit low hydraulic conductivities. No relationships were identified between the variation in dry density and hydraulic conductivity.

Gradation analysis on CLS218 resulted in fines content of about 8% (see Table 22). But the field measurements showed a variation between 5% to 11% (Figure F25).

Using the mean hydraulic conductivity value and assuming a 0% longitudinal gradient of the base, 2% of cross-slope, and 30% effective porosity, drainage times were estimated using the PDE 1.0 program. The estimate of time for 90% drainage is < 2 hour and for 50% drainage is < 1 hour, and is rated "Excellent" (Table 35).

#### *US151 Permeable Base Construction*

This site is located on US 151 East Bound near Springville, Cedar Rapids, Iowa. An aerial photograph of the test location is shown in Figure F26, and the grid test pattern used for testing the full width of the pavement is shown in Figure F27. Figure 57 shows a photograph taken during sampling and testing at this test section. A crushed limestone base (CLS151) of about 8 in. thickness on the edges and 10 in. thickness on the center (cross-slope of about 1%) was constructed at this location and then overlaid with PCC layer. The final base layer was compacted using a 5 ton steel drum roller with no vibration for 2 roller passes.

GeoGauge vibration test results show a mean modulus (MOD) of about 69 MPa with a coefficient of variation at 17%. The contour plots (Figure F28) show the variation in modulus over the test section with lower modulus on the northern edge. With this mean modulus value, the base is also rated as "weak."

DCP test results show a mean penetration index (PI) of about 27 mm/blow with a coefficient of variation at 51%. Mean CBR estimated from the PI is about 9% with a high coefficient of variation at 44%. Similar to the variation in modulus, the contour plot for CBR (Figure F29) shows lower values on the northern edge. The modulus of subgrade reaction

value estimated from CBR is about 190 pci.

Clegg Impact Hammer test results show a mean CIV of about 14 with a coefficient of variation at about 16%. The contour plots for variation in CIV indicate lower values on the north-western part of the test section (Figure F30).



**Figure 57 Photograph showing the process of measurements at grid points on US151 Test section**

The mean value for moisture content is about 4% with a low coefficient of variation at about 18%. The contour plot (Figure F31) and results show that there is no significant variation in moisture content. Dry densities were in the range 1500 to 1850 kg/m<sup>3</sup> with a low coefficient of variation at about 6%. Similar to moisture content, there is no significant variation in dry density (Figure F32). There is no predictable relationship between the variation in dry density and strength/stiffness (CBR, modulus, and CIV).

Results from the APT show a mean hydraulic conductivity of 5.6 cm/sec, with a coefficient of variation at about 57%. The contour plots (Figure F32) show that the southern half of the test section has the lowest hydraulic conductivity. The mean fines content is about 4% with a coefficient of variation at 18%. By comparing the contour plots for variation in fines content (Figure F33) and hydraulic conductivity (Figure F32), it can be seen that the locations of high fines contents exhibit low hydraulic conductivities. However, the variation in fines content is not significant at this site.

Using the mean hydraulic conductivity value and assuming a 0% longitudinal gradient of the base, 2% of cross-slope, and 30% effective porosity, the time of drainage was estimated using the PDE 1.0 program. The estimate of time for 50% and 90% degree of drainage is < 1 hour and is rated “Excellent” (Table 35).

#### *University-Guthrie Avenue, Permeable Base Construction*

This site is located on the exit towards University Avenue from I235 West Bound in Des Moines, Iowa. An aerial photograph of the test location is shown in Figure F35, and the grid test pattern used for testing (only half the width of the pavement) is shown in Figure F36. A crushed limestone granular subbase (CLSUG) of about 6 in. thickness was constructed at this location and overlaid with PCC layer. The final base layer was compacted using a 5 ton steel drum roller with no vibration for 2 roller passes as shown in Figure 55

Results from GeoGauge tests show a mean modulus of about 114 MPa with a coefficient of variation at 14% (Table 33). The contour plot (Figure F37) shows that there are many locations over the test section with modulus between 100 and 130 MPa, whereas only few locations with modulus greater than 130 MPa. With this mean modulus value, the base is rated “Weak/Good” (Table 34).

DCP test results show a mean penetration index (PI) of about 4.7 mm/blow with a coefficient of variation at 17%. Mean CBR estimated from the PI is about 53 with a coefficient of variation at 21% (Table 33). The contour plot (Figure F38) shows that the variation in CBR is in between 40 and 80 with relatively lower CBR on the northern half of the test section. The modulus of subgrade reaction value estimated from CBR is about 500 pci.

Clegg Impact Hammer test results show a mean CIV of about 25 with a coefficient of variation at 24%. The contour plots (Figure F39) show that variation in CIV is similar to CBR (Figure F38) with relatively low values on the northern half.

Results from the APT show a mean hydraulic conductivity of 2.6 cm/sec, with a high coefficient of variation of at 158%. The hydraulic conductivity values ranged from 0.1 to 18 cm/sec (see Table E5). The contour plot (Figure F40) shows that there are many areas with hydraulic conductivity less than 2 cm/sec. The coefficient of variation in fines content is 36%

with a mean value of about 8.5%. Figure F41 shows that there is significant variation in fines content (from 4%–12%) over the test section. By comparing the contour plots for variation in fines content and hydraulic conductivity, it can be seen that the central part of the test section in Figure F41 having high fines content coincides with low hydraulic conductivities in Figure F42.

Using the mean hydraulic conductivity value and assuming a 0% longitudinal gradient of the base, 2% of cross-slope, and 30% effective porosity, the drainage times were estimated using the PDE 1.0 program. The estimated of time for 50% and 90% degree of drainage is < 1 hour and is rated “Excellent”

Dry density and moisture content results were not determined at this project location.

#### *University-Guthrie Avenue Subbase Construction*

This site is located on the University Avenue exit from I235 West Bound in Des Moines, Iowa. An aerial photograph of the test location is shown in Figure F42, and the grid test pattern used for testing (only half width of pavement) is shown in Figure F43. A subbase using special back fill material (RAUG) of about 12 in. thickness was constructed at this location and then overlaid with a granular subbase layer and PCC pavement. The final subbase layer was compacted using a 5 ton steel drum roller with vibration for about 14 to 16 roller passes.

Results from the GeoGauge vibration test show a mean modulus (MOD) of about 136 MPa with a coefficient of variation at 22% (Table 33). The contour plot (Figure F44) shows that the modulus is lowest near the edge of the pavement.

DCP test results show a mean penetration index (PI) of about 9 mm/blow with a high coefficient of variation at 90%. Mean CBR estimated from the PI is about 12 with a coefficient of variation at 138% (Table 33). The contour plot (Figure F45) shows the variation in CBR over the test section, which is similar to the modulus having lower values towards the edge of the pavement.

Results from Clegg Impact Hammer test show a mean CIV of about 29 with a coefficient of variation at 40% (Table 33). The variation in CIV on the test section (Figure F 46) is similar to the variation in CBR and modulus, having lower values towards the edge of

the pavement.

The mean value for moisture content is about 7% with a coefficient of variation at 47% (Table 33). The contour plots (Figure F47) show that the southern half of the section has a uniform moisture content of about 9%, whereas the northern half is at about 3%. Dry densities were in range 1450 to 1750 kg/m<sup>3</sup>, with a coefficient of variation at 5% (Table 33). There is no significant spatial variation in dry density (Figure F48).

Results from the APT show a mean saturated hydraulic conductivity of about 5 cm/sec, with a high coefficient of variation at 81% (Table 33). The hydraulic conductivity values ranged from 0.76 to 18 cm/sec (see Table G6). The fines content ranged from 0.1% to 0.6% (Figure F50).

### *I35 South Bound, Permeable Base Construction*

This site is located on I35 South Bound about 2 miles south the US20/I35 intersection, Hamilton County Iowa. An aerial photograph of the test location is shown in Figure F51, and the grid test pattern used for testing the full width of the pavement is shown in Figure F52. A recycled concrete base (RPCC35) of about 6 in. thickness with a cross-slope of about 2% was constructed at this location and overlaid with PCC pavement. The final base layer was compacted using a 5 ton steel drum roller with no vibration in 3 to 4 roller passes.

Results from GeoGauge tests show a mean modulus of about 48 MPa with a coefficient of variation at 13%. The contour plots (Figure F53) show the variation in modulus over the test section with relatively low values on the edges of the pavement. With this mean modulus value, the base is rated “Weak” (Table 34).

DCP test results show a mean Penetration Index (PI) of about 24 mm/blow with a coefficient of variation at 50%. Mean CBR estimated from the PI is about 10 with a coefficient of variation at 38%. The contour plot for variation in CBR (Figure F54) is similar to modulus with lower values on the edges than on the center of the test section. The modulus of subgrade reaction value estimated from CBR is about 230 pci.

Clegg Impact Hammer test results show a mean CIV of about 13 with a coefficient of variation at 26%. The contour plots (Figure F55) show that the variation in CIV is similar to CBR and modulus with lower values on the edges of the test section. Also few locations on



the center of the test section exhibit a lower CIV

The mean value for moisture contents is about 11% with a coefficient of variation at 15%. There is no significant variation in moisture content over the test section (Figure F56). Dry densities were in the range of 1300 to 1600 kg/m<sup>3</sup> with a low coefficient of variation at 6% (Table 33).

Results from the APT show a mean hydraulic conductivity of about 6 cm/sec, with a high coefficient of variation at 107% (Table 33). Hydraulic conductivity values varied between 0.8 cm/sec and 26 cm/sec (see Table G3). The contour plot (Figure F58) shows that there is significant spatial variation in hydraulic conductivity over the test section. However, many locations on the test section exhibit a hydraulic conductivity less than 2 cm/sec. The coefficient of variation in fines content is about 37% with a mean value of about 6% (Table 33). By comparing the contour plots for variation in fines content (Figure F59) and hydraulic conductivity (Figure F58), it can be seen that the locations of high fines contents exhibit low hydraulic conductivity

Gradation analysis on RPCC35 resulted in fines content of about 2.4% (see Table 22). But field measurement shows a variation from 4% to 11%, which gives an indication of increased fines possibly due to particle breakage during construction. Figure 58 shows evidence of segregation in fines at this construction site.

Using the mean hydraulic conductivity value and assuming a 0% longitudinal gradient of the base, 2% of cross-slope, and 30% effective porosity, the drainage times were estimated using the PDE 1.0 program. The estimate of time for 50% and 90% drainage is < 1 hour and is rated as "Excellent" (Table 35).



**Figure 58. Picture showing segregation in fines on the final base layer**

Observing the test results and contour plots from all the projects it is indicative that the mean values of strength/stiffness and hydraulic conductivity meet the design criteria. But spatial variability of most parameters is observed, of which the degree and consequences are poorly understood. The pavement supporting layers including base/subbase and subgrade having non-uniform support capacity could lead to differential settlements causing failure on the surface layer. It should be recognized that though the measurements may meet the design criteria, variability in these parameters could influence the long-term performance of the pavement.

### **Statistical Analysis of Test Results**

Beyond calculating the mean and coefficient of variation values for each project, statistical analyses were performed on results for all projects with granular base (138 points). Table 36 summarizes the mean (M), standard deviation (SD), and coefficient of variation (CV) for all parameters. Further, using linear regression techniques, Pearson's correlation coefficients were determined for relationships between all parameters and are shown in Table 37. R-squared values were also calculated from the Pearson's correlations to better understand the influence of fines content, dry density, water content and degree of saturation on various strength/stiffness measurements and hydraulic conductivity (see Table 38).

Results from statistical analyses show a coefficient of variation of about 9% for density 83% for CBR and about 97% for hydraulic conductivity, indicating significant variation.

The R-squared values from Table 38 show that fines content accounts for more variation in strength and stiffness than any other parameter. The R-squared value calculated on a linear regression for fines content versus hydraulic conductivity is about 0.13 Figure 59 clearly shows however, that the relationship is non-linear (i.e. exponential). With an exponential fit, the R-squared value improves to 0.5. A similar relationship is observed from the laboratory investigation on RPCC (see Figure 31).

Relationships between strength/stiffness (CBR, MOD and CIV) and hydraulic conductivity (K) shows R-values in the range of -0.004 to 0.078 (Table 37), indicating poor correlations. No relationship was identified even considering a range of multiple regression analyses performed on several combinations of these parameters.

**Table 36. Statistics of all field data**

Parameter	Statistics		
	M	SD	CV
K (cm/sec)	4.4	4.2	96.8
MOD (MPa)	83.2	34.3	41.3
S (MN/m)	9.6	4.0	41.3
PI (mm/blow)	20.5	14.0	68.2
CBR <sup>1</sup> %	17.8	14.7	82.7
CIV	18.6	9.0	48.4
% fines	5.4	3.5	64.3
w%	6.7	3.6	53.5
$\gamma_d$ (kg/m <sup>3</sup> )	1654.6	119.4	7.2
S%	32.1	17.2	53.5

For symbols, refer to the Notes in Table 33

Relationships between the parameters estimated from in situ tests are shown in Figures 37 through 39. A strong relationship between CIV measured from Clegg Hammer test and PI (mm/blow) measured from DCP test is observed with an R-squared value of 0.65, as shown in Figure 60. Linear relationship between CIV vs. GeoGauge Modulus (MPa) as well as CBR vs. GeoGauge Modulus (MPa) is observed with an R-squared value of 0.54 and 0.59 respectively as shown in Figures 61 and 62 respectively.

Table 37. Pearson's correlation coefficient (R) between various parameters measured

Parameter	K (cm/sec)	MOD (MPa)	S (MN/m)	PI (mm/blow)	CBR %	CIV	% fines	w %	$\gamma_d$ (kg/m <sup>3</sup> )	S %
K (cm/sec)	1.000	-0.004	-0.004	-0.069	0.078	0.016	-0.357	0.163	-0.242	0.097
MOD (MPa)	-0.004	1.000	1.000	-0.582	0.870	0.840	-0.568	-0.080	0.240	0.168
S (MN/m)	-0.004	1.000	1.000	-0.582	0.870	0.840	-0.568	-0.080	0.240	0.168
PI (mm/blow)	-0.069	-0.582	-0.582	1.000	-0.748	0.673	0.352	-0.327	0.116	-0.445
CBR %	0.078	0.870	0.870	-0.748	1.000	0.924	-0.564	0.197	0.018	0.391
CIV	0.016	0.840	0.840	-0.673	0.924	1.000	-0.402	0.175	0.132	0.385
% fines	-0.357	-0.568	-0.568	0.352	-0.564	0.402	1.000	0.094	0.173	0.044
w %	0.163	-0.080	-0.080	-0.327	0.197	0.175	0.094	1.000	-0.563	0.905
$\gamma_d$ (kg/m <sup>3</sup> )	-0.242	0.240	0.240	0.116	0.018	0.132	0.173	-0.563	1.000	-0.228
S %	0.097	0.168	0.168	-0.445	0.391	0.385	0.044	0.905	-0.228	1.000

Note: For symbols refer to Notes in Table 33

Table 38. R-Squared coefficients calculated from Pearson's Correlations

Influencing Parameter	R-Squared Values					
	K (cm/sec)	MOD (MPa)	S (MN/m)	PI (mm/blow)	CBR <sup>1</sup> %	CIV
% fines	0.13	0.32	0.32	0.12	0.32	0.16
w %	0.03	0.01	0.01	0.11	0.04	0.03
$\gamma_d$ (kg/m <sup>3</sup> )	0.06	0.06	0.06	0.01	0.00	0.02
S %	0.01	0.03	0.03	0.20	0.15	0.15

For symbols, refer to Notes in Table 33

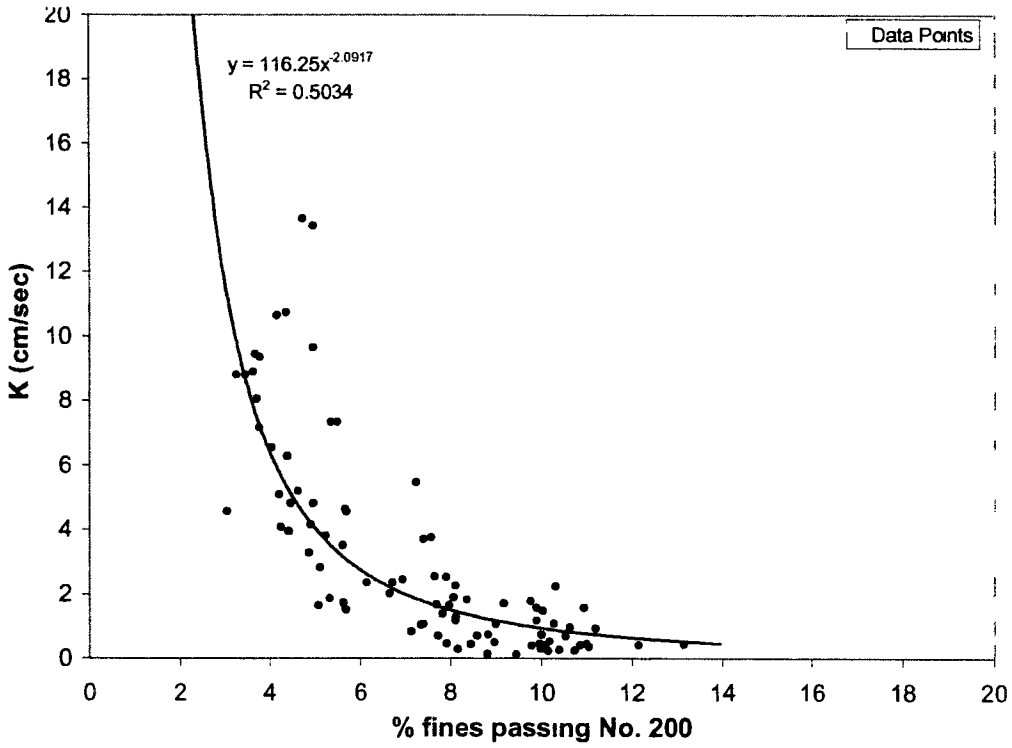


Figure 59 Relationship between hydraulic conductivity and fines content

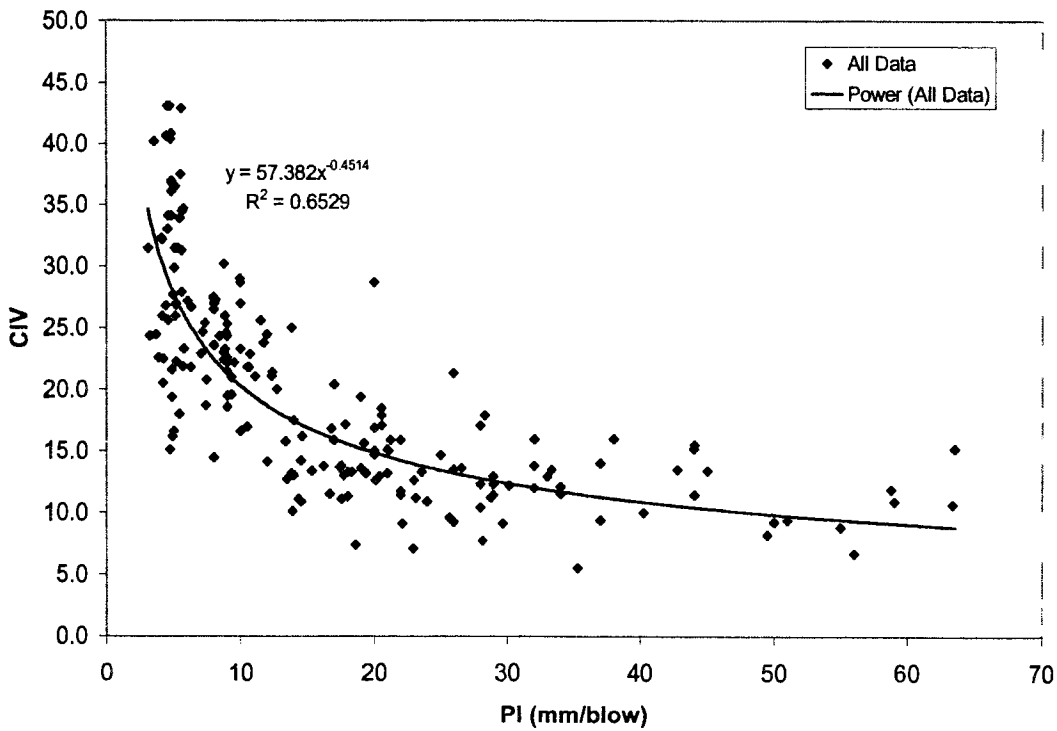


Figure 60. Relationship between CIV and PI (mm/blow)

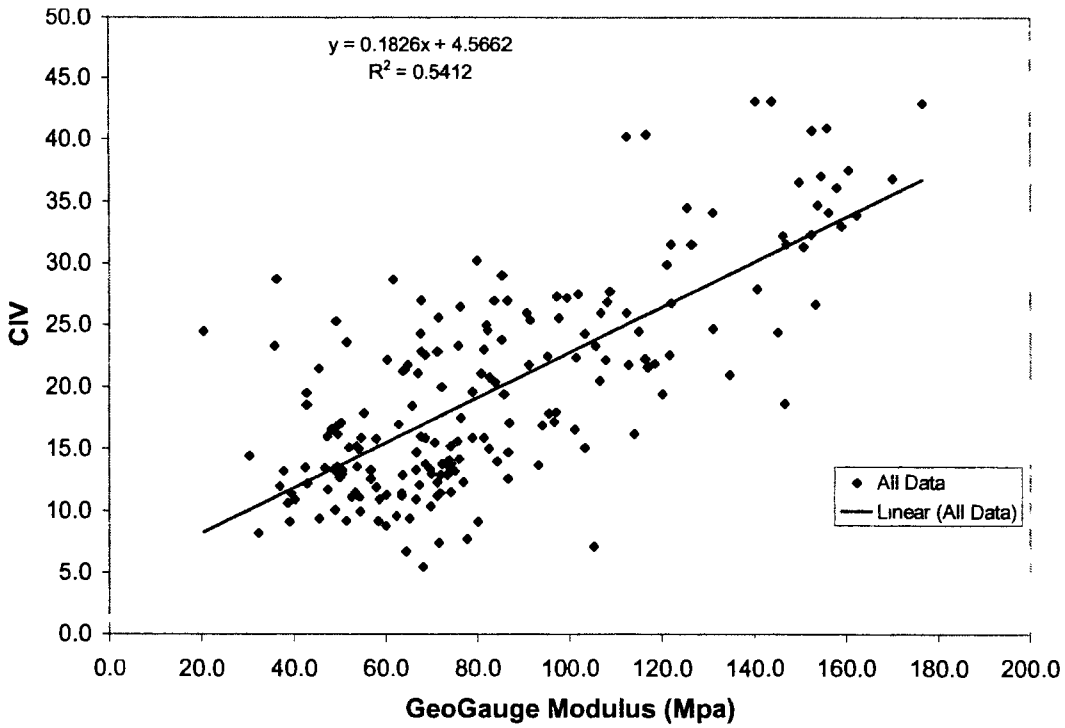


Figure 61. Relationship between CIV and GeoGauge Modulus (MPa)

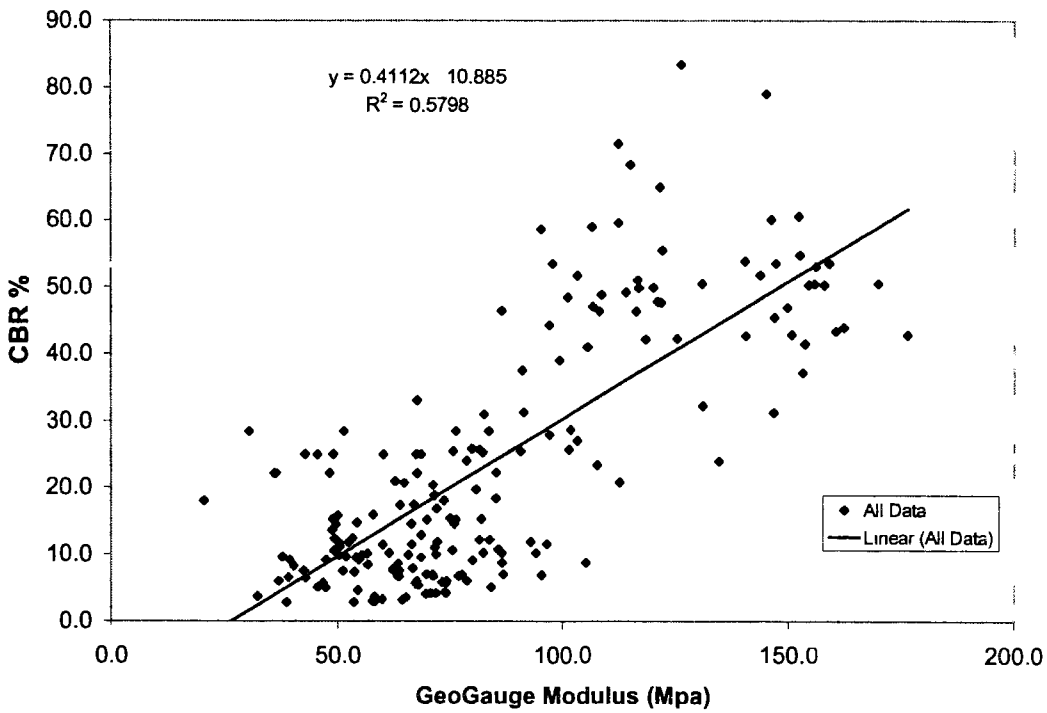


Figure 62. Relationship between estimated CBR from DCP and GeoGauge Modulus (MPa)

### Significance of the Test Results in Design

The field test results show that generally drainability of granular base materials is excellent. According to AASHTO (1986), excellent drainage is defined as the state at which the drainage coefficient,  $C_d$ , is between 1.0 and 1.25 (Table 35). Using the AASHTO 1986 PCC pavement thickness design procedures and assuming various design parameters, the thickness required and reliability on design were determined. Results show that if a drainage coefficient,  $C_d$ , of 1.0, is assumed, the thickness required is about 9.5 in. at 95% reliability. Whereas on assuming a  $C_d$  of 1.2, the thickness required is reduced to 8.5 in, maintaining 95% reliability. Additionally, it can be shown that reliability can be increased over 99% if the thickness is maintained at 9.5 in and using a  $C_d$  of 1.2.

Assumptions:

$k^*$  = Modulus of Subgrade Reaction = 150 pci

$E_c$  = Concrete Elastic Modulus =  $5 \times 10^6$  psi

$S'_c$  = Mean Concrete Modulus of Rupture = 650 psi

$J$  = Load Transfer Coefficient = 3.2

$C_d$  = Drainage Coefficient = 1.0 to 1.2

$\Delta$ PSI = Design Serviceability Loss = 1.7

$W_{18}$  = Estimated Total 18-kip ESAL Applications =  $5.1 \times 10^6$

$S_0$  = Overall Standard Deviation = 0.29

*Results*

$C_d$	Thickness (in)	Reliability %
1.0	9.5	0.95
1.2	8.5	0.95
1.2	9.5	> 99%

### Feasibility of Various In-Situ Testing Methods

Based on the experiences gained during the field testing phase of this project and a review of literature, a summary of comparisons between the various in-situ testing methods is provided in Table 39. Clegg Hammer and GeoGauge tests are more rapid and need fewer

people to perform as compared to DCP tests. Although the GeoGauge test is considered rapid, no correlations are available yet to relate the measurements to a standard plate load test (i.e. modulus of subgrade reaction). Also, vibrations caused from construction traffic influenced the measurements made by the GeoGauge during testing. Various correlations available to estimate CBR from DCP test are well established and also the test method was recently standardized according to ASTM D6951-03. The DCP test can measure up to a depth of 39 in, where other tests are limited to surface measurements. The Clegg Hammer test is standardized according to ASTM D5874, but the correlations are not well established and are subject to change with soil type (Clegg, 1986). However, Clegg Hammer and GeoGauge can be used as rapid quality control tools to investigate the uniformity of a layer.

The APT was demonstrated as a rapid quality control tool to measure the in-situ hydraulic conductivity within few seconds. Spatial variability of hydraulic conductivity over the final compacted base can be measured for quality control purposes in a few minutes.

**Table 39 Comparison between various in-situ testing methods**

Test	Parameter measured	Correlated parameter/s	Time (minutes)	Simplicity	Depth (in)	Labor needed	Skill level	Cost (\$)
Clegg Impact Hammer Test	CIV	CBR	0.2	1	6'	One	Low	
GeoGauge™ Vibration Test	Stiffness and Modulus	—	1.5	2	9**	One	Low	
DCP Test	Penetration Index, PI	CBR, Modulus, UCS	3	3	39***	Two	Low	\$2500
Air Permeameter Test (APT)	Saturated Hydraulic Conductivity	—	0.5	1	0 – 4	One	Low	\$2000
Nuclear Density Gauge Test	Moisture Content, and Dry density	—	5	1	12	One	High	\$5000

### Key Observations from Field Testing

- Estimated modulus of subgrade reaction values for all projects with granular subbase is 1.1 to 2.8 times greater than the Iowa DOT pavement design value of 150 pci.
- Time estimates for 50% and 90% drainage for all granular subbase projects is < 2



hours and can be rated “Excellent” according to AASHTO (1986).

- Significant spatial variability of most parameters is observed in each project. Considering all projects with granular subbase, the calculated coefficient of variations are as follows: 9% for density, 41% for modulus, 53% for water content, 64% for fines, 83% for CBR, and 97% for hydraulic conductivity
- Considering variations in density water content, degree of saturation, and fines content, results show that fines content accounts for more variation in strength/stiffness than the other parameters.
- The strongest correlation from linear regression analyses between fines content and the other measured parameters with hydraulic conductivity ( $R^2$  value equals 0.5).
- No significant relationship was identified from a range of multiple regression analyses to correlate strength/stiffness properties with hydraulic conductivity measurements.
- Relationships between Clegg Hammer, DCP and GeoGauge measurements show indications of non-linear and/or linear correlations with  $R^2$  values of 0.54 to 0.65
- A comparison of the field testing techniques shows that although the DCP may require more effort in the field, the results are better correlated to establish parameters and the depth of measurement is much greater. The APT is established as a simple and rapid technique for determination of hydraulic conductivity

## DESCRIPTION OF THE PAVEMENT DRAINAGE ESTIMATOR (PDE)

The *Pavement Drainage Estimator (PDE) Version 1.04* is an Excel-based spreadsheet program that can be used to estimate the minimum required hydraulic conductivity of a pavement base layer and/or the time to achieve a given percent drainage. Estimation of these parameters is determined from several factors which can be broadly addressed as properties of aggregates, dimensions of the pavement, rainfall intensity and the amount of drainage required. Results obtained from this program account only for the flow of water caused due to infiltration from the surface of the pavement. In locations where other sources of water are significant, adjustments to the calculations may be warranted. A brief description of the program with an example calculation is described in this section.

### What is PDE used for?

The user provides information including dimensions of the pavement, infiltration rate and effective porosity of the base material. *PDE (1.04)* can then be used to estimate the required hydraulic conductivity (K) based on steady-state flow analysis, and the time for any given percentage of drainage based on unsteady-state flow analysis (see Moulton, 1980). Typical values for all these parameters are provided in the description page of the program. The program considers the effect of the geometry of the pavement which has a significant impact on the results.

### How is it used?

- Figure 63 shows the introductory page of the program which begins with a flowchart describing the options available in the program. Next the user selects an option and clicks on “Go To Main Menu”
- The main menu has three options for the estimation of parameters, and one option which describe all the parameters (see Figure 64).

- If the user knows or has an estimate for hydraulic conductivity of the base material, then depending on the degree of drainage required, pick one of the top two options (e.g. if the user is estimating time to achieve 90% drainage in the pavement base then pick DEGREE OF DRAINAGE > 50%). This step leads to a page similar to Figure 65.
- Enter all the values under the “Enter Values Here” (yellow bar). If the description of any parameter is needed, just click on the parameter button. This leads to the description page of the program as shown in Figure 66. After all the parameters are entered, output can be viewed under “Output” (pink bar) as “Required Permeability” (cm/sec and ft/day) and “Time to Drain” (hours and days).

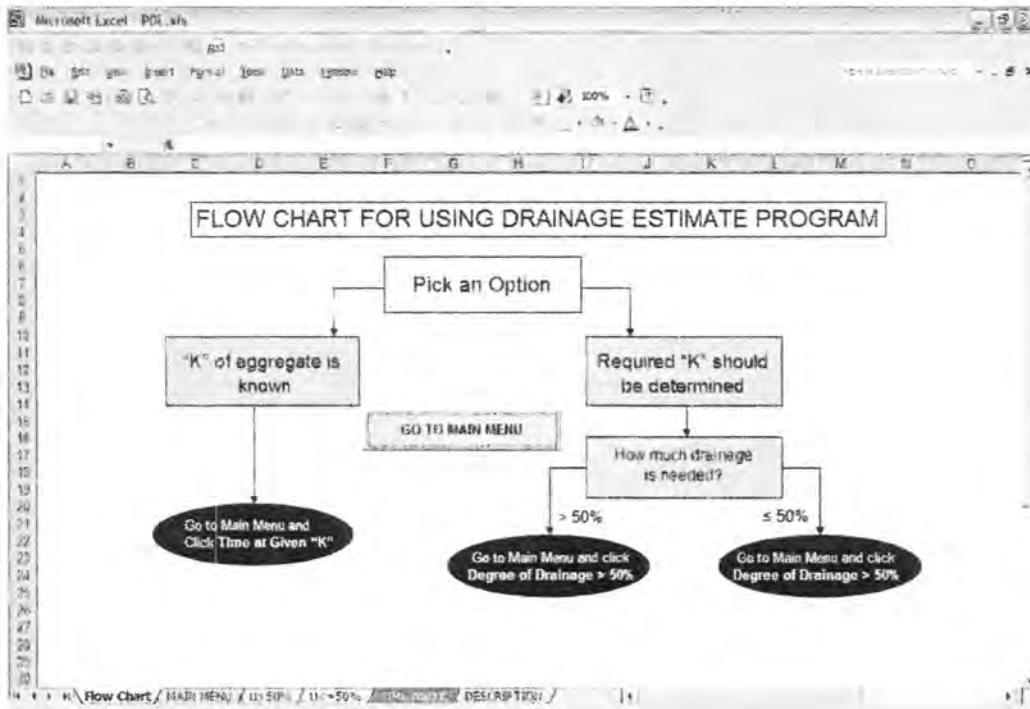


Figure 63. Flow chart of PDE version 1.04

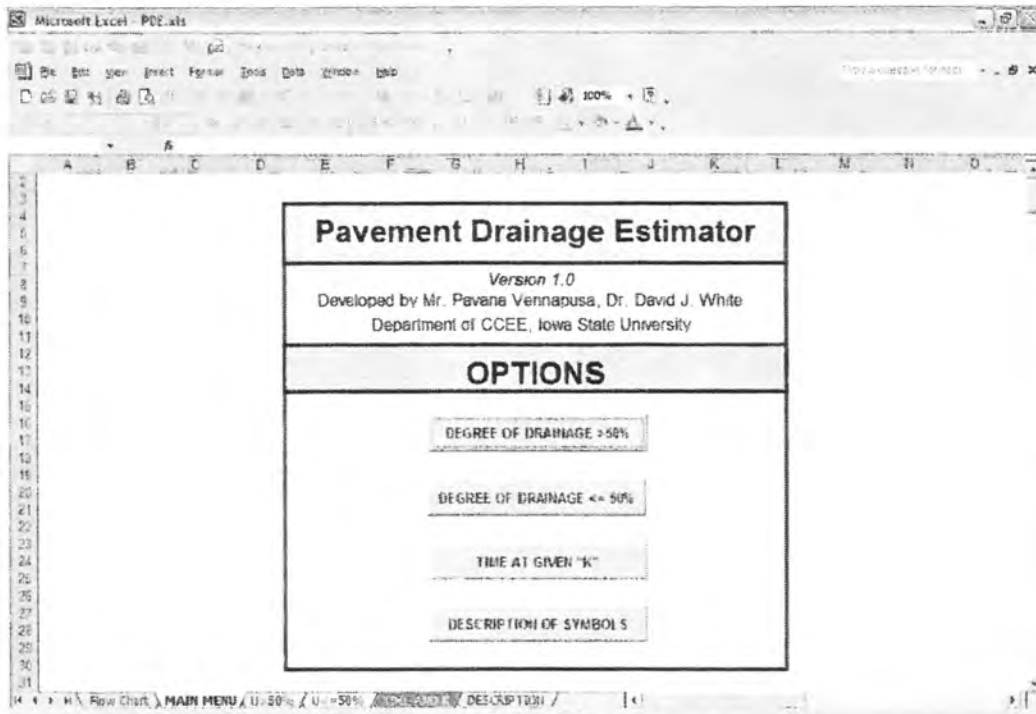


Figure 64. Options in main menu of PDE version 1.04

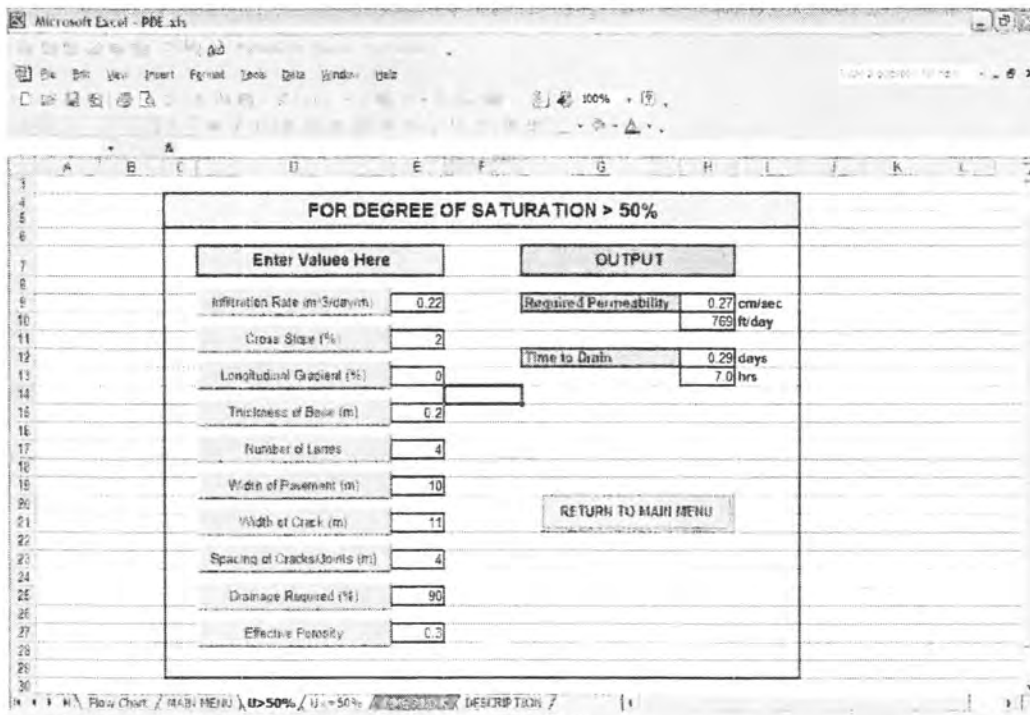


Figure 65. Option in the program for PDE version 1.04

### Sample Calculation

For the pavement section shown in Figure 66, and for a given set of geometric conditions, calculations for steady and un-steady state flow conditions are provided as follows:

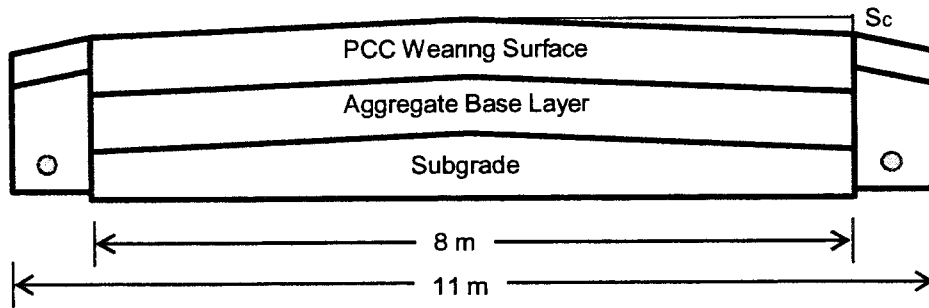


Figure 66. Cross-section of pavement

Given data:

Infiltration rate per crack =  $I_c = 0.22 \text{ m}^3/\text{day}/\text{m}$ ,

Width of the pavement =  $W_p = 8 \text{ m}$ ,

Width of crack =  $W_c = 11 \text{ m}$ ,

Spacing of transverse cracks =  $C_s = 4\text{m}$ ,

No. of lanes =  $N = 4$ ,

Thickness of base layer =  $H = 0.15 \text{ m}$ ,

Effective porosity of the material =  $n_e = 37\%$ ,

Cross-slope =  $S_c = 2\%$ ,

Longitudinal gradient =  $g = 1\%$ .

Calculations:

Using the above information, the infiltration rate per unit area of crack can be calculated using Equation 1

$$\Rightarrow q_i = I_c \left( \frac{N+1}{W_p} + \frac{W_c}{W_p C_s} \right) = \left( \frac{4+1}{8} + \frac{11}{8*4} \right) = 0.213 \text{ m}^3/\text{day}/\text{m}^2$$

Assuming that there is constant infiltration throughout the crack, the infiltration rate

per unit width of crack is given by  $q$ , which is equal to the discharge capacity of the drainage layer, and can be calculated using Equation 4.

$$\Rightarrow q = q_i \times W_c = 0.213 \times 11 = 2.344 \text{ m}^3/\text{day}/\text{m}$$

Flow-path gradient and flow-path length can be calculated using Equations 2 and 3

$$\Rightarrow S = \sqrt{S_c^2 + g^2} = \sqrt{0.02^2 + 0.01^2} = 0.0223$$

$$\Rightarrow L = \frac{W_p}{2} \sqrt{1 + \left(\frac{g}{S_c}\right)^2} = \frac{8}{2} \sqrt{1 + \left(\frac{0.01}{0.02}\right)^2} = 4.47 \text{ m}$$

Substituting the values of  $L$ ,  $S$ ,  $q$  in Equation 2, the required hydraulic conductivity of the drainage layer,  $k$ , can be computed as

$$\Rightarrow k = \left( \frac{q}{H(S + H/2L)} \right) = \left( \frac{2.344}{0.15(0.0223 + 0.15/2 \times 4.47)} \right) = 399.88 \text{ m/day} = 0.46 \text{ cm/sec}$$

Assuming that the material used in the base layer has the hydraulic conductivity of 0.46 cm/sec and using Figure 14, the time for 50% degree of drainage may be computed as

$$S_1 = LS/H = 4.47 \times 0.0223/0.15 = 0.664$$

for  $U = 0.5$  and  $S_1 = 0.664$ , Time factor  $T = 0.298$

Hence the time required for 50% drainage is:

$$t = \left( \frac{n_e L^2}{k \times H} \right) \times T = \frac{0.37 \times 4.47^2}{399.88 \times 0.15} \times 0.298 = 0.0367 \text{ days} = 0.9 \text{ hrs.}$$

So, for the given set of conditions of the pavement, the material used in the drainage layer should have a hydraulic conductivity of 0.46 cm/sec (1310 ft/day) to drain 50% of the water infiltrated in  $< 1$  h.

## FIELD INVESTIGATION OF PAVEMENT PATCHING PROJECTS

Field observations and testing were recently conducted on subgrade/base layers at locations of full-depth patching on I-235 and Hwy 30. The objectives of the investigation were to document in-place engineering properties of the subgrade/base layers and thus improve our understanding of conditions that lead to poor pavement performance. After the pavement sections had been removed, in situ tests including APTs and DCP tests were performed. Bag samples were also collected for material classification. Unfortunately none of the patching projects visited were supported by granular subbase materials. Future investigations should include an evaluation of in-service granular subbase layers. A brief summary of the test results and information gained from the patching projects is summarized in the following.

### **I 235 East Bound, West Des Moines, Iowa**

This patching site is located on I-235 east bound in West Des Moines, Iowa. The existing PCC pavement in this corridor is riddled with hundreds of patches. Our investigation shows that the pavement is underlain with about 4–6 inches of leveling sand (SAND235) underlain by weathered shale subgrade (CLAY235). Figure 67 shows a cross-section of the pavement. In order to prepare the existing PCC pavement for an ACC overlay deteriorated sections of the pavement were saw cut, excavated, leveled, and replaced with new PCC. Figure 68 shows a typical patching section. After removing the pavement layer, about 6 inches of recycled concrete base (RPCC235) was placed over the existing subbase (Figure 69). RPCC235 in this case is well-graded and only served as a leveling course, not a drainage material.

### *Materials*

Grain-size distribution curves for SAND235 and RPCC235 are shown in Figure 70. The Iowa DOT gradation for granular subbase is also shown for comparison. A summary of the results is provided in Table 40. The coefficient of uniformity  $C_u$ , coefficient of curvature,  $C_c$ , classification and percent fractions of gravel, sand, and silt/clay and Atterberg limits are provided in Table 41 for SAND235, RPCC235 and CLAY235. Grain-size analyses show that

the newly placed base layer (RPCC235) fits the Iowa DOT modified subbase gradation. The SAND235 material meets the gradation requirements for granular backfill.

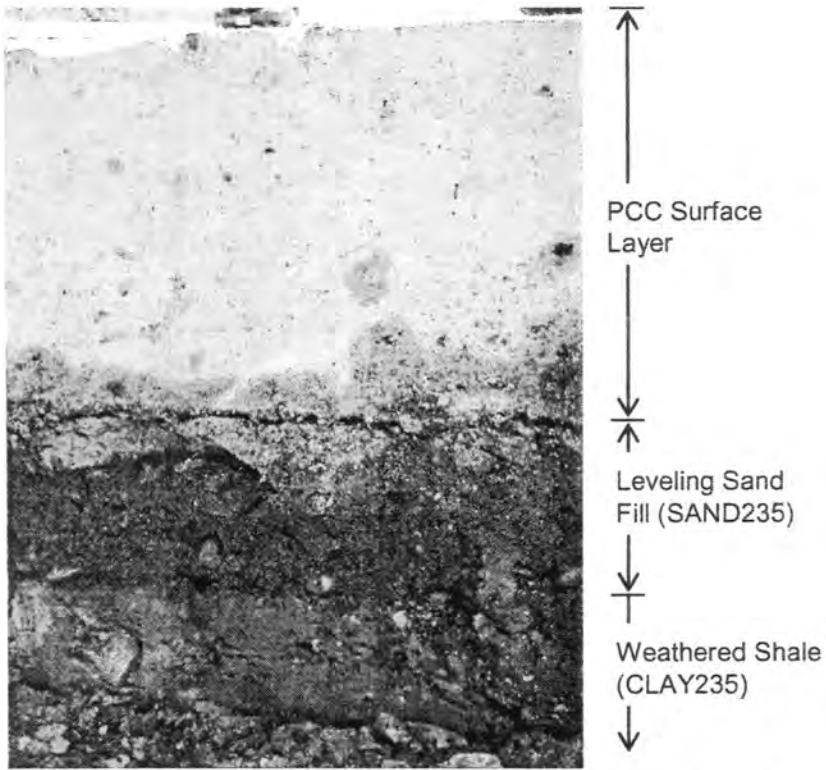


**Figure 67** Cross-section of the existing pavement on I-235, West Des Moines, Iowa

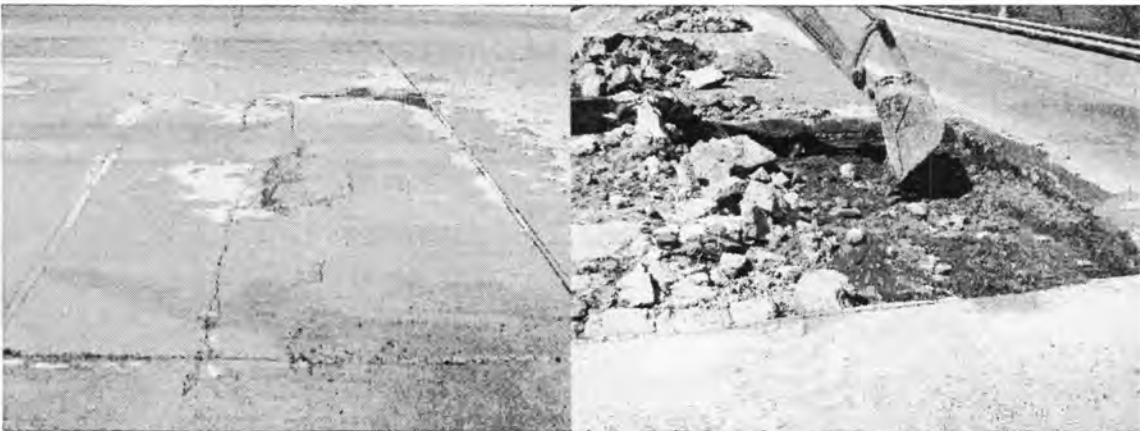


**Figure 68.** I-235 deteriorated PCC surface on the left, and excavation on the right



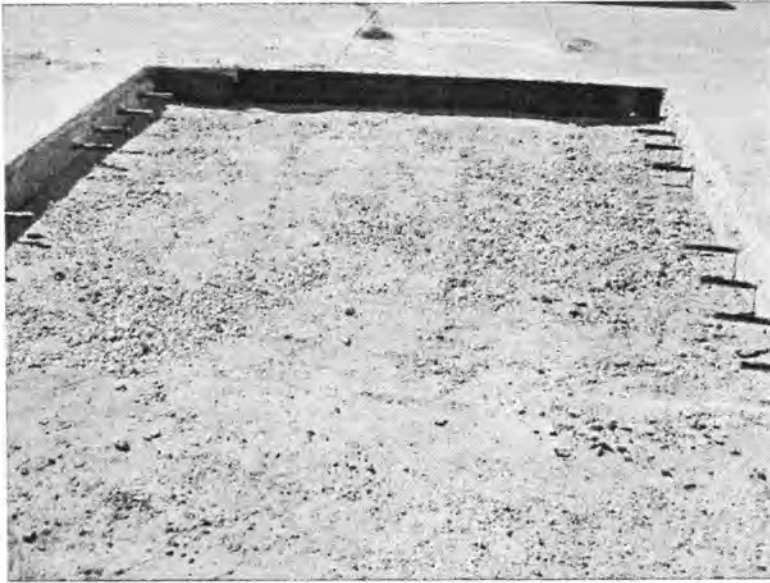


Figure 69. Recycled PCC aggregate placed over the existing subbase I-235

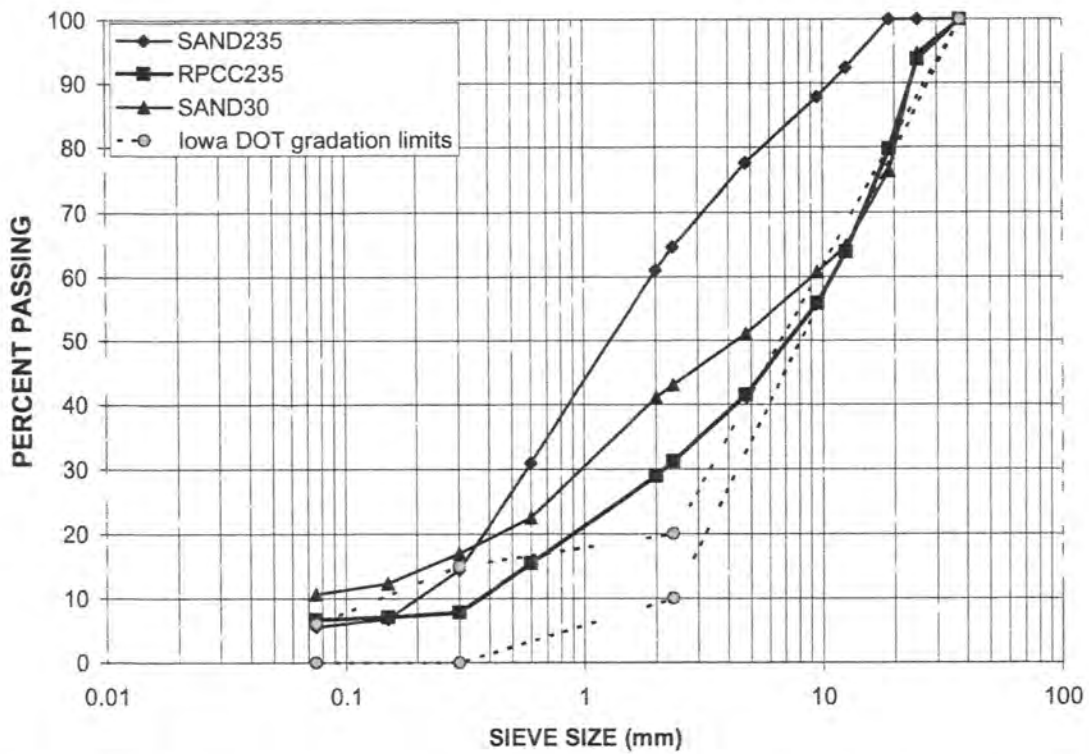


Figure 70. Grain-size distribution curves for subbase materials from patching projects compared to the Iowa DOT granular subbase gradation limits

**Table 40. Grain-size distribution data for samples from patching projects**

Sieve No.	Sieve Size (mm)	Percent Passing				
		SAND235	SAND30	Iowa DOT <sup>1</sup>	RPCC235	Iowa DOT <sup>2</sup>
1.5"	37.5	100	100	—	100	100
1	25	100	94.6	—	93.7	—
0.75"	19	100	76.3	—	79.7	70-90
0.5"	12.5	92.3	64.8	—	63.9	—
0.375"	9.5	87.9	60.8	—	55.9	—
No. 4	4.75	77.6	51	—	41.5	—
No. 8	2.36	64.6	43	20-100	31.2	10-40
No. 10	2	61	41.1	—	29	—
No. 30	0.6	30.9	22.5	—	15.4	—
No. 50	0.3	14.4	17	—	7.9	—
No. 100	0.15	6.7	12.4	—	7.1	—
No. 200	0.075	5.6	10.7	0-10	6.7	3-10

<sup>1</sup> Iowa DOT specified gradation according to section No. 4133 – granular backfill

<sup>2</sup> Iowa DOT specified gradation according to section No. 4123 – modified subbase

### *In-Situ Testing*

DCP tests were performed at 7 locations on the east bound lane and 1 location on the west bound lane of I-235. Tests were conducted up to a depth of about 800 mm from the surface of the RPCC235 layer in the east bound lane. Tests performed on the west bound lane only included the subgrade (CLAY235) layer. APTs were conducted at 4 locations on the new recycled concrete base layer (RPCC235).

CBR values were estimated from DCP Penetration Index (mm/blow) results using Equation No. 4 of Table 19. Figure 71 shows the mean CBR with depth through the various soil layers. All eight CBR profiles for individual test results are provided in Appendix H. From Figure 71, it can be seen that the SAND235 layer, which was directly under the pavement layer exhibits a CBR value in the range of 19 to 28. The RPCC235 material placed as a leveling layer was very low in the range of 2 to 4. The subgrade layer (CLAY235) has a CBR value in the range of 5 to 14.

Table 41 Summary of index properties of all samples from patching projects

Source	Material	Layer	% material gravel > #4 sand < #4 > #200 silt/clay < #200	LL	PI	C <sub>u</sub>	C	AASHTO	Unified soils classification
I 235 East Bound West Des Moines (CLAY235)	Clayey Sand	Subgrade	gravel = 0.0% sand = 18.3% silt/clay = 81.7%	42	33	—	—	A 7 6	CI
I 235 East Bound West Des Moines (SAND235)	Sand	Leveling Base	gravel = 22.4% sand = 72.0% silt/clay = 5.6%	—	NP	10.0	0.6	A 1 b	SP
I 235 East Bound West Des Moines (RPCC235)	Recycled Concrete	New Base	gravel = 58.5% sand = 34.7% silt/clay = 6.7%	—	NP	30.6	1.2	A 1 a	GW
US 30 East Bound Boone (CLAY30)	Sandy Clay	Subgrade	gravel = 0.0% sand = 47.3% silt/clay = 52.7%	29	16	—	—	A 6	CL
US 30 East Bound Boone (SAND30)	Sand	Leveling Base	gravel = 49.0% sand = 40.4% silt/clay = 10.7%	—	NP	128.6	1.4	A 1 a	SW

## Notes:

\* Tests not performed

LL - Liquid Limit

PI - Plasticity Index

NP - Non Plastic

C<sub>u</sub> - Coefficient of Uniformity

C - Coefficient of Curvature

D<sub>10</sub> - Particle diameter at 10% passing (mm)

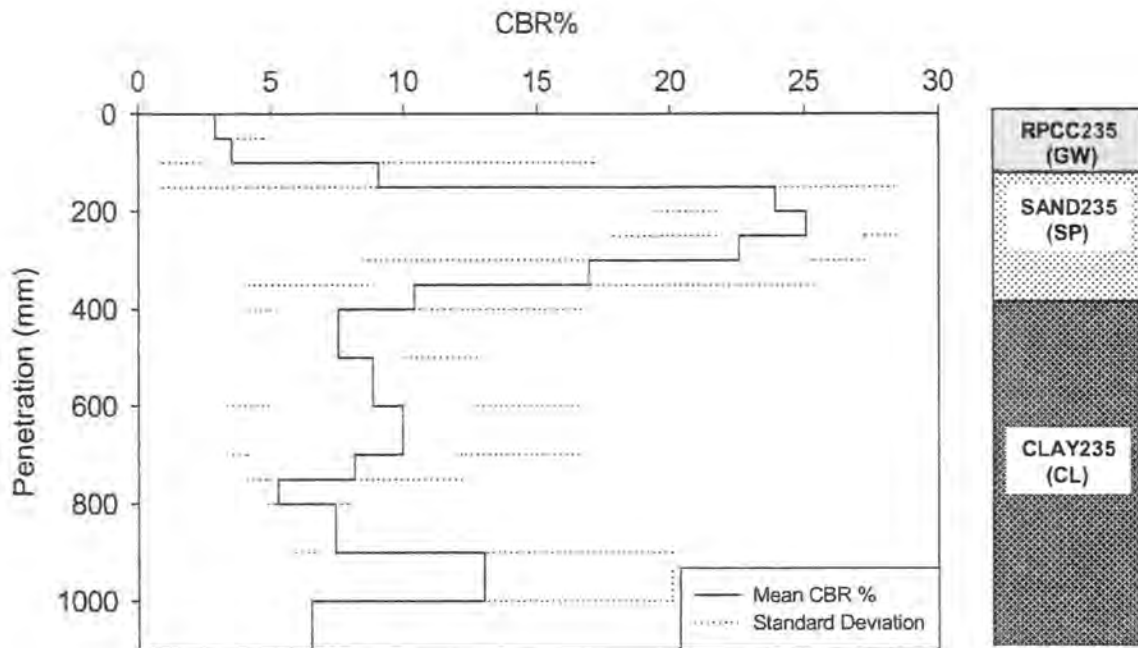


**Figure 71. Change in CBR with depth: I-235 patch project**

Test results from APT measurements are shown in Table 42. Samples of about 1000 g were obtained at each test location to determine the fines content. Test results show that hydraulic conductivity decreases significantly with increasing fines. To investigate the variability in fines and hydraulic conductivity two APTs were conducted within a patch area only 3 feet apart (A and B). Results show that the hydraulic conductivity changes from 0.4 to 0.8 cm/sec, indicating significant variability over a short distance.

**Table 42. I-235 fines content and APT results in RPCC**

Location	K (cm/sec)	% fines
1	5.2	2.2
2A	0.4	9.0
2B	0.8	7.0
3	0.5	5.0

### US Hwy 30 East Bound, Boone, Iowa

This PCC patching site is located on US Hwy 30 in the east bound lane about 3 miles west of Boone, Iowa. The existing PCC layer was underlain by 4–6 inches of leveling sand fill (SAND30) and glacial till as subgrade (CLAY30). Full-depth patching of the existing

pavement was carried out on various areas at this location by completely removing and replacing the concrete slab.

### *Materials*

The grain size distribution curve for SAND30 is shown in Figure 70. The coefficient of uniformity,  $C_u$ , coefficient of curvature,  $C_c$ , percent fractions of gravel, sand, and silt/clay Atterberg limits and classification for SAND30 and CLAY30 are shown in Table 41

### *In-Situ Testing*

DCP tests were performed at four different patches to a depth of about 800 mm from the surface of the SAND30 layer. CBR values were estimated from the DCP Penetration Index (mm/blow) using Equation No. 4 of Table 19. Figure 72 shows the change in mean and standard deviation of CBR with depth. All CBR profiles for individual locations are provided in Appendix H. Unlike the I-235 measurements, Figure 72 shows that there is no significant change in CBR with depth.

DCP tests were also conducted at 15 randomly located points within a patching area of about 12 ft by 12 ft as shown in Figure 73. The purpose of multiple DCP tests was to investigate the spatial variability of CBR for the pavement support layers. Tests were conducted by measuring the number of blows required to penetrate the upper to 150 mm and the underlying 300 mm (total of 450 mm from the bottom of pavement). The spatial CBR plots are shown in Figures 74 and 75. The variation in CBR for the sand layer (SAND30 for top 150 mm) is from 4 to 9 with a coefficient of variation of 20%, whereas for the underlying subgrade layer (CLAY 30 from 150 to 450 mm deep) varies from 6 to 11 with a coefficient of variation of 18%. CBR values are generally lower towards the edge of the pavement.

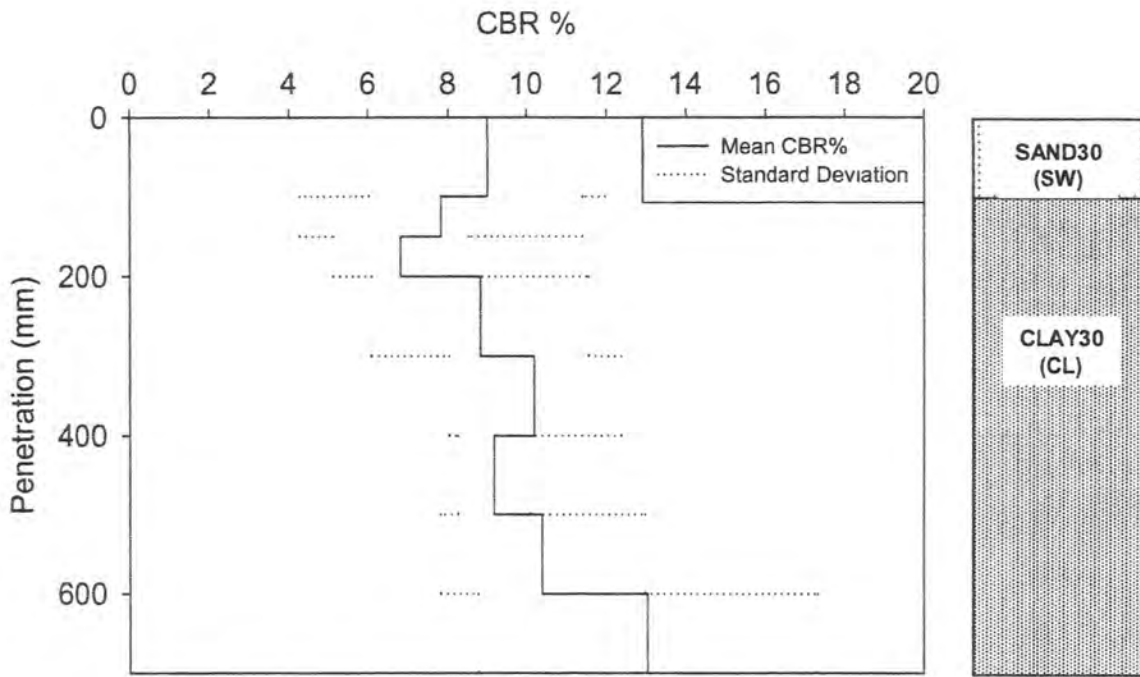
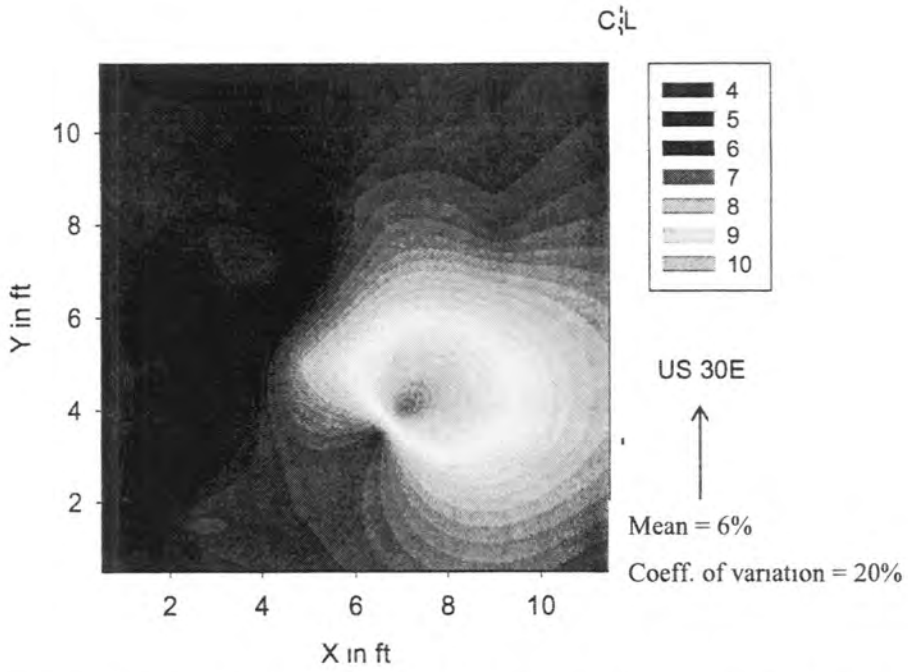


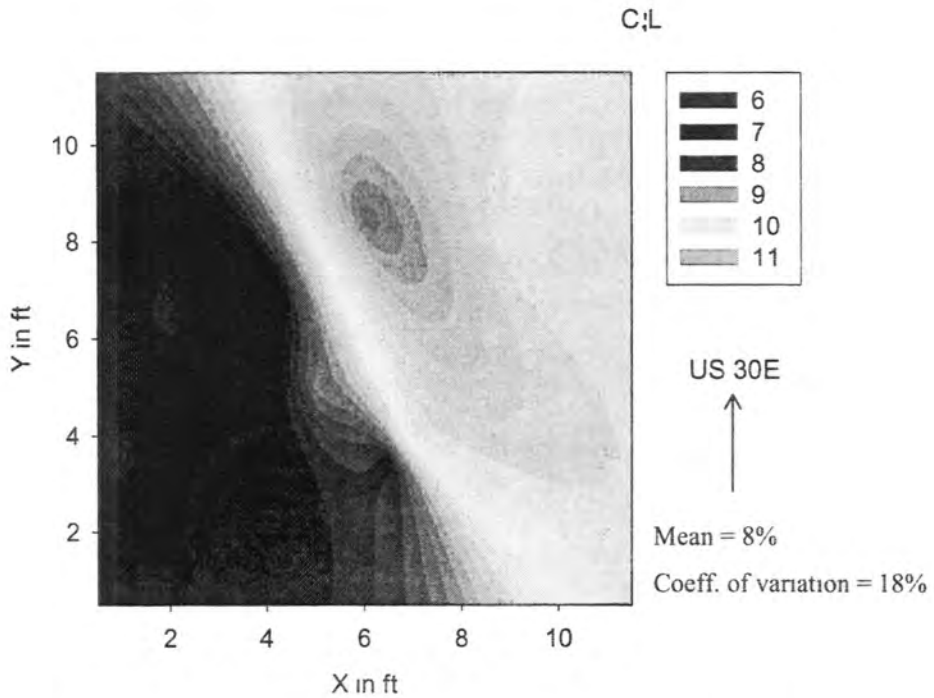
Figure 72. Change in CBR with depth: US Hwy 30



Figure 73. Test section used for DCP testing to investigate the spatial variability US Hwy 30



**Figure 74. Contour plot for variation in CBR for subbase layer (0 to 150 mm deep): US Hwy 30**



**Figure 75. Contour plot for variation in CBR for subgrade layer (150 to 450 mm deep): US Hwy 30**

**Key Observations from Patching Projects**

- Excavations of PCC pavement sections for patches on I-235 revealed 4–6 inches of poorly graded leveling sand overlying weathered shale subgrade with high plasticity (PI = 33). Hwy 30 PCC patches revealed 4–6 inches of well-graded leveling sand overlying glacial till subgrade with moderate plasticity (PI = 16).
- CBR values for the leveling sand and subgrade at the I-235 patching project are in the range of 19 to 28 and 5 to 14, respectively. CBR values for the leveling sand and subgrade at the US Hwy 30 patching project are in the range of 4 to 9 and 6 to 11, respectively.
- Spatial variation in CBR observed over a 12 ft x 12 ft patch section on US Hwy 30 shows that the CBR values are higher under the centerline of the pavement and that the coefficient of variation is approximately 20%.
- Recycled PCC used as a leveling course on the I-235 project has CBR value in the range of 2 to 4 and variable hydraulic conductivity in the range of 0.4 to 0.8 cm/s.



## SUMMARY AND CONCLUSIONS

The main conclusions developed from this research are summarized as follows:

### Laboratory Investigation

- None of the aggregates obtained from the quarry and only a two from the field meet the specified Iowa DOT gradation requirements for granular subbase.
- Maximum CBR is achieved at fines contents between 6% and 14% for granular subbase materials. All crushed limestone materials (CLS, ALS, and AALS) exhibit higher CBR values than recycled concrete materials (RPCC, RPCCAmes).
- The degradation/abrasion loss is higher for recycled concrete than crushed limestone and gravel.
- Hydraulic conductivity decreases exponentially with increasing fines content.
- The fines content of RPCC must be 2% or less to meet the drainage requirement of 90% in < 2h or less than 10% to achieve 50% drainage in < 2h.
- CBR decreases from dense to open gradations.
- Hydraulic conductivity can significantly decrease with increasing compaction energy (i.e. density), but depends on the aggregate type. RPCC exhibited a 16 times decrease in hydraulic conductivity with increased compaction energy. The crushed limestone granular subbase materials achieved adequate hydraulic conductivity even at high compaction energies.

### Construction Operations

- The construction equipment and procedures varied between projects.
- Trimming aggregate with the Gomaco type trimmers leads to segregation, especially for dry base materials.
- There was no moisture control during placement or compaction of final base layer.
- Low moisture content is believed to contribute to increased segregation as there is poor adhesion between finer and larger particles.
- Significant segregation and increase in fines content was observed in two of the three projects visited.

- Construction traffic was allowed with no restriction on only one of the three projects visited. Although segregation was observed, it can not be solely linked to increased construction track, as other projects with no construction traffic showed similar segregation problems.

### **Field Investigations**

- Estimated modulus of subgrade reaction values for all projects with granular subbase is 1.1 to 2.8 times greater than the Iowa DOT pavement design value of 150 pci.
- Time estimates for 50% and 90% drainage for all granular subbase projects is < 2 hours and can be rated “Excellent” according to AASHTO (1986).
- Significant spatial variability of most parameters is observed in each project. Considering all projects with granular subbase, the calculated coefficient of variations are as follows: 9% for density, 41% for modulus, 53% for water content, 64% for fines, 83% for CBR, and 97% for hydraulic conductivity
- Considering variations in density, water content, degree of saturation, and fines content, results show that fines content accounts for more variation in strength/stiffness than the other parameters.
- The strongest correlation from linear regression analyses between fines content and the other measured parameters with hydraulic conductivity ( $R^2$  value equals 0.5).
- No significant relationship was identified from a range of multiple regression analyses to correlate strength/stiffness properties with hydraulic conductivity measurements.
- Relationships between Clegg Hammer, DCP and GeoGauge measurements show indications of non-linear and/or linear correlations with  $R^2$  values of 0.54 to 0.65
- A comparison of the field testing techniques shows that although the DCP may require more effort in the field, the results are better correlated to establish parameters and the depth of measurement is much greater. The APT is established as a simple and rapid technique for determination of hydraulic conductivity

**Patching Projects**

- Excavations of PCC pavement sections for patches on I-235 revealed 4–6 inches of poorly graded leveling sand overlying weathered shale subgrade with high plasticity (PI = 33). Hwy 30 PCC patches revealed 4–6 inches of well-graded leveling sand overlying glacial till subgrade with moderate plasticity (PI = 16).
- CBR values for the leveling sand and subgrade at the I-235 patching project are in the range of 19 to 28 and 5 to 14, respectively. CBR values for the leveling sand and subgrade at the US Hwy 30 patching project are in the range of 4 to 9 and 6 to 11, respectively.
- Spatial variation in CBR observed over a 12 ft x 12 ft patch section on US Hwy 30 shows that the CBR values are higher under the centerline of the pavement and that the coefficient of variation is approximately 20%.
- Recycled PCC used as a leveling course on the I-235 project has CBR value in the range of 2 to 4 and variable hydraulic conductivity in the range of 0.4 to 0.8 cm/s.

## RECOMMENDATIONS

### Optimal Range for In-Place Stability and Permeability

Target in-place stability and permeability values can be established to ensure design assumptions are met or exceeded in the field. For stability, the design assumption is a modulus of subgrade reaction ( $k$ ) equal to 150 pci. Because it is very difficult and time consuming to determine  $k$  in the field (i.e. plate load tests), the authors recommend correlating  $k$  to CBR, which can be determined from a number of in situ testing techniques. According to Middlebrooks (1942), a  $k$  of 150 pci is approximately equal to a CBR of 6. However, given the significant variation of CBR documented in this report, it is further recommended that the field target value be increased by three standard deviations above the minimum target value (according to the “three-sigma rule” described by Dai and Wang (1992), 99.73% of all normally distributed values fall within three standard deviations of the average). Thus, assuming a coefficient of variation of 50% (average of individual projects in this report), the target average CBR value determined in situ should be  $\geq 15$ . The average CBR value determined from all granular subbase projects in this study was 17.8.

For permeability a rating of “excellent” (AASHTO, 1986) indicates that pavement drainage occurs in  $< 2$  hours. For a two lane highway minimum threshold values of 1.0 cm/s and 0.21 cm/s corresponding to 90% and 50% drainage were determined from *PDE (version 1.04)*. Similar to the “three sigma rule” applied to the target CBR values, given that the coefficient of variation for hydraulic conductivity determined from projects tested in this study is 100%, the minimum target values for in-place hydraulic conductivity should be 4.0 cm/s and 0.84 cm/s to achieve 90% and 50% drainage, respectively in  $< 2$  hours. The average value determined for granular subbase project in this study was 4.4 cm/s.

### Field Quality Control/Quality Assurance

Based on the recommendation for in-place stability and permeability described above, and the relationships identified between various in situ test measurements from this study, a DCP Penetration Index (PI) of  $\leq 14$  mm/blow a Clegg impact value (CIV) of  $\geq 20$ , and a GeoGauge modulus of  $\geq 80$  MPa are recommended as target quality control values to ensure

stability of granular subbase materials. The average recommended PI value is similar to the value recommended by Burnham (1997) at about 19 mm/blow for a pavement base immediately after compaction. Because of the added advantage of generating a profile plot, DCP tests are recommended over the Clegg impact hammer and GeoGauge. For determination of hydraulic conductivity use of the Air Permeameter Test is recommended.

### **End-Results Specifications**

Based on guidelines developed by Trenter and Charles (1996), it is recommended that the field quality control tests be performed at a frequency of at least every 200 ft. along the length of the final compacted granular subbase layer. The average tests results should meet the established criteria discussed above.

### **Alternative Construction Practices**

Significant segregation of fines was observed on all projects, contributing to the high variation (coefficient of variation = 100%) in the measured in-place permeability. To reduce segregation, the following construction operations are recommended:

- 1 Do not spread the aggregate material longitudinally along the pavement section, but rather use a motor grader to push the aggregate transversely from a center windrow/pile. A motor grader with a sharp angle (i.e. 45 degrees) can facilitate this process (Pavement Technology Workshop, 2000).
2. Do not use recycled PCC for permeable granular subbase in areas where the construction traffic must haul over the placed aggregate (narrow or no shoulders)
3. As an alternative to trimming equipment (e.g. Gomaco type), use a motor grader with GPS assisted grading (i.e. stakeless grading control). If trimming equipment must be used, however, ensure that the aggregate is delivered to the site with sufficient water content (7%–10 %) to bind the fines during trimming.

### **Future Research Needs**

The future of pavement material characterization will involve repeated triaxial loading as means to detect permanent strain behavior under dynamic loading. It is recommended that the Iowa DOT conduct resilient modulus testing of representative granular

subbase aggregates to ensure no long-term permanent strain problems will develop. It is anticipated that recycled aggregates from PCC and ACC may exhibit poor performance in this regard and may require gradation changes or stabilization to ensure adequate long-term performance. Further, it is recommended that intact core samples of granular subbase materials from in-service pavements be sampled and characterized in detail to document gradation, particle breakdown, contamination, and permeability especially for the recycled aggregates. Computed tomography (CT) techniques could provide useful information in this effort.

**BIBLIOGRAPHY**

- AASHTO 1986. Guide for Design of Pavement Structures. American Association of State Highway and Transportation Officials, Washington D.C.
- ASTM D2940, 2003. Standard Specification for Graded Aggregate Material For Bases or Subbases for Highways or Airports. American Standard Testing Methods.
- ASTM D1241, 2000. Standard Specification for Materials for Soil-Aggregate Subbase, Base, and Surface Courses. American Standard Testing Methods.
- ASTM D1883, 1999 Standard Test Method for CBR (California Bearing Ratio) of Laboratory-Compacted Soils. American Standard Testing Methods.
- ASTM D4429 1993 Standard Test Method for CBR (California Bearing Ratio) of Soils in Place. American Standard Testing Methods.
- ASTM D6951, 2003 Standard Test Method for Use of the Dynamic Cone Penetrometer in Shallow Pavement Applications. American Standard Testing Methods.
- ASTM D5874, 2002. Standard Test Method for Determination of the Impact Value (IV) of a Soil. American Standard Testing Methods.
- ASTM WK2080, 2003. Standard Guide for General Pavement Deflection Measurements. American Standard Testing Methods.
- ASTM D2434-68, 2000. Standard Test Method for Permeability of Granular Soils (Constant Head). American Standard Testing Methods.
- ASTM D3385 2003 Standard Test Method for Infiltration Rate of Soils in Field Using Double-Ring Infiltrometer. American Standard Testing Methods.
- ASTM D5093, 2002. Standard Test Method for Field Measurement of Infiltration Rate Using a Double-Ring Infiltrometer with a Sealed-Inner Ring. American Standard Testing Methods.
- Adams, L.G., 1969 Report on Flexible Pavement Distress in the Atlanta Area. State Highway Department of Georgia, unpublished report.
- Aggregate Handbook, 1996. National Stone Association, Washington, D C.
- Amini, F., 2003. Potential Applications of Dynamic and Static Cone Penetrometers in MDOT Pavement Design and Construction. FHWA/MS-DOT-RD-03-162,

Department of Civil Engineering, Jackson State University, submitted to Mississippi Department of Transportation, Mississippi.

Army Corps of Engineers (COE), 1992. Engineer Technical Letter 1110-3-435 Department of Army, Washington D C., 19-20.

Army Corps Engineers Report, EM1110-1-4001, 2001 Recommended Estimation Methods for Air Permeability Appendix D, <http://www.usace.army.mil/usace-docs/eng-manuals/em1110-1-4001/a-d.pdf>.

Barber, E.S., and Sawyer, C.L. , 1952. Highway Subdrainage. *Proceedings: Highway Research Board*, 643-666.

Barenberg, E., Thompson, M., 1970. Behavior and Performance of Flexible Pavements Evaluated in the University of Illinois Test Track. Highway Engineering Series 6, Cooperative High Research Program Series 108, Urbana, 511.

Baumgardner, H.R., 1992. Overview of Permeable Bases. Materials: Performance and Prevention of Deficiencies and Failures, 1992. Materials Engineering Congress, Atlanta, GA, 275-287

Bouwer, H., 1966. Rapid Field Measurement of Air-Entry value and Hydraulic Conductivity of Soil as significant parameters in Flow System Analysis. *Journal of Water Resources Research*, Vol. 2(4), 729-732.

Bowders, J.J., Blanco, A.M., Parra, J.R., 2003. Characterization of Permeability of Pavement Bases in Missouri Department of Transportation s System. Report No. RI 01 006/RDT 03-005, Prepared for Missouri Department of Transportation, Research, Development and Technology MO

Briaud, J.L., 2003. The GeoGauge and Compaction Control. Department of Civil Engineering, Texas A&M University College Station, Texas.

Brooks, R.H., and Corey A.T., 1964. Hydraulic Properties of Porous Media. Hydrology Papers, Colorado State University Fort Collins, Colorado.

Brown, F.S., 1997 Keynote Address: Achievements and Challenges in Asphalt Pavement Engineering. ISAP-8<sup>th</sup> International Conference on Asphalt Pavements, Seattle, Washington, 1-23

Burnham, R.T., 1997 Application of Dynamic Cone Penetrometer to Minnesota Department of Transportation Pavement Assessment Procedures. Minnesota Department of Transportation.



- Carpenter, S.H., 1990. Highway Subdrainage Design by Microcomputer (DAMP) Drainage Analysis and Modeling Programs. FHWA-IP-90-012, Civil Engineering Department, University of Illinois-Urbana, submitted to FHWA, Illinois.
- Casagrande, A., and Shannon, W.L., 1952. Base Course Drainage for Airport Pavements. *Transactions: American Society of Civil Engineering*, 792-814.
- Cedergren, R.H., 1974. Drainage of Highway and Airfield Pavements. John Wiley & Sons, Inc, New York.
- 1988. *Seepage, Drainage, and Flow Nets*. 3<sup>rd</sup> Edition.
- 1994. "America's Pavement: World's Longest Bathtubs." *Civil Engineering* v 64, n 9, 56-58.
- Chai, G., and Roslie, N., 1998. The Structural Response and Behavior Prediction of Subgrade Soils Using Falling Weight Deflectometer in Pavement Construction. Proceedings: 3<sup>rd</sup> International Conference on Road and Airfield Pavement Technology
- Chapuis, P.R., Gill, E.D., Baass, K., 1989 Laboratory Permeability Tests on Sand: Influence of the Compaction Method on Anisotropy *Canadian Geotechnical Journal* 26(1), 614-622.
- Charles R. Marek, 1997 Compaction of Graded Aggregate Bases and Subbases. *Transportation Engineering Journal* v 103, 103-113
- Chen, D.H., and Bilyeu, J., 1999 Comparison of Resilient Moduli Between Field and Laboratory Testing: A Case Study Internal Document, Texas Department of Transportation, Design Pavement Section, Austin, Texas.
- Cheung, L.W., Dawson, R.A., 2002. Effects of Particle and Mix Characteristics on Performance of Some Granular Materials. *Transportation Research Record*, n. 1787 90-98.
- Clegg, B., 1986. Correlation with California Bearing Ratio. *News Letter 2*, <http://www.clegg.com.au/information%20list12.htm>, Date Accessed: 04/28/2004.
- Crovetti, A. J., and Dempsey, B. J., 1993. Hydraulic Requirements of Permeable Bases. *Transportation Research Record*, n. 1425, 28-36.
- Coonse, J., 1999 Estimating California Bearing Ratio of Cohesive Piedmont Residual Soil Using the Scala Dynamic Cone Penetrometer. Master's Thesis submitted to Department of Civil Engineering, North Carolina State University Raleigh, N.C.

- Dai, S. H., and Wang, M. O., 1992. Reliability Analysis in Engineering Applications. Van Nostrand Reinhold, New York.
- Das, M.B., 1990. *Principles of Geotechnical Engineering*, 2<sup>nd</sup> Edition. PWS-KENT Publishing Company, Boston.
- Dawson, A.R., 1995. The Unbound Aggregate Pavement Base. Keynote Paper, Center for Aggregates Research, 3rd Annual Symposium, Austin, Texas.
- Dawson, A.R., and Plaistow, L., 1996. Parametric Study: Flexible Pavements. Flexible Pavements, Balkema, 229–237
- Dawson, A R, Mundy M J & Huhtala, M., 2000. European Research into Granular Material for Pavement Bases and Sub-bases. *Transportation Research Record*, n. 1721, 91-99
- Eigenbrod, K.D., Knutsson, S., 1992. Measurement of Pore Water Pressures at the interfaces of Asphalt Cement Concrete Pavement and Soil. Proceedings of 45<sup>th</sup> Canadian Geotechnical Conference, Toronto, Ontario, Canada, 44/1–44/10.
- Ese Dag, Myre Jostein, Noss Per, Vaerness Einar, 1994. The Use of Dynamic Cone Penetrometer (DCP) for Road Strengthening Design in Norway 4<sup>th</sup> International Conference on Bearing Capacity of Roads and Airfields, Vol 1, 343–357
- Evans, D.D., and Kirkham, D., 1949 Measurement of Air Permeability of Soil In-Situ. American Soil Science Society Proceedings, v14, 65–73
- Evans, D.D., 1965 Gas Movement, Chapter 23. *Methods of Soil Analysis—Part 1* Ed. Black C.A, No. 9 series, American Society of Agronomy Inc., Wisconsin.
- Federal Aviation Agency (FAA), 2003. (<http://www.airtech.tc.faa.gov/pavement/28ndt.asp>), Date accessed: 11/10/2003.
- Federal Highway Administration (FHWA), 1973b. Final Report: Studies for the Development of Guidelines for the Design of Subsurface Drainage systems for Highway Structural Sections. Washington, DC.
- Ferguson, E.G. 1972. Repetitive Triaxial Compression of Granular Base Course Material with Variable Fines Content. PhD Dissertation submitted to Department of Civil Engineering, Iowa State University, Ames, Iowa.
- Fernuik, N., Haug, M., 1990. Evaluation of In Situ Permeability Testing Methods. *Journal of Geotechnical Engineering*, Vol. 116, No. 2, ASCE.

- Freeman, B.R., Aderton, L.G., 1994. Unbound drainable base courses: Permeability Versus Unsurfaced Stability Infrastructure: New Methods of Repair, Proceedings of third material engineering conference, San Diego, California. 685–692.
- Fwa, T.N., Tan, S.A, Chua, C.T., 1998. Permeability Measurement of Base Materials Using Falling Head Test Apparatus.” *Transportation Research Record* 1615, 94–99
- George, K. P., and Uddin, W., 2000. Subgrade Characterization for Highway Pavement Design. Final Report, Mississippi Department of Transportation, Jackson, Mississippi.
- Goggin, J.D, Thrasher, L. R., Lake W.L., 1988. A Theoretical and Experimental Analysis of Minipermeameter Response Including Gas Slippage and High Velocity Flow Effects. *In situ*, Vol. 12, 79–116.
- Haiping, Z., Moore, L., Huddleston, J., Gower, J., 1993 Determination of Free-Draining Base Materials Properties. *Transportation Research Record*, n. 1425, 54–63
- Hall T.K., Correa E. C., 2003. Effects of Subsurface Drainage on Performance of Asphalt and Concrete Pavements. NCHRP Report 499, Transportation Research Board, Washington, D.C.
- Harrison, J. R., 1987 Correlation Between California Bearing Ratio and Dynamic Cone Penetrometer Strength Measurement of Soils. Proceedings: Institute of Civil Engineers, London, Part 2, 83–87
- Harrigan, T.E., 2002. Performance of Pavement Subsurface Drainage. NCHRP *Research Results Digest*, Number 268.
- Hassan, A., 1996. The Effect of Material Parameters on Dynamic Cone Penetrometer Results for Fine-Grained Soils and Granular Materials. Ph.D Dissertation, Oklahoma State University Stillwater, Oklahoma.
- Hazen, A., 1930. Water Supply *American Civil Engineering Handbook*, Wiley, New York.
- Head K. H., 1982. Manual of Soil Laboratory Testing. Chapter 10, v II, Pentech Press, Plymouth, London.
- Highlands, K.L., Hoffman, L.G., 1988. Subbase Permeability and Pavement Performance. *Transportation Research Record*, n. 1159 7–20.
- Hight, D W., and Stevens, M.G.H. (1982). “An Analysis of the California Bearing Ratio in Saturated Clays.” *Geotechnique*, v 32, No. 4, 315-322.

- Hoover, J.M., 1967 Final Report: Factors affecting Stability of Granular Base Course Mixes. Iowa Highway Research Board Project No. HR-99 Engineering Research Institute, Iowa State University Ames, Iowa.
- Huang H. Yang, 2004. *Pavement Analysis and Design*, 2<sup>nd</sup> Edition, Pearson Prentice Hall, NJ, 334–364.
- Humboldt Mfg Co., 2000. GeoGauge User Guide: Version 3.8. Norridge, Illinois.
- Iowa Department of Natural Resources (IDNR), 2004. <http://ortho.gis.iastate.edu/cir/cir.html>  
Date Accessed: 04/20/2004
- Iowa Department of Transportation (Iowa DOT), 2004, <http://i235.com>, Date Accessed: 04/20/2004
- Ismail, I., Raymond, G., 2002. Investigation into the Behavior of Crushed Aggregate when Loaded Repeatedly Ground and Water: Theory and Practice, Proceedings of 55<sup>th</sup> Canadian Geotechnical and 3<sup>rd</sup> Joint IAH-CNC Groundwater Specialty Conference, Niagara Falls, Ontario.
- Jackson, T.J., and Ragan, R.M. 1974. Hydrology of Porous Pavement Parking Lots. *Journal of the Hydraulics Division*, American Society of Civil Engineers, v 100, n. HY12.
- Jones, T.R. Jr., Otten, L.E., Machemehl, A.C. Jr., Carlton, T.A., 1972. Effect of Changes in Gradation on Strength and Unit Weight of Crushed Stone Base. *Highway Research Record*, Issue 405, 19–23
- Jones, H.A., and Jones, R.H., 1989 Technical Note: Horizontal Permeability of Compacted Aggregates. Proceedings of the 3<sup>rd</sup> International Symposium, University of Nottingham, April 11–13
- Kazmierowski, T.J., Bradbury, A., Hajek J., 1994. Field Evaluation of Various Types of Open-Graded Drainage Layers. *Transportation Research Record*, n. 1434, 29–36.
- Kenny, T.C., Lau, D., and Ofoegbu, G.I., 1984. Permeability of Compacted Granular Materials. *Canadian Geotechnical Journal*, v 21, No.4, 726–729
- Kolisaja, P., 1997 Factors Affecting Deformation Properties of Coarse Grained Granular Materials. Proceedings of 14<sup>th</sup> International Conference on Soil Mechanics and Foundation Engineering, Hamburg, Germany 337–342.
- Kolisaja, P., Saarenketo, T., Peltoniemi, H., Vuorimies, N., 2002. Laboratory Testing of Suction and Deformation Properties of Base Course Aggregates. *Transportation Research Record*, n. 1787, 83–89

- Lambe and Whitman, 1979 Soil Mechanics. John Wiley and Sons, New York, 287–291
- Livneh, M., 1989 Validation of Correlations between a Number of Penetration Tests and In Situ California Bearing Ratio Tests. *Transportation Research Record* 219 Transportation Research Board, Washington, D.C., pp. 56–67
- Livneh, M., Ishai, I., and Livneh, N. A., 1992. Automated DCP Device Versus Manual DCP Device. *Road and Transportation Research*, Vol. 1, No. 4.
- LTTP Protocol P 46, 1996. Resilient Modulus of Unbound Granular Base/Subgrade Materials and Subgrade Soils. US Department of Transportation, FHWA, Virginia.
- Miyagawa, K.F., 1991 Permeability of Granular Subbase Materials. Interim Report for MLR-90-4, Iowa Department of Transportation, Iowa.
- McElvaney, J., and Djatnika, I., 1991 Strength Evaluation of Lime-Stabilized Pavement Foundations Using the Dynamic Cone Penetrometer. *Australian Road Research*, v 21, n. 1, pp. 40–52.
- Middlebrooks, T A. and Bertram, G.E., 1942. Soil Tests for Design of Runway Pavements. *Proceedings of Highway Research Board*.
- Minnesota Department of Transportation (MnDOT), 1994. Permeable Aggregate Base Drainage Systems: Guideline Development. Materials Engineering Committee, MnDOT Minnesota.
- Moulton, L.K., Seals, K.R., 1979 Determination of the In-Situ Permeability of Base and Subbase Courses. Final Report No. FHWA-RD-79-88, Department of Civil Engineering, West Virginia University, Morgantown, West Virginia.
- Moulton, L.K., 1980. Highway Subdrainage Design. Report No. FHWA-TS-80-224, Federal Highway Administration, Washington, D.C.
- Muskat and Botset, H.G., 1931 Flow of Gas through Porous Media. *Physics, I*: 21–48.
- Muskat, 1937 The Flow of Homogenous Fluids through Porous Media. McGraw Hill Book Company London, 75–78.
- Pavement Conditions Survey Manual*, 1998. North Carolina Department of Transportation, Raleigh, N.C.
- Pau Chang Lu, 1979 Fluid Mechanics: An introductory course. Appendixes, 1<sup>st</sup> Edition, Iowa State University Press, 433–447.3
- Pavement Technology Workshop, 2000. A Videotape from the South Africa/United States

Pavement Technology Workshop. University of California— Berkeley Field Station, Richmond, California.

Rajasekharan 1985 Numerical Methods in Science and Engineering. Wheeler Publishing, Allahabad, India.

Randolph W.B., Heydinger G.A., Gupta D.J., Jiangeng Cai, Edward Stienhauser, Quinglu Xie, 2000. Permeability and Stability of Base and Subbase Materials. Final Report No. FHWA/OH 2000/017 submitted to the Ohio Department of Transportation, Department of Civil Engineering, University of Toledo, Ohio.

Reed C.M., 1995 Impact of Open-Graded Drainage Layers on the Construction of Concrete Pavements in Illinois. *Transportation Research Record*, n. 1478, 67–75

Ridgeway H.H., 1976. Infiltration of water through the Pavement Surface. *Transportation Research Record* 616, Transportation Research Board, 98–100.

———, 1982. Pavement Subsurface Drainage Systems. *Synthesis of Highway Practice* 96, Transportation Research Board.

Richardson, N. D., 1997 Drainability Characteristics of Granular Pavement Base Material. *Journal of Transportation Engineering*, v 123, n. 5, 385–392.

Shahabi, A.A., Das, M.B., and Tarquin, A.J., 1984. An Empirical Relation for Coefficient of Permeability of Sand. Proceedings: Fourth Australia-New Zealand Conference on Geomechanics, v 1, 54–57

Siekmeier, J., Burnham, T., and Beberg, D., 1998. MnDOT's New Base Compaction Specification Based on the Dynamic Cone Penetrometer. 46<sup>th</sup> Geotechnical Engineering Conference, University of Minnesota, Minnesota.

Smith, K.D., Peshkin, D.G., Darter, M.I., Mueller, A.L., and Carpenter, S.H., 1990. Performance of Jointed Concrete Pavements, Volume I: Evaluation of Concrete Pavement Performance and Design Features. Publication No. FHWA-RD-89-136.

Thompson, M.R., Smith, K.L., 1990. Repeated Triaxial Characterization of Granular Bases. *Transportation Research Record*, n. 1278, 7–17

Thornton, S.I., Elliott, P.R., 1988. Fines Content of Granular Base Material. Final Report TRC-8703, submitted to Arkansas Highway and Transportation Department, Department of Civil Engineering, University of Arkansas, Fayetteville, Arkansas.

Thornton, S.I., Leong C.T., 1995. Permeability of Pavement Base Course. Submitted to Arkansas Highway and Transportation Department, and Mack-Blackwell National

Rural Transportation Study Center, Department of Civil Engineering, University of Arkansas, Fayetteville, Arkansas.

- Trenter N.A., and Charles, J. A., 1996. A Model Specification of Engineered Fill for Building Purposes. Proceedings of Institute of Civil Engineers, Geotechnical Engineering, v 119, 219–230.
- Van Til, C.J., McCullough, B.A., Val-lerga, and Hicks, R.G., 1972. Evaluation of AASHTO Interim Guides for Design of Pavement Structures. NCHRP 128, Highway Research Board.
- Webster, S. L., Grau, R. H., and Williams, T P., 1992. Description and Application of Dual Mass Dynamic Cone Penetrometer. Final Report GL-92 3, Department of Army Waterways Experiment Station, Vicksburg, Mississippi.
- Webster, S.L., Brown, R.W., and Porter, J. R., 1994. Force Projection Site Evaluation Using the Electric Cone Penetrometer (ECP) and the Dynamic Cone Penetrometer (DCP). Technical Report No. GL-94-17 Air Force Civil Engineering Support Agency, U.S. Air Force, Tyndall Air Force Base, Florida.

## ACKNOWLEDGEMENTS

First of all I would like to acknowledge my major professor Dr. David J White, Assistant Professor, Department of CCEE, for his incredible support and advice throughout this study, Dr. Charles T Jahren, Professor In-Charge, Department of CCEE, and Dr. Jonathan A. Sandor, Department of Agronomy for their constructive comments on this project.

I would like to thank the Highway Division of the Iowa Department of Transportation and the Iowa Highway Research Board who sponsored this study Input and review comments provided by the Technical Steering Team members: Tim Mallicoat, Richard White, Mark Trueblood, David Anthony, David Heer, John Vu, Chris Brakke, and Bob Stanley were very helpful in directing the research tasks for this project.

I would also like to thank Bob Youmie, John Heggen, Wes Musgrove, Doug McDonald, Don Stevens, Dirk Zaiser, Ron Harvey for providing assistance in identifying pavement base and patching projects for testing, and Todd Sirodiak, Adjunct Associate Professor, Department of CCEE, for his timely assistance with project coordination.

I greatly appreciate Dr. Glen Ferguson for his input during development of the new APT device, which was based on the prototype model he developed. Special appreciation and thanks to Dr. Muhannad Suleiman, who wrote the finite difference algorithm to derive the geometric factors for the new APT device.

Mike Adams and Eric Weaver from FHWA provided timely assistance in answering questions of use and interpretation of GeoGauge test measurements. Gerald Voigt from ACPA provided helpful insight into current base material practices at the national level.

The assistance provided in field and laboratory testing by Blake Vosburg, Clinton Halverson, Matthew Cushman, and Deepak Makarla is greatly appreciated.

Last but not the least; I would like to thank my family members, friends, and colleagues for their amenable support throughout my studies, and can not be expressed in words.



**APPENDIX A. GRADATIONS USED BY VARIOUS STATE AND FEDERAL  
AGENCIES**

Sieve Size	Percent Passing																	
	Alabama		Alaska		Arizona		Arkansas		California		Colorado							
	UL	LL	UL	LL	UL	LL	UL	LL	UL	LL	UL	LL						
3"	100	100									100	95						
2 1/2"																		
2"		100		100					100	100								
1 1/2"							100	100	100	87								
1 1/4"																		
1"					100	100	100	60										
3/4"					100	90	90	50	90	45								
5/8"																		
1/2"																		
3/8"					70	50												
1/4"																		
#4																		
#8	75	22			35	23			55	25	50	20						
#10																		
#16																		
#20																		
#30																		
#40									30	10								
#50																		
#60																		
#100					17	5												
#200	38	3	6	0	55	2	10	3	12	0	15	3						

Sieve Size	Percent Passing													
	Connecticut		Delaware		Florida		Georgia		Hawaii		Idaho			
	UL	LL	UL	LL	UL	LL	UL	LL	UL	LL	UL	LL		
3"														
2 1/2"	100	100	100	100					100	100				
2"	100	95			100	100	100	100						
1 1/2"					100	95	100	97	90	65				
1 1/4"														
1"			80	50										
3/4"	75	50			90	65	95	60	70	45				
5/8"														
1/2"														
3/8"					75	45								
1/4"	45	25												
#4			50	20	60	35			45	25				
#8														
#10					45	25	45	25						
#16														
#20			30	10										
#30														
#40	20	5												
#50					25	5								
#60							30	10						
#100	12	2												
#200			20	2	10	0	20	7	9	3				

Sieve Size	Percent Passing													
	Illinois		Indiana		Iowa		Kansas		Kentucky		Louisiana			
	UL	LL	UL	LL	UL	LL	UL	LL	UL	LL	UL	LL		
3"														
2 1/2"									100	100				
2"									100	100				
1 1/2"	100	100			100	100			100	90	100	100		
1 1/4"														
1"	100	90	100	100							100	100		
3/4"			95	75					95	60	100	70		
5/8"														
1/2"	90	60	70	40					70	30				
3/8"			50	20										
1/4"														
#4	60	30	15	0					55	15	65	35		
#8			10	0	20	10								
#10														
#16	40	10												
#20														
#30									20	5				
#40											32	12		
#50					15	0								
#60														
#100														
#200	12	4			6	0			8	0	12	5		

Sieve Size	Percent Passing													
	Maine		Maryland		Massachusetts		Michigan		Minnesota		Mississippi			
	UL	LL	UL	LL	UL	LL	UL	LL	UL	LL	UL	LL		
3"							100	100						
2 1/2"														
2"			100	100					100	100				
1 1/2"			100	70										
1 1/4"														
1"						100	60							
3/4"			85	50										
5/8"														
1/2"	70	45												
3/8"														
1/4"	55	30												
#4			55	30					100	35				
#8														
#10									100	20				
#16														
#20														
#30								35	0					
#40	20	0								50	5			
#50			24	8										
#60														
#100														
#200	5	0	10	3	7	0	0	10	5					

Sieve Size	Percent Passing													
	Missouri		Montana		Nebraska		New Hampshire		Nevada		New Jersey			
	UL	LL	UL	LL	UL	LL	UL	LL	UL	LL	UL	LL		
3"							100	85						
2 1/2"														
2"		100		100										
1 1/2"			100		100	100	90	60			100	100		
1 1/4"														
1"	100	100	80	50							100	95		
3/4"					88	73	70	40						
5/8"														
1/2"	90	55												
3/8"					62	45					80	60		
1/4"														
#4			50	20			40	15						
#8														
#10	50	25			25	15					55	40		
#16											25	5		
#20											8	0		
#30														
#40	30	10												
#50											5	0		
#60														
#100														
#200	3	0	8	0	8	3	5	0						

Sieve Size	Percent Passing													
	New Mexico		New York		North Carolina		North Dakota		Ohio		Oklahoma			
	UL	LL	UL	LL	UL	LL	UL	LL	UL	LL	UL	LL		
3"			100	100										
2 1/2"														
2"			100	90					100	100				
1 1/2"					100	100								
1 1/4"														
1"	100	100			100	80	100	100	100	100	70			
3/4"	100	90					100	95	90	50				
5/8"														
1/2"					83	58	100	85						
3/8"	55	20					90	60						
1/4"			65	30										
#4	10	0			60	38	25	15	60	30				
#8							10	2						
#10					50	28								
#16							5	2						
#20														
#30									33	9				
#40			40	5	33	15								
#50														
#60														
#100														
#200	2	0	10	0	13	6	3	0	13	0				





Sieve Size	Percent Passing													
	Texas		Utah		Vermont		Virginia		Washington		West Virginia			
	UL	LL	UL	LL	UL	LL	UL	LL	UL	LL	UL	LL		
3"														
2 1/2"														
2"														
1 1/2"	100	100	100	100			100	100			100	100		
1 1/4"									100	100				
1"							95	85						
3/4"					91	81					90	50		
5/8"									80	50				
1/2"					77	67								
3/8"	70	50					69	50						
1/4"									50	30				
#4	55	35	53	43							50	20		
#8														
#10							36	20						
#16			29	23										
#20														
#30														
#40	30	15					19	9	18	3	20	5		
#50														
#60														
#100														
#200			10	6			7	4	7.5	0	7	0		



Sieve Size	% Passing					
	AASHTO No. 57		ASTM D 1241		ASTM D 2940	
	UL	LL	UL	LL	UL	LL
3"						
2 1/2"						
2"			100	100	100	100
1 1/2"	100	100			100	95
1 1/4"						
1"	100	95				
3/4"					92	70
5/8"						
1/2"	60	25				
3/8"			65	30	70	50
1/4"						
#4	10	0	55	25	55	35
#8	5	0				
#10			40	15		
#16						
#20						
#30					25	12
#40			20	8		
#50						
#60						
#100						
#200			8	2	8	0

**APPENDIX B: TEST PROCEDURE FOR LABORATORY PERMEABILITY  
TESTING USING LARGE SCALE AGGREGATE COMPACTION MOLD  
PERMEAMETER (ACP)**

### LARGE SCALE AGGREGATE COMPACTION MOLD PERMEAMETER (ACP)

The large scale ACP was built to measure hydraulic conductivity of granular materials. Both constant head and falling head tests can be performed. The ACP consists of a 60 liter capacity water reservoir, large compaction mold with 1 inch diameter hole porous disk at the base and a base mold attached connected to 10 inch diameter butterfly valve. The dimensions of the large scale ACP are shown in Figure B1. The permeameter was built for testing aggregate with particles sizes up to 2 inches.

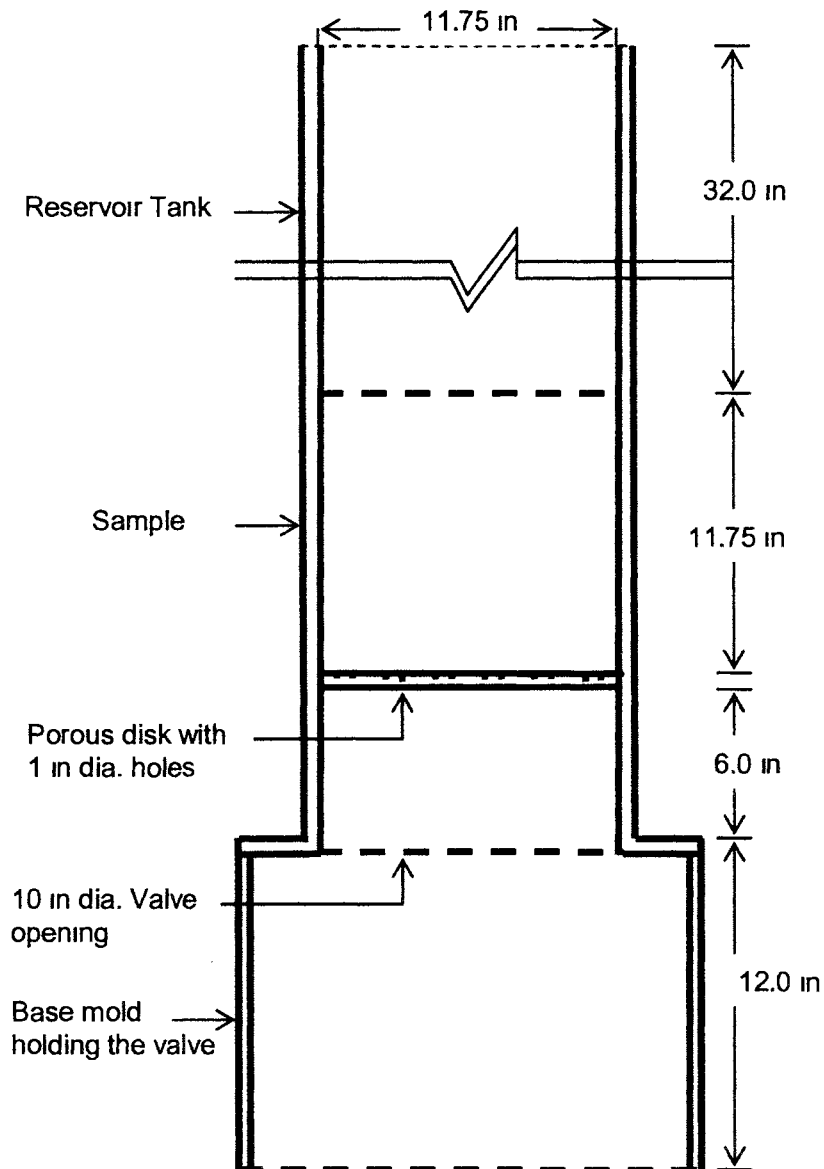


Figure B1. Cross-section of the large scale AC

## EQUIPMENT

The Aggregate Compaction Mold Permeameter (ACP)  
Stop-watch with a precision of up to 1/100<sup>th</sup> second  
Calibrated level indicator attached to the reservoir  
1 inch hose connected from a water supply tank  
Bubble level  
Marshal Impact Hammer

## TEST PROCEDURE

- 1 A level surface should be selected for testing. Place the base mold on two spacer blocks as shown in the Figure B2.



**Figure B2. Base mold placed on the concrete blocks**

2. Place the aggregate compaction mold on the top of base mold. Then place one or two fine screens on the porous disk to minimize washout of finer particles during testing (Figure B3).



**Figure B3. Aggregate compaction mold with screens placed over the base mold**

3. A marshal impact compaction hammer of 6.7 kg weight with 45 cm drop height can be used to compact the sample (Figure B4). To achieve standard proctor compaction energy, the sample should be compacted in 5 lifts with 67 blows per each lift.



**Figure B4. Marshall impact hammer (left) and compaction procedure (right)**

4. After compaction, the reservoir tank is placed over the sample mold. The joints between the reservoir tank and the mold, as well as the mold and the bottom base, are sealed with hose clamps at the joints (Figure B5).



**Figure B5. Final setup ready for testing**

- 5 Next, close the valve attached to the base mold, and fill the reservoir tank to the desired head level. Because of entrapped air in the sample, air bubbles usually appear

in the reservoir tank after filling it with water. The test should not be started until air bubbling has stopped.

6. Falling Head Test: Open the valve, and record the time taken ( $t$ ) for drop in head for each 100 mm as  $H_0$  and  $H_1$ . Repeat for five readings from 90 to 80 cm, 80 to 70 cm, 70 to 60 cm, 60 to 50 cm, and 50 to 40 cm. The water level indicator attached to the reservoir tank is used to measure the change in head.
7. Constant Head Test: Open the valve and adjust the inlet flow of water to maintain constant head in the reservoir. The level indicator attached to the reservoir tank is used to monitor for a steady state flow condition. Once steady state flow is achieved, use the same inlet flow and measure the quantity of water ( $Q$ ) to fill a known volume in time ( $t$ ).
8. Repeat steps 5 and 6 for falling head tests and 5 and 7 for constant head tests.

## MEASUREMENTS AND CALCULATIONS

### *Falling Head Test:*

$H_0$	Initial Head (cm)
$H_1$	Final Head (cm)
$\Delta H$	Change in Head (cm)
$H$	Average Head $(H_0 + H_1)/2$ (cm)
$t$	Time for change in head (sec)
$L$	Length of the sample (cm)
$i$	Hydraulic Gradient, $H/L$ (cm/cm)
$v$	Velocity of flow, $\Delta H/L$ (cm/sec)
$n$	"n" slope of the line in plot between $\log i$ vs. $\log v$

Plot a logarithmic scale with hydraulic gradient ( $\log i$ ) on the x-axis and velocity of flow ( $\log v$ ) on the y-axis. The slope of the line is equal to "n". Use equation  $K = vi^n$  to compute the saturated hydraulic conductivity (cm/sec).

### *Constant Head Test:*

$H$	Head (mm)
$Q$	Quantity of flow in the inlet for a time ( $t$ ), ( $\text{cm}^3/\text{sec}$ )
$t$	Time (sec)
$L$	Length of the sample (cm)
$A$	Area of the sample ( $\text{cm}^2$ )
$i$	Hydraulic Gradient ( $H/L$ ), (cm/cm)

Use Darcy's equation to compute the saturated hydraulic conductivity  $K$  ( $\text{cm}/\text{sec}$ ) =  $Q/(i.A)$ .



**Falling Head Test Measurements**

Test No	$H_0$ (cm)	$H_1$ (cm)	$\Delta H$ (cm) = $H_1 - H_0$	$H$ (cm) = $(H_1 + H_0)/2$	$t$ (sec)	$L$ (cm)	$i = H/L$	$v = \Delta H / t$	$K = v i^n$
1									
2									
3									
4									


**CONSTANT HEAD TEST MEASUREMENTS**

Test No	$H$ (cm)	$Q$ (cm <sup>3</sup> )	$t$ (sec)	$L$ (cm)	$i = H/L$	$A$ (cm <sup>2</sup> )	$K$ (cm/sec) = $Q/(i A)$
1							
2							
3							
4							
5							

**APPENDIX C: RAW DATA FROM LABORATORY TESTING**

Table C1. Summary of results from CBR testing

Material	Penetration	% fines							
		0%	2%	4%	6%	8%	10%	12%	14%
AALS	0.5"	48	<b>55</b>	47	42	38	42	16	19
	0.4"	39	46	46	<b>52</b>	34	40	15	18
	0.3"	29	42	<b>44</b>	40	30	38	16	18
	0.2"	20	34	<b>35</b>	34	23	37	12	17
	0.1"	11	15	<b>18</b>	18	12	35	7	9
	DD (kg/m <sup>3</sup> )	2253.7	2347.0	2423.9	2418.3	2390.1	2412.7	2409.3	2430.0
	DD(pcf)	140.7	146.5	151.3	151.0	149.2	150.6	150.4	151.7
CLS	0.5"	13	17	35	34	<b>55</b>	40	43	35
	0.4"	10	14	30	24	<b>52</b>	35	37	30
	0.3"	7	10	23	19	<b>54</b>	25	34	26
	0.2"	3	5	21	13	<b>45</b>	25	42	19
	0.1"	2	4	18	7	<b>40</b>	12	33	9
	DD (kg/m <sup>3</sup> )	1982.1	1996.0	2058.7	2072.3	2150.7	2159.7	2218.4	2208.8
	DD(pcf)	123.7	124.6	128.5	129.4	134.3	134.8	138.5	137.9
RPCC	0.5"	6	20	23	22	22	<b>22</b>	19	
	0.4"	3	18	19	20	<b>22</b>	19	18	
	0.3"	2	14	14	18	<b>22</b>	16	16	
	0.2"	2	11	10	13	<b>19</b>	11	11	
	0.1"	1	7	5	6	<b>11</b>	5	5	
	DD (kg/m <sup>3</sup> )	1976.9	2016.6	2040.3	2036.1	2229.5	2262.8	2265.1	
	DD(pcf)	123.4	125.9	127.4	127.1	139.2	141.3	141.4	
AG	0.5"	22	<b>43</b>	0	31	0	0	32	25
	0.4"	31	46	0	21	<b>44</b>	18	17	31
	0.3"	20	0	0	18	<b>38</b>	17	20	33
	0.2"	11	26	<b>40</b>	14	27	14	25	20
	0.1"	9	32	<b>43</b>	13	15	6	21	10
	DD (kg/m <sup>3</sup> )	2322.6	2342.4	2392.6	2454.2	2442.7	2448.3	2428.0	2548.0
	DD(pcf)	145.0	146.2	149.4	153.2	152.5	152.8	151.6	159.1
ALS	0.5"	12	20	25	29	32	<b>57</b>	45	39
	0.4"	10	18	24	25	27	<b>45</b>	39	33
	0.3"	9	17	25	21	25	<b>34</b>	25	29
	0.2"	6	15	26	18	21	<b>29</b>	12	23
	0.1"	5	12	25	8	<b>18</b>	15	4	12
	DD (kg/m <sup>3</sup> )	2048.2	2074.7	2190.5	2247.8	2295.4	2340.4	2366.3	2276.7
	DD(pcf)	127.9	129.5	136.7	140.3	143.3	146.1	147.7	142.1
RPCC Ames	0.5"	20	16	18	19	18	31	25	<b>31</b>
	0.4"	21	16	17	19	19	31	23	<b>31</b>
	0.3"	23	18	18	20	20	27	24	<b>33</b>
	0.2"	27	18	18	18	21	18	22	<b>33</b>
	0.1"	30	14	16	14	23	9	20	<b>33</b>
	DD (kg/m <sup>3</sup> )	2303.6	2275.5	2296.1	2287.9	2318.7	2305.6	2251.4	2279.4
	DD(pcf)	143.8	142.1	143.3	142.8	144.8	143.9	140.5	142.3

 indicates the maximum CBR value during respective penetration

**APPENDIX D: DERIVATION AND VALIDATION FOR APT**

## ESTIMATION OF SATURATED HYDRAULIC CONDUCTIVITY FROM APT

Derivation of a relationship to determine the saturated hydraulic conductivity from Air Permeameter Test (APT) field measurements is described in this section. The derivation expands Darcy's Law to consider air compressibility, viscosity of air, and partially saturated field conditions. First, an equation to estimate air permeability ( $L^2$ ) from APT field measurements is derived and then the effect of partial saturation in the aggregate is taken into account to determine intrinsic permeability ( $L^2$ ) and the saturated hydraulic conductivity ( $L/T$ ).

### Darcy's Law

In 1856, Henry Darcy developed a simple equation describing one-dimensional flow of water in saturated porous media for viscous/laminar, steady state, and horizontal flow conditions (neglecting the effect of gravity). The simplified form of Darcy's equation is written as shown in Equation 1. Equation 2 shows the differential form of Darcy's equation (Evans *et al.* 1965)

$$q = KiA \quad (1)$$

$$v = (k/\mu) (dp/dx) \quad (2)$$

Where

$q$  = the flow rate [ $L^3/T$ ]

$K$  = saturated hydraulic conductivity [ $L/T$ ]

$i$  = the hydraulic gradient [ $L/L$ ]

$A$  = the cross sectional area through which the fluid is flowing [ $L^2$ ]

$v$  = Velocity of flow or volume of water per unit time passing unit cross-section [ $L/T$ ]

$k$  = permeability of the medium [ $L^2$ ]

$\mu$  = viscosity of water [ $FT/L^2$ ]

$dp/dx$  = change of pressure with distance [ $F/L^2/L$ ]

Figure D1 shows a soil sample having a cross-sectional area,  $A$ , length,  $L$ , and inlet and outlet pressures of  $P_1$  and  $P_2$ , respectively. For water flowing through the soil, compressibility effects are neglected, and velocity of flow ( $v$ ) is assumed to be uniform along the length of the sample. Thus, the change in pressure with distance ( $dp/dx$ ) is constant along the length of the sample (Equation 3). Velocity of flow ( $v$ ) can be related to the quantity of water flowing through the cross-sectional area ( $A$ ) per unit time as shown in Equation 4. Substituting Equations 3 and 4 into Equation 1, Equation 5 can be used to calculate the flow rate (Muskat, 1937).

$$dp/dx = \text{constant} = (P_1 - P_2)/L \quad (3)$$

$$v = Q/A \quad (4)$$

$$Q = (k/\mu) A (P_1 - P_2)/L \quad (5)$$

Where:

$Q$  = flow rate or quantity of water flowing through a sample per unit time [ $L^3/T$ ],

$A$  = cross-sectional area of the sample [ $L^2$ ],

$L$  = Length of the sample [ $L$ ],

$P_1$  = Inlet Pressure [ $F/L^2$ ],

$P_2$  = Outlet Pressure [ $F/L^2$ ].

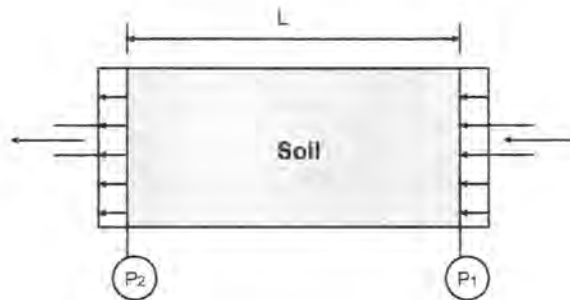


Figure D1. Sample indicating pressure at inlet and outlet

### Derivation of Air Permeability

Muskat (1937) reported that Darcy's law is valid for air permeability by only considering the compressibility of air. This implies that air velocity and change in pressure,  $dp/dx$ , are no longer uniform through the sample. Muskat (1937) made the following assumptions:

1. Steady state mass flux along the flow path is constant ( $\gamma V = \text{constant}$ ), where  $\gamma$  is the density of air, and  $V$  is volume. Considering volume of flow per unit cross-section per unit time,  $\gamma v$  is also constant, where  $v$  is velocity of flow
2. Flow is isothermal,  $p = \gamma RT$  where  $R$  is the gas constant and  $T$  is the temperature in degrees Kelvin.

Combining these assumptions,  $p v$  is also a constant. If Equation 2 is multiplied by  $p$  (Equation 6), the left hand side becomes constant and can be integrated along the tube length,  $L$  resulting in Equation 7. Next take  $p$  as  $P_1$ , and  $v=Q/A$ , and substitute in Equation 7 to form Equation 8. This relationship was proven experimentally by Muskat and Botset (1931). The coefficient of permeability  $k$ , can then be calculated by rearranging Equation 8 as shown in Equation 9

$$p v = (k/\mu) p (dp/dx) \quad (6)$$

$$pvL = (k/\mu) (P_1^2 - P_2^2)/2 \quad (7)$$

$$P_1 (Q/A) L = (k/\mu) (P_1^2 - P_2^2)/2 \quad (8)$$

$$k = (2 Q \mu P_1)/(A/L) (P_1^2 - P_2^2)/2 \quad (9)$$

Equations 6 through 9 were derived for one dimensional flow however air permeability field measurements is a three dimensional problem (Figure D2). Therefore, geometry of the instrument, sample boundary conditions, and pressure distributions must to be considered. Evans and Kirkham (1949) used an analogy of flow of electricity to calculate a geometric factor ( $A'$ ) to account for inlet and outlet diameters of an air permeameter (Figure D3). This geometric factor did not consider the sample dimensions or the pressure distribution however. Goggin *et al.* (1988) introduced an alternative geometric factor ( $G_o$ ) for steady state gas flow that considers instrument and sample geometry, and pressure distributions (Figures D2 and D4). The relationships proposed by Goggin *et al.* (1988) use a modified form of Darcy's law to determine  $G_o$ .

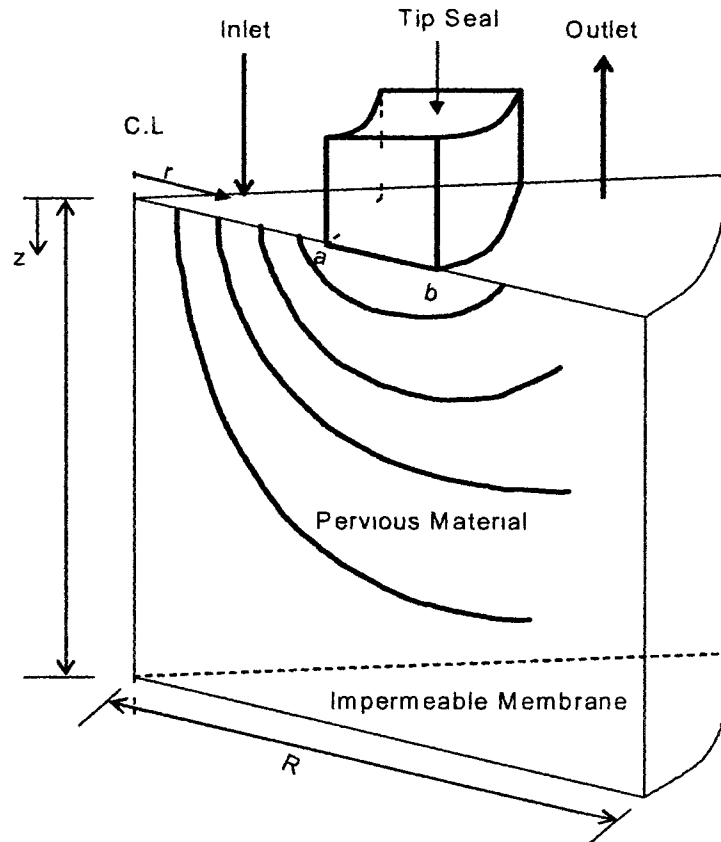


**Figure D2. Showing a three dimensional setup for Air Permeability Testing (Modified from Goggin et al. 1988)**

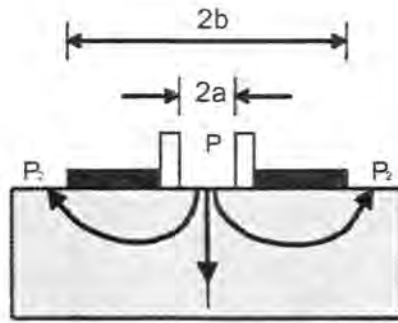


Figure D3. Geometrical effect used by Evans and Kirkham (1949)

According to Darcy's theory the velocity of flow and quantity of discharge through a porous media are directly proportional to the hydraulic gradient which is true only for viscous/laminar flow conditions. The water flow condition in open-graded base material is very often seen to be non-laminar even at low hydraulic gradients (Aggregate Handbook, 1996). The transition between laminar and non-laminar flow can be represented using Reynolds Number ( $R_e$ ).  $R_e$  less than 2000 represents laminar flow conditions (Cedergren, 1988). To avoid the complexities of non-laminar flow the APT device was designed to determine the permeability at a low pressure, low flow and laminar condition.

Figures D2 and D4 show the cross-section and geometry of the APT device, having an inlet diameter of  $2a$  and a tip seal outer diameter of  $2b$ , and a soil sample having a thickness of  $L$  and radius of  $R$ . The theory and procedures used to calculate the geometric factor for the device are summarized below

First, all dimensions can be expressed in dimensionless form by dividing by "a" (Equations 10 to 14).

$$b_D = b/a, \quad (10)$$

$$L_D = L/a, \quad (11)$$

$$R_D = R/a, \quad (12)$$

$$r_D = r/a, \text{ and} \quad (13)$$

$$z_D = z/a, \quad (14)$$



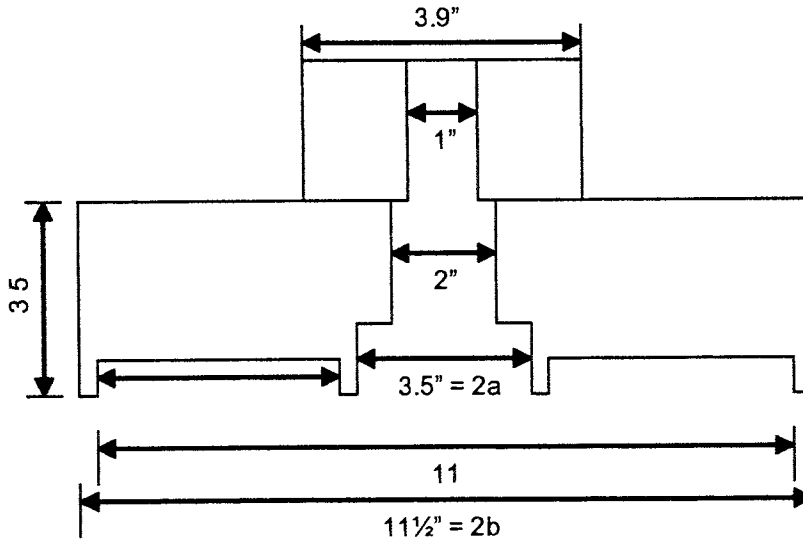


**Figure D4. Cross-section of the Air Permeability Testing (APT) Device developed at Iowa State University**

### *Modified Darcy's Law*

As discussed earlier, Darcy's law indicates that the rate of flow of fluid through a cross sectional area (mass flux) equals the hydraulic conductivity multiplied by the hydraulic gradient. Using this relationship, but considering a two-dimensional flow condition Goggin *et al.* (1988) defined the mass flux across the inlet surface of an air permeameter as the permeability of the medium ( $k$ ) multiplied by the partial derivative of the pressure spatial distribution ( $m\{\phi\}$ ) with respect to depth ( $z$ ) as the modified Darcy's law or the differential form of Darcy's law (Equation 15). Assuming radially symmetrical flow in a homogenous and isotropic material, the gas inlet mass rate is given by Equation 16. Replacing the vertical mass flux ( $\rho u_z$ ) across the inlet face by the differential form of Darcy's law as a function of the spatial pressure distribution ( $m\{\phi\}$ ) (Equation 15), the inlet mass rate can be written as shown in Equation 17 where  $G_o$  is defined using dimensionless parameters as shown in Equation 18. This relationship indicates that the geometric factor is a function of spatial pressure distribution, tip seal size and soil sample size.

$$\rho u_z = k_0 \frac{\partial m\{\phi\}}{\partial z} \quad (15)$$

$$m_o = \int_0^{2\pi} \int_0^a \{\rho u_z\}_{z=0} r dr d\theta \quad (16)$$

$$m_o = -a G_o (b_D, R_D, L_D) k_0 \Delta m\{\phi\} \quad (17)$$

$$G_o(b_D, R_D, L_D) = 2\pi \int_0^1 \left\{ \frac{\partial m_D}{\partial z_D} \right\}_{z_D=0} r_D dr_D \quad (18)$$

Where:

$\rho u_z$  = mass flux in z direction [M/T L<sup>2</sup>],

$k_o^\infty$  = sample permeability [L<sup>2</sup>],

$m\{\phi\}$  = pressure as a function of z and r coordinates (spatial pressure distribution) [M/TL<sup>3</sup>],

$m_o$  = inlet mass rate [M/T],

$G_o$  = Geometric factor which is a function of ( $b_D, R_D, L_D$ ) [dimensionless].

### Mass Conservation

Considering the steady state flow of a compressible fluid (i.e. air in this case) in a homogenous and isotropic media, the mass conservation equation in a cylindrical coordinate system is shown in Equation 19. Substituting the mass flux using the differential form of Darcy's law, Equation 19 can be presented as shown in Equation 20. This equation is presented in dimensionless terms as shown in Equation 21 where  $m_D$  is the dimensionless spatial pressure distribution.

$$\frac{1}{r} \frac{\partial}{\partial r} (r \rho u_r) + \frac{\partial}{\partial z} (\rho u_z) = 0 \quad (19)$$

$$\frac{1}{r} \frac{\partial}{\partial r} \left[ r k_o^\infty \frac{\partial m\{\phi\}}{\partial r} \right] + \frac{\partial}{\partial z} \left[ k_o^\infty \frac{\partial m\{\phi\}}{\partial z} \right] = 0 \quad (20)$$

$$\frac{1}{r_D} \frac{\partial}{\partial r_D} \left[ r_D k_o^\infty \frac{\partial m_D}{\partial r_D} \right] + \frac{\partial}{\partial z_D} \left[ k_o^\infty \frac{\partial m_D}{\partial z_D} \right] = 0 \quad (21)$$

The boundary conditions for the dimensional equation (Equation 20) are summarized in Equation 22 and the boundary conditions for the dimensionless equation (Equation 21) are provided in Equation 23

Dimensional Boundary Conditions:

$$\begin{aligned} P_{\text{inlet}} &= P_1 && \text{for } 0 \leq r \leq a, z=0 \\ P_{\text{outlet}} &= P_o && \text{for } b \leq r \leq R, z=0 \text{ and } 0 \leq z \leq L, r=R \\ \frac{\partial P}{\partial z} &= 0 && \text{for } a \leq r \leq b, z=0 \text{ and } 0 \leq r \leq R, z=L \end{aligned} \quad (22)$$

Dimensionless Boundary Conditions:

$$\begin{aligned}
 m_D\{\phi_0\} &= 0 \quad \text{for } b_D \leq r_D \leq R_D, z_D = 0; \quad 0 \leq z_D \leq L_D, r_D = R_D, \quad \text{and } 0 \leq r_D \leq R_D, z_D = L_D \\
 m_D\{\phi_1\} &= 1 \quad \text{for } 0 \leq r_D \leq 1, z_D = 0 \\
 \frac{\partial m_D\{\phi\}}{\partial z} \Big|_{z=0} &= 0 \quad \text{for } 1 \leq r_D \leq b_D, z_D = 0
 \end{aligned} \tag{23}$$

### *Finite Difference Analysis*

To calculate the geometric factor using Equation 18, the dimensionless spatial distribution of the pressure as a function of  $z_D$  and  $r_D$  is required. However, Equation 21 with the boundary conditions provided in Equation 23, cannot be solved analytically. Hence, the finite difference numerical method using an iterative approach was used to solve the dimensionless spatial pressure distribution parameter ( $m_D$ ). The procedure followed is outlined in Figure D5. The soil sample was discretized into a number of nodes (or points) representing the corners of small squares with a length ( $h = 0.1$  in). The dimensionless spatial pressure at a node  $i, j$  was calculated as a function of the dimensionless pressure at the surrounding nodes.

After calculating the dimensionless spatial pressure at all nodes, the calculated value of dimensionless pressure at each node was compared with the values calculated in the previous step at the same node. If the maximum difference (Max X) of dimensionless pressure at a node  $i, j$  calculated at two successive iterations was greater than the preset convergence criteria,  $\epsilon$ , (0.01), a new set of dimensionless pressure distribution parameters are calculated. However, if the calculated maximum difference is less than  $\epsilon$ , the system converges and the iterative solution is stopped.

Once convergence is achieved, the derivative of the dimensionless spatial pressure (Equation 18) is calculated using the forward derivative definition and the converged values of the dimensionless spatial pressure. The integration shown in Equation 18 was evaluated numerically using Simpson's rule (see Rajasekaran, 1985).

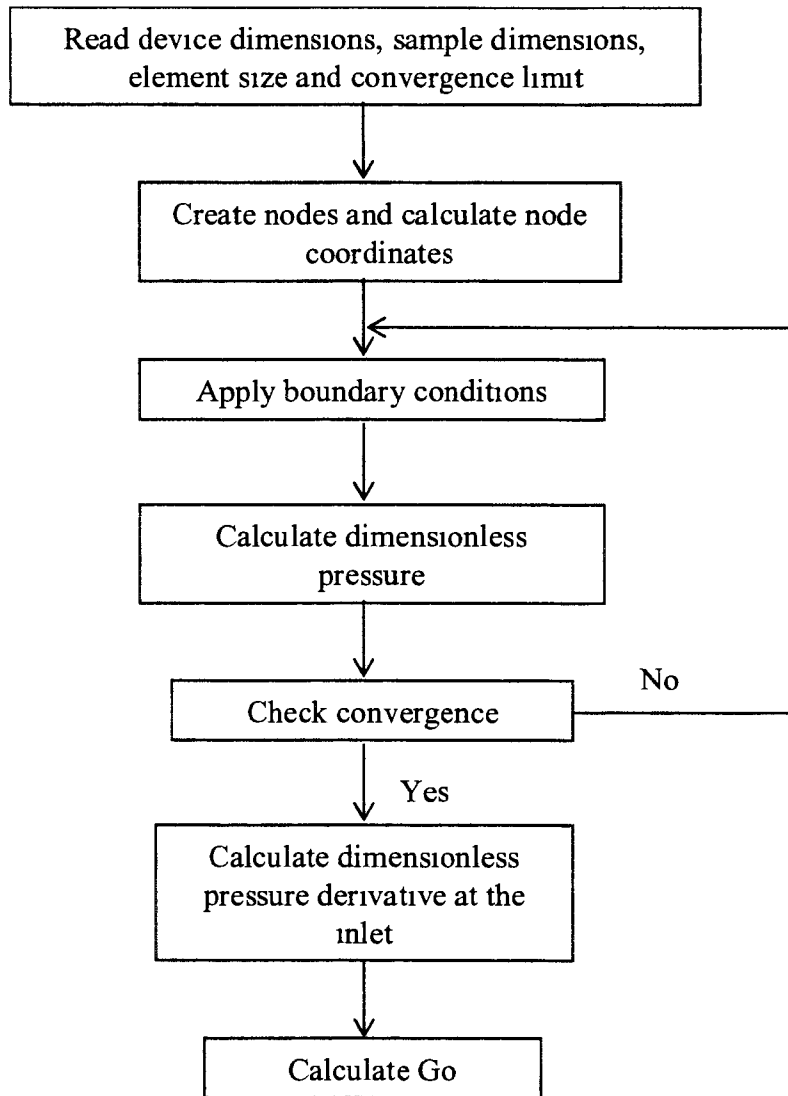


**Figure D5.** Flowchart of the code written to calculate the geometric factor  $G_o$ .

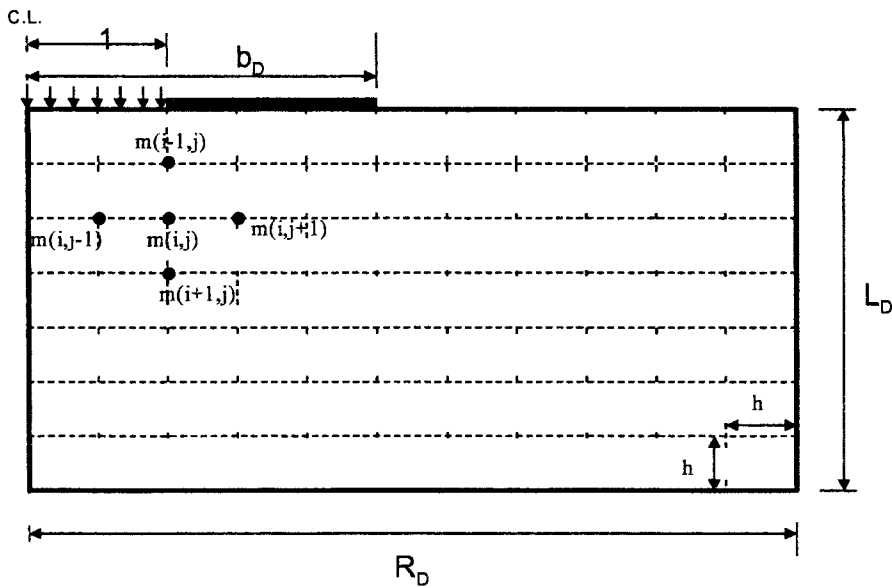


**Figure D6. Finite difference nodes and the dimensions of the sample used in the analysis**

### Results

Figure D7 shows the dimensionless spatial pressure distribution calculated using the code written by the research team. It shows that, the flow of gas is concentrated near the contact surface of the tip seal, which indicate that this region dominates the flow pattern and consequently the mass rate versus injection pressure relationship and the geometric factor value. To validate the results several points were compared with the results reported in Goggin *et al.* (1988). Figure D8 shows an  $R^2$  value of 0.9882 for the compared points and a  $45^\circ$  line of  $R^2$  value of 1. Values of  $G_o$  were also compared with the values presented in Goggin *et al.* (1988) for different  $R_D$  and  $L_D$  values which showed a difference less than 1%.  $G_o$ , for the device dimensions shown in Figure D4, were calculated for two soil samples having radius of 18 and 12 inches and thickness of 4, 6, 8, 12 and 24 inches. Figure D9 shows the geometric factor results for the Air Permeability Testing (APT) device developed at Iowa State University as a function of sample radius and thickness.

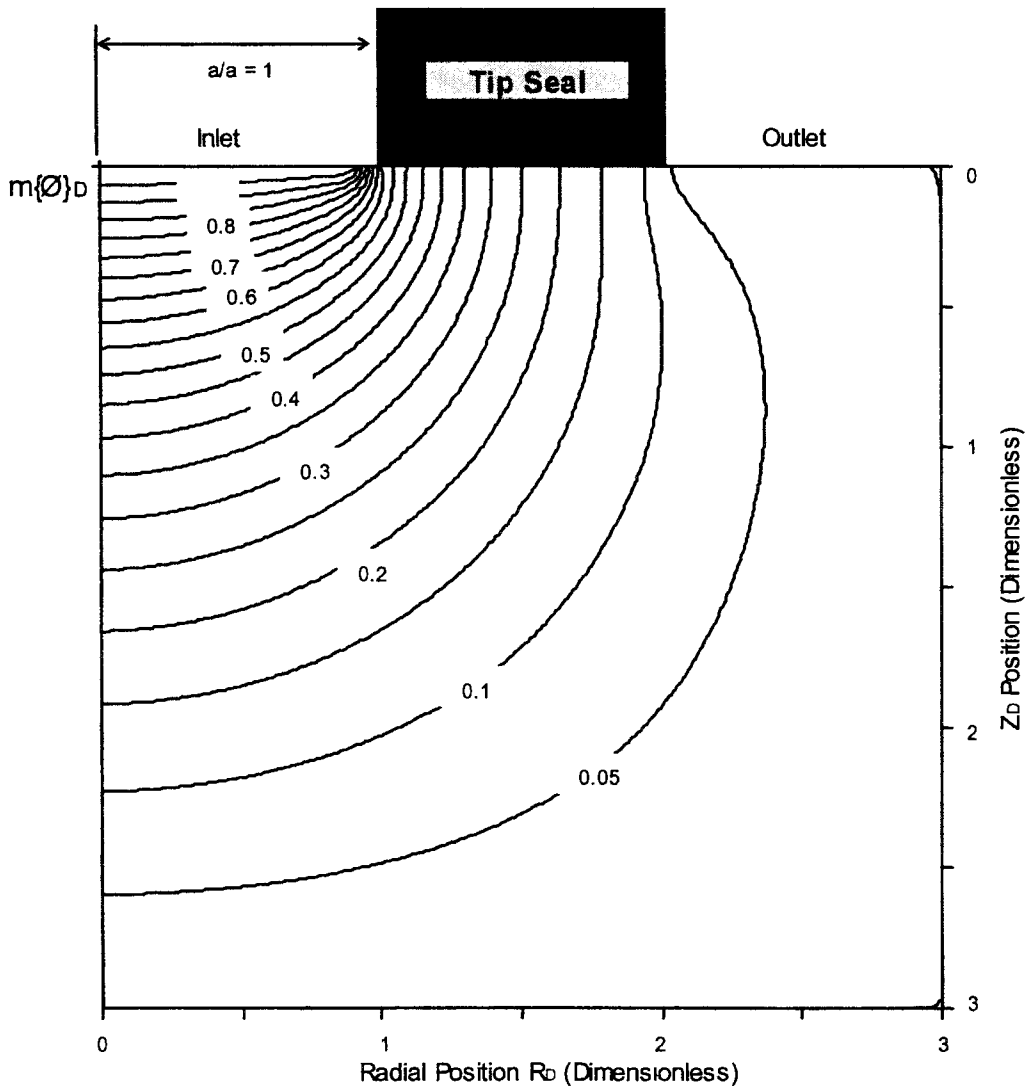


**Figure D7 Showing Dimensionless Pseudo-Potential Contours for the case of  $bD=2$ ,  $RD=LD=3$ ,  $a=1$**

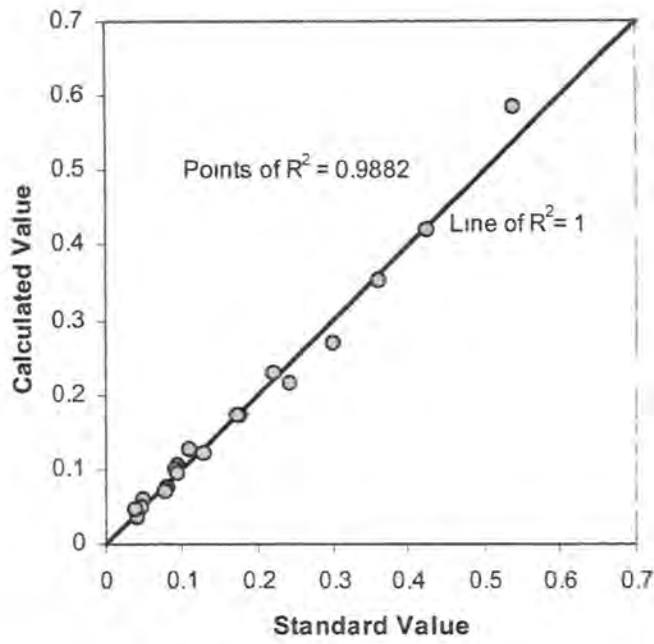


Figure D8. Comparison of calculated  $m \{ \phi \}$  values with values from Goggin et al. (1988).

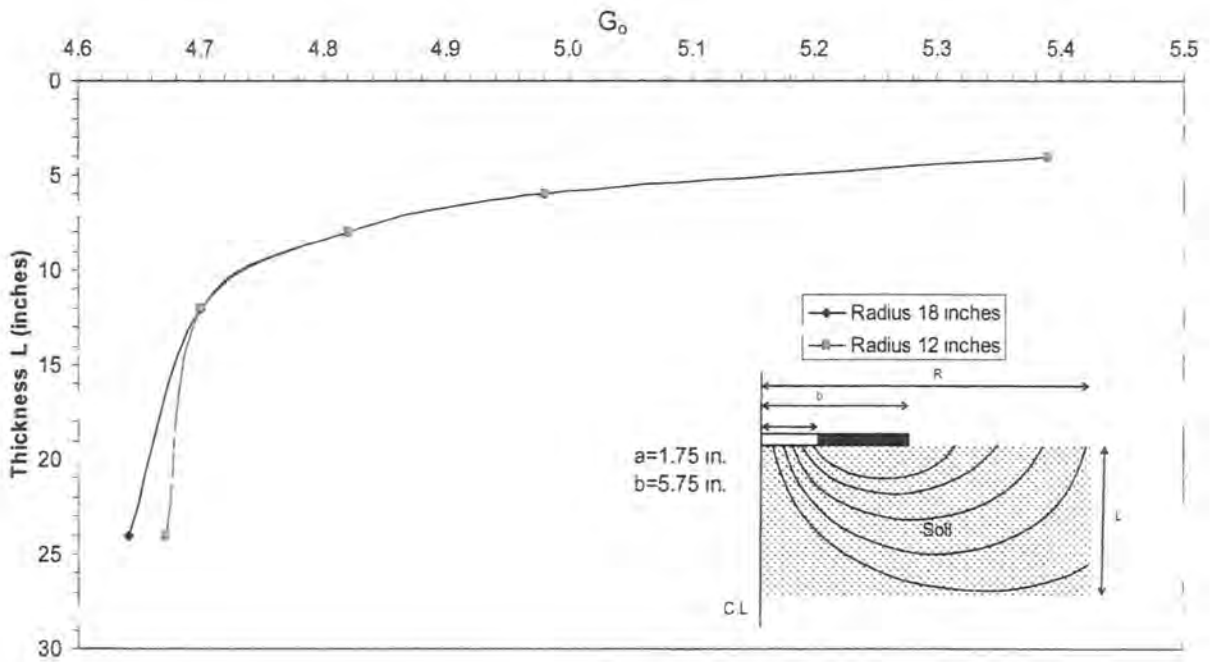


Figure D9  $G_0$  curve showing the effect of sample size

Using the calculated geometric factor,  $G_o$ , which depends on the sample dimensions, the sample air permeability can be calculated using Equation 24 (Goggin *et al.* 1998):

$$k_{\text{air}} = 2\mu_{\text{air}}Q P_1 / a G_o (P_1^2 - P_2^2) \quad (24)$$

Where:

- $k_{\text{air}}$  = air permeability ( $\text{cm}^2$ )
- $\mu_{\text{air}}$  = kinematic viscosity of air (Pa.S)
- $Q$  = volumetric flow rate ( $\text{m}^3/\text{sec}$ )
- $P_1$  = inlet pressure (Pa)
- $P_2$  = outlet pressure or atmospheric pressure (Pa)
- $b_D$  = dimensionless tip radius ( $b/a$ )
- $a$  = radius of tip (cm)
- $b$  = outer radius of tip
- $G_o$  = Geometric factor (dimensionless)

As mentioned earlier the air permeability decreases as soil saturation increases since less area is available through which flow can take place (Evans *et al.* 1965). To calculate a material property at full saturation (intrinsic permeability in this case), the effect of partial saturation needs to be considered as a function of saturation and particle size distribution.

### Effect of Partial Saturation

Brooks and Corey (1964) developed an expression to calculate the relative permeability to air as a function of degree of saturation and pore-size distribution of the sample (Equation 25).

$$k_{\text{ra}} = (1 - S_e)^2 (1 - S_e^{(2+\lambda/\lambda)}) \quad (25)$$

Where:

- $k_{\text{ra}}$  = relative permeability to air (dimensionless),
- $S_e$  = effective water saturation [ $S_e = (S - S_r)/(1 - S_r)$ ],
- $\lambda$  = Brooks-Corey pore size distribution index assumed as 4.0,
- $S_r$  = residual water saturation, assumed as water saturation at bulking moisture content,
- $S$  = water saturation.

### Calculation of Saturated Hydraulic Conductivity



Knowing the air permeability ( $L^2$ ) and the relative permeability to air using the procedure described above, the next step is to calculate the intrinsic permeability (Equation 26) which in turn can be used to calculate saturated hydraulic conductivity (Equation 27) (Army Corps, 2001).

$$k_{air} = k_i * k_{ra} \quad (26)$$

$$K = (k_i \rho g) / \mu_{water} \quad (27)$$

Where:

$k_{air}$  = air permeability ( $cm^2$ ) (from Equation 16)

$k_i$  = intrinsic permeability ( $cm^2$ )

$k_{ra}$  = relative air permeability (dimensionless)

$K$  = Saturated hydraulic conductivity ( $cm/sec$ )

$\rho$  = density of water ( $g/cm^3$ )

$g$  = acceleration due to gravity ( $cm/sec^2$ )

$\mu_{water}$  = absolute viscosity of water ( $gm/cm-sec$ )

Substituting equations 24, 25 and 26 in to 27, the saturated hydraulic conductivity can be determined (Equation 28).

Therefore:

$$K = \left[ \frac{2\mu_{air}QP_1}{a G_o(P_1^2 - P_2^2)} \right] \times \frac{\rho g}{\mu_{water}(1 - S_e)^2(1 - S_e^{(2+\lambda/\lambda)})} \quad (28)$$

## Conversions

As the field data is not similar as the units mentioned above, conversion of all these factors is required. The standard values of water at 20° C are as follows (Pau chang lu, 1979):

$$\begin{aligned} \mu_{air} &= 1.81 \text{ E-5 Pa-sec} \\ \mu_{water} &= 0.01 \text{ gm/cm-sec} \\ a &= 1.75 \text{ in} = 4.45 \text{ cm} \\ P_2 &= 101325 \text{ Pa} \\ \rho &= 1 \text{ g/cc} \\ g &= 981 \text{ cm/sec}^2 \\ \lambda &= 4.0 \text{ (assumed)} \end{aligned}$$

Pressure measured in the field needs to be multiplied by 249.08 to convert from inches of water to Pa. Hence  $P_1 = (101325 + 249.08 P)$ , where  $P$  is the measured pressure in the field.

Flow rate  $Q$  measured in the field needs to be multiplied by 7.8659 to convert from  $\text{ft}^3/\text{hr}$  to  $\text{cm}^3/\text{sec}$ . Hence the final equation to compute the saturated hydraulic conductivity  $K$  ( $\text{cm}/\text{sec}$ ) using the Air Permeability Testing Device is given as:

$$K \text{ (cm/sec)} = \frac{6.277 Q (249.08 P + 101325)}{\{G_o ((249.08 P + 101325)^2 - 1.0266E10) \times (1 - S_e)^{-1} (1 - S_e^{1.5})\}} \quad (21)$$

### Sample Calculation

Data from field:

- $Q$  = flow rate =  $80 \text{ ft}^3/\text{hr}$
- $P$  = pressure =  $0.285 \text{ in. of water}$
- $L$  = thickness of base =  $6 \text{ in.}$
- $S$  = saturation =  $40\%$
- $S_r$  = residual saturation =  $5\%$  (assumed)

*Calculations:*

$$S_e = (0.4 - 0.05) / (1 - 0.05) = 0.368$$

$$G_o = 4.97 \text{ (from Figure D9)}$$

Substituting all the values in Equation 21

$$K \text{ (cm/sec)} = \frac{6.277 \times 80 \times (249.08 \times 0.285 + 101325)}{\{4.97 \times ((249.08 \times 0.285 + 101325)^2 - 1.0266E10) \times (1 - 0.368)^{-1} (1 - 0.368^{1.5})\}}$$

$$\Rightarrow K = 2.18 \text{ cm/sec}$$

### Air Permeameter Test (APT) Results Vs. Laboratory Permeability Test Results

Hydraulic conductivity determinations from the APT at maximum and minimum densities measured in the field are compared to the laboratory measurements on samples compacted to similar densities. Laboratory tests were performed using the Large Scale Aggregate Compaction Mold Permeameter (ACP) in accordance with the test procedure provided in Appendix B.

The hydraulic conductivity measurements of various materials at maximum and minimum densities from both field and lab are provided in Table D1. Figure D10 shows the mean hydraulic conductivity values from field and lab with their upper and lower limits of measurement. The variation between lab and field measurements is attributed to the non-uniformity of the material in the field. The comparison tests in the lab were uniformly mixed and compacted. Thus, it should be recognized that a material with change in gradation, particle orientation etc., changes the hydraulic conductivity properties significantly but not necessarily the global density calculations.

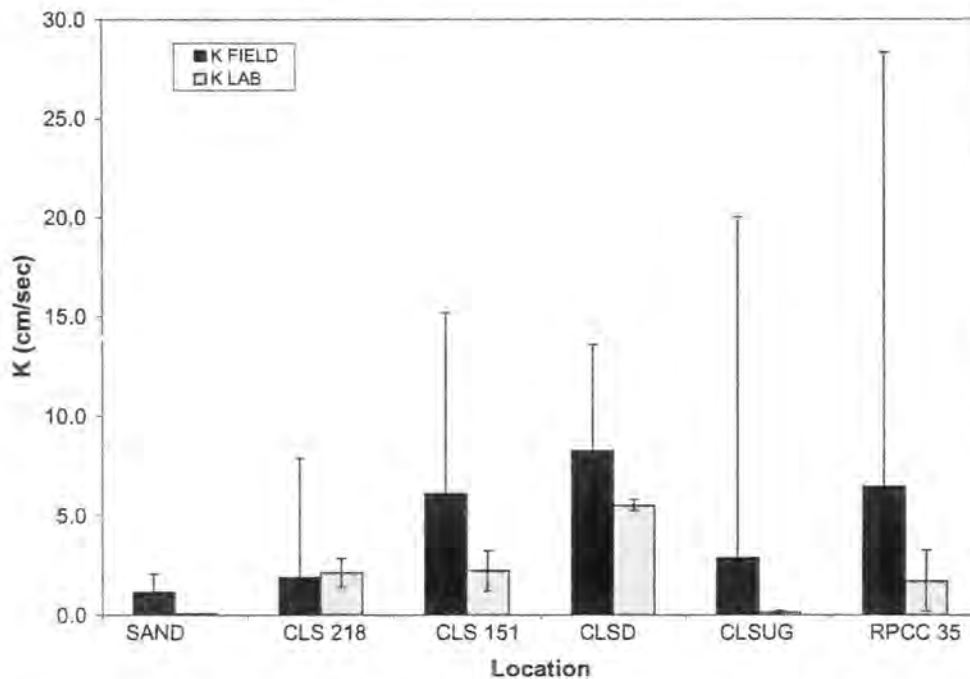
**Table D1. Maximum and Minimum Hydraulic Conductivity values in Field and Lab**

Material	FIELD		LAB	
	$K_{Max}$	$K_{Min}$	$K_{Max}$	$K_{Min}$
Sand	2.06	0.25	0.09	0.07
CLS218	7.91	0.23	2.83	1.39
CLS151	15.18	0.83	3.22	1.22
CLSD	13.60	6.43	5.81	5.25
CLSUG	20.02	0.10	0.21	0.06
RPCC35	28.35	0.93	3.24	0.20

Notes:

 $K_{Max}$  = Hydraulic Conductivity at Minimum Density $K_{Min}$  = Hydraulic Conductivity at Maximum Density

Variability in hydraulic conductivity measurements in field are shown in Figure D11. The left part of the figure shows APT results from the field, whereas the right part shows the water permeability tests from the lab. The final compacted sections both in lab as well as the field can result in segregated layers with changes in local density. First considering the laboratory testing, the water should pass through all the layers present in the sample, thus measuring the lowest possible permeability. Secondly, considering the field testing, the air tends to move through the pores having least resistance, thus measuring the highest possible permeability. However, it should be noticed that the movement of water in the pavement base will also be through the material having least resistance. Thus it can be concluded that the air permeability measurement simulates the field conditions in a more appropriate way than the conventional laboratory test methods.

**Figure D10. Comparison of Laboratory vs. Field Hydraulic Conductivity Measurements**

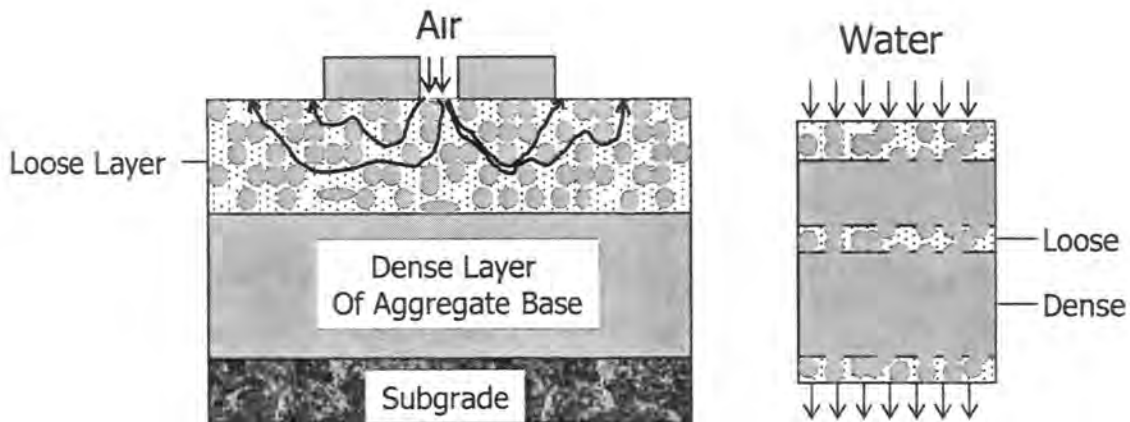


**Figure D11. Comparing the Type of Measurement in Field (left) and Lab (right)**

The APT device demonstrates as a rapid quality control tool in determining the saturated hydraulic conductivity of granular bases in few seconds. Also, tests can be performed at various locations in a few minutes to ensure uniformity of the final base layer. However, there are also a few limitations of APT as follows:

- The APT can not be performed on areas having steep slopes ( $> 10\%$ ).
- Material properties including dry density and degree of saturation are needed to determine the saturated hydraulic conductivity. An approximate of all these parameters for a wide range of base materials has been established. But for better accuracy measurement of in-situ dry density and moisture content is recommended.

**APPENDIX E. METHOD OF TEST IN-SITU PERMEAMETER TEST (APT) FOR  
GRANULAR MATERIALS**

## METHOD OF TEST IN-SITU AIR PERMEAMETER TEST (APT) FOR GRANULAR MATERIALS

### SCOPE

This test method describes the procedure for determining the in-situ hydraulic conductivity of granular base materials using the air permeameter test (APT). Measurements are limited to materials with hydraulic conductivity  $\geq 10^{-2}$  cm/s.

### DEFINITION

**Air Permeability** – It is defined as a factor of proportionality between the rate of air flow and the pressure gradient along the flow distance.

**Saturated Hydraulic Conductivity** – It is defined as the rate of discharge of water at 20°C under conditions of laminar flow through a unit cross-sectional area of a soil medium under a unit hydraulic gradient

### APPARATUS

The APT device is shown in Figure 1. The device consists of the contact ring, console, two flow meters and two differential pressure gauges (DGP's). The DGP's are attached to the outflow end of the contact ring. A compressed air tank with regulator is connected to the APT through a ¼ in. diameter hose. Neoprene foam is attached to the bottom of the contact ring to prevent leakage between the bottom of the contact ring and the ground surface.

### EQUIPMENT

- A. Air Permeameter Test (APT) device with two flow meters (0 to 100 cu ft/hr and 0 to 200 cu ft/hr) and two differential pressure gauges (0 to 0.25 in of water and 0 to 1 in of water),
- B. Compressed air tank and regulator
- C. ¼ in. hose with quick connections at both ends,
- D. A wrench to fix the regulator to the compressed air tank,
- E. 1 in. thick neoprene foam of 11 in. diameter with a 4 in. diameter hole in the center

### TEST PROCEDURE

The APT is a rapid in-situ test device for determining the hydraulic conductivity of granular bases in 20 to 30 seconds. Air permeability measurements are converted to saturated hydraulic conductivity values using Equation A. Steps to perform the test are as follows:

- A. Connect the pressure regulator to the compressed air tank.
- B. Connect the compressed air source to the APT device using the ¼ in. hose and quick connector
- C. Seat the instrument at the test location by leveling the instrument using a bubble level. The initial pressure reading will not be zero unless the instrument is leveled. If the instrument cannot be leveled, note the initial pressure reading as  $P_0$ .
- D. Start by turning the DPG valve towards the pressure gauge which has a measuring range of 0 to 0.25 in. of water

- E. Open the pressure regulator connected to the air tank to about 20 psi.
- F. Gently open the flow regulator fixed on the flow meter which has 0 to 100 cu ft/hr measuring range, and let the air flow through the system. During this process the 0 to 200 cu ft/hr flow meter should be closed. As the air flows through the system a rise in the bubble level can be seen in the flow meter
- G. As the air flows into the aggregate layer pressure builds up as indicated by a rise in pressure in the DPG. Increasing the flow rate increases the pressure.
- H. Record the flow reading as "Q" and its respective pressure reading as "P<sub>1</sub>" at five different flow rates (e.g. 20, 40, 60, 80, 100 cu ft/hr).
- I. If the flow rate exceeds 100 cu ft/hr close the flow meter and slowly open the 0 to 200 cu ft/hr flow meter
- J. If the pressure exceeds 0.25 in. of water stop the air flow by closing the flow regulator and turn the DPG value towards the pressure gauge having 0 to 1 in. of water measuring range.
- K. After measuring the pressures at five different flow rates close the flow meters and relocate the APT for additional tests. Because of the rapid data collection, several test points can be tested and averaged.

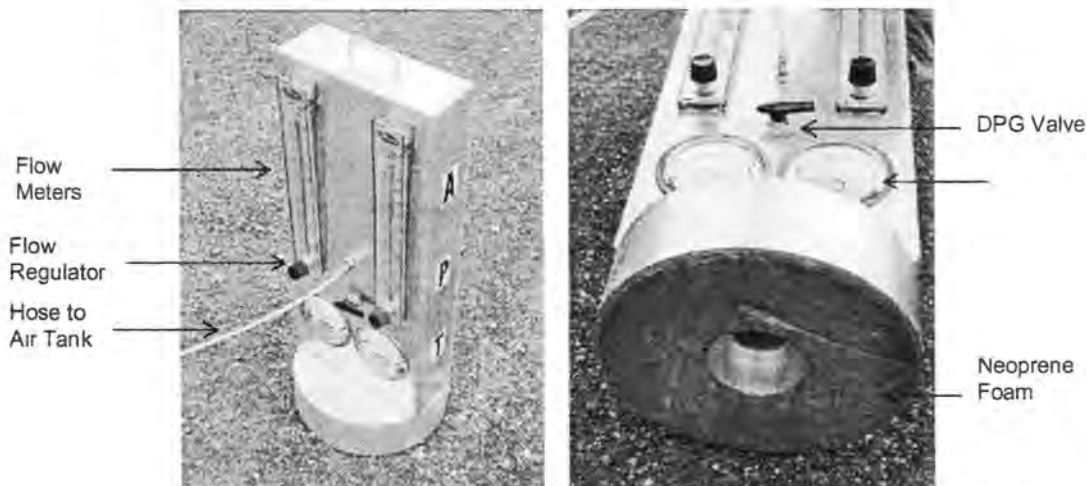


Figure 1. Air Permeameter Test (APT) Device

### CALCULATIONS

- A. Determine the Geometric Factor ( $G_0$ ) based on the estimated thickness of the aggregate layer (L) at the test location.
- B. Use the range of saturation values provided in Table 1 to estimate "S" for the calculations. For better accuracy, determine the in-situ dry density and moisture contents at each test location.
- C. Calculate the saturated hydraulic conductivity K (cm/sec) using the relationship:

$$K \text{ (cm/sec)} = \frac{6.277 Q (249.08 P + 101325)}{\{G_0((249.08 P + 101325)^2 - 1.0266E10) \times (1 - S_e)^2 (1 - S_e^{1.5})\}} \quad [A]$$

Where:

- K = saturated hydraulic conductivity (cm/sec)
- P =  $P_1 - P_0$  = measured pressure – initial pressure (inches of water)
- Q = flow rate (cu ft/hr)
- $G_0$  = Geometric factor determined from Figure 2
- $S_e$  = Effective saturation [ $S_e = (S - S_r)/(1 - S_r)$ ]
- S = Field saturation (from Table 1)
- $S_r$  = Residual saturation % (assumed to be 5% for most granular materials)

**Table 1. Typical saturation values (S) for various base materials**

Material	Range of Saturation, S%
Open-Graded Crushed Limestone	18 to 26
Dense-Graded Crushed Limestone	22 to 40
Open-Graded Recycled Concrete	18 to 26
Dense-Graded Recycled Concrete	34 to 46
Special Back Fill Material	22 to 46
Modified subbase	35 to 55

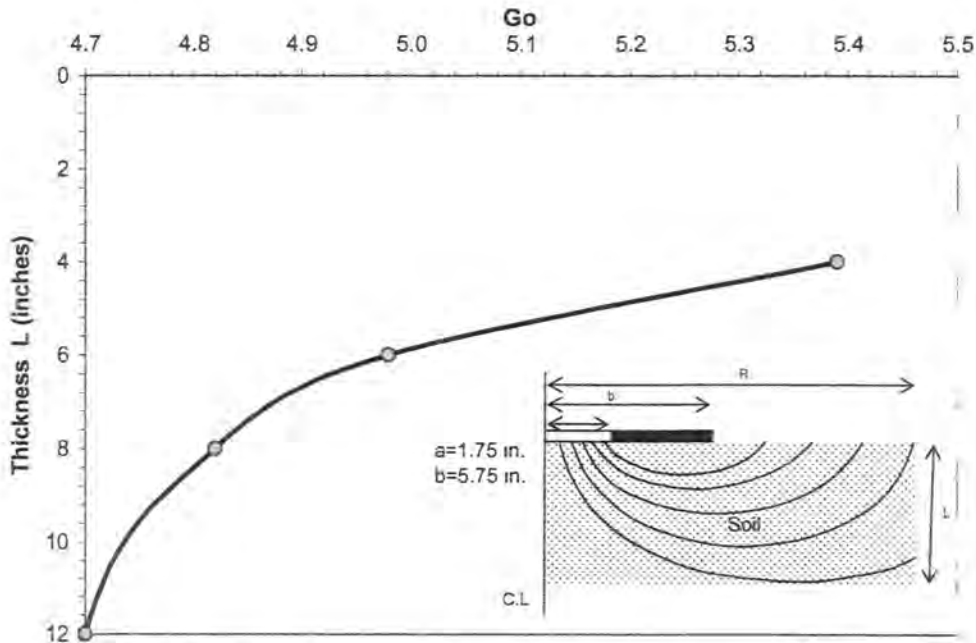


**Figure 2. Graph to determine Geometric factor  $G_0$  for APT Device**



**SAMPLE CALCULATIONS**

A. Data obtained from test location 1 in field:

$P_0$  = Initial pressure = 0.015 in of water

$P_1$  = Measure pressure = 0.3 in of water

$Q$  = Flow rate = 80 cu ft/hr

$L$  = Thickness of base = 6 in.

$S$  = Field saturation = 40%

$S_r$  = Residual Saturation = 5% (assumed)

Calculations:

$P$  = Actual  $P = P_1 - P_0 = 0.285$  in of water

$G_o$  = Geometric factor from Figure 2 for  $L$  at 6 in = 4.97

$S_e = (0.4 - 0.05) / (1 - 0.05) = 0.368$

Substituting all the values in Equation A.

$$K \text{ (cm/sec)} = \frac{6.277 \times 80 \times (249.08 \times 0.285 + 101325)}{\{4.97 \times ((249.08 \times 0.285 + 101325)^2 - 1.0266E10) \times (1 - 0.368)^2 (1 - 0.368^{1.5})\}}$$

$\Rightarrow K = 2.18$  cm/sec.

*Note: 1 cm/sec = 2835 ft/day*



**APPENDIX F · CONTOUR GRAPHS**

**CONTOUR GRAPHS FOR THE DATA FROM 35TH STREET MODIFIED  
SUBBASE CONSTRUCTION**



Figure F1. Aerial Photograph of the Test Location (Iowa DOT, 2004)

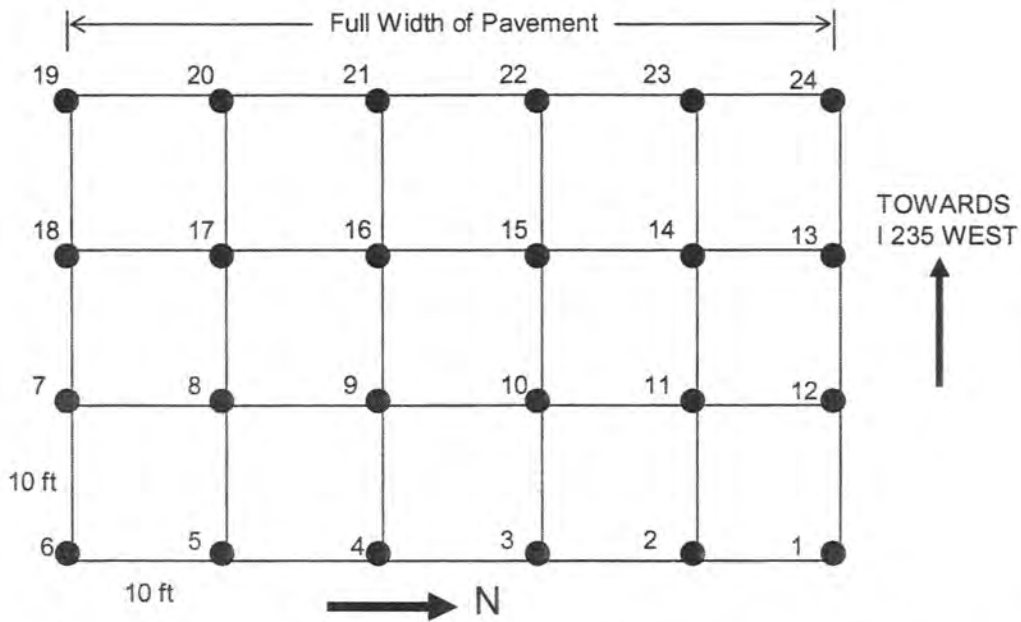


Figure F2. Grid Setup for Testing at 35<sup>th</sup> street Modified Subbase Construction Site

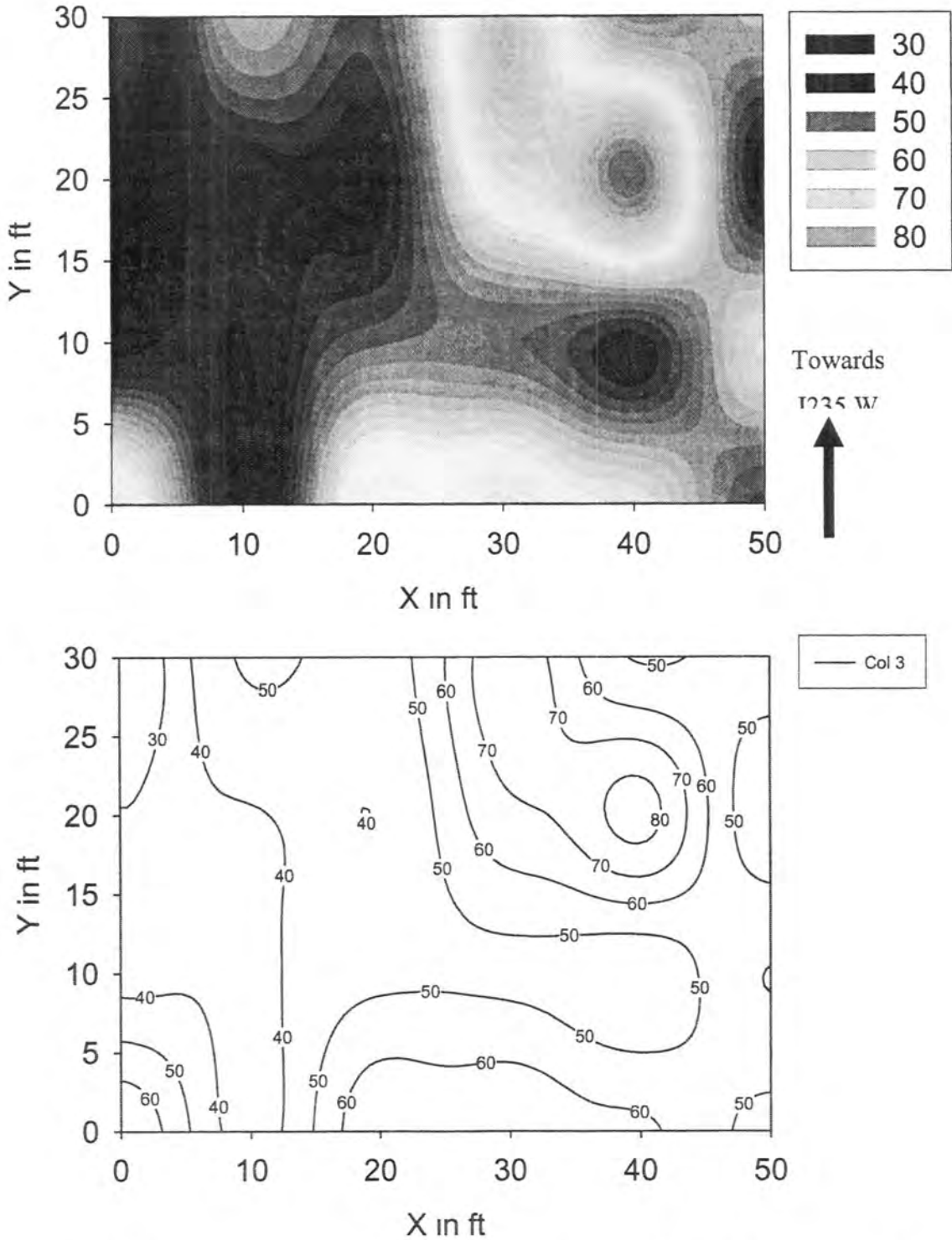


Figure F3. Spatial variation of GeoGauge Modulus (MPa) at 35<sup>th</sup> Street, DSM, Pavement Subbase Test Section

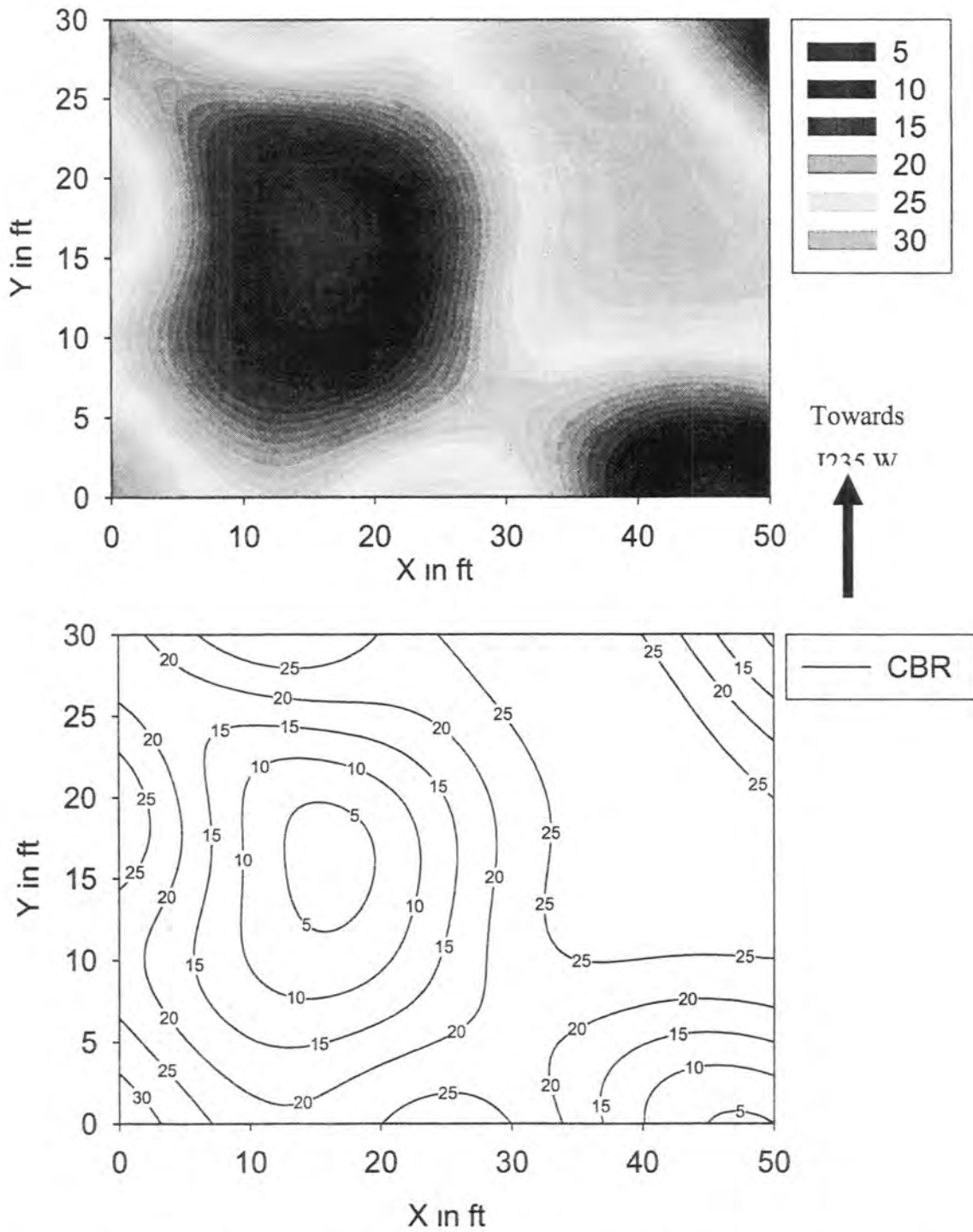


Figure F4. Spatial variation of CBR% at 35<sup>th</sup> Street, DSM, Pavement Subbase Test Section

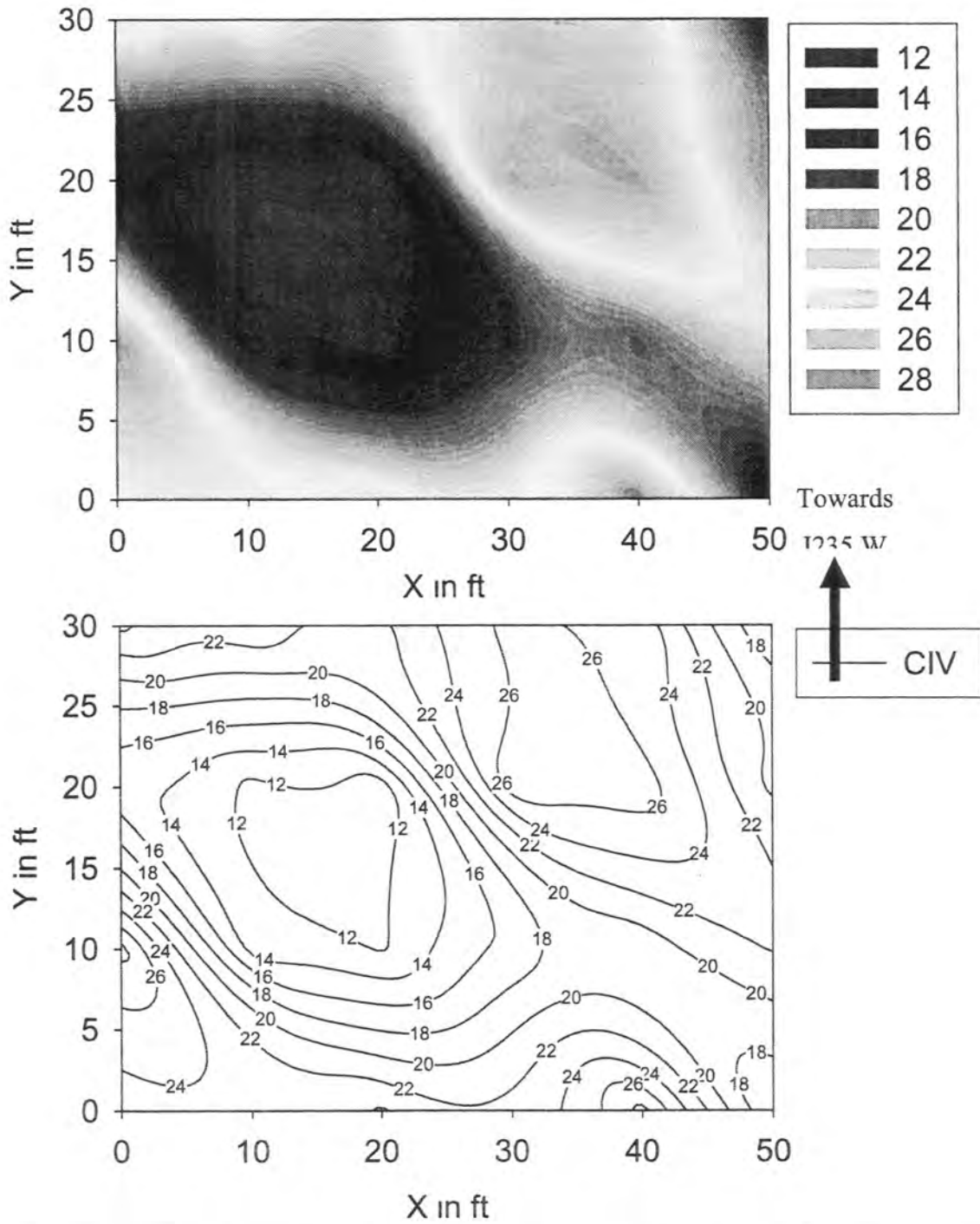


Figure F5. Spatial variation of Clegg Impact Value (CIV) at 35<sup>th</sup> Street, DSM, Pavement Subbase Test Section



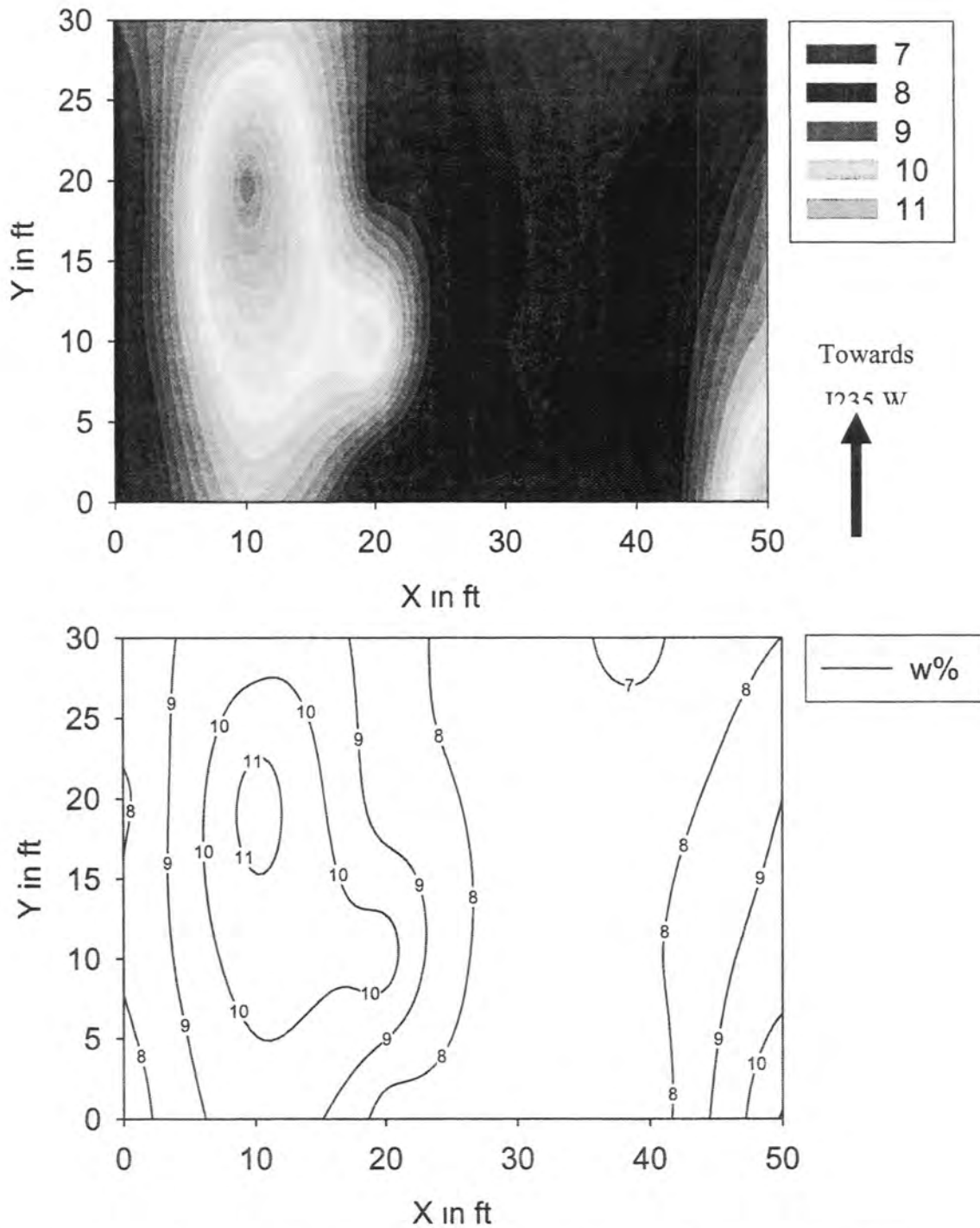


Figure F6. Spatial variation of Moisture Content (w %) at 35<sup>th</sup> Street, DSM, Pavement Subbase Test Section

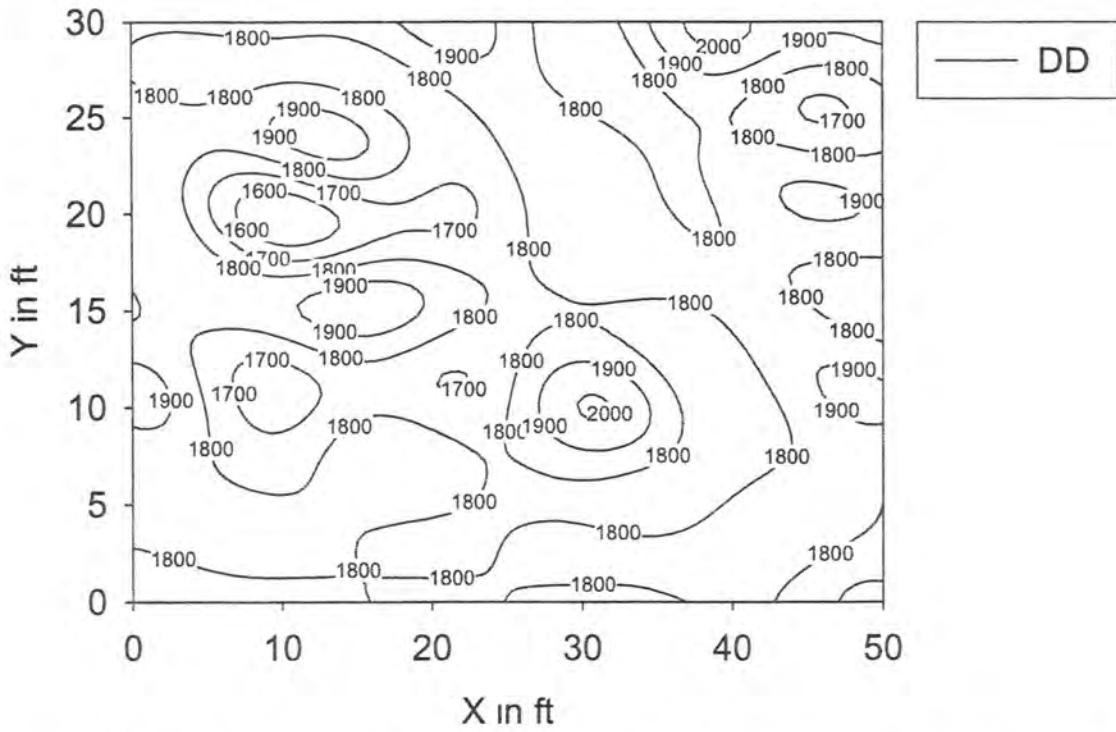
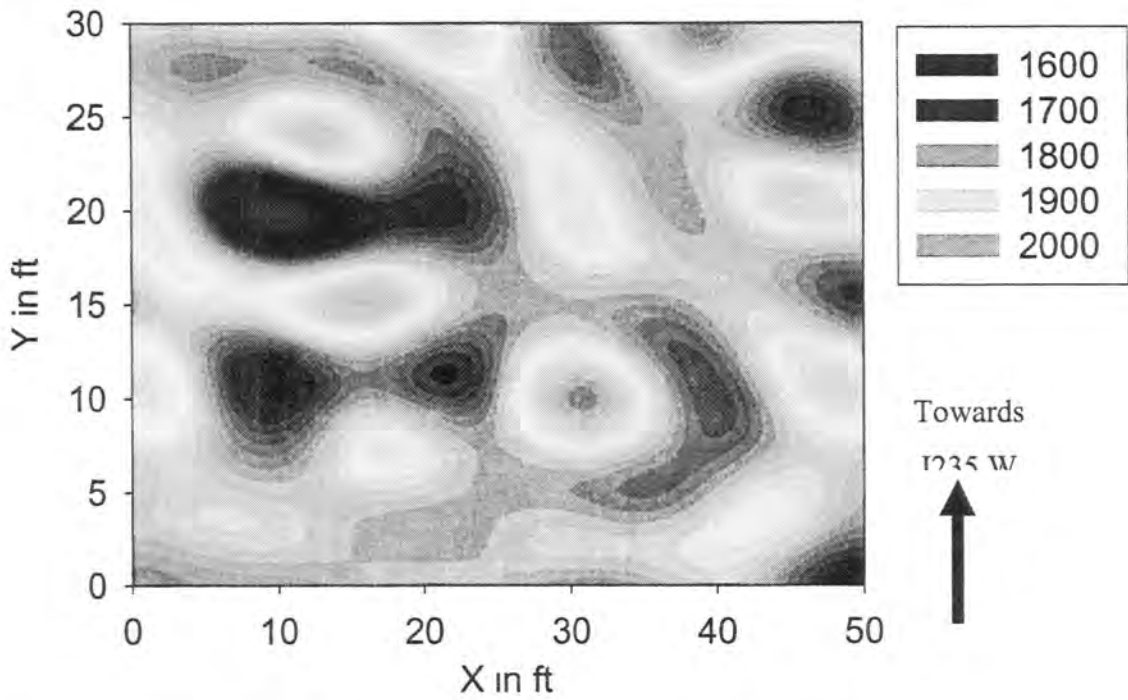


Figure F7 Spatial variation of Dry Density ( $\text{kg/m}^3$ ) at 35<sup>th</sup> Street, DSM, Pavement Subbase Test Section

**CONTOUR GRAPHS FOR THE DATA FROM KNAPP STREET BASE  
CONSTRUCTION**



Figure F8. Aerial Photograph of the Test Location (IDNR, 2004)

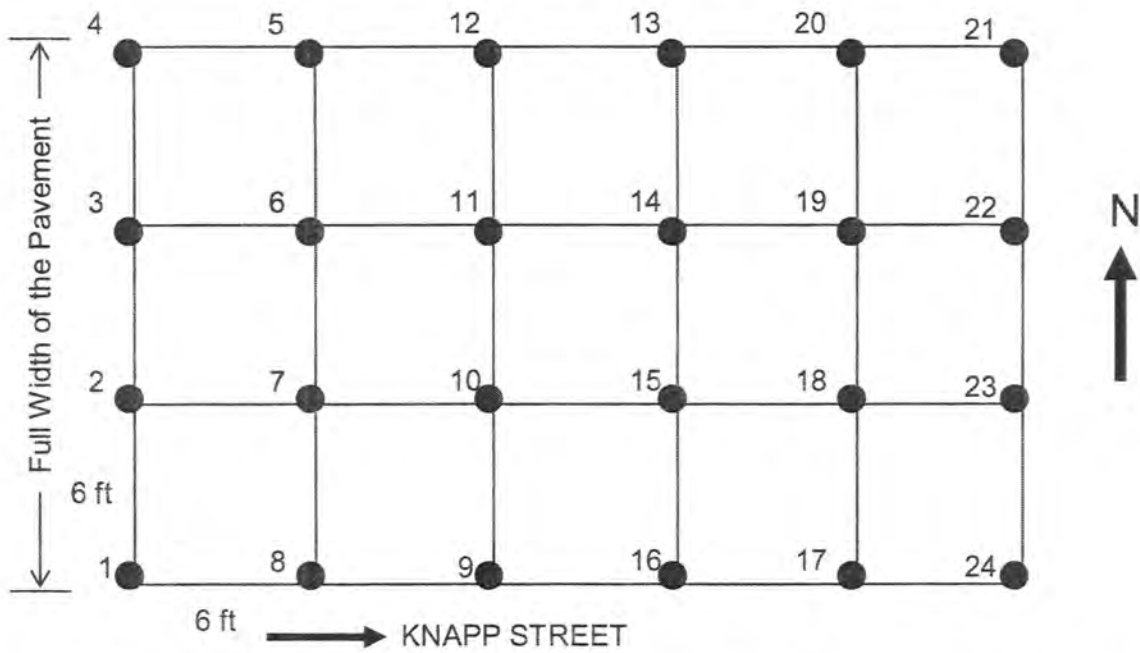
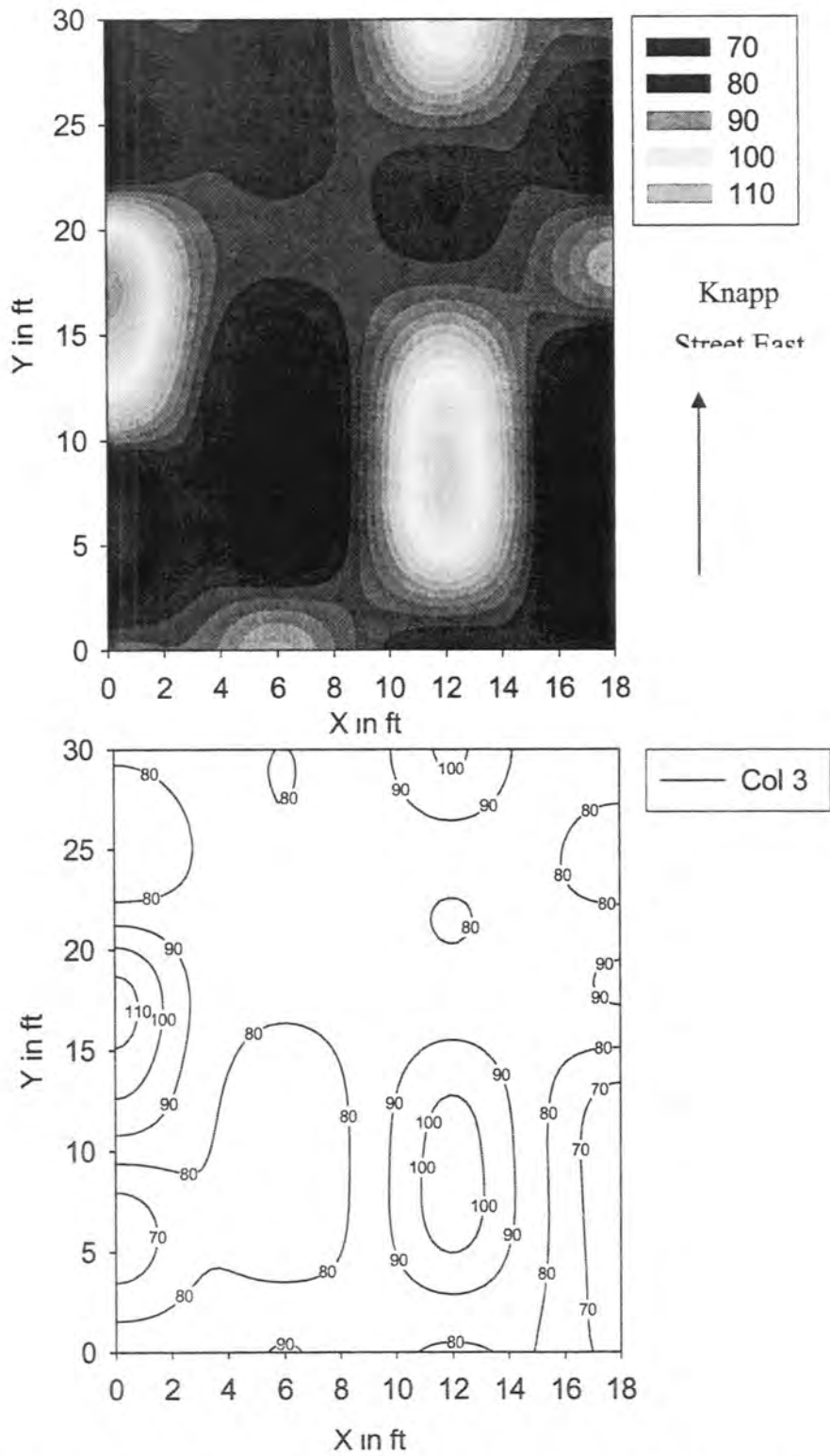


Figure F9. Grid Setup for Testing at Knapp Street Base Construction Site



**Figure F10. Spatial variation of GeoGauge Modulus (MPa) at Knapp Street, Ames, Pavement Base Test Section**

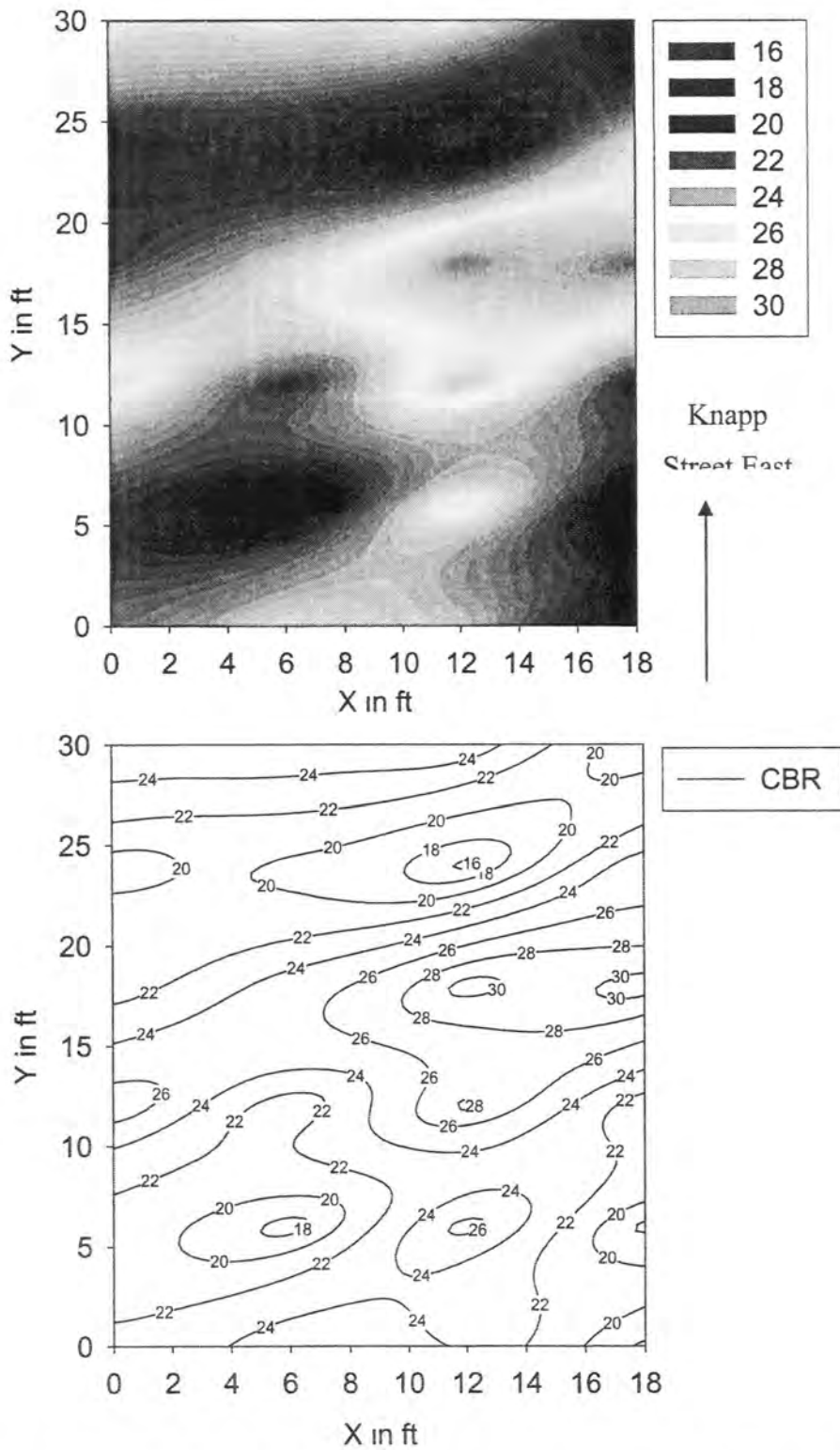


Figure F11. Spatial variation of CBR% at Knapp Street, Ames, Pavement Base Test Section

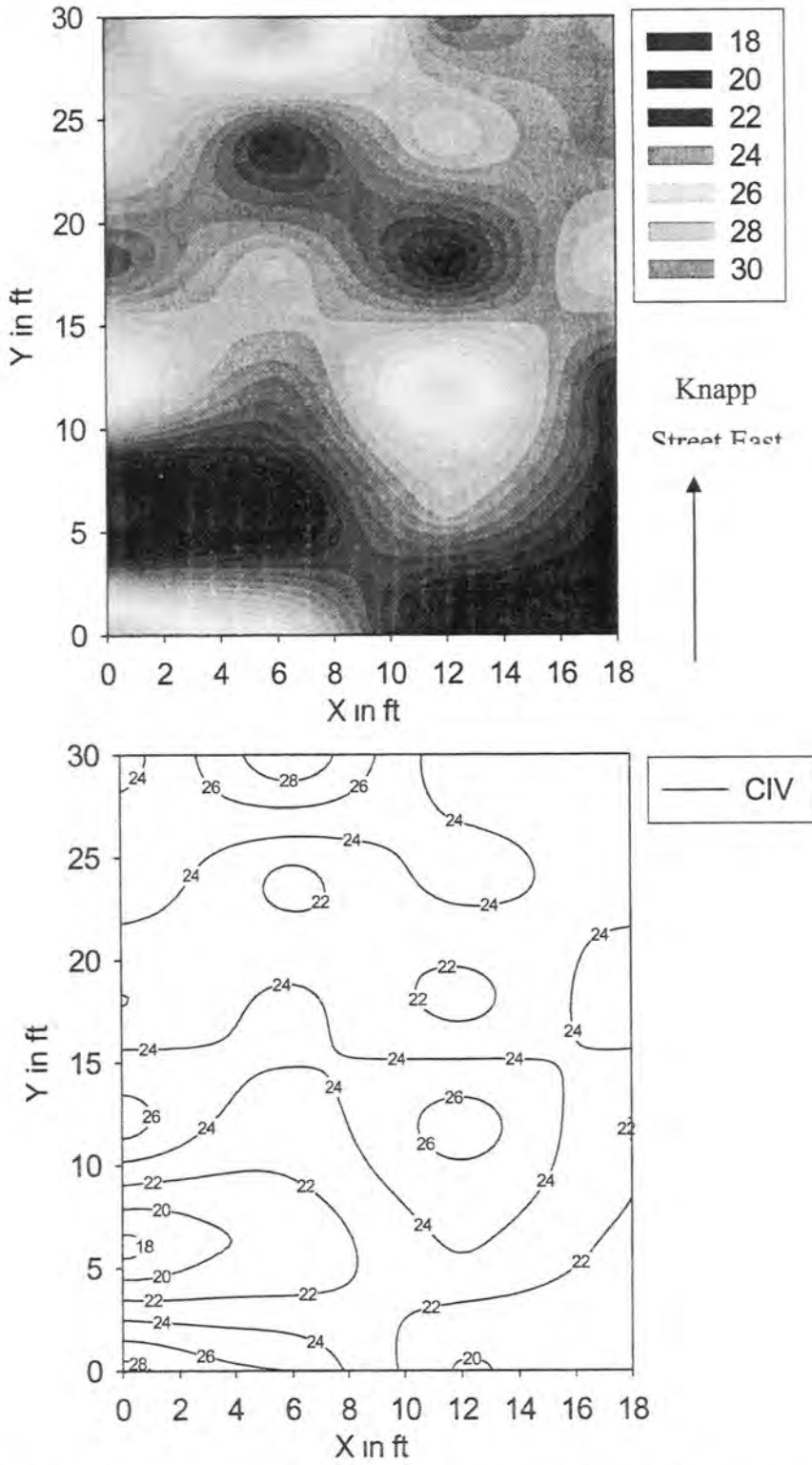
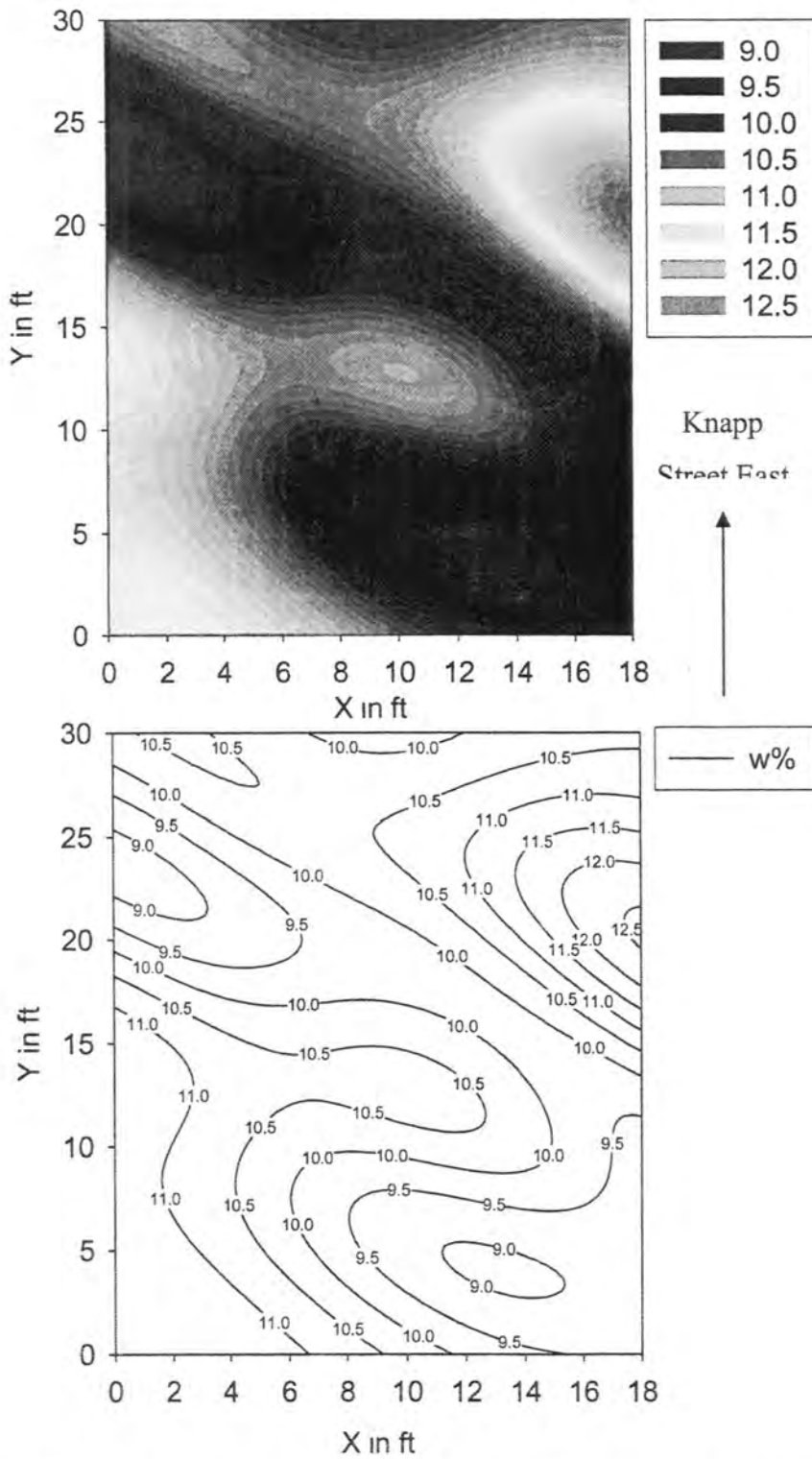


Figure F12. Spatial variation of Clegg Impact Value (CIV) at Knapp Street, Ames, Pavement Base Test Section



**Figure F13. Spatial variation of Moisture Content (w%) at Knapp Street, Ames, Pavement Base Test Section**



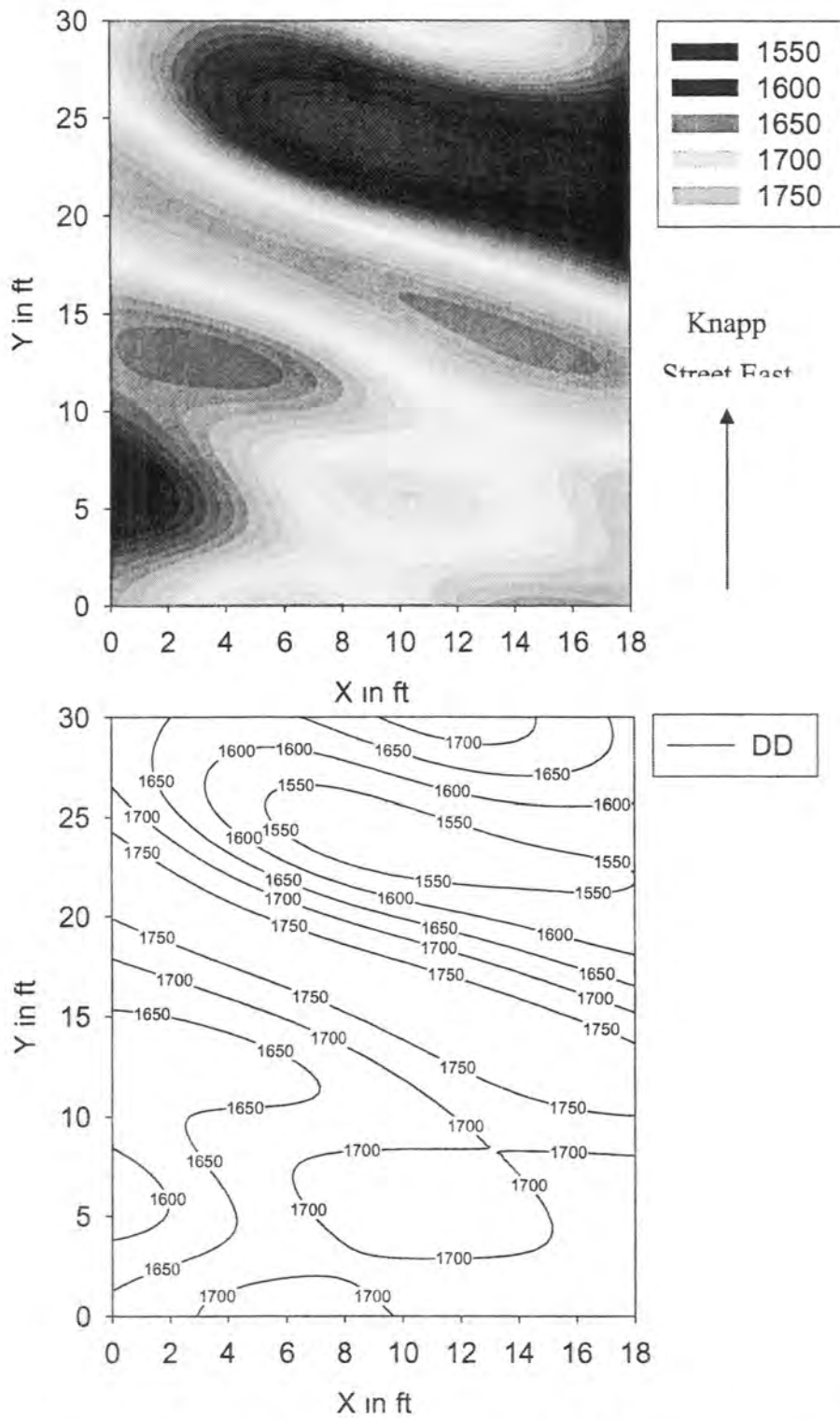
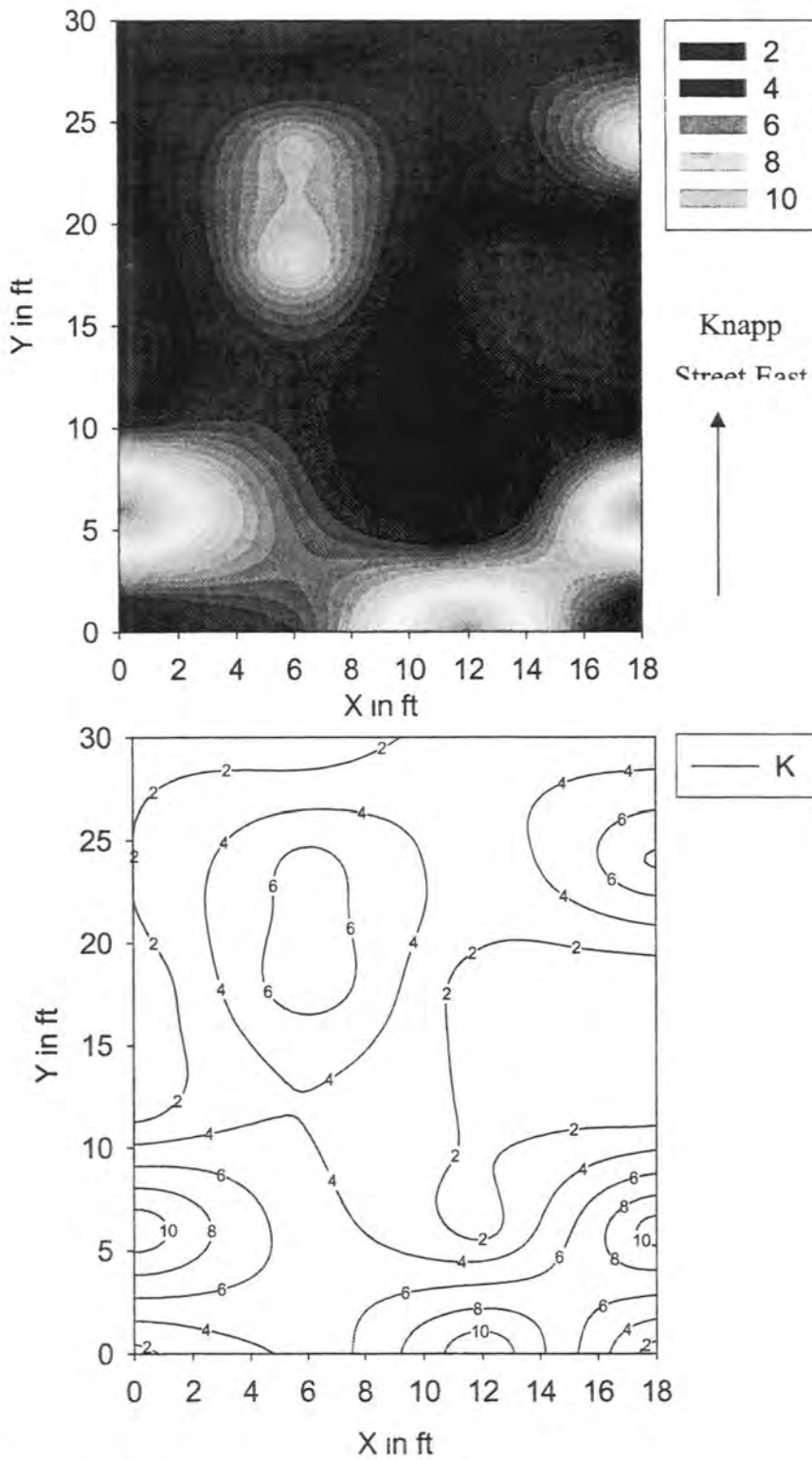


Figure F14. Spatial variation of Dry Density ( $\text{kg/m}^3$ ) at Knapp Street, Ames, Pavement Base Test Section



**Figure F15. Spatial variation of Saturated Hydraulic Conductivity (cm/sec) at Knapp Street, Ames, Pavement Base Test Section**

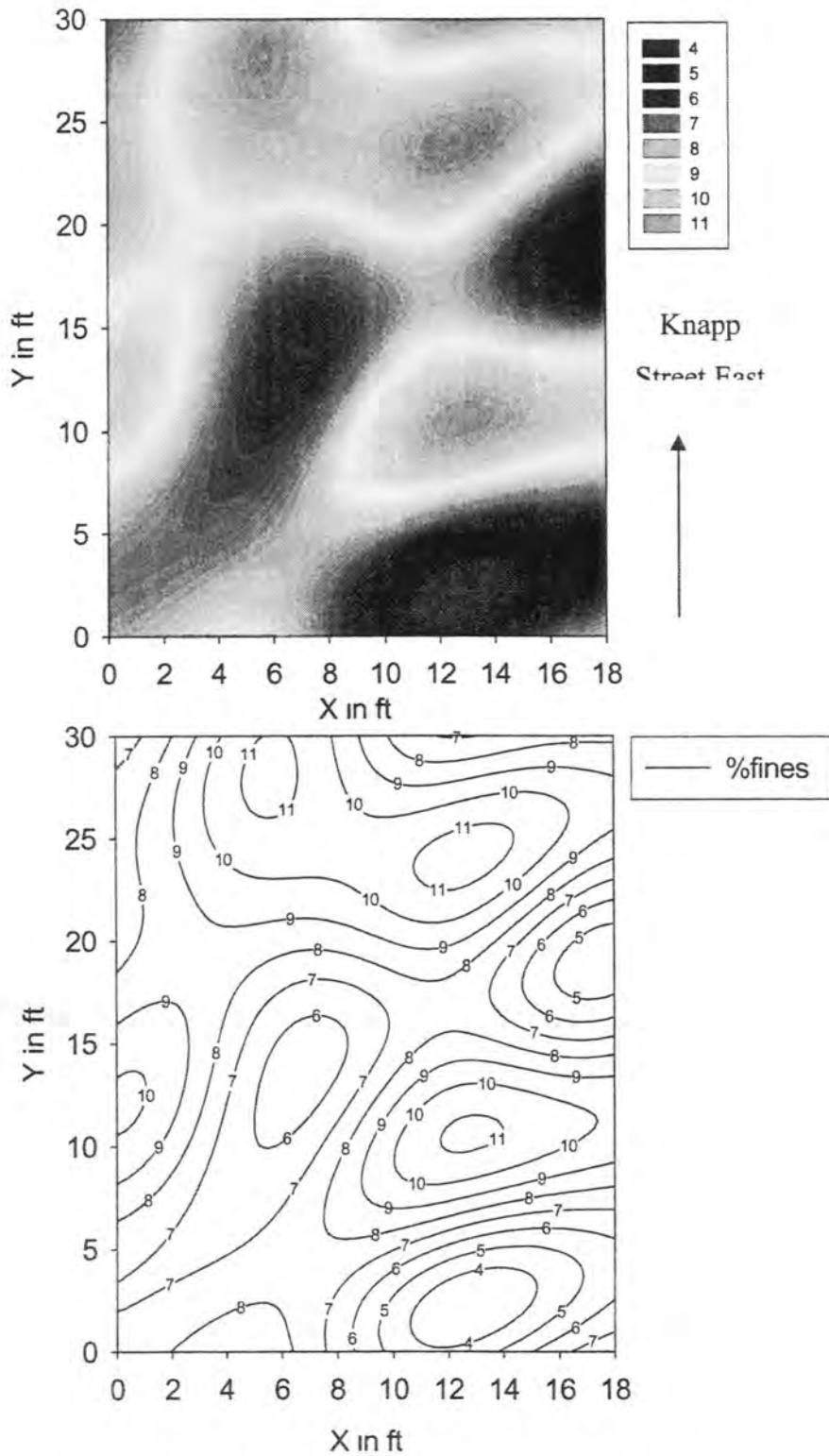


Figure F16. Spatial variation of fines content (% passing No. 200) at Knapp Street, Ames, Pavement Base Test Section

**CONTOUR GRAPHS FOR THE DATA FROM US 218 GRANULAR BASE  
CONSTRUCTION**



Figure F17 Aerial Photograph of the Test Location (IDNR, 2004)

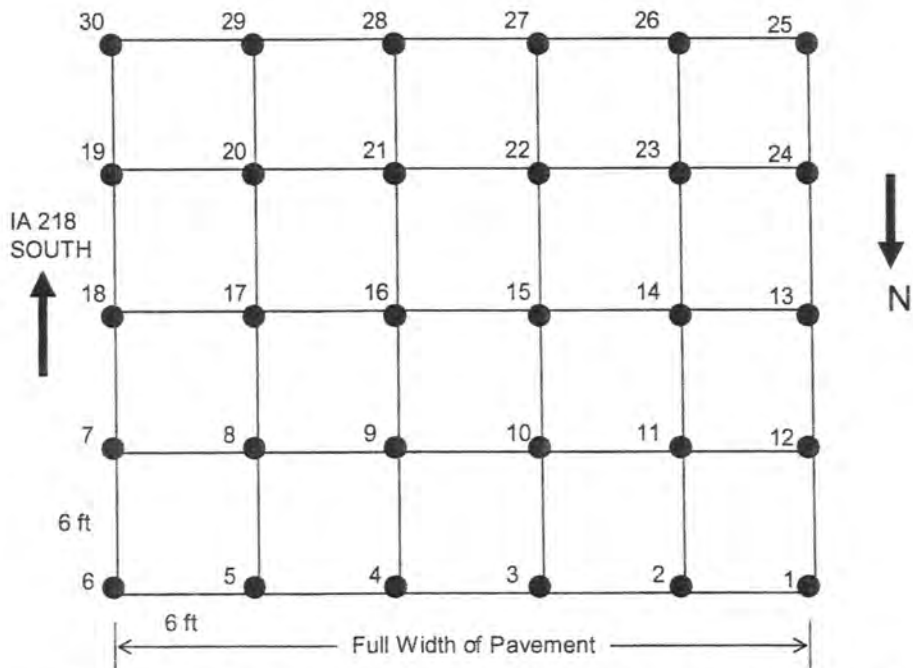


Figure F18. Grid Setup for Testing on US 218 Base Construction Site

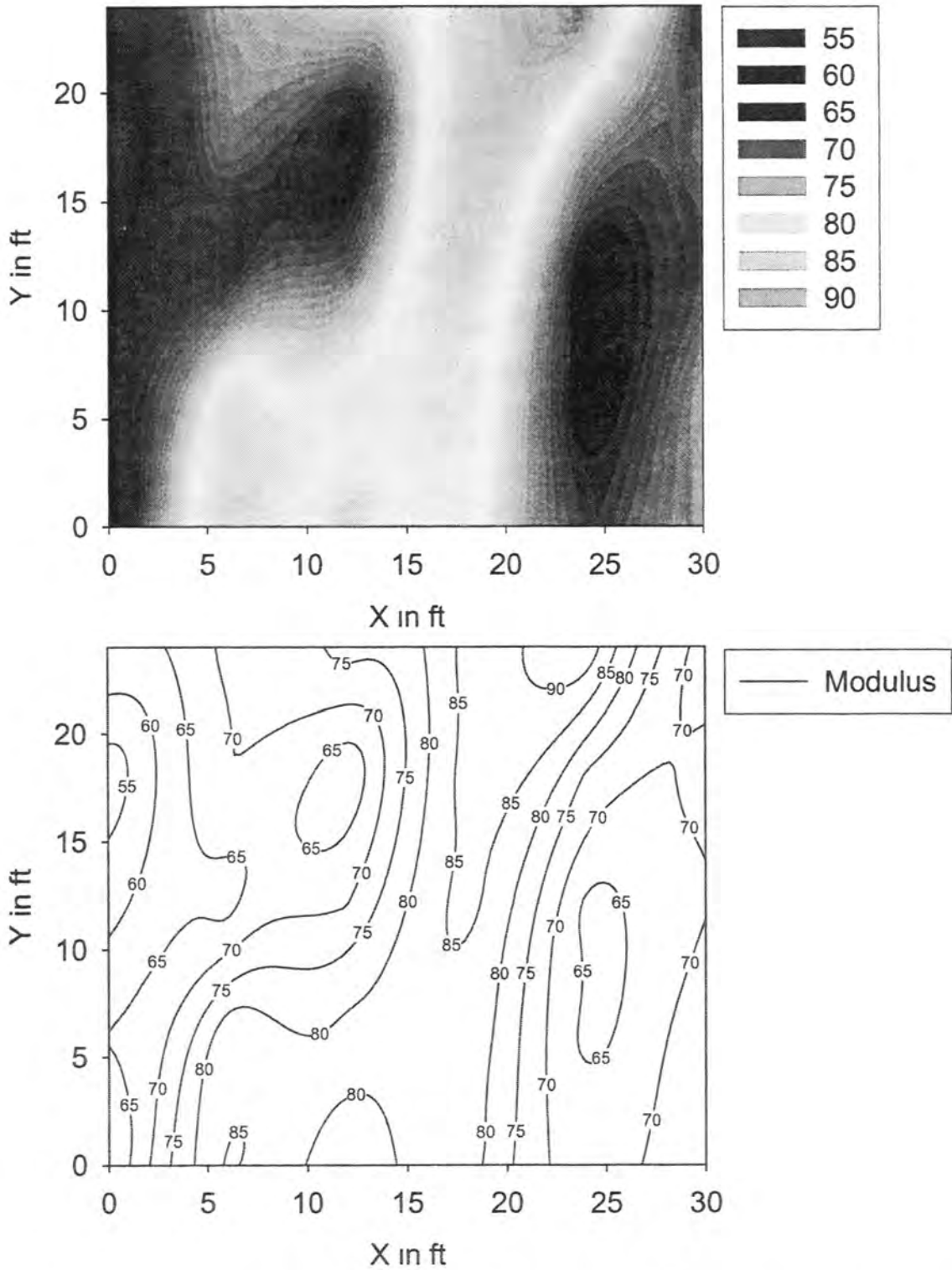


Figure F19. Spatial variation of GeoGauge Modulus (MPa) at US 218 South, Pavement Base Test Section

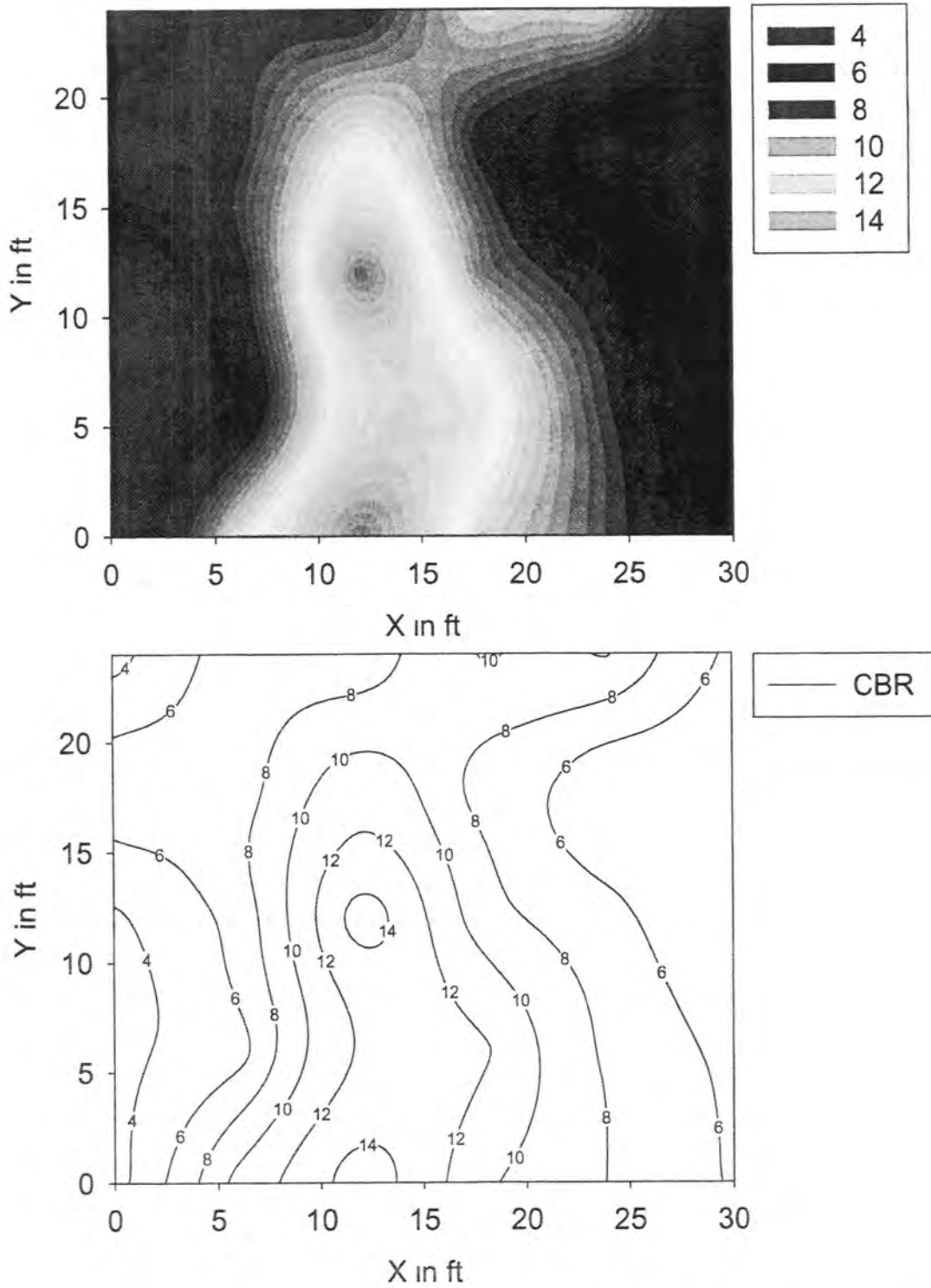


Figure F20. Spatial variation of CBR (%) at US 218 South, Pavement Base Test Section

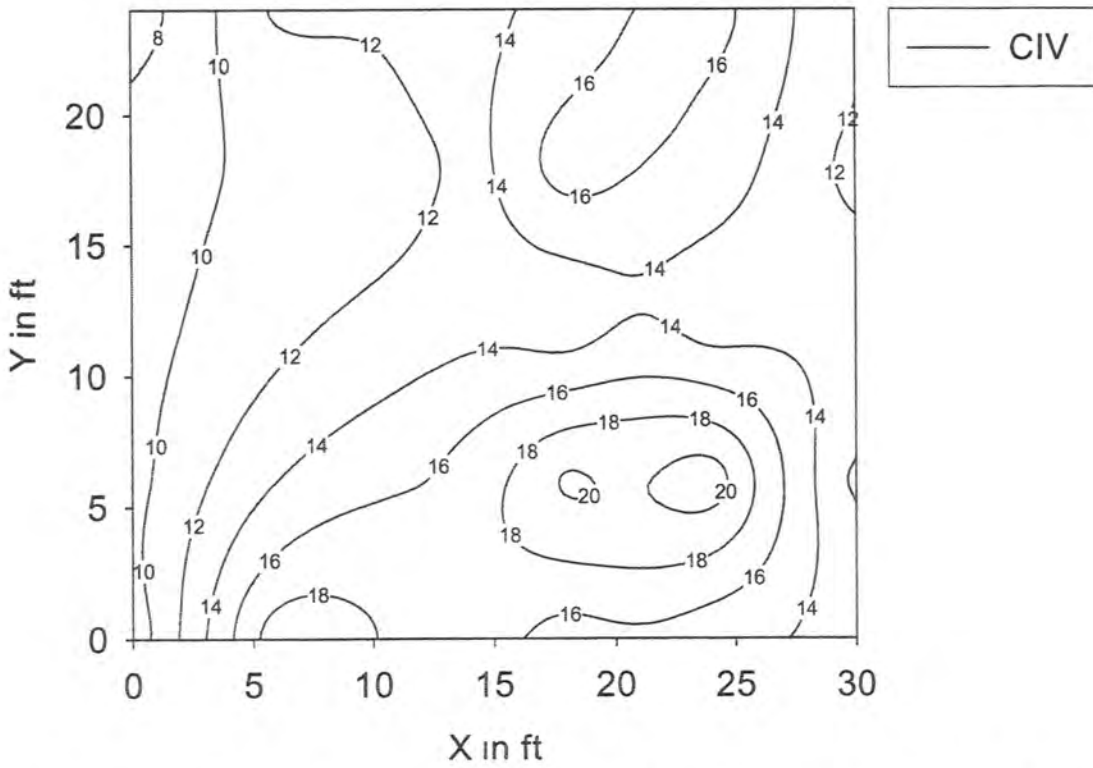
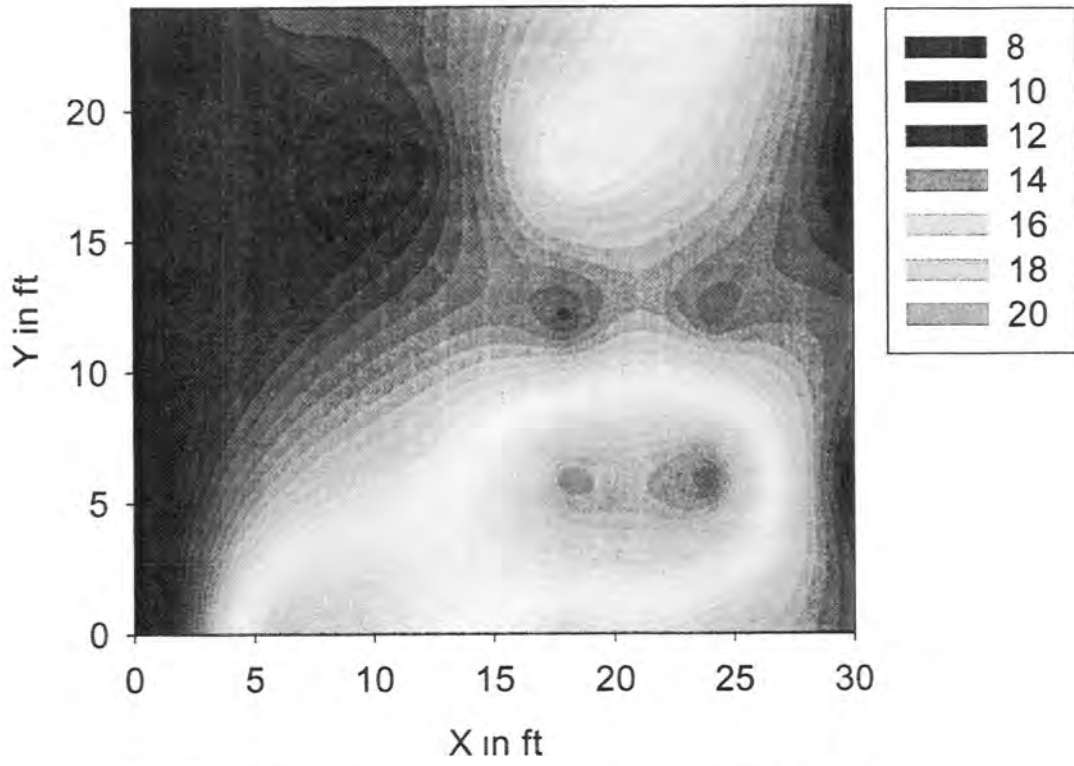


Figure F21. Spatial variation of Clegg Impact Value (CIV) at US 218 South, Pavement Base Test Section



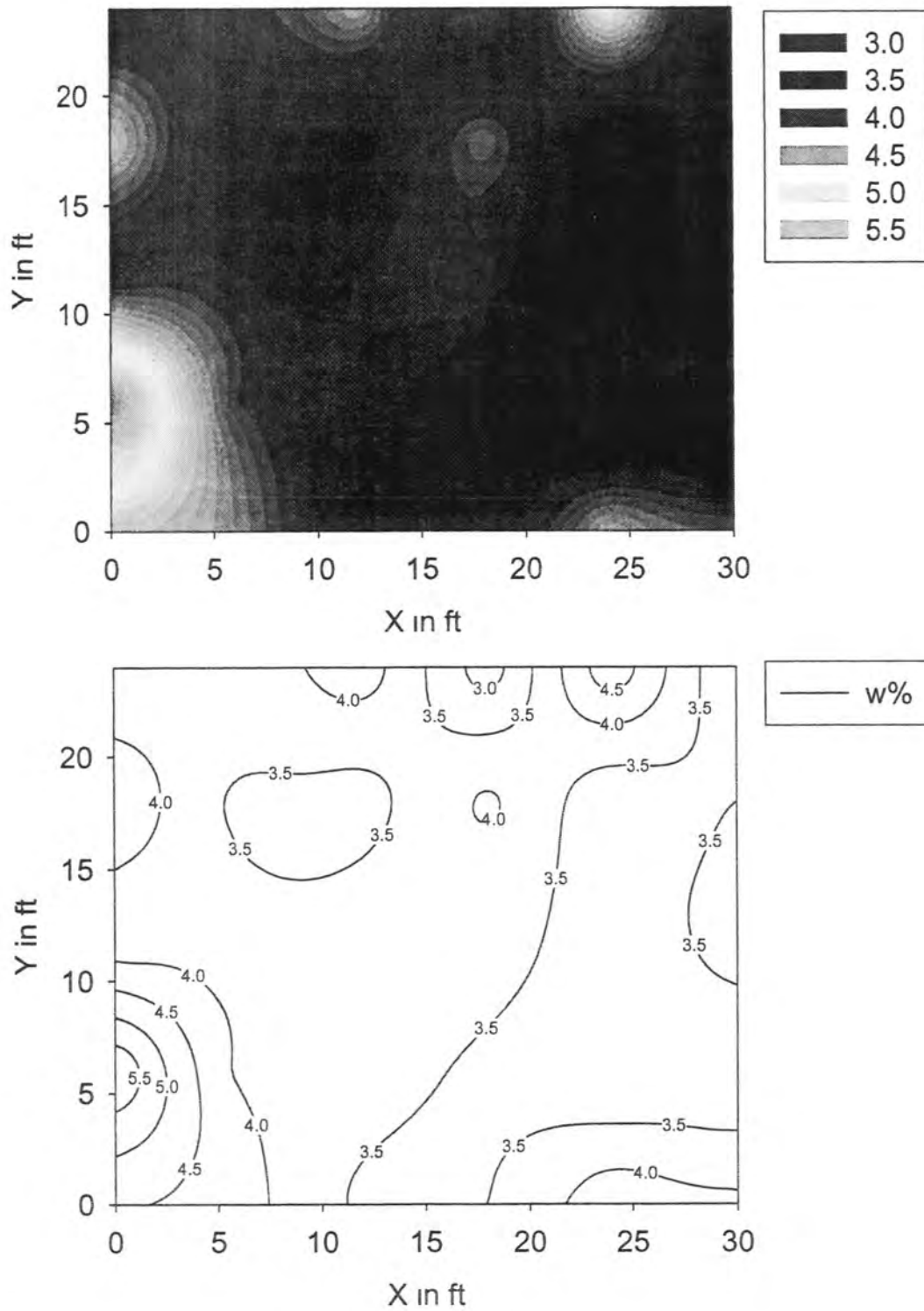


Figure F22. Spatial variation of Moisture Content (w %) at US 218 South, Pavement Base Test Section

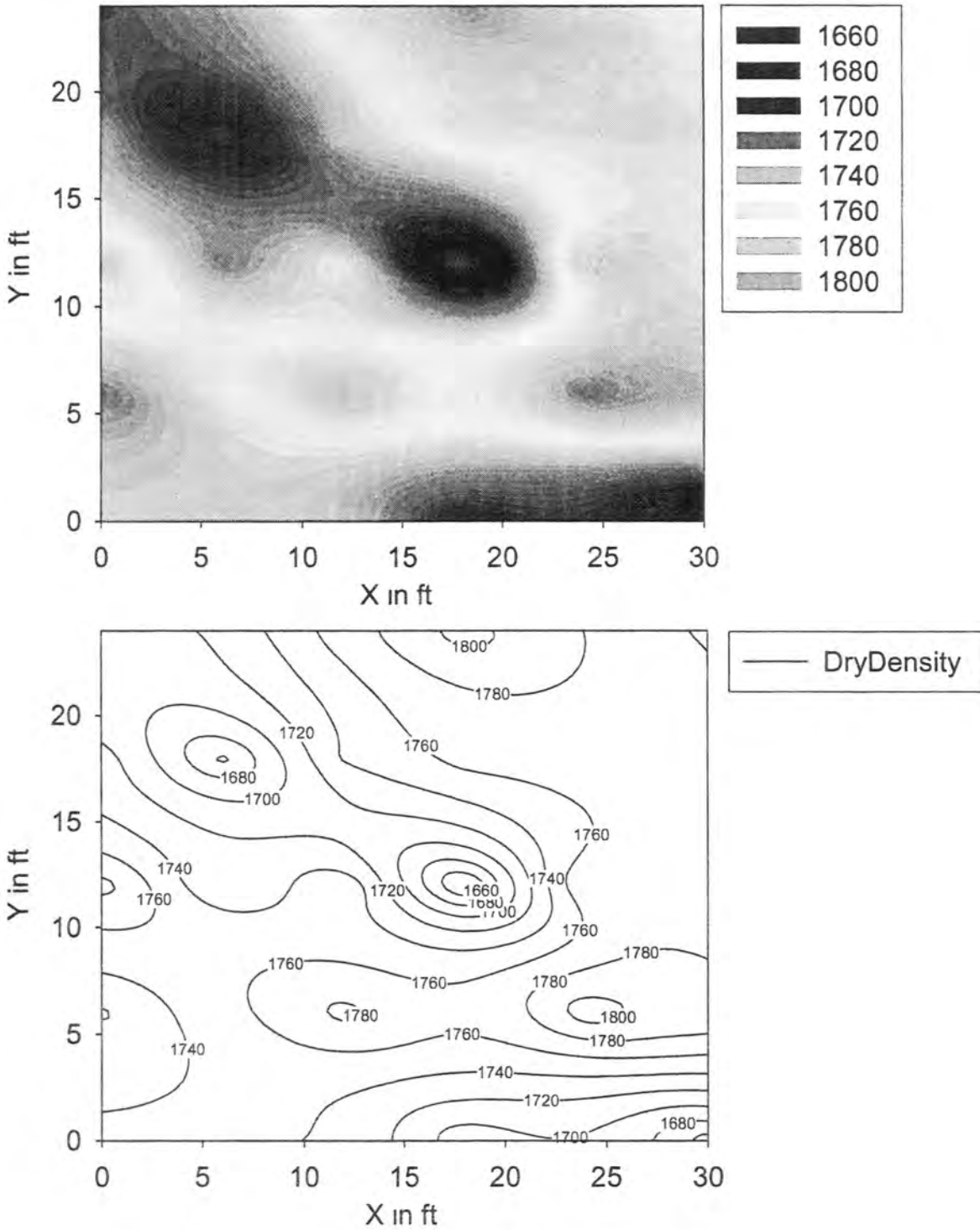
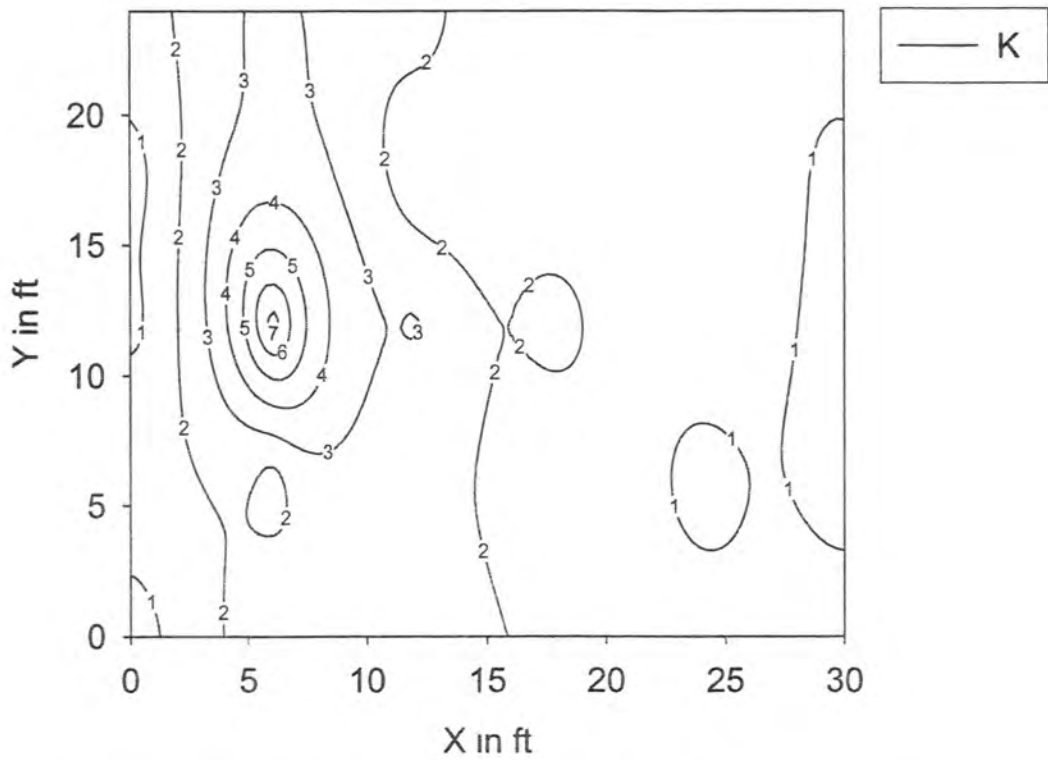
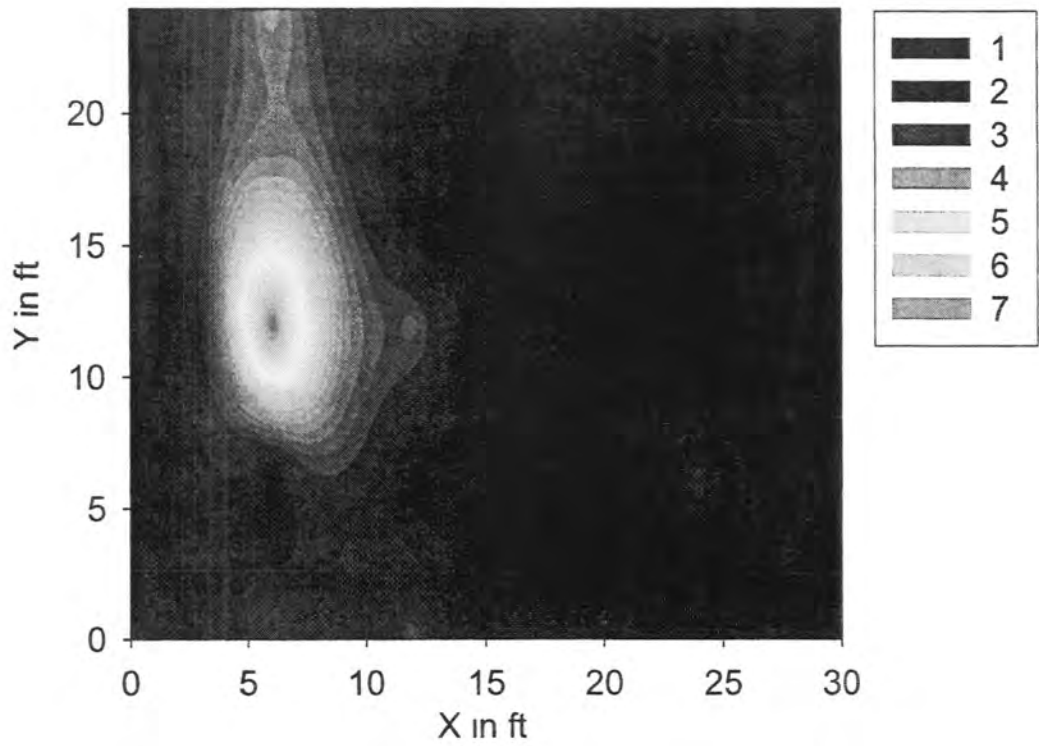
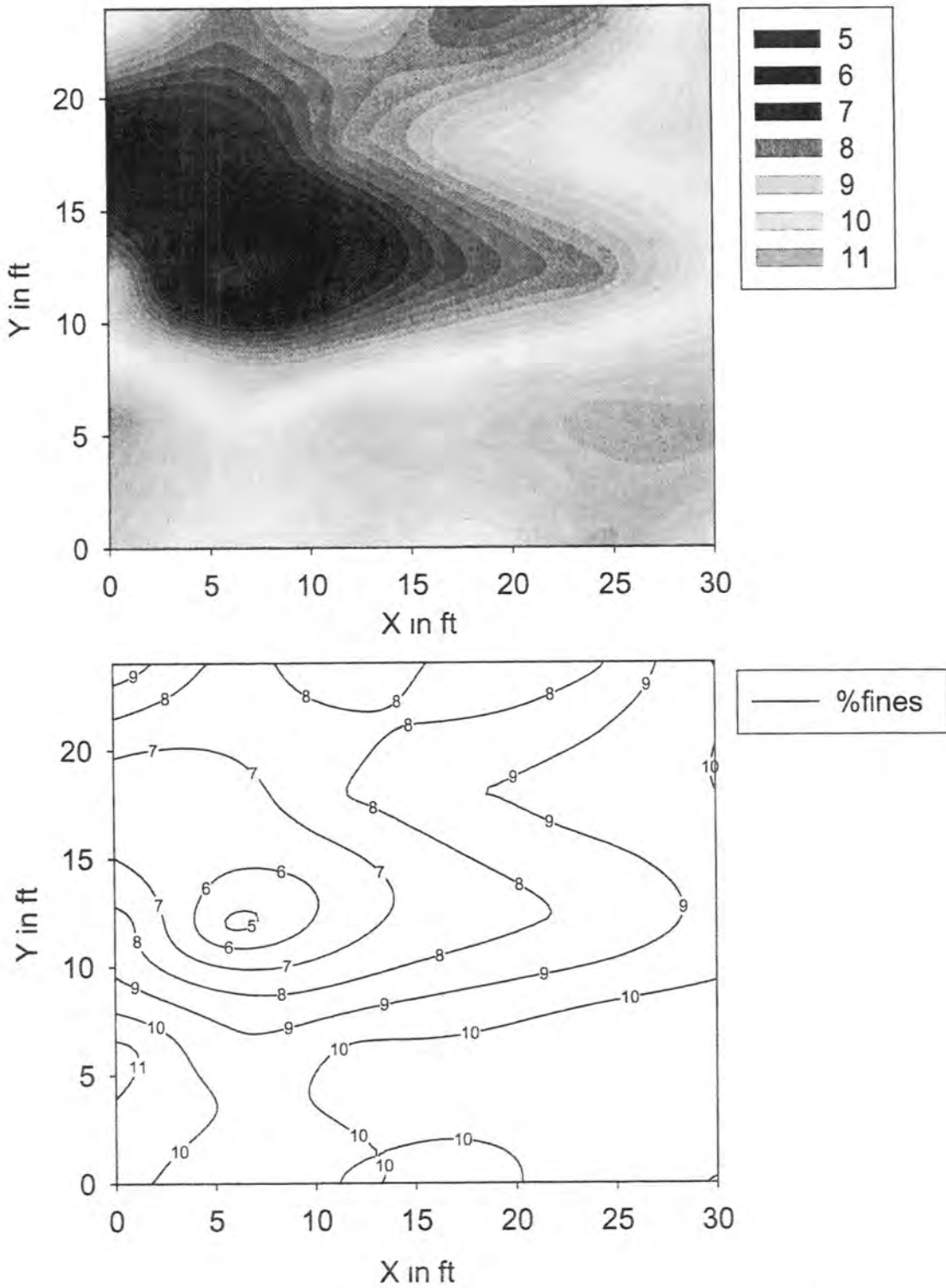


Figure F23. Spatial variation of Dry Density ( $\text{kg/m}^3$ ) at US 218 South, Pavement Base Test Section



**Figure F24. Spatial variation of Saturated Hydraulic Conductivity at US 218 South, Pavement Base Test Section**



**Figure F25. Spatial variation of fines content (% passing No. 200) at US 218 South, Pavement Base Test Section**

**CONTOUR GRAPHS FOR THE DATA FROM US 151 BASE CONSTRUCTION**

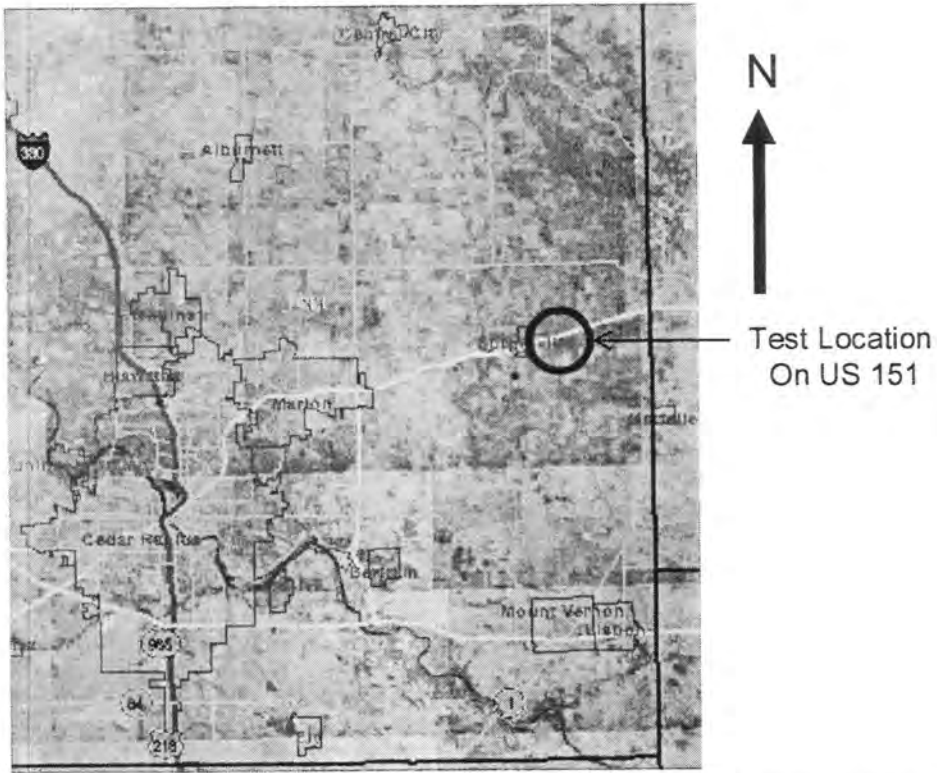


Figure F26. Aerial Photograph of the Test Location (IDNR, 2004)

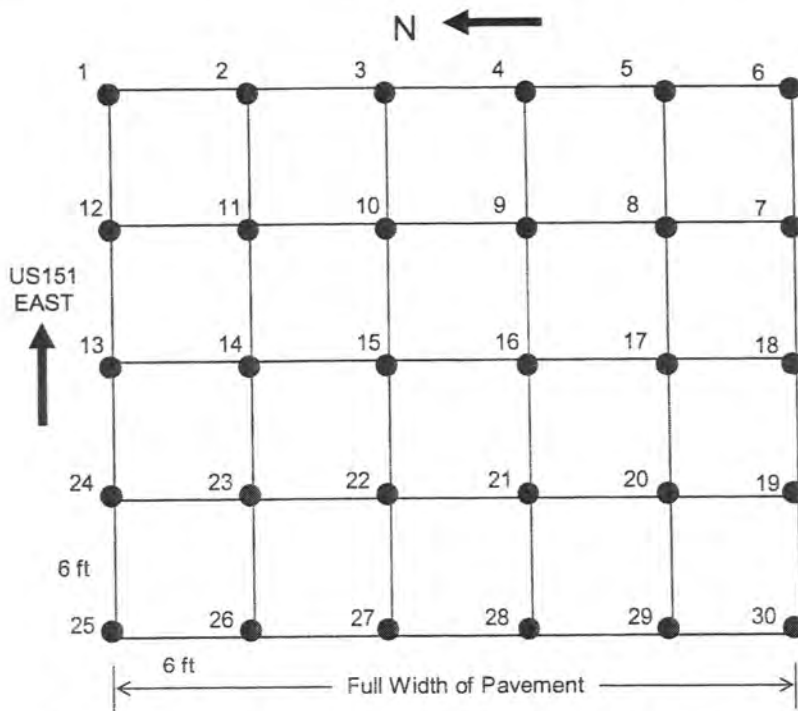


Figure F27 Grid Setup for Testing at US 151 Base Construction Site

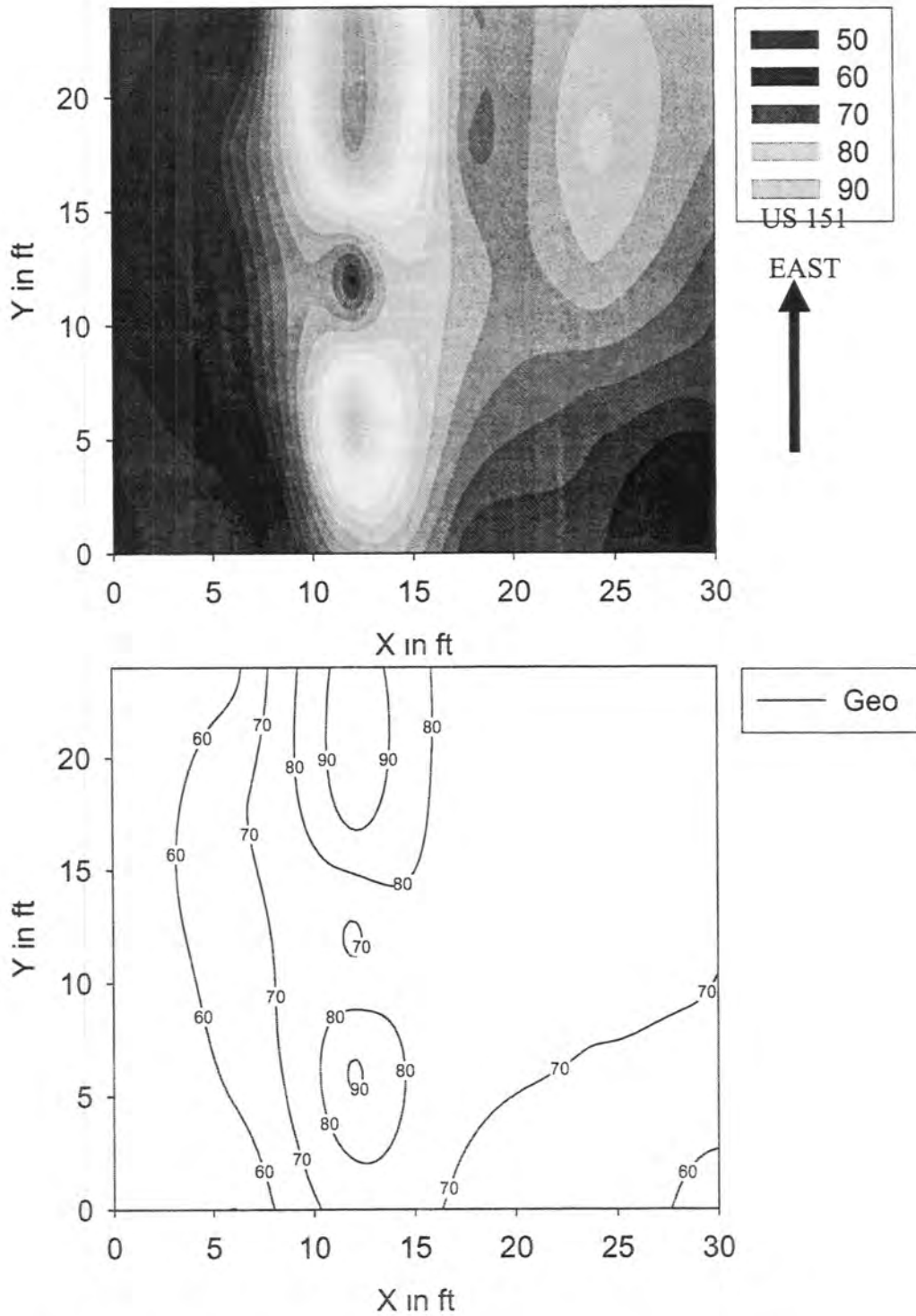


Figure F28. Spatial variation of GeoGauge Modulus (MPa) at US151, Pavement Base Test Section

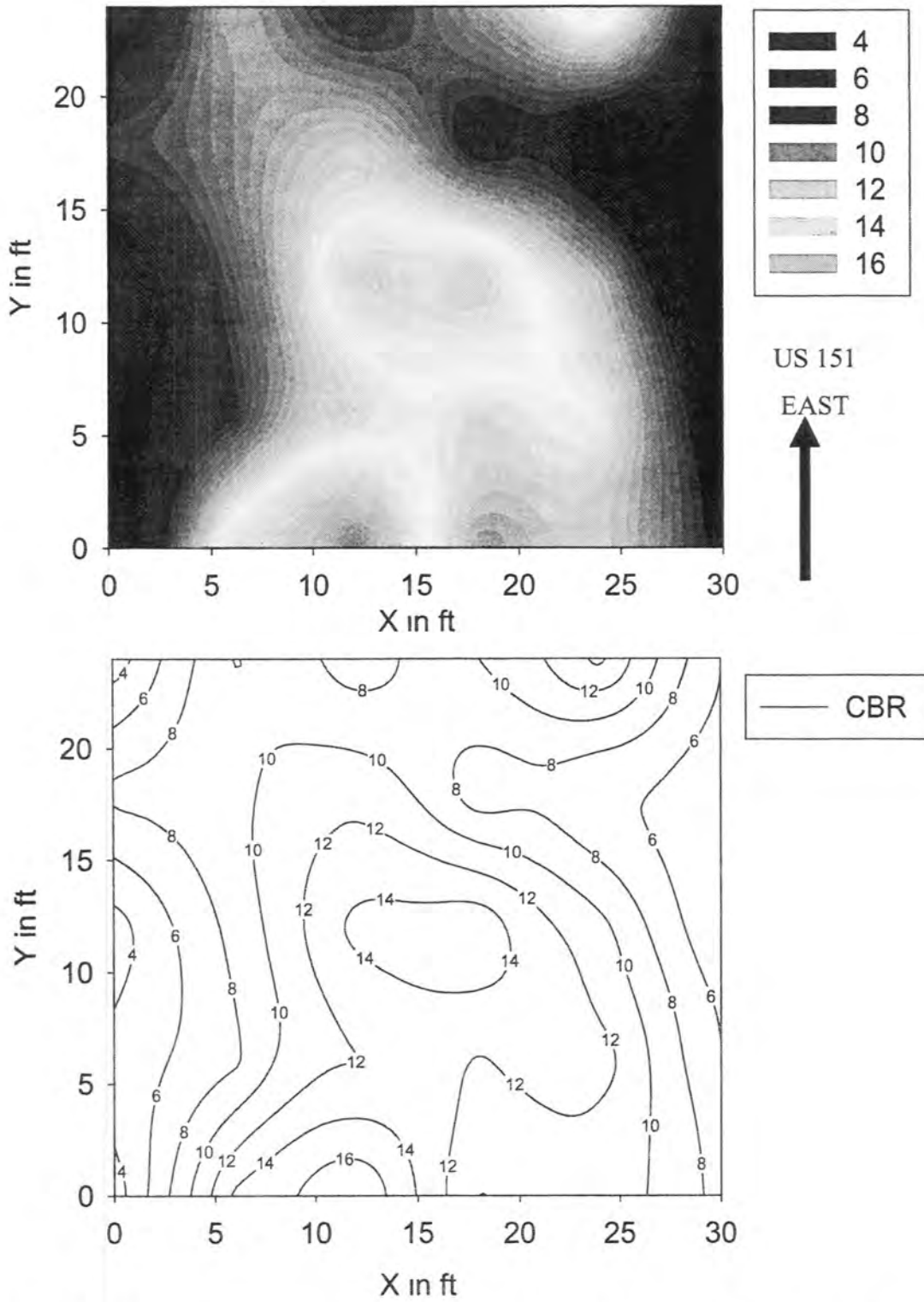
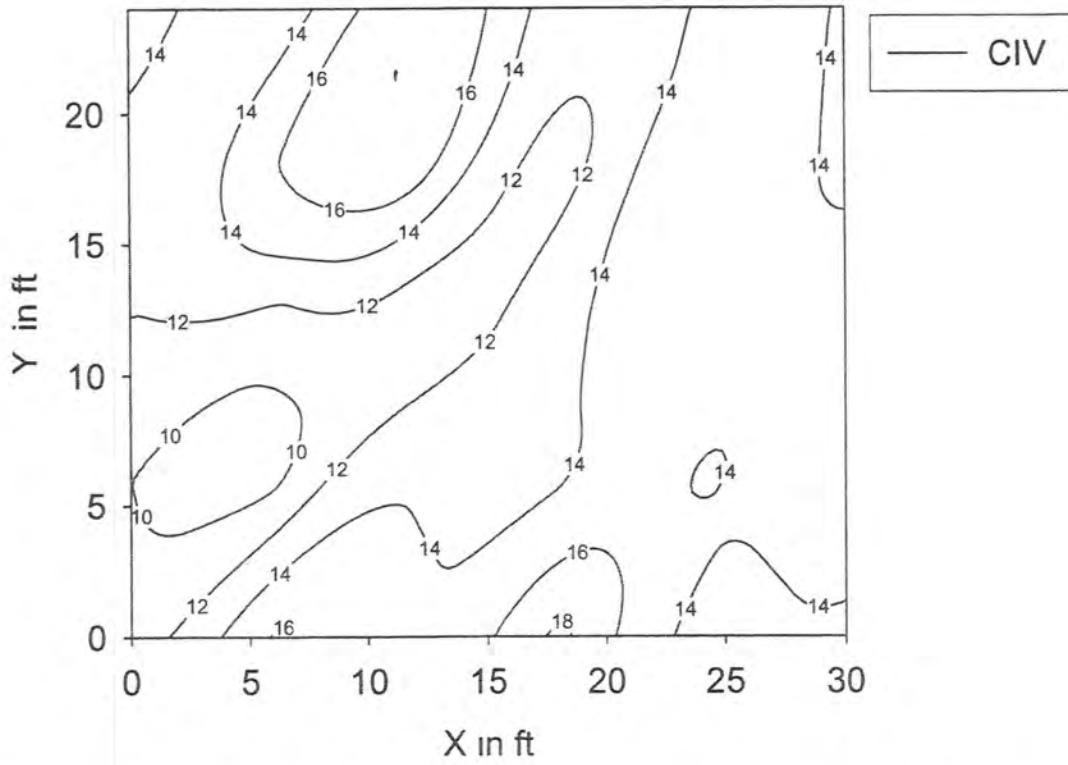
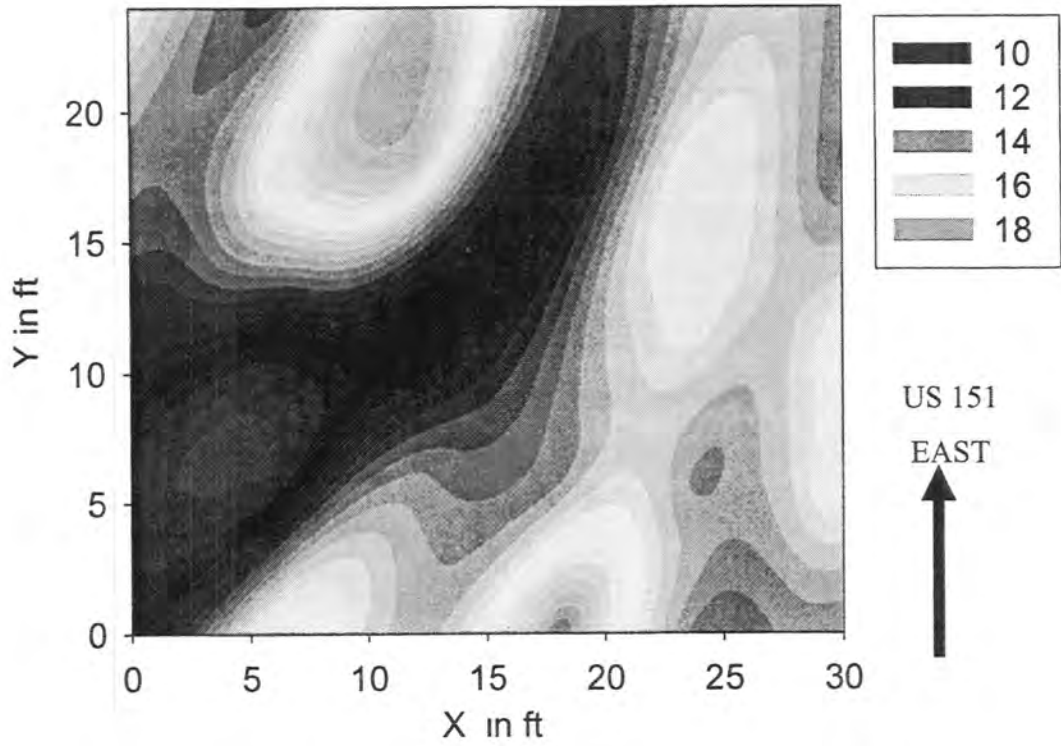


Figure F29. Spatial variation of CBR (%) at US151, Pavement Base Test Section





**Figure F30. Spatial variation of Clegg Impact Value (CIV) at US151, Pavement Base Test Section**

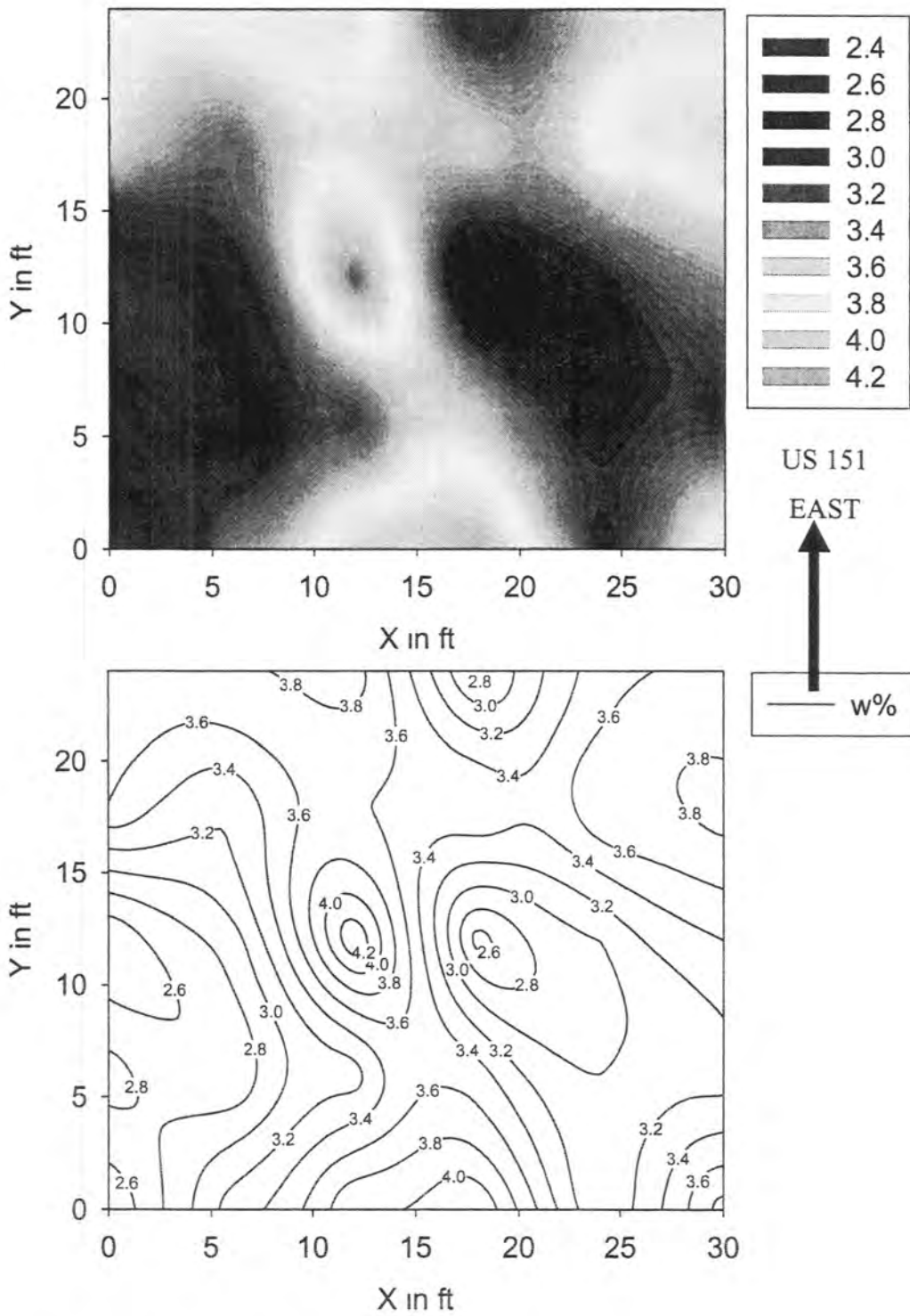


Figure F31. Spatial variation of Moisture Content (%) at US151, Pavement Base Test Section

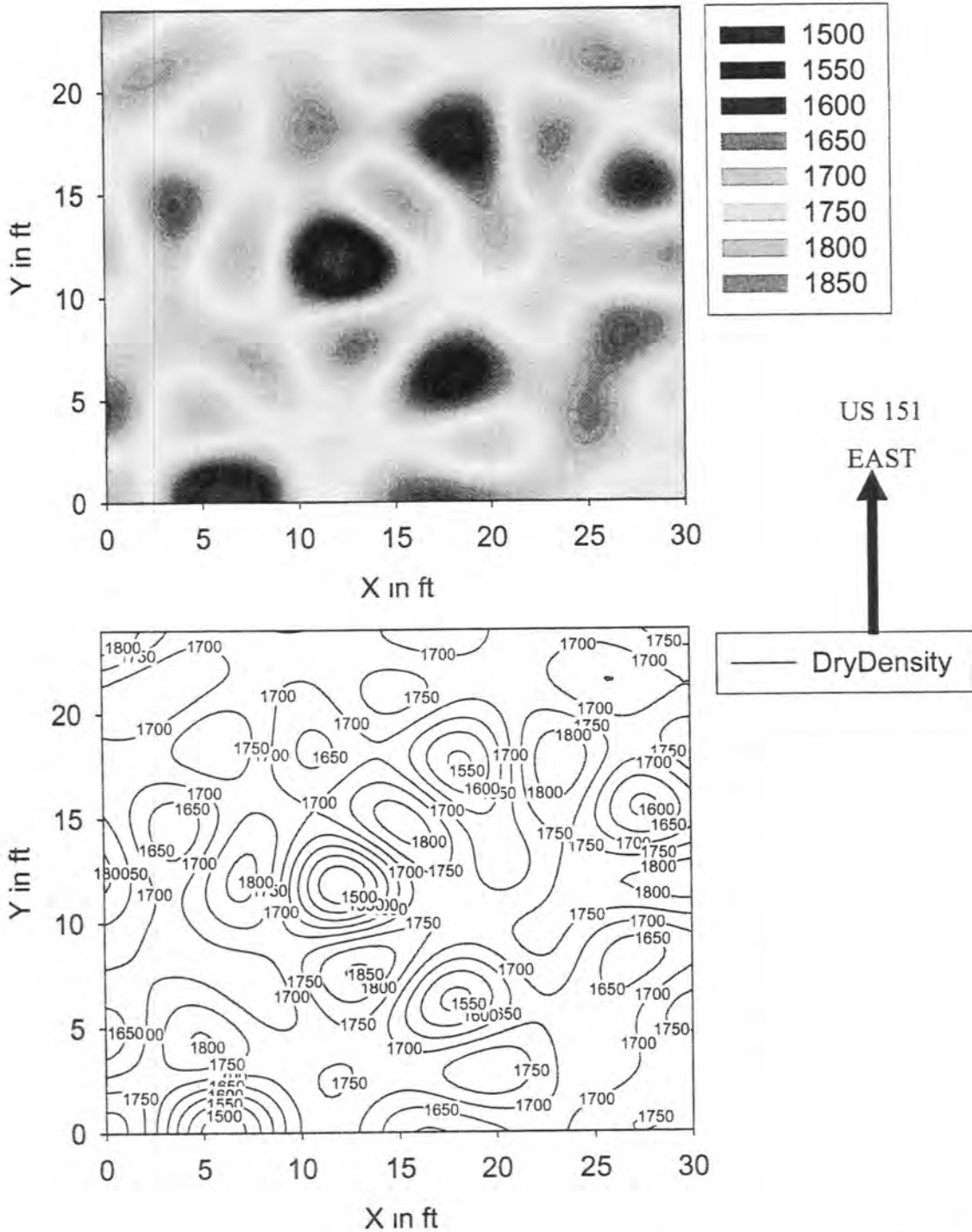


Figure F32. Spatial Variation of Dry Density ( $\text{kg/m}^3$ ) at US 151, Pavement Base Test Section

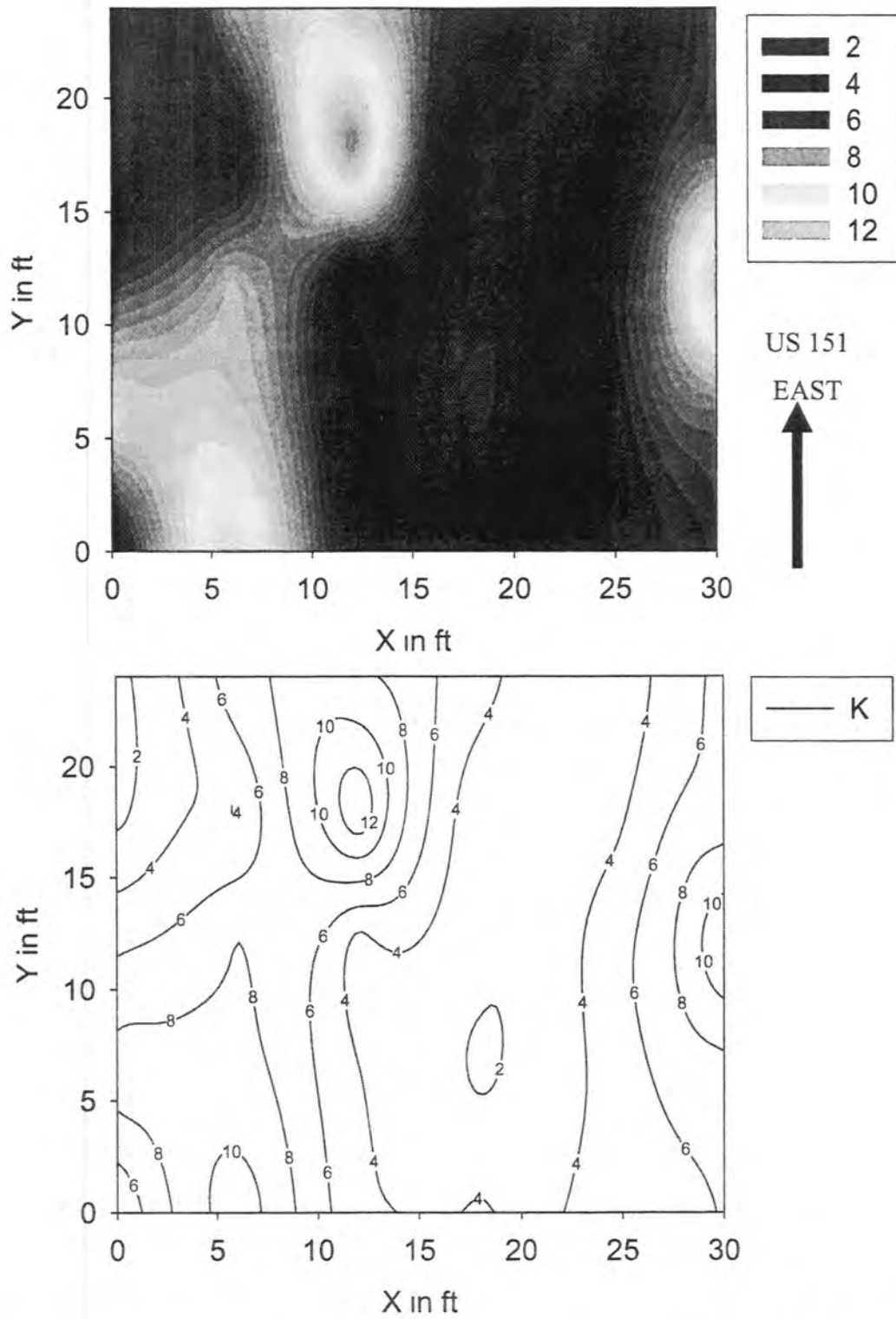
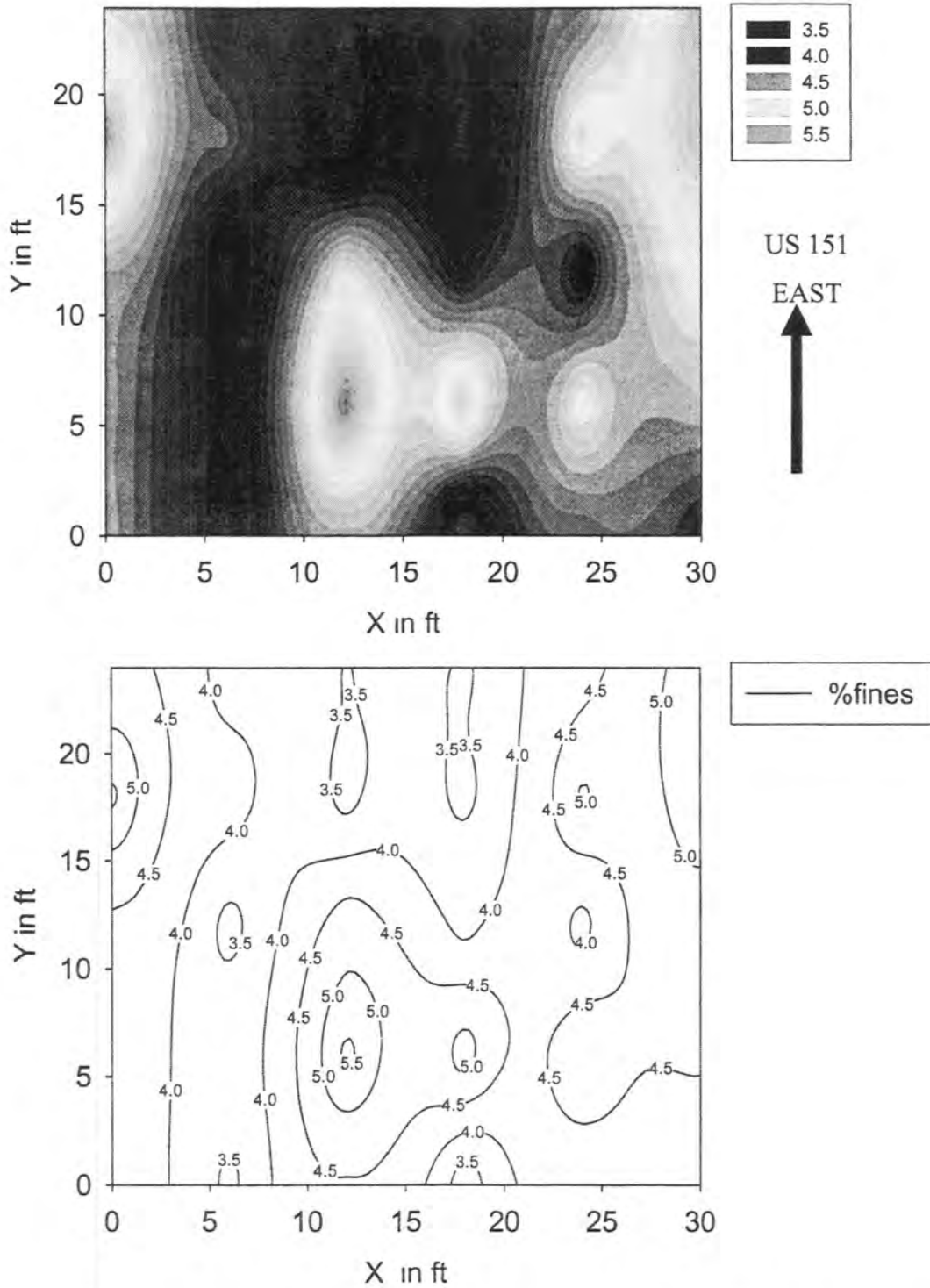


Figure F33. Spatial variation of Saturated Hydraulic Conductivity at US151, Pavement Base Test Section



**Figure F34. Spatial variation of fines content (% fines passing No. 200) at US151, Pavement Base Test Section**

**CONTOUR GRAPHS FOR THE DATA FROM UNIVERISTY-GUTHRIE AVENUE  
BASE CONSTRUCTION**

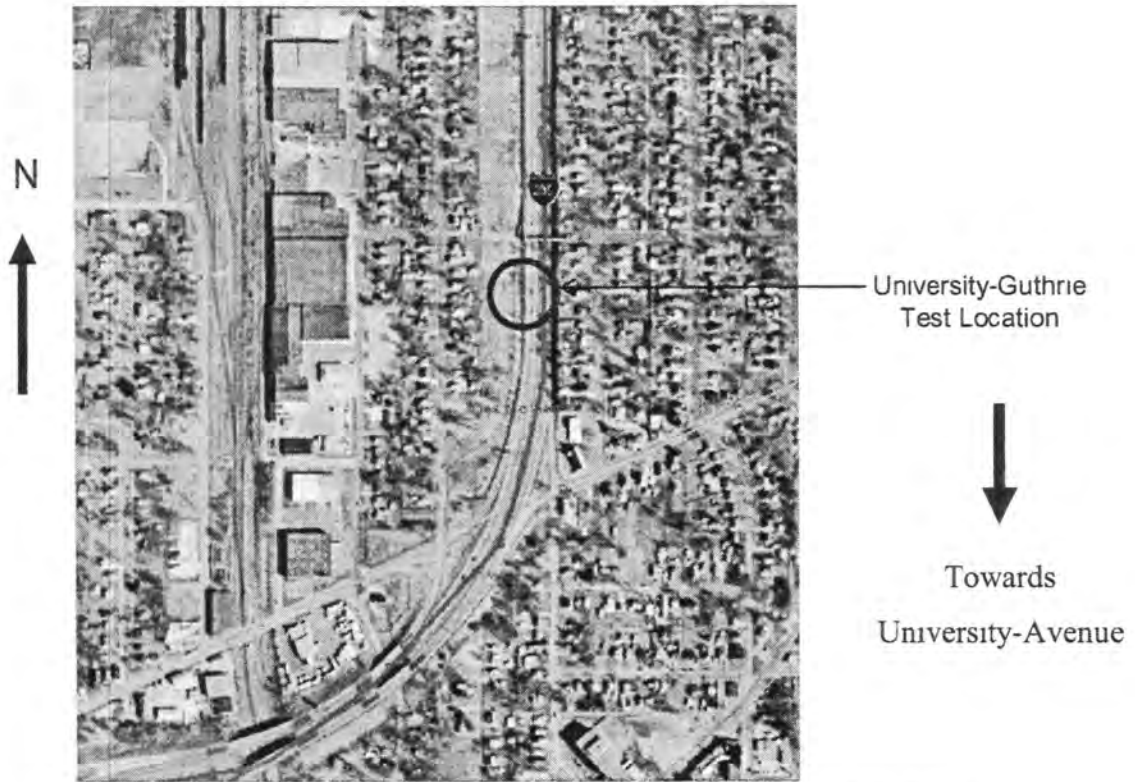


Figure F35. Aerial Photograph of the Test Location (IDNR, 2004)

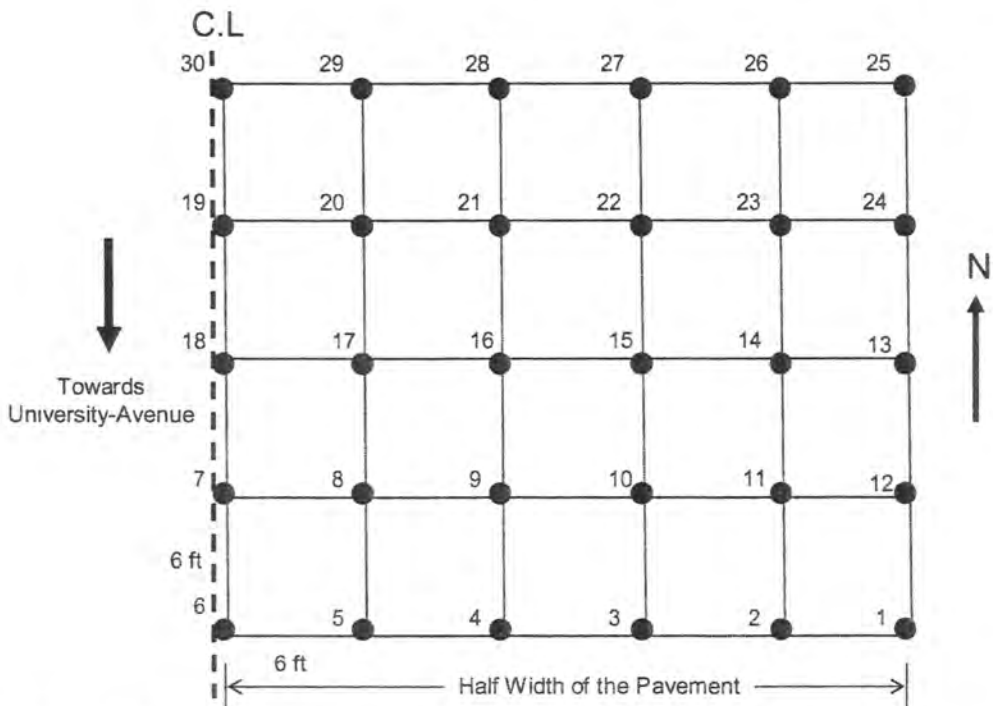
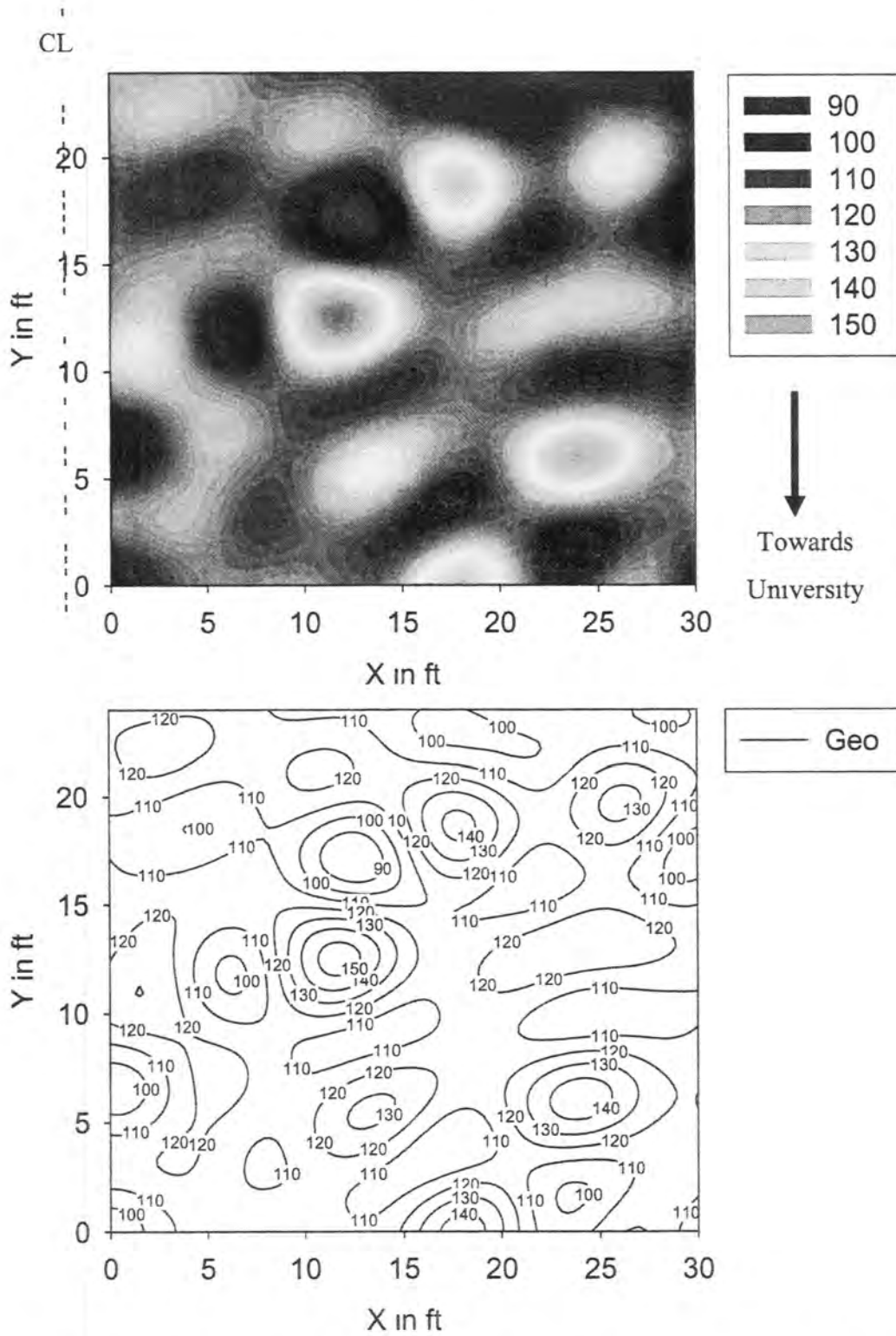


Figure F36. Grid Setup for Testing at University-Guthrie Base Construction Site



**Figure F37 Spatial variation of GeoGauge Modulus (MPa) at University-Guthrie Pavement Base Test Section**



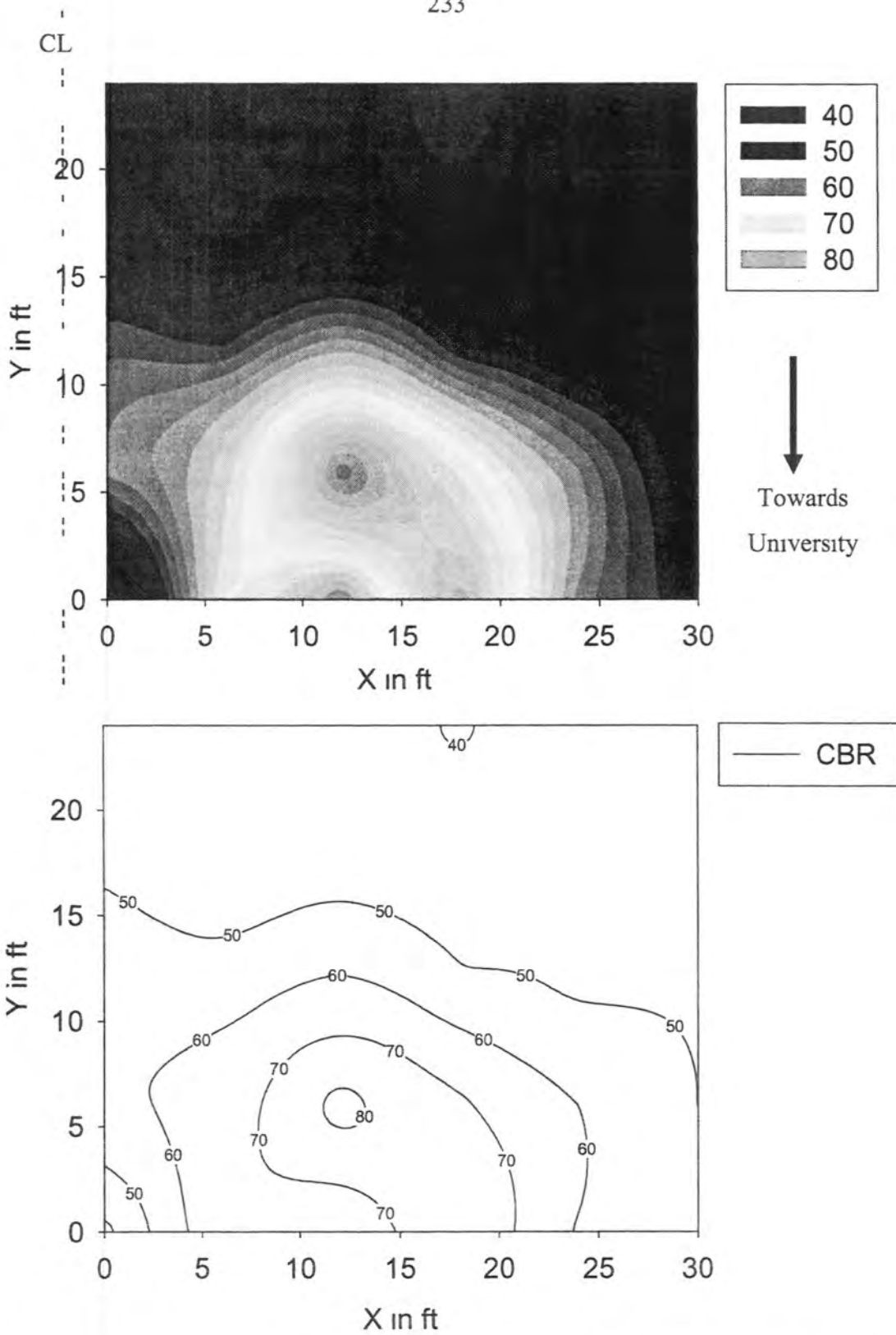
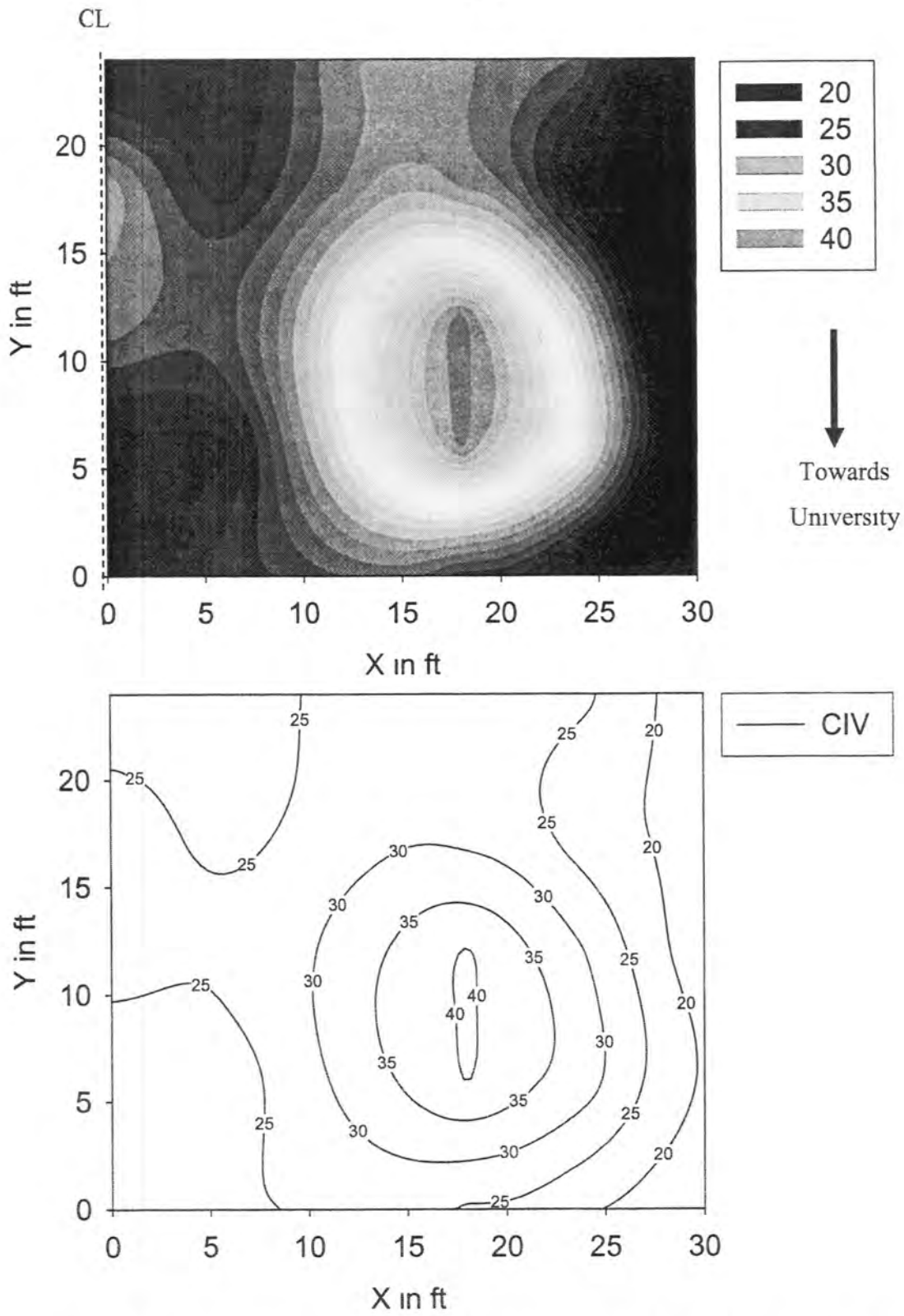
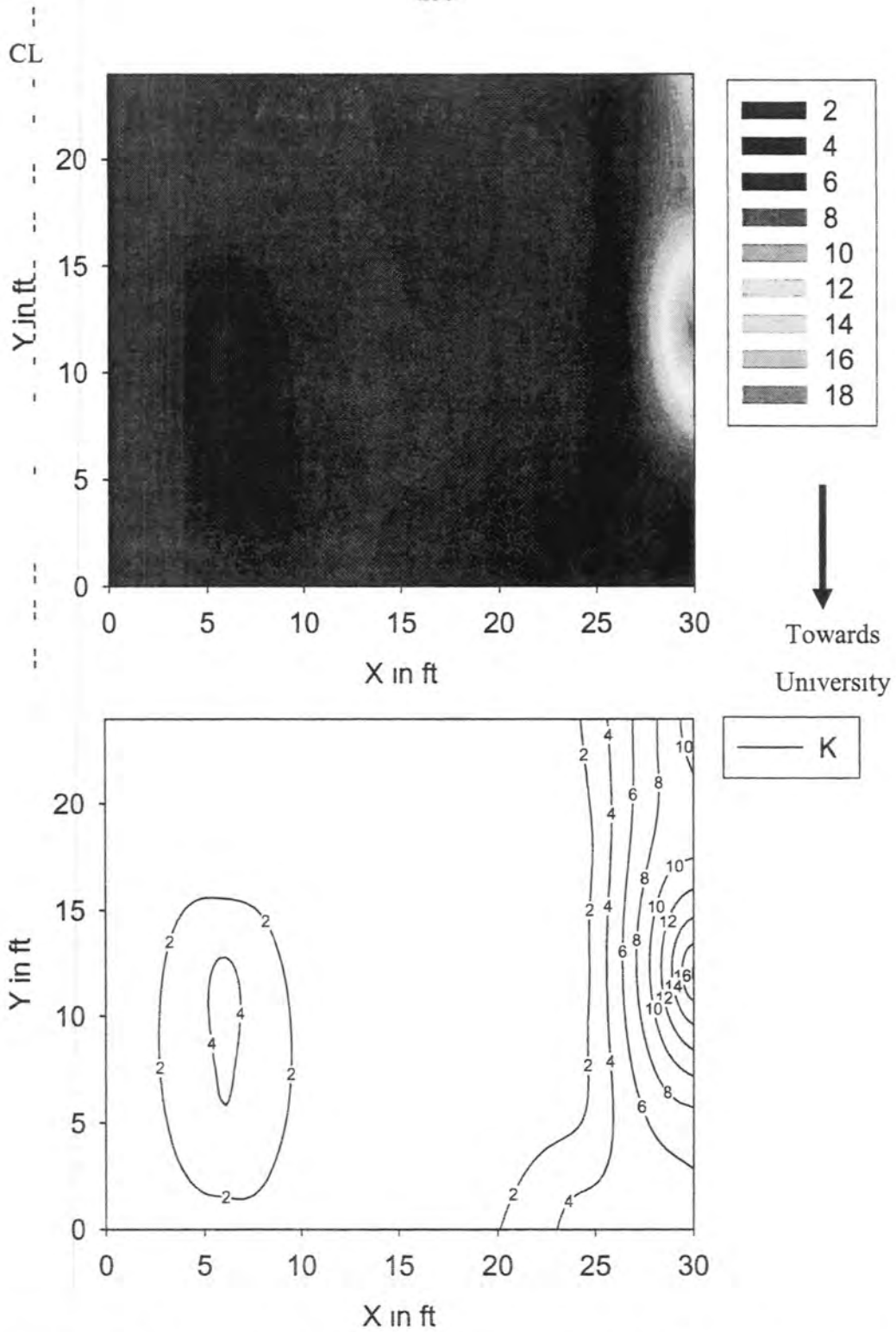


Figure F38. Spatial variation of CBR (%) at University-Guthrie Pavement Base Test Section



**Figure F39. Spatial variation of Clegg Impact Value (CIV) at University-Guthrie Pavement Base Test Section**



**Figure F40. Spatial variation of Saturated Hydraulic Conductivity (cm/sec) at University-Guthrie Pavement Base Test Section**

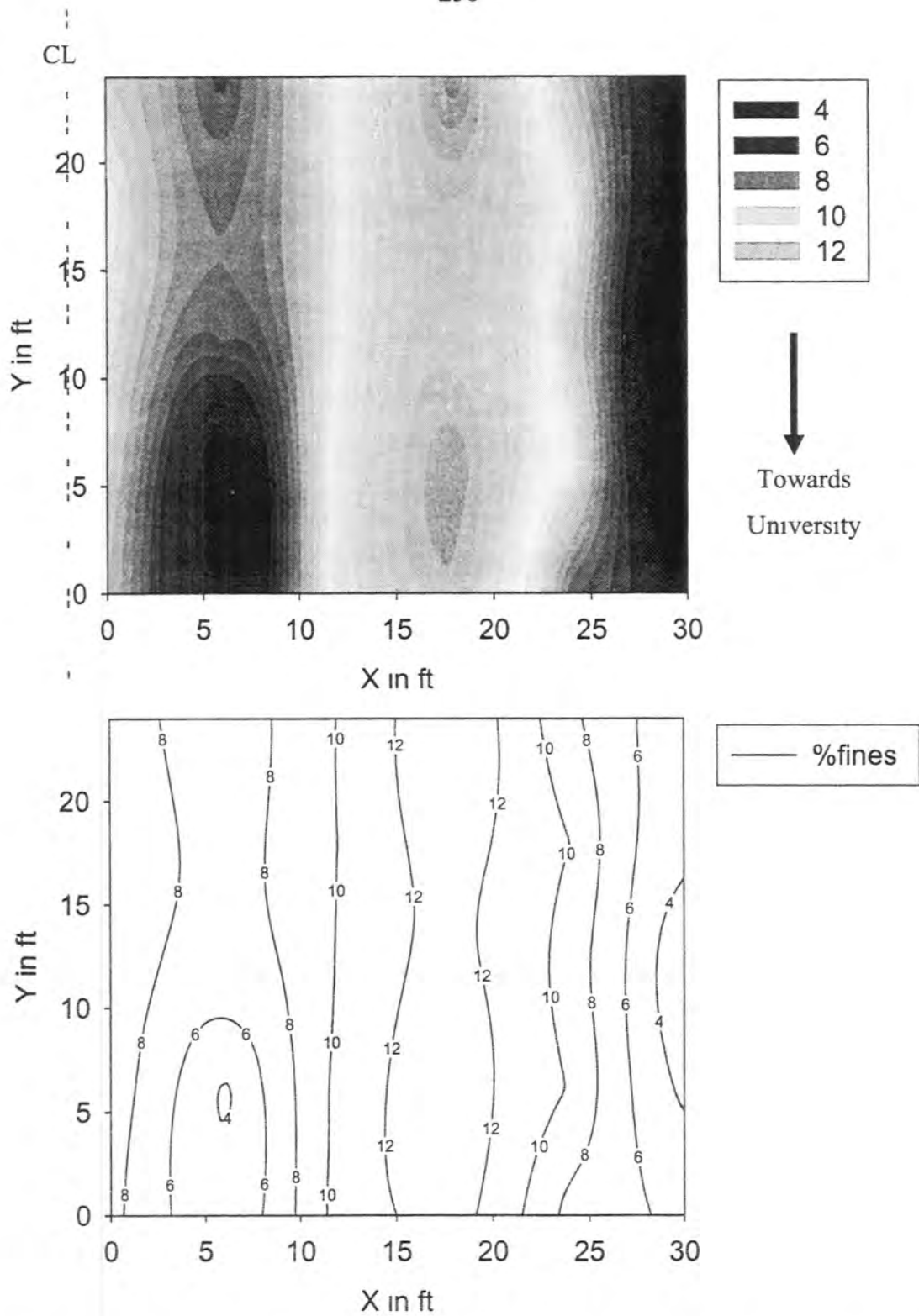


**Figure F41. Spatial variation of fines content (% fines passing No. 200) at University-Guthrie Pavement Base Test Section**

**CONTOUR GRAPHS FOR THE DATA FROM UNIVERSITY GUTHRIE SPECIAL  
BACKFILL CONSTRUCTION**



Figure F42. Aerial Photograph of the Test Location (IDNR, 2004)

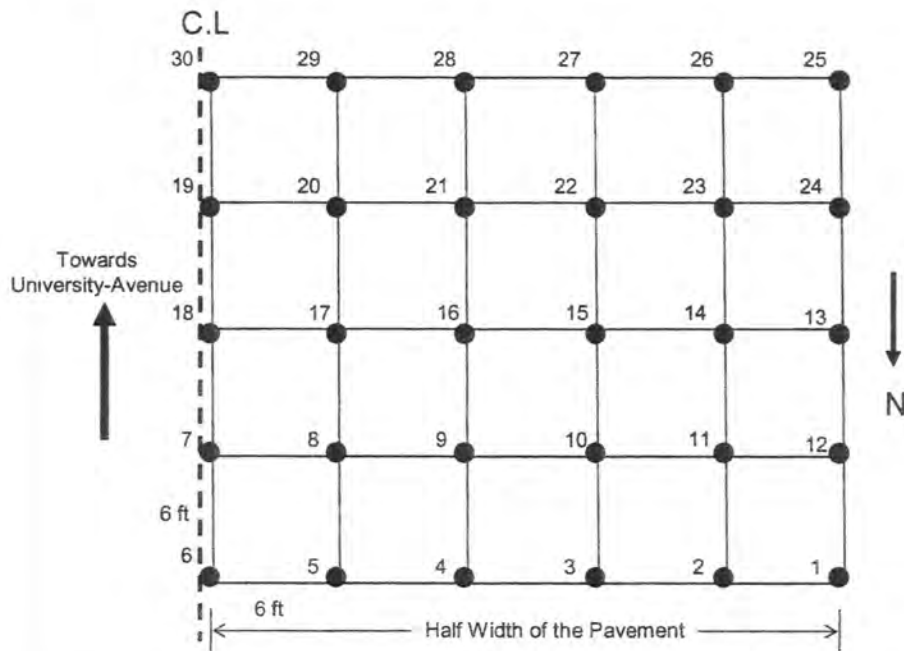
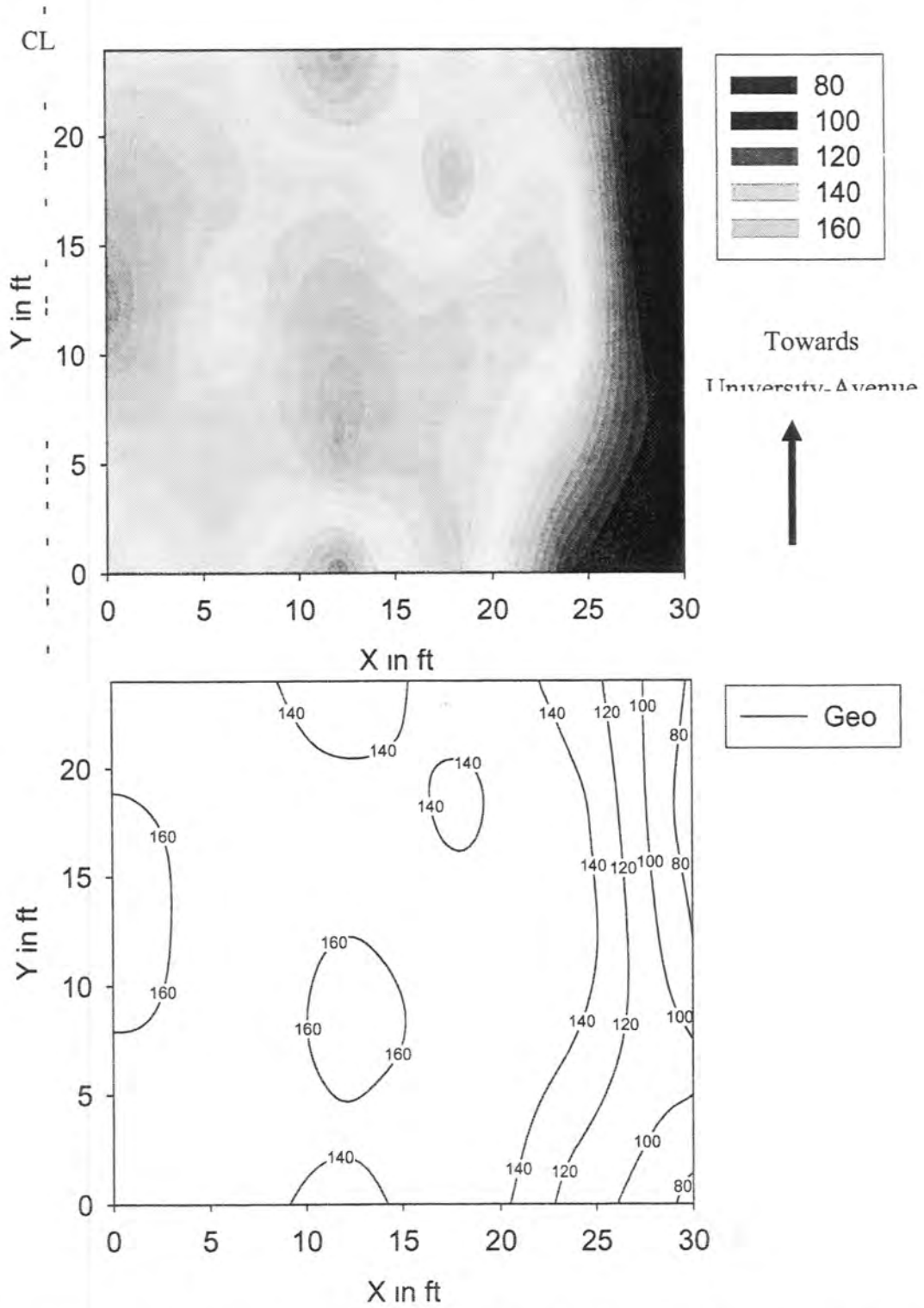


Figure F43. Grid Setup for Testing at University-Guthrie Base Construction Site



**Figure F44. Spatial variation of GeoGauge Modulus (MPa) at University-Guthrie Special Backfill Test Section**

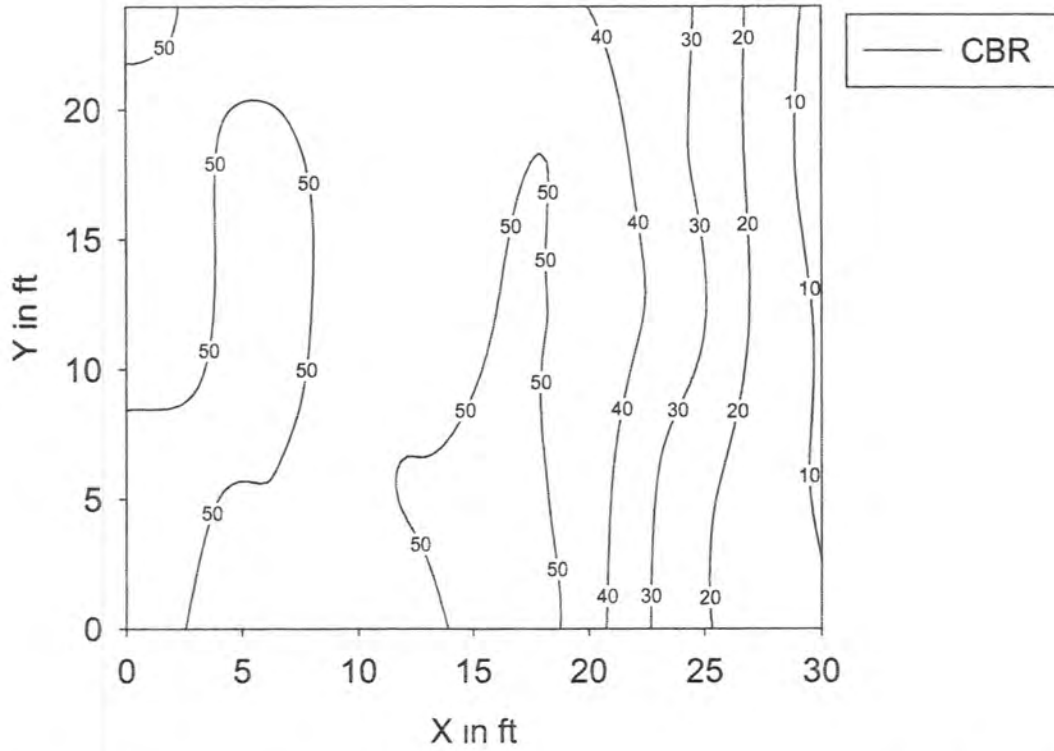
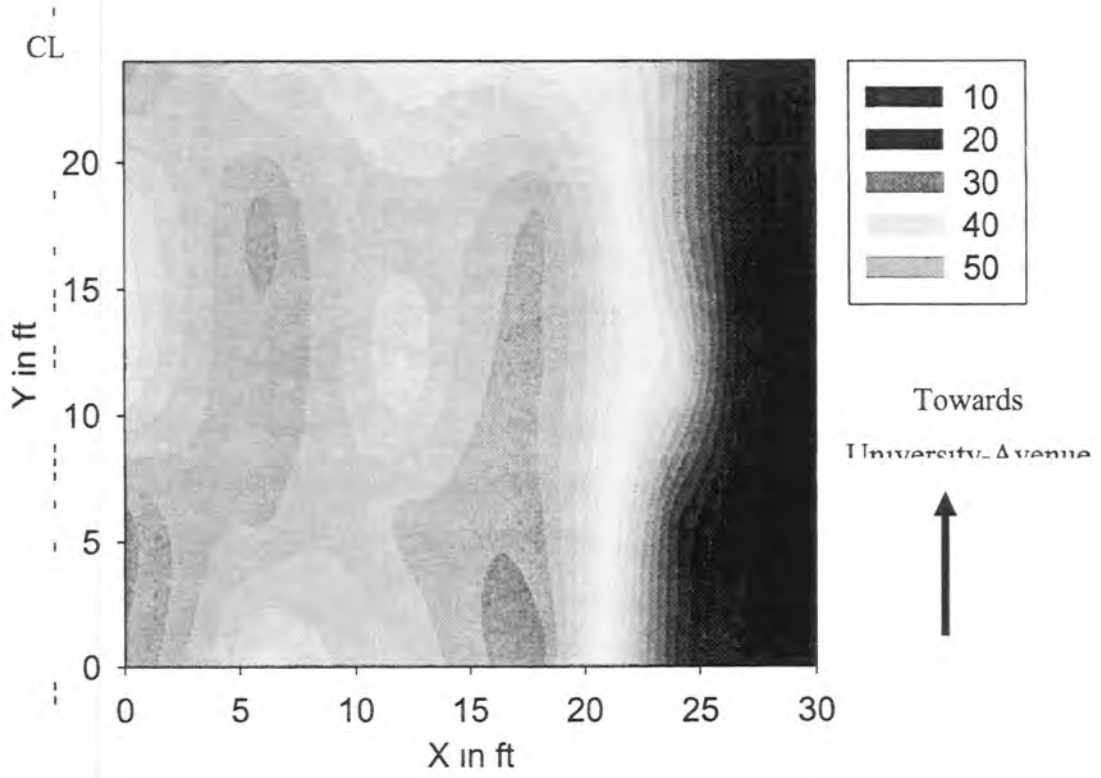


Figure F45. Spatial variation of CBR (%) at University-Guthrie Special Backfill Test Section



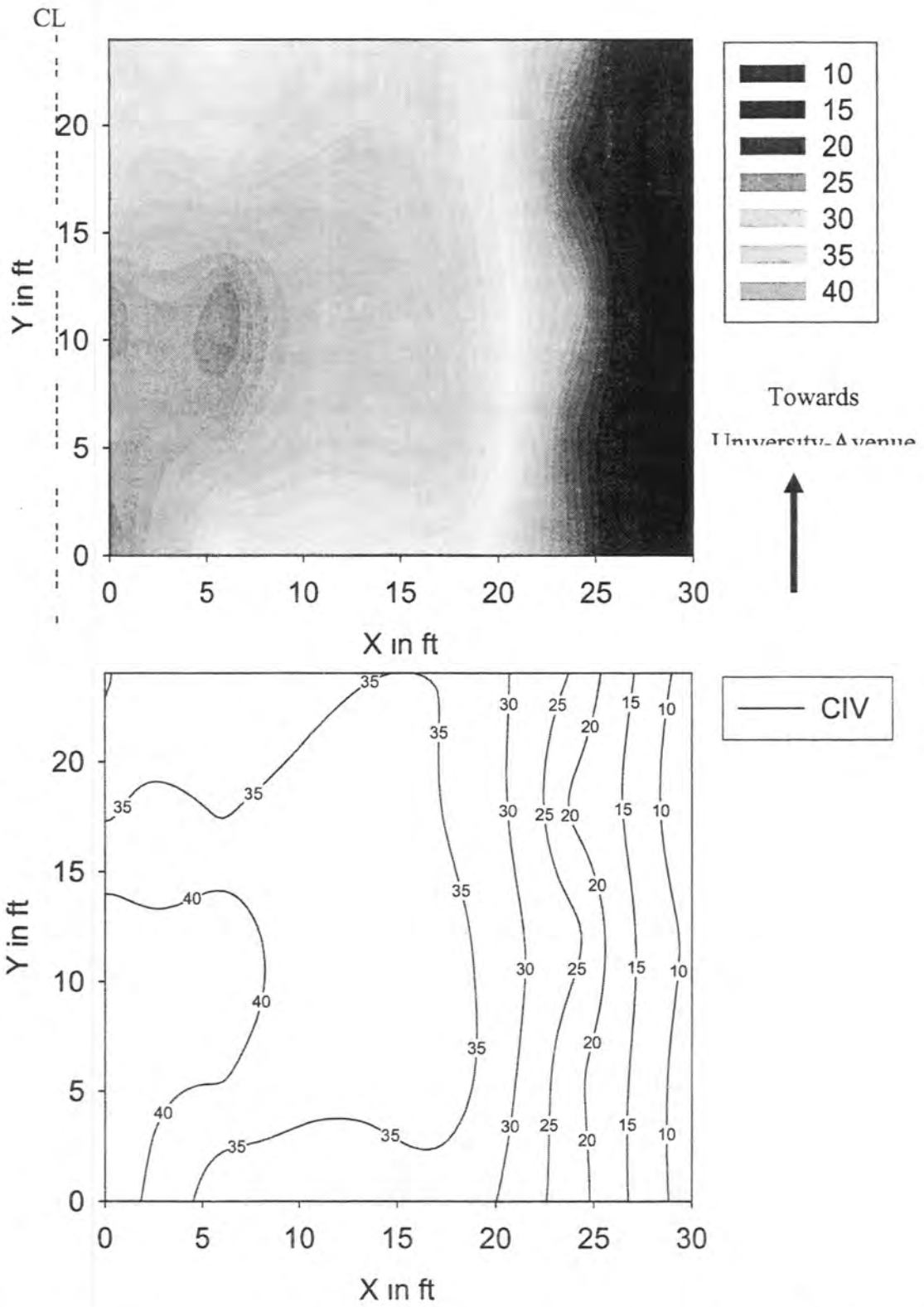


Figure F46. Spatial variation of Clegg Impact Value (CIV) at University-Guthrie Special Backfill Test Section

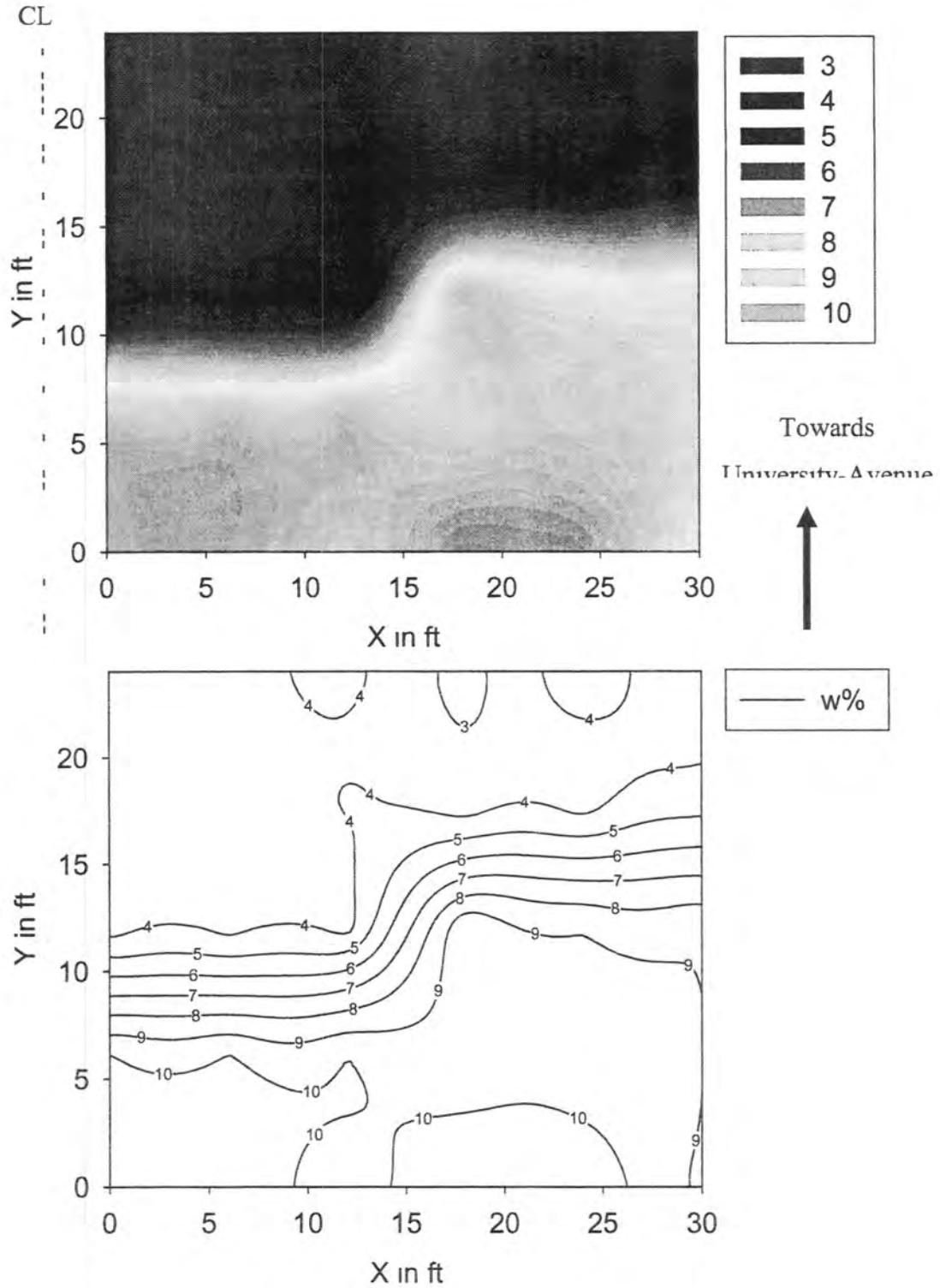


Figure F47 Spatial variation of Moisture Content (w %) at University-Guthrie Special Backfill Test Section

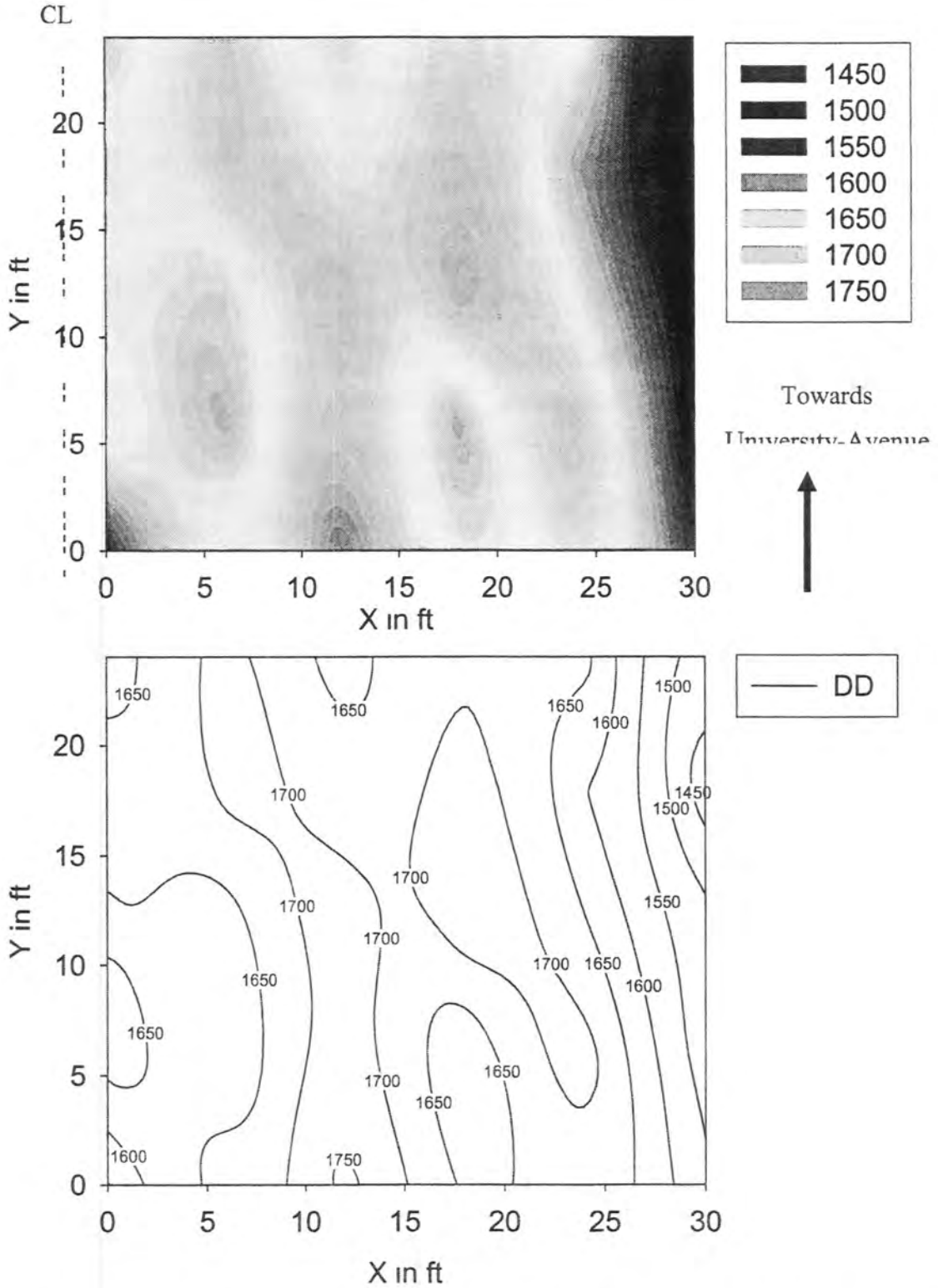
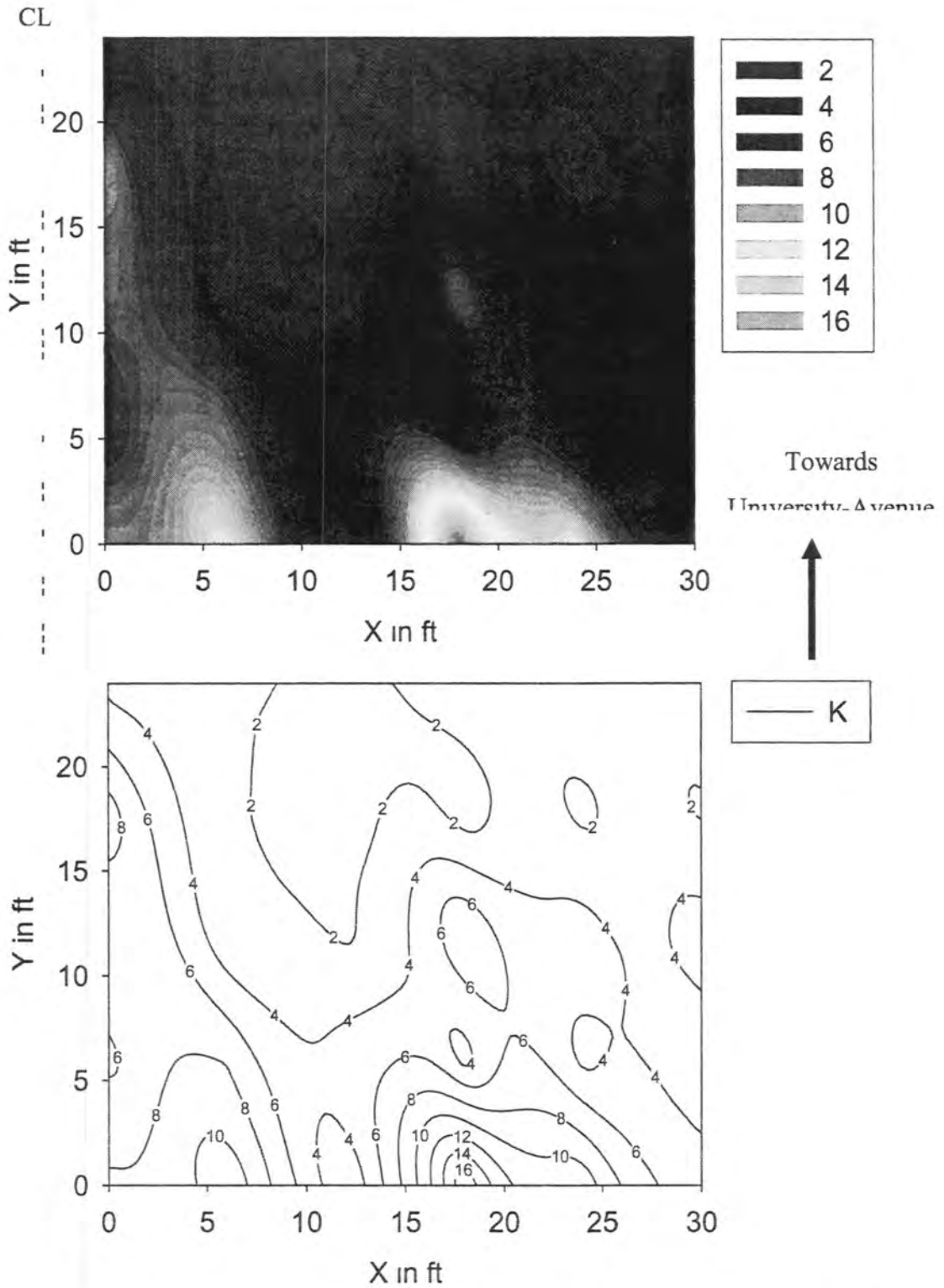
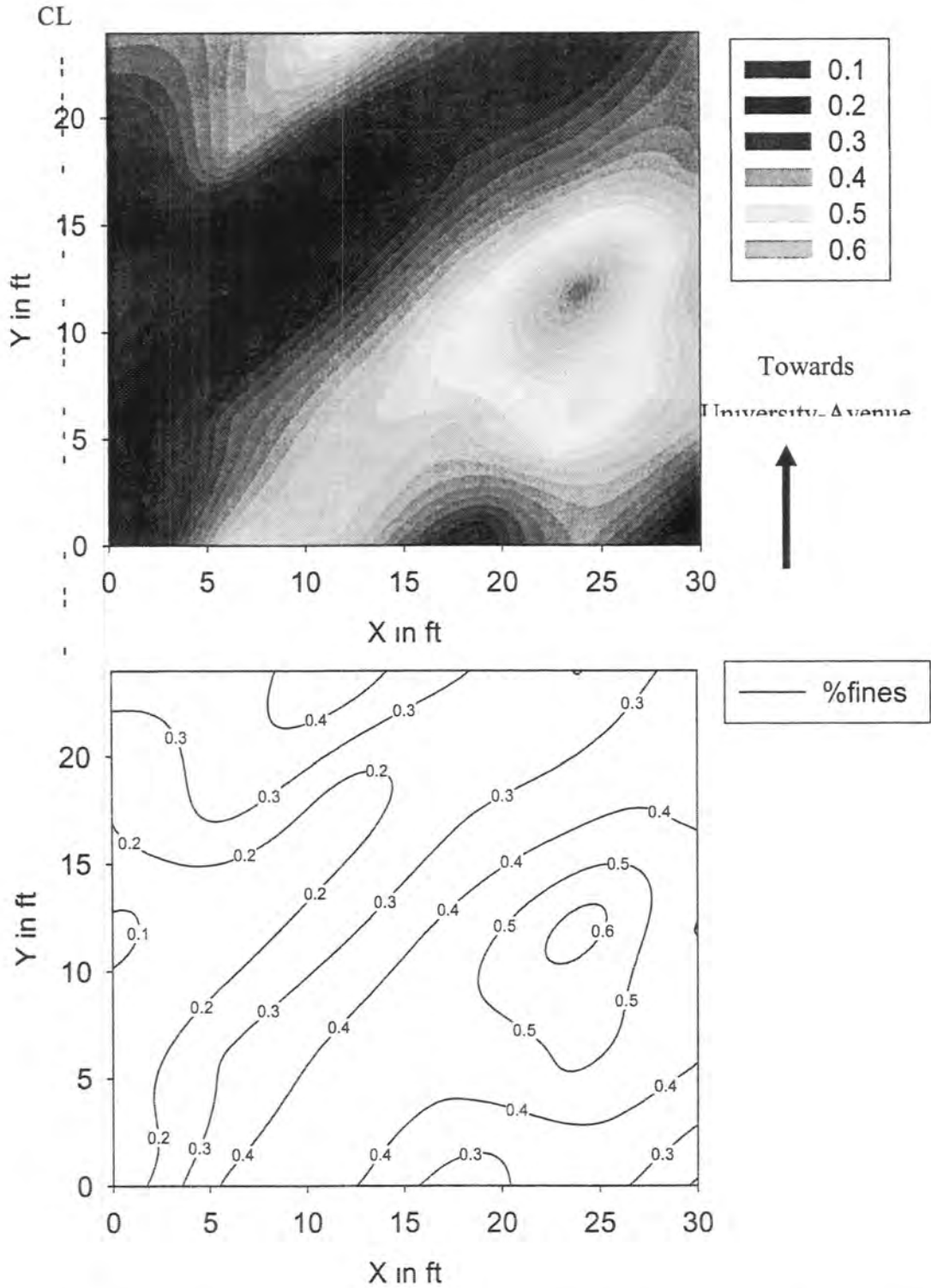


Figure F48. Spatial variation of Dry Density ( $\text{kg/m}^3$ ) at University-Guthrie Special Backfill Test Section



**Figure F49. Spatial variation of Saturated Hydraulic Conductivity at University-Guthrie Special Backfill Test Section**



**Figure F50. Spatial variation of fines content (% fines passing No.200) at University-Guthrie Special Backfill Test Section**

**CONTOUR GRAPHS FOR THE DATA FROM I35 SOUTH BOUND PAVEMENT  
BASE CONSTRUCTION**

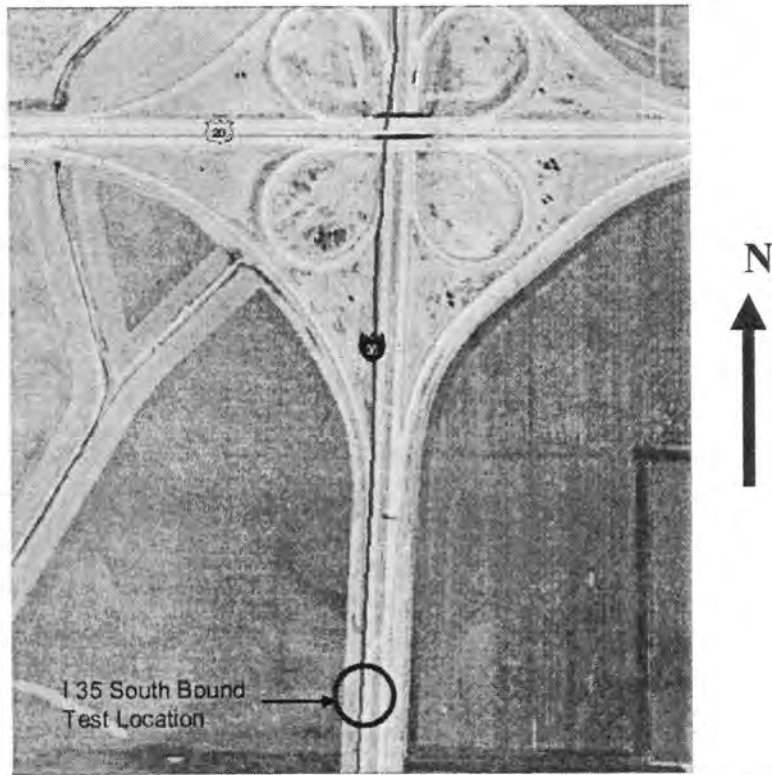


Figure F51. Aerial Photograph of the Test Location (IDNR, 2004)

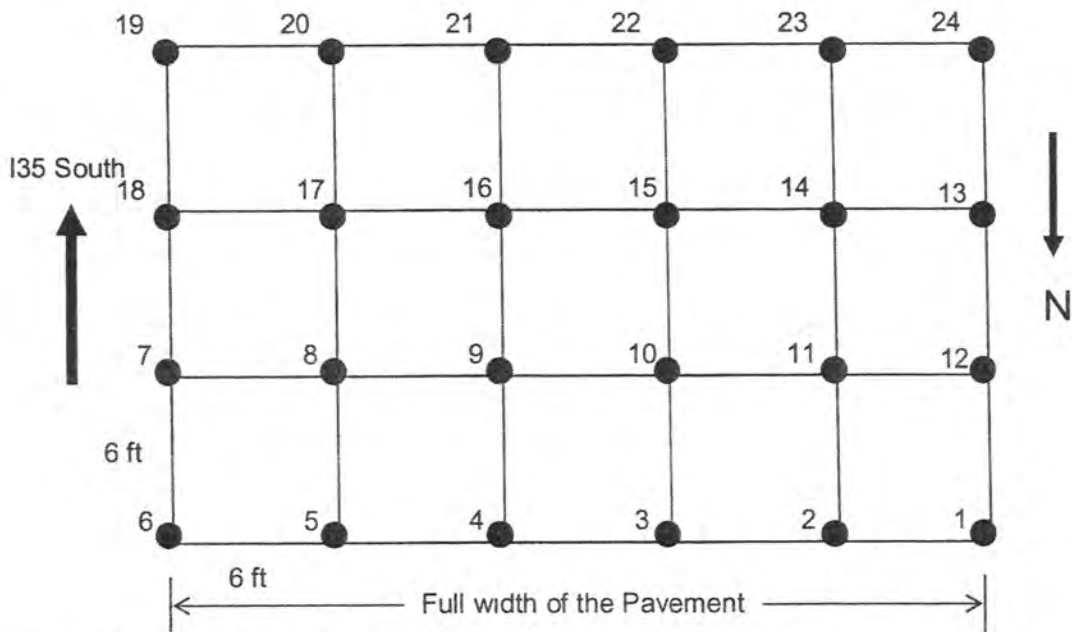
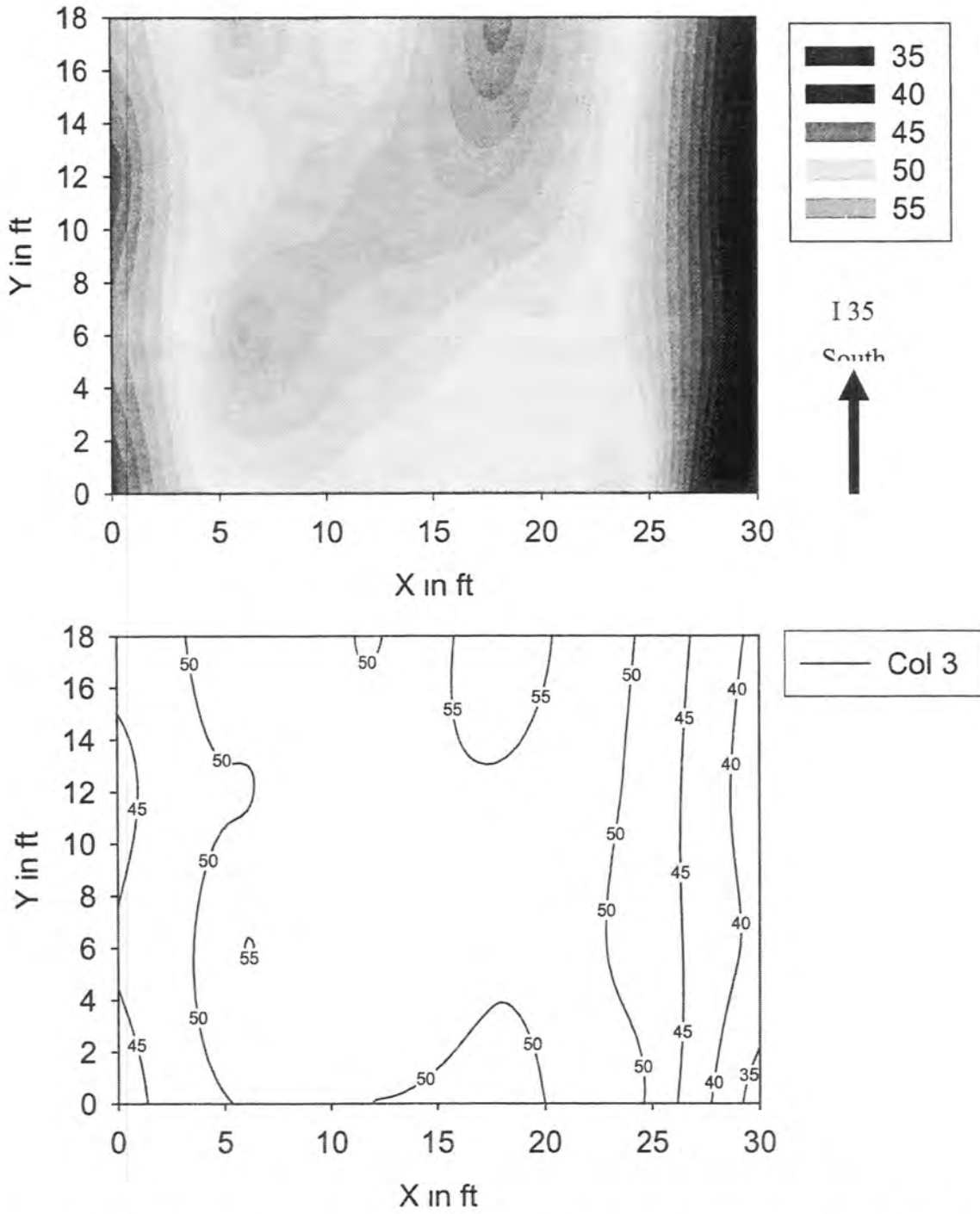


Figure F52. Grid Setup for Testing at I 35 South Bound Base Construction Site



**Figure F53. Spatial variation of GeoGauge Modulus (MPa) at I35 South Bound Pavement Base Test Section**



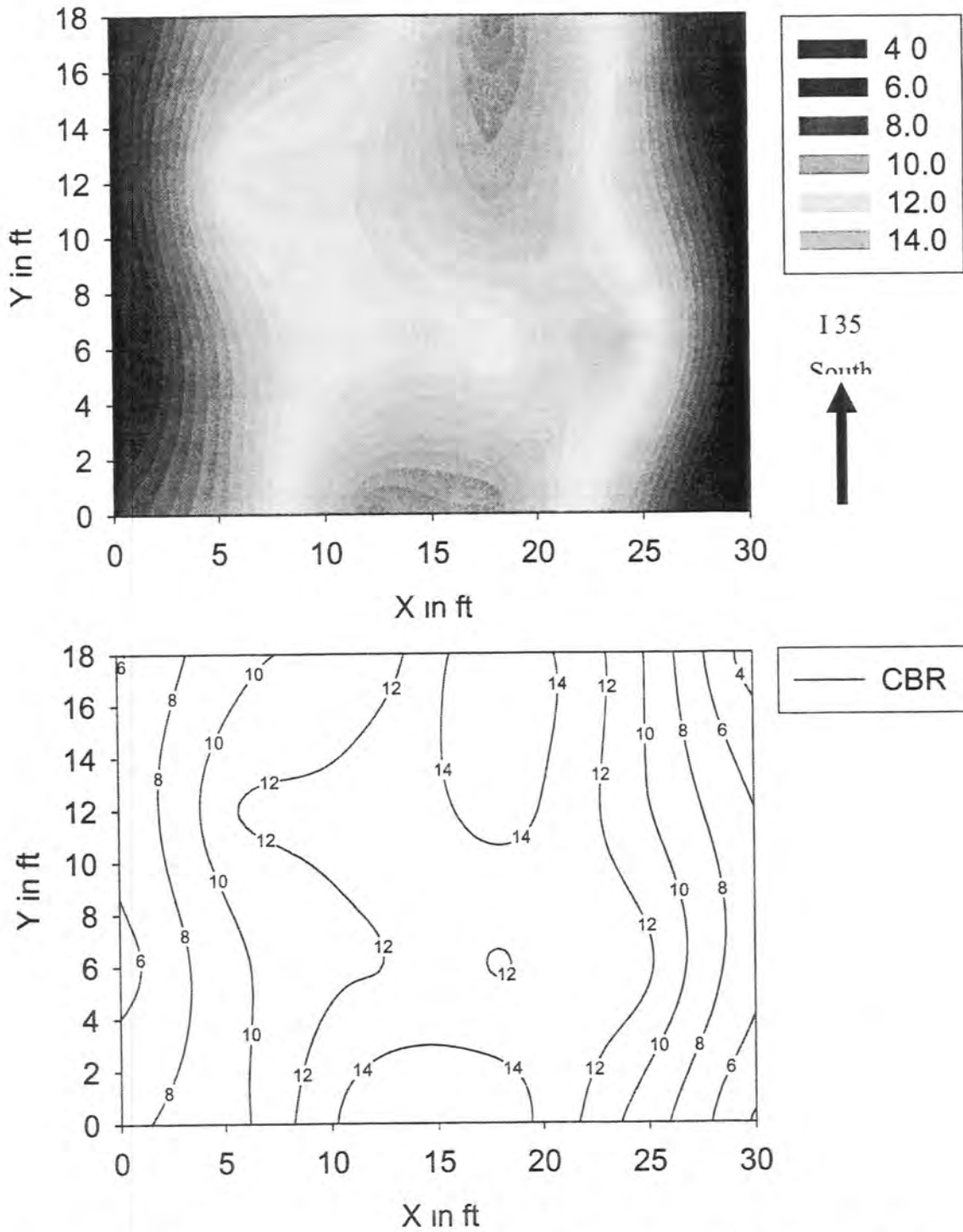


Figure F54. Spatial variation of CBR (%) at I35 South Bound Pavement Base Test Section

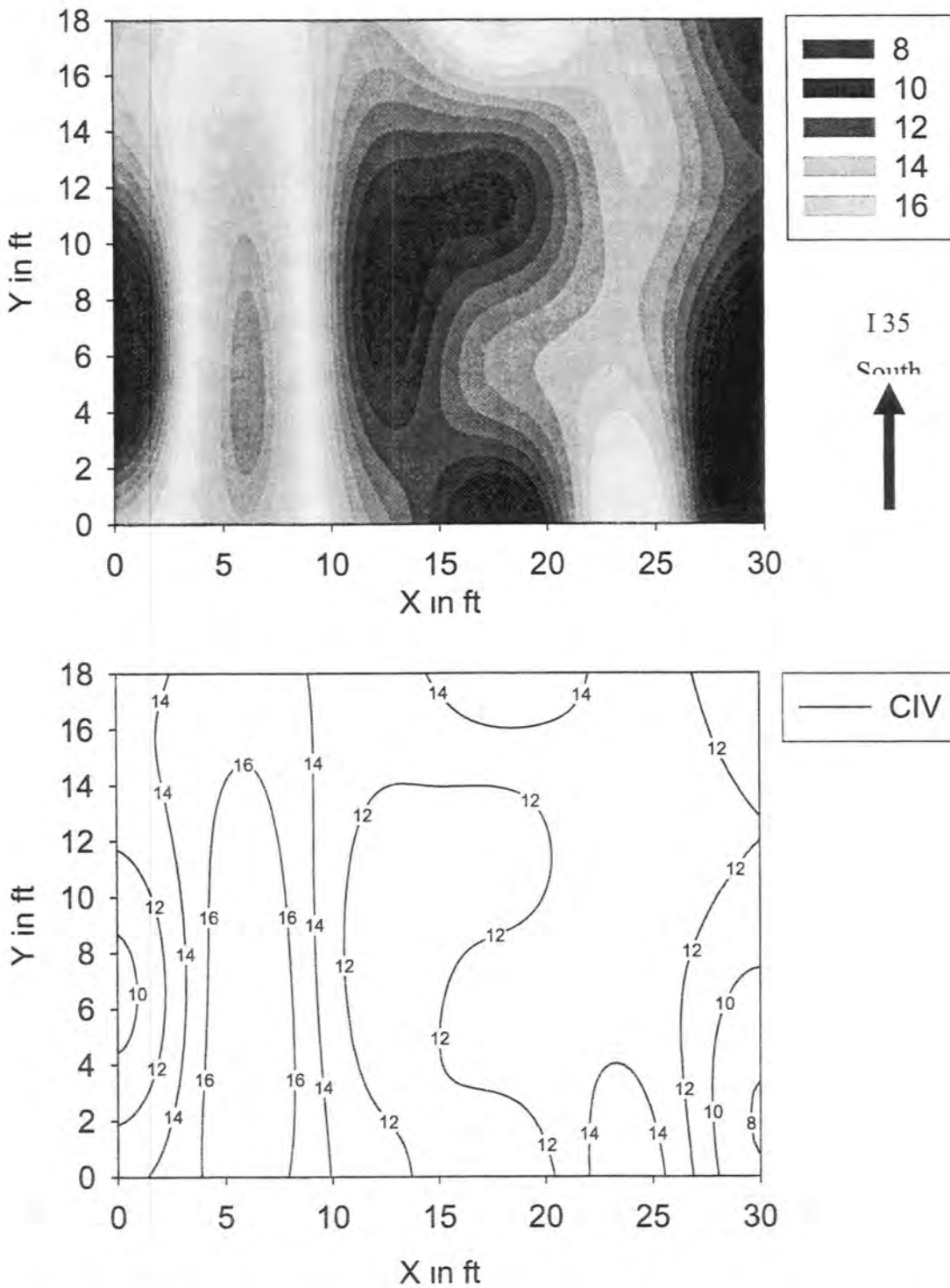
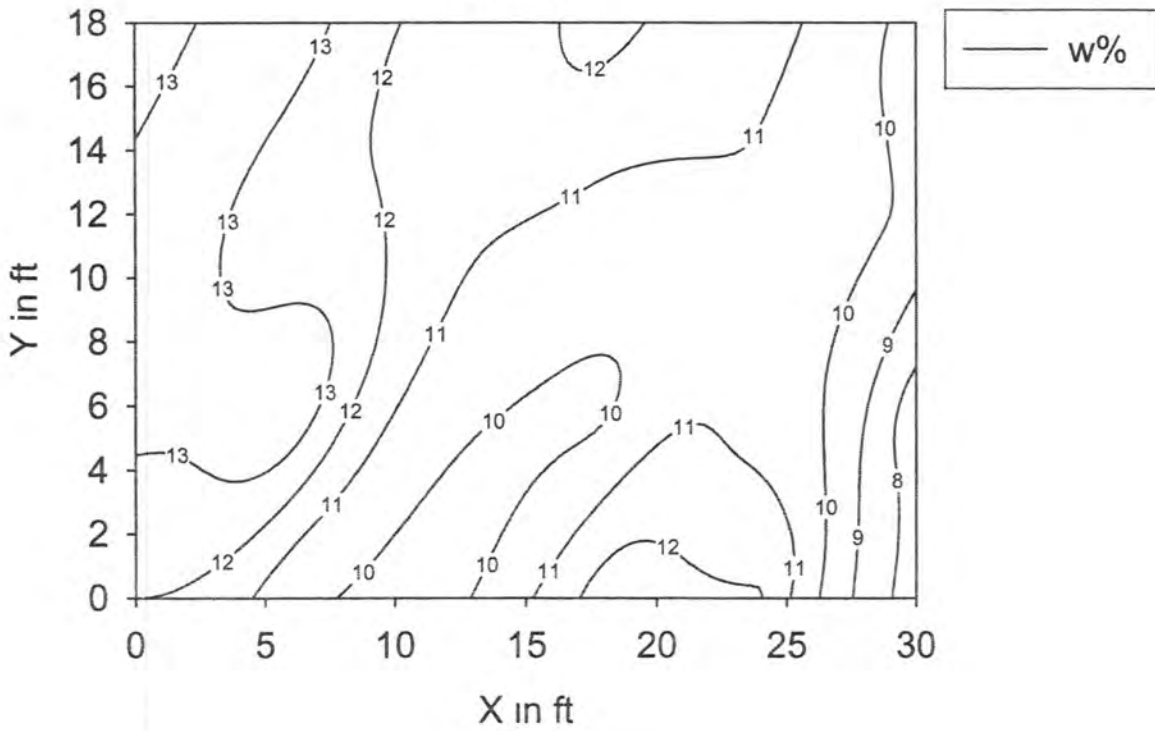
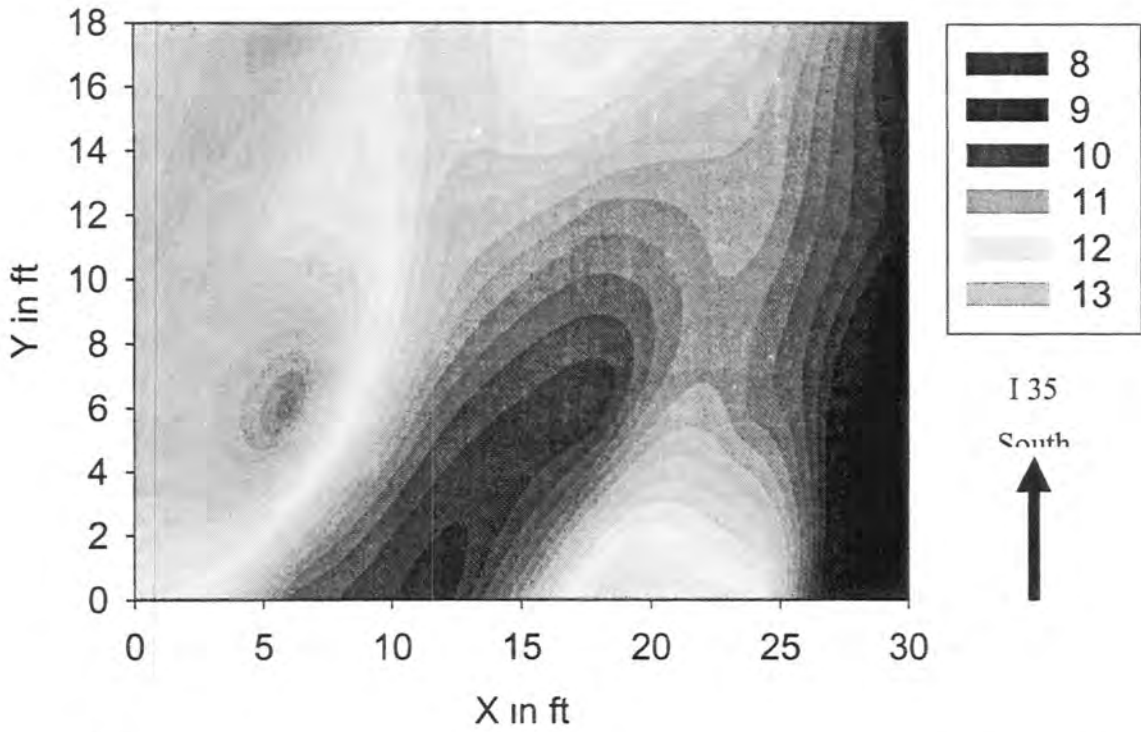
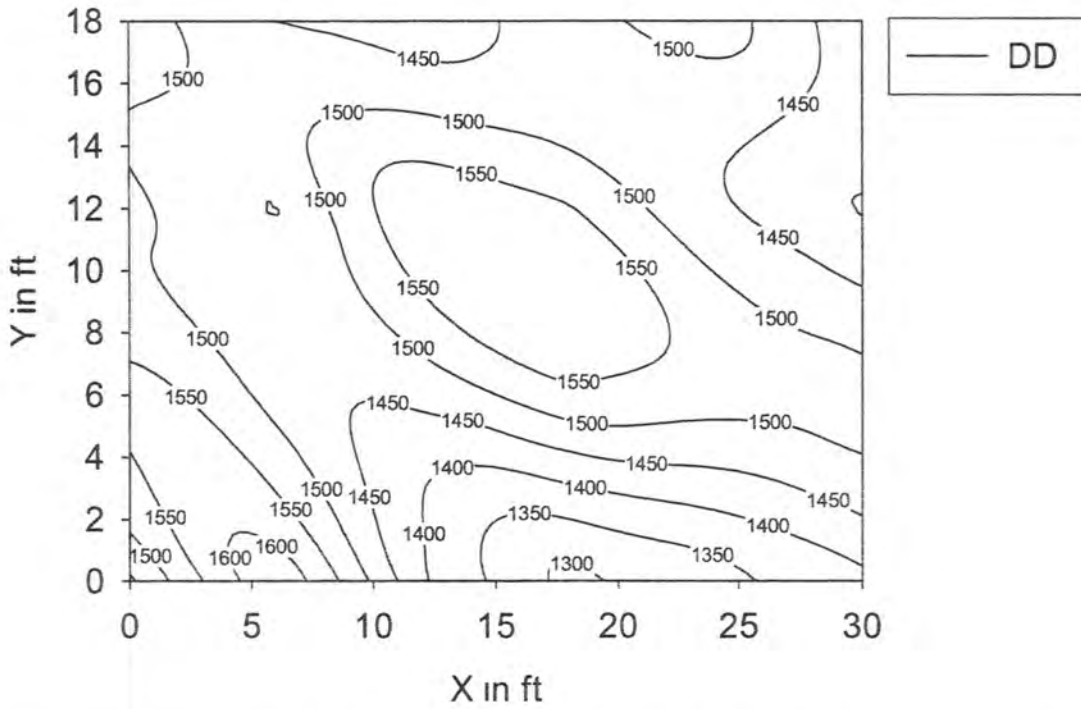
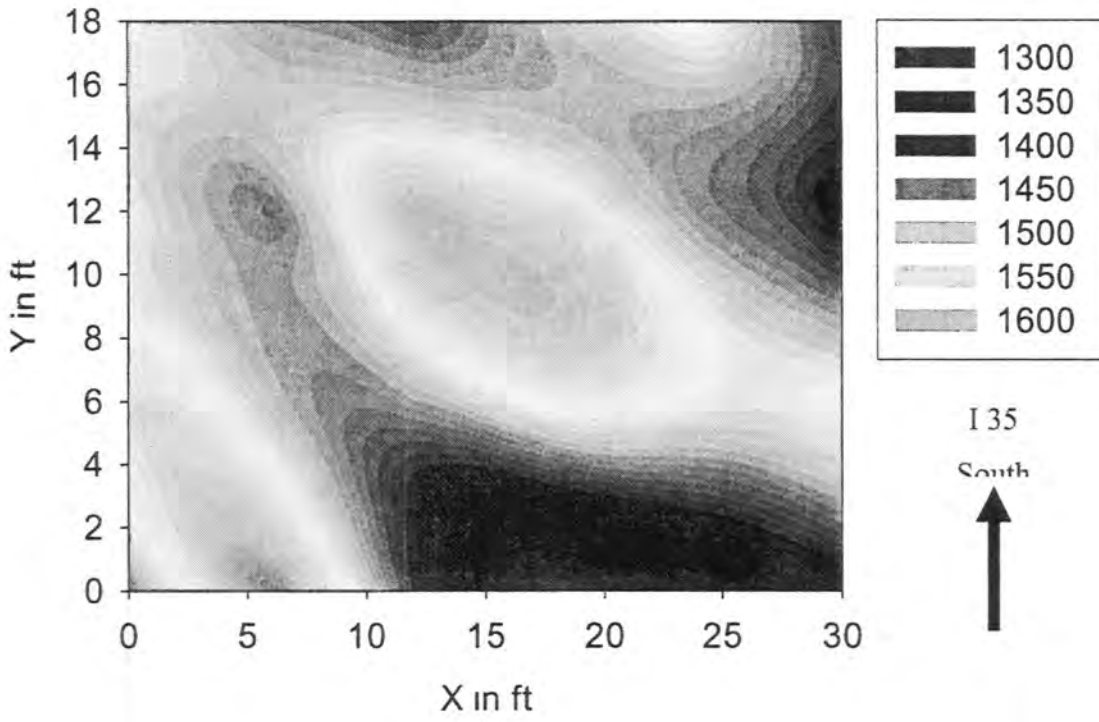


Figure F55. Spatial variation of Clegg Impact Value (CIV) at I35 South Bound Pavement Base Test Section



**Figure F56. Spatial variation of Moisture Content (w %) at I35 South Bound Pavement Base Test Section**



**Figure F57 Spatial variation of Dry Density ( $\text{kg/m}^3$ ) at I35 South Bound Pavement Base Test Section**

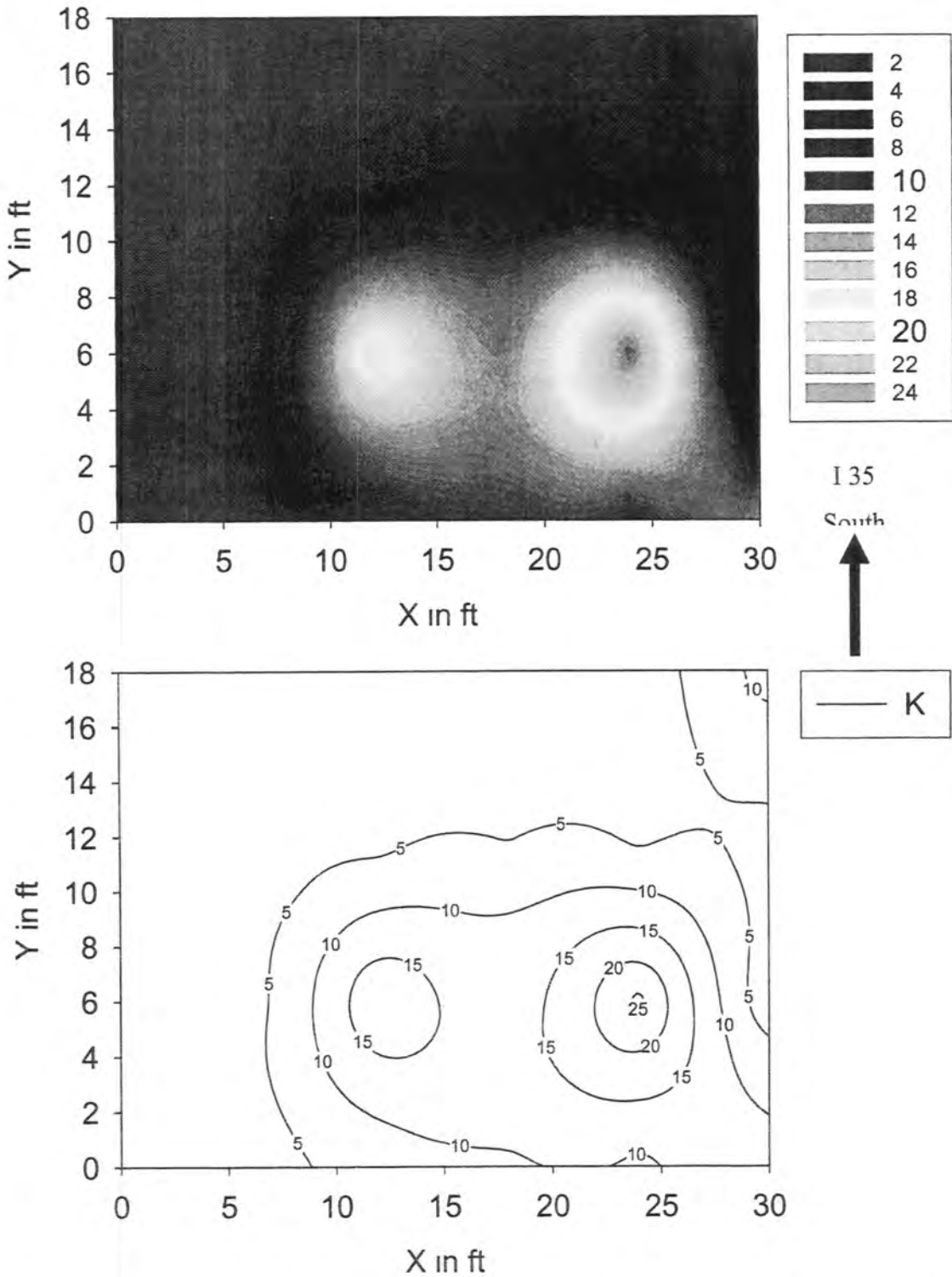
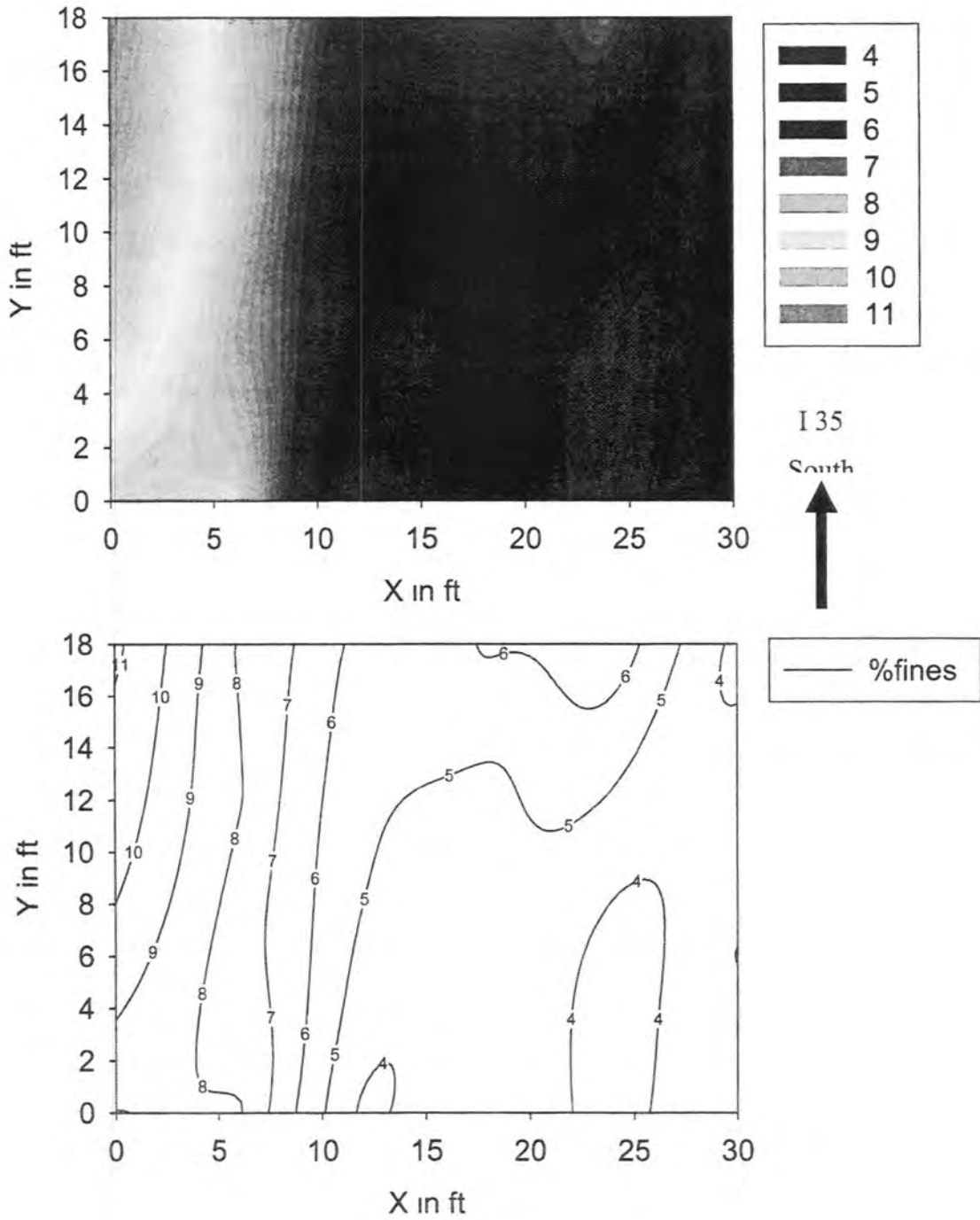


Figure F58. Spatial variation of Saturated Hydraulic Conductivity (cm/sec) at I35 South Bound Pavement Base Test Section



**Figure F59. Spatial variation of fines content (% fines passing No. 200) at I35 South Bound Pavement Base Test Section**

**APPENDIX G: RAW DATA FROM FIELD PROJECTS**

### Glossary of Terms Used for Field Test Results

$\gamma_d$	Dry Density measured from Nuclear Density Gauge Test ( $\text{kg/m}^3$ )
CBR	California Bearing Ratio (%)
CBR <sup>1</sup>	CBR calculated from PI, using Equation No. 4 of Table 19
CBR <sup>2</sup>	CBR calculated from CIV using correlation $\text{CBR} = (0.24 \text{ IV} + 1)^2$
CIV	Clegg Impact Value measured from Clegg Impact Hammer Test
CV	Coefficient of Variation (%)
K	Saturated Hydraulic Conductivity (cm/sec)
M	Mean
MOD	Modulus calculated from GeoGauge <sup>TM</sup> vibration test (MPa)
PI	Penetration Index measured from DCP testing (mm/blow)
S	Stiffness calculated from GeoGauge <sup>TM</sup> vibration test (MN/m)
S%	Degree of Saturation (%)
SD	Standard Deviation
w%	Moisture Content measured from Nuclear Density Gauge Test (%)
% fines	Fines Passing No. 200 sieve size



Table G1 Summary of results from testing on 35<sup>th</sup> street Modified Subbase

Location	MOD (MPa)	S (MN/m)	DCP Test		Clegg Hammer		K (cm/sec)	% fines	w%	Y <sub>d</sub> (kg/m <sup>3</sup> )	Y <sub>d</sub> (pcf)
			PI(mm/blow)	CBR %	CIV	CBR %					
1	473	545	38	50	160	179	208		111	16760	1046
2	615	709	20	102	287	577	26		74	18230	1138
3	686	791	9	249	226	358	14		75	17640	1101
4	676	779	9	249	243	413	139		74	18230	1138
5	360	415	10	222	233	380	54		96	17680	1104
6	677	780	7	330	229	367	53		74	17470	1091
7	364	420	10	222	287	577	28		81	19380	1210
8	378	436	21	96	132	122	63		105	16580	1035
9	475	547	22	92	117	96	294		106	17370	1084
10	483	556	10	222	166	193	46		74	20060	1252
11	428	494	9	249	186	242	47		79	17260	1078
12	602	694	9	249	222	345	35		95	19180	1197
13	428	494	9	249	195	266	31		90	18810	1174
14	837	965	8	284	270	510	40		76	18160	1134
15	678	781	10	222	270	510	38		75	18920	1181
16	403	465	24	83	109	83	91		83	16800	1049
17	395	455	22	92	114	91	107		116	15170	947
18	304	351	8	284	145	147	141		78	18990	1186
19	205	236	12	181	245	420	34		86	18190	1136
20	514	592	8	284	236	390	165		95	18440	1151
21	455	525	9	249	215	324	311		85	19460	1215
22	763	880	8	284	265	492	42		72	17340	1083
23	491	566	9	249	253	448	243		68	20260	1265
24	547	630	22	92	159	177	67		80	19150	1195

Table G2 Summary of results from testing on Knapp Street pavement base

Location	MOD (MPa)	S (MN/m)	DCP Test		Clegg Hammer		K (cm/sec)	% fines	w%	$\gamma_d$ (kg/m <sup>3</sup> )	$\gamma_d$ (pcf)
			PI(mm/blow)	CBR %	CIV	CBR %					
1	67.1	7.73	12	17.5	21.1	31.2	0.79	7.7	9.5	1661.1	103.7
2	78.9	9.09	9	24.0	19.6	26.9	12.09	4.2	9.9	1669.1	104.2
3	90.6	10.44	9	25.5	26.0	47.3	4.34	8.2	11.1	1730.0	108.0
4	85.3	9.83	10	22.3	29.0	58.9	1.25	7.4	11.3	1657.9	103.5
5	62.9	7.25	11	20.9	17.0	20.2	12.00	7.8	11.2	1568.2	97.9
6	72.2	8.32	13	16.9	20.0	28.0	5.00	7.3	10.1	1693.2	105.7
7	103.3	11.91	8	26.9	24.3	41.3	0.97	7.1	9.1	1723.6	107.6
8	64.1	7.39	12	17.4	21.4	32.1	11.42	6.3	9.2	1670.7	104.3
9	64.8	7.47	11	20.6	21.8	33.3	0.50	9.8	9.6	1773.2	110.7
10	101.8	11.74	8	28.6	27.5	52.9	1.70	10.5	10.6	1741.2	108.7
11	71.3	8.21	11	20.4	22.9	36.7	3.97	5.6	10.5	1640.3	102.4
12	97.1	11.19	8	27.8	27.3	52.2	0.60	10.2	11.3	1641.9	102.5
13	112.9	13.01	11	20.8	21.8	33.3	0.34	8.2	10.6	1702.8	106.3
14	82.3	9.48	9	25.2	24.6	42.4	7.80	7.2	9.7	1773.2	110.7
15	82.6	9.53	7	31.0	20.8	30.3	0.53	7.9	9.9	1704.4	106.4
16	91.4	10.53	7	31.2	25.4	45.2	0.34	4.6	12.1	1601.8	100.0
17	75.9	8.75	9	25.5	23.3	38.0	8.55	8.0	11.9	1566.6	97.8
18	81.9	9.44	14	15.3	25.0	43.8	2.93	11.4	11.0	1537.8	96.0
19	80.7	9.31	11	19.7	21.1	31.2	6.81	10.4	10.1	1552.2	96.9
20	71.6	8.25	12	18.8	25.6	45.9	1.95	7.7	8.8	1755.6	109.6
21	81.5	9.39	9	25.7	23.0	37.0	1.45	6.5	10.4	1680.3	104.9
22	80.0	9.22	9	25.8	30.2	63.8	0.39	11.1	10.1	1643.5	102.6
23	101.5	11.70	9	25.7	22.4	35.1	2.94	6.9	10.0	1728.4	107.9
24	85.2	9.82	12	18.4	23.8	39.7	2.43	7.8	10.4	1635.5	102.1

Table G3 Summary of results from testing on IA218 pavement base

Location	MOD (MPa)	S (MN/m)	DCP Test		K (cm/sec)	% fines	w%	$\gamma_d$ (kg/m <sup>3</sup> )	$\gamma_d$ (pcf)		
			PI (mm/blow)	CBR %							
1	73.4	8.46	33	5.8	12.9	11.6	1.50	9.9	4.1	1649.9	103.0
2	66.7	7.69	25	7.9	14.7	15.1	1.49	10.9	4.4	1698.0	106.0
3	82.5	9.51	20	10.2	15	15.8	1.96	9.4	3.5	1685.1	105.2
4	76.4	8.80	14	15.2	17.5	21.4	2.92	10.2	3.4	1736.4	108.4
5	85.7	9.88	19	10.8	19.4	26.3	2.90	9.0	4.2	1744.4	108.9
6	59.9	6.90	55	3.3	8.8	5.4	0.25	10.4	4.5	1742.8	108.8
7	65.3	7.52	51	3.6	9.4	6.2	1.81	11.5	6.0	1717.2	107.2
8	84.2	9.70	37	5.1	14	13.7	1.60	9.2	3.9	1754.0	109.5
9	81.5	9.39	17	12.2	15.9	17.7	2.10	10.3	3.7	1786.1	111.5
10	83.8	9.66	17	12.2	20.4	29.1	1.03	10.3	3.4	1763.6	110.1
11	63.8	7.35	26	7.6	21.3	31.8	0.43	11.0	3.0	1811.7	113.1
12	74.2	8.55	34	5.6	11.5	9.3	0.40	10.9	3.0	1797.3	112.2
13	69.7	8.04	45	4.1	13.4	12.6	0.67	9.3	3.9	1766.8	110.3
14	63.8	7.35	29	6.7	12.9	11.6	1.81	8.1	3.1	1781.3	111.2
15	86.4	9.96	23	8.7	12.6	11.1	2.45	7.6	3.9	1633.9	102.0
16	70.0	8.07	14	15.2	13	11.8	3.11	6.7	3.7	1755.6	109.6
17	63.4	7.31	29	6.7	11.4	9.1	7.53	4.6	3.7	1720.4	107.4
18	58.2	6.71	50	3.7	9.2	5.9	0.66	8.6	3.6	1787.7	111.6
19	51.2	5.90	26	7.6	9.2	5.9	0.47	6.1	4.5	1728.4	107.9
20	69.8	8.05	28	7.0	10.4	7.6	3.45	6.7	3.4	1654.7	103.3
21	60.1	6.93	18	11.5	11.3	8.9	1.23	8.1	3.3	1742.8	108.8
22	86.7	9.99	28	7.0	17.1	20.5	0.98	9.0	4.1	1766.8	110.3
23	74.1	8.55	44	4.2	15.2	16.2	1.30	9.6	3.1	1768.4	110.4
24	71.9	8.28	44	4.2	11.4	9.1	0.70	10.0	3.5	1770.0	110.5
25	67.4	7.77	34	5.6	12.1	10.2	1.40	10.0	3.0	1757.2	109.7
26	94.0	10.84	20	10.2	16.9	20.0	1.31	7.8	4.9	1779.7	111.1
27	86.5	9.97	20	10.2	14.7	15.1	0.99	7.3	2.7	1810.1	113.0
28	77.0	8.88	29	6.7	12.3	10.6	2.46	8.9	4.3	1771.6	110.6
29	71.2	8.21	28	7.0	12.3	10.6	3.56	7.6	3.8	1725.2	107.7
30	64.5	7.43	56	3.2	6.7	3.1	1.68	9.8	3.5	1701.2	106.2

Table G4. Summary of results from testing on US151 pavement base

Location	MOD (MPa)	S (MN/m)	DCP Test		Clegg Hammer		K (cm/sec)	% fines	w%	$\gamma_d$ (kg/m <sup>3</sup> )	$\gamma_d$ (pcf)
			PI (mm/blow)	CBR %	CIV	CBR %					
1	53.8	6.20	27	7.4	13.6	12.9	6.08	4.04	3.9	1738.0	108.5
2	66.6	7.67	18	11.5	13.3	12.4	4.62	4.20	3.0	1709.2	106.7
3	65.8	7.58	21	9.9	18.5	24.0	4.28	3.05	4.2	1608.3	100.4
4	73.8	8.50	12	18.1	14.1	13.9	4.46	4.45	4.0	1730.0	108.0
5	49.6	5.71	15	14.5	16.2	18.4	11.37	3.33	3.3	1465.7	91.5
6	58.5	6.74	59	3.0	10.9	8.3	3.90	4.37	2.4	1816.5	113.4
7	54.4	6.27	40	4.7	10.0	7.0	9.16	4.36	2.9	1649.9	103.0
8	62.4	7.19	26	7.7	9.6	6.5	8.54	3.68	2.6	1728.4	107.9
9	93.0	10.72	17	11.9	13.7	13.1	4.09	5.69	3.1	1784.5	111.4
10	72.3	8.33	18	11.8	13.8	13.3	1.70	5.32	3.5	1541.0	96.2
11	68.6	7.91	16	12.9	13.8	13.3	4.41	4.94	3.0	1675.5	104.6
12	67.7	7.80	32	6.0	16.0	17.9	6.99	4.59	3.1	1765.2	110.2
13	70.7	8.15	44	4.2	15.5	16.8	12.09	4.95	3.4	1827.7	114.1
14	75.6	8.72	19	10.6	15.6	17.0	5.01	3.80	3.0	1774.8	110.8
15	75.1	8.66	14	15.4	13.2	12.2	2.35	3.82	2.5	1734.8	108.3
16	66.5	7.67	15	14.6	10.9	8.3	2.99	4.86	4.4	1459.3	91.1
17	63.5	7.32	23	8.7	11.2	8.8	8.10	3.26	2.9	1789.3	111.7
18	57.8	6.66	59	3.0	11.9	9.9	5.68	4.39	2.4	1810.1	113.0
19	56.7	6.54	24	8.5	13.3	12.4	1.36	5.67	3.6	1722.0	107.5
20	68.6	7.91	21	9.5	15.9	17.7	3.86	4.24	3.2	1786.1	111.5
21	96.6	11.13	18	11.6	17.2	20.7	14.06	3.27	3.6	1657.9	103.5
22	71.3	8.22	29	6.8	11.2	8.8	2.46	3.33	3.6	1545.8	96.5
23	78.9	9.09	32	6.0	15.9	17.7	2.78	5.10	3.8	1827.7	114.1
24	74.0	8.52	43	4.4	13.5	12.8	6.69	5.34	3.9	1784.5	111.4
25	74.3	8.56	32	6.0	13.8	13.3	6.69	5.49	3.6	1770.0	110.5
26	76.0	8.76	15	14.6	14.2	14.1	2.26	4.27	3.5	1723.6	107.6
27	72.0	8.29	20	10.0	12.9	11.6	4.91	3.39	2.7	1670.7	104.3
28	95.3	10.99	28	6.9	17.9	22.4	8.03	3.47	3.9	1734.8	108.3
29	56.6	6.53	20	10.1	12.6	11.1	7.36	3.71	3.8	1718.8	107.3
30	53.6	6.18	64	2.8	15.2	16.2	1.47	4.68	3.8	1840.5	114.9

Table G5 Summary of results from testing on University-Guthrie pavement base

Location	MOD (MPa)	S (MN/m)	DCP Test		Clegg Hammer		K (cm/sec)	% fines	w%	$\gamma_d$ (kg/m <sup>3</sup> )	$\gamma_d$ (pcf)
			PI (mm/blow)	CBR %	CIV	CBR %					
1	103.3	11.91	5	51.8	15.1	16.0	4.27	5.66			
2	106.5	12.28	4	59.0	20.5	29.4	5.05	7.23			
3	145.0	16.72	3	79.0	24.4	41.7	1.13	12.71			
4	112.4	12.96	4	59.6	26	47.3	0.22	10.75			
5	115.1	13.27	4	68.3	24.5	42.0	1.42	4.28			
6	91.0	10.49	6	37.5	21.8	33.3	0.40	8.45			
7	95.2	10.97	4	58.7	22.5	35.4	0.46	8.97			
8	121.6	14.02	4	64.9	22.6	35.8	4.11	3.70			
9	126.3	14.56	3	83.4	31.5	69.5	0.64	10.54			
10	112.4	12.96	4	71.5	40.2	113.1	0.41	13.14			
11	146.2	16.85	4	60.0	32.2	72.6	1.09	9.90			
12	120.1	13.85	5	49.9	19.4	26.3	8.23	3.64			
13	114.2	13.16	5	49.2	16.2	18.4	18.52	2.12			
14	121.1	13.96	5	47.8	29.9	62.6	0.69	8.83			
15	116.8	13.46	5	51.0	40.4	114.3	0.39	12.15			
16	152.2	17.55	4	60.6	32.3	73.0	0.22	10.15			
17	97.7	11.26	5	53.4	25.6	45.9	4.63	7.32			
18	122.1	14.07	4	55.5	26.8	50.3	0.11	9.44			
19	108.9	12.55	5	48.8	27.7	53.7	0.42	9.96			
20	105.7	12.18	6	41.0	23.3	38.0	0.40	7.54			
21	86.4	9.96	5	46.3	27	51.0	0.34	10.03			
22	140.5	16.20	6	42.6	27.9	54.5	1.32	12.31			
23	117.0	13.49	5	49.8	21.6	32.7	0.28	10.00			
24	97.0	11.18	5	44.2	18	22.7	9.26	4.64			
25	101.1	11.66	5	48.5	16.6	19.3	11.11	4.22			
26	106.8	12.31	5	47.1	26	47.3	1.68	8.36			
27	99.3	11.45	6	39.0	27.2	51.8	0.17	13.95			
28	108.3	12.48	5	46.4	26.9	50.7	0.37	10.08			
29	116.5	13.43	5	46.3	22.3	34.8	1.85	6.63			
30	118.5	13.66	6	42.0	21.9	33.6	0.11	8.81	No Data	No Data	No Data

Table G6 Summary of results from testing on University-Guthrie special backfill

Location	MOD (MPa)	S (MN/m)	DCP Test		Clegg Hammer		K (cm/sec)	% fines	w%	$\gamma_d$ (kg/m <sup>3</sup> )	$\gamma_d$ (pcf)
			PI (mm/blow)	CBR %	CIV	CBR %					
1	71.7	8.26	19	11.0	7.4	3.8	4.65	0.18	8.8	1557.0	97.2
2	107.9	12.43	10	23.3	22.2	34.5	11.52	0.36	10.7	1686.7	105.3
3	158.9	18.32	5	53.6	33.0	76.2	18.04	0.22	10.9	1643.5	102.6
4	121.9	14.05	5	47.6	31.5	69.5	2.09	0.42	9.4	1763.6	110.1
5	150.8	17.38	6	42.8	31.3	68.6	11.93	0.42	10.4	1672.3	104.4
6	140.2	16.16	5	53.9	43.1	130.0	8.35	0.10	10.2	1547.4	96.6
7	105.4	12.15	23	8.7	7.1	3.5	2.80	0.41	9.0	1525.0	95.2
8	134.6	15.52	9	23.9	21.0	30.9	3.50	0.53	9.4	1718.8	107.3
9	154.5	17.80	5	50.3	37.0	95.8	3.18	0.42	9.2	1601.8	100.0
10	169.9	19.59	5	50.6	36.8	94.8	4.66	0.43	10.0	1714.0	107.0
11	155.8	17.96	5	50.4	40.9	117.1	7.89	0.32	10.1	1601.8	100.0
12	152.6	17.59	4	54.7	40.7	116.0	5.50	0.16	10.1	1675.5	104.6
13	80.1	9.23	22	9.1	9.1	5.8	4.87	0.39	8.8	1518.6	94.8
14	153.2	17.66	6	37.2	26.7	49.9	4.75	0.67	8.9	1653.1	103.2
15	157.9	18.20	5	50.3	36.1	91.2	8.23	0.45	9.9	1730.0	108.0
16	160.4	18.49	5	43.3	37.5	98.4	1.66	0.28	3.7	1722.0	107.5
17	143.7	16.56	5	51.8	43.1	130.0	2.22	0.14	3.7	1627.5	101.6
18	176.4	20.34	6	42.8	42.9	128.8	7.78	0.07	3.6	1643.5	102.6
19	68.1	7.85	35	5.4	5.5	2.1	1.68	0.36	4.5	1420.8	88.7
20	146.7	16.91	7	31.1	18.7	24.5	1.45	0.35	3.4	1601.8	100.0
21	130.8	15.07	5	50.5	34.1	81.4	0.76	0.28	3.3	1714.0	107.0
22	149.7	17.26	5	46.9	36.5	93.3	0.97	0.14	4.1	1670.7	104.3
23	156.0	17.99	5	53.0	34.1	81.4	2.20	0.36	3.1	1712.4	106.9
24	162.2	18.69	5	43.9	33.9	80.4	8.86	0.20	3.5	1680.3	104.9
25	77.7	8.96	28	6.9	7.7	4.2	2.90	0.35	3.0	1480.1	92.4
26	130.9	15.09	7	32.3	24.7	42.7	3.55	0.19	4.9	1665.9	104.0
27	153.7	17.71	6	41.4	34.7	84.3	3.19	0.31	2.7	1698.0	106.0
28	125.4	14.46	6	42.3	34.5	83.3	0.89	0.49	4.3	1627.5	101.6
29	146.9	16.93	5	45.5	31.5	69.5	2.28	0.35	3.8	1714.0	107.0
30	147.1	16.95	5	53.5	35.3	87.2	3.42	0.33	3.5	1621.1	101.2

Table G7 Summary of results from testing on I35 South Bound pavement base

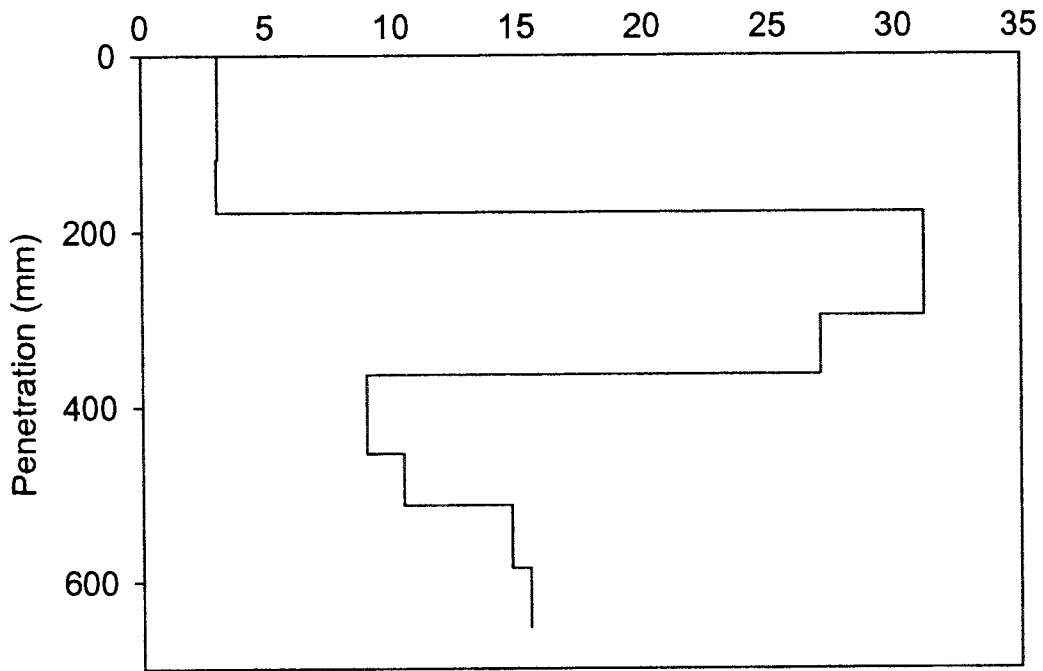
Location	MOD (MPa)	S (MN/m)	DCP Test		Clegg Hammer		K (cm/sec)	% fines	w%	$\gamma_d$ (kg/m <sup>3</sup> )	$\gamma_d$ (pcf)
			PI(mm/blow)	CBR %	CIV	CBR %					
1	32.3	3.72	50	3.7	8.2	4.7	12.41	4.19	7.5	1385.6	86.5
2	51.9	5.99	21	9.6	15.1	16.0	8.94	3.78	12.1	1326.3	82.8
3	49.0	5.64	14	15.3	10.1	7.1	9.27	4.95	12.6	1284.7	80.2
4	49.9	5.76	14	15.8	12.7	11.3	6.87	3.77	9.7	1404.8	87.7
5	50.2	5.79	21	9.9	17.1	20.5	1.96	8.10	10.1	1641.9	102.5
6	42.6	4.91	26	7.6	13.5	12.8	1.52	7.97	12.0	1441.7	90.0
7	45.6	5.26	37	5.1	9.4	6.2	2.08	9.73	13.2	1566.6	97.8
8	55.4	6.39	21	9.9	17.9	22.4	3.29	7.40	14.0	1478.5	92.3
9	52.4	6.04	18	11.8	11.1	8.6	19.69	4.75	10.3	1468.9	91.7
10	50.4	5.81	18	11.7	13.0	11.8	12.61	4.72	9.8	1539.4	96.1
11	48.8	5.62	15	13.7	13.4	12.6	26.14	3.51	10.5	1518.6	94.8
12	39.1	4.51	30	6.5	9.1	5.8	1.57	5.05	7.4	1529.8	95.5
13	37.0	4.27	32	6.0	12.0	10.1	3.77	4.41	9.9	1395.2	87.1
14	49.5	5.70	19	10.8	13.6	12.9	3.88	4.90	11.0	1456.1	90.9
15	54.3	6.26	14	14.8	11.1	8.6	4.70	4.61	10.7	1553.8	97.0
16	53.4	6.16	17	12.5	11.5	9.3	3.32	5.22	11.2	1600.2	99.9
17	49.3	5.68	17	12.4	16.8	19.8	1.10	8.11	12.3	1446.5	90.3
18	42.9	4.95	30	6.4	12.2	10.4	0.84	10.64	13.2	1513.7	94.5
19	46.8	5.39	33	5.7	13.5	12.8	0.82	11.19	12.5	1528.2	95.4
20	54.1	6.24	21	9.6	15.0	15.8	2.30	7.90	13.6	1449.7	90.5
21	49.2	5.67	19	10.5	13.2	12.2	1.63	5.63	11.4	1419.2	88.6
22	57.9	6.67	13	16.0	15.8	17.5	2.15	6.13	12.4	1478.5	92.3
23	50.4	5.81	18	11.2	13.3	12.4	2.12	6.71	11.4	1531.4	95.6
24	38.7	4.46	63	2.8	10.6	7.9	12.01	3.73	9.6	1417.6	88.5

**APPENDIX H. DCP PROFILES FROM PATCHING INVESTIGATION**



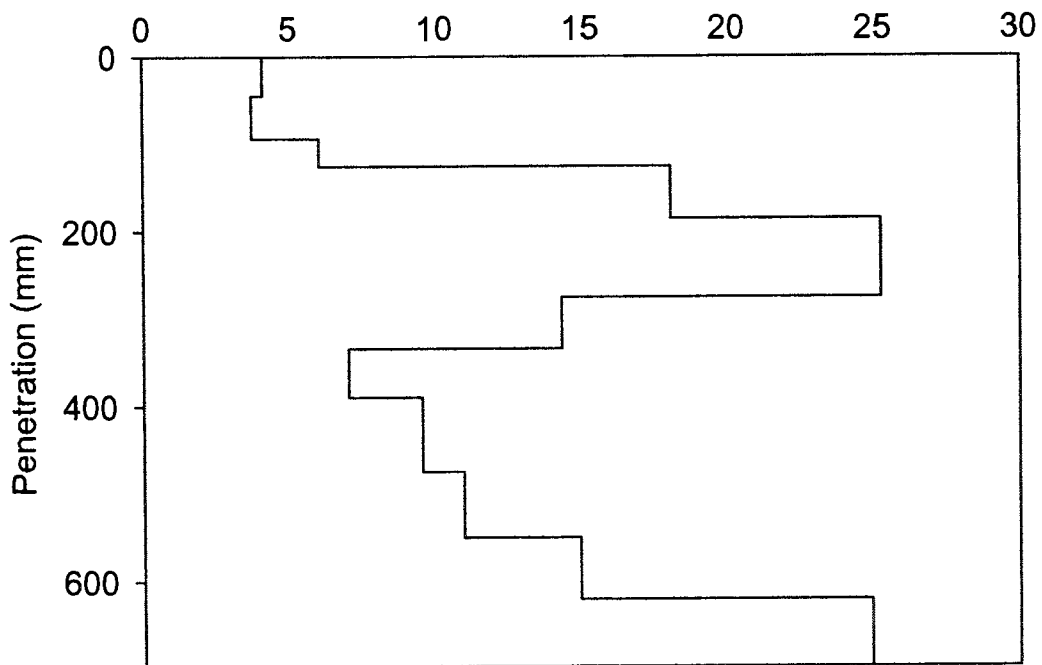
CBR at Location 1 on I235

CBR%

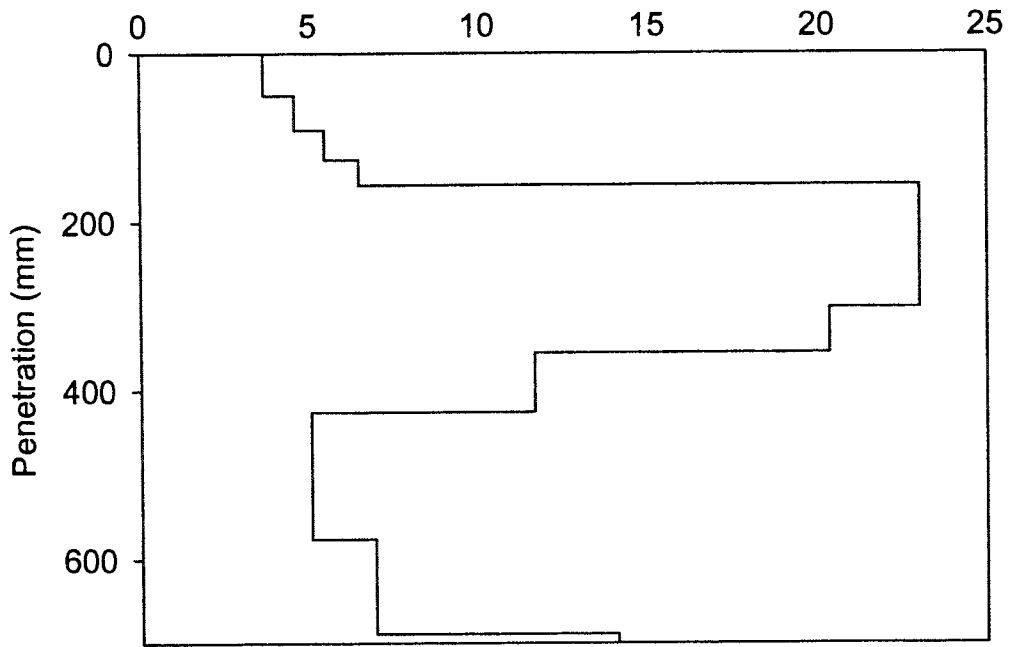


CBR at Location 2 on I235

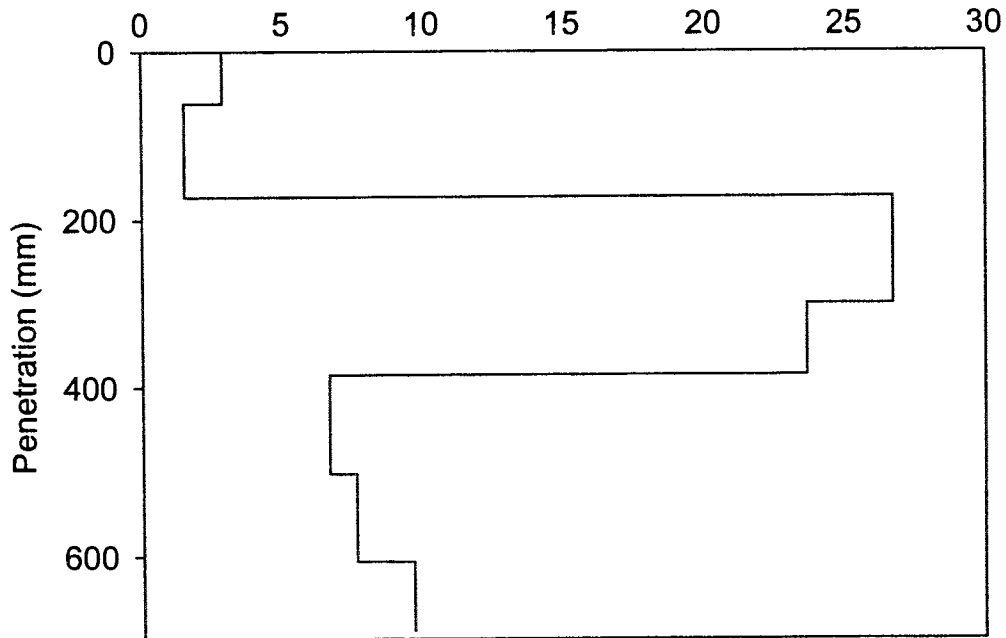
CBR%



CBR at Location 3 on I235  
CBR%

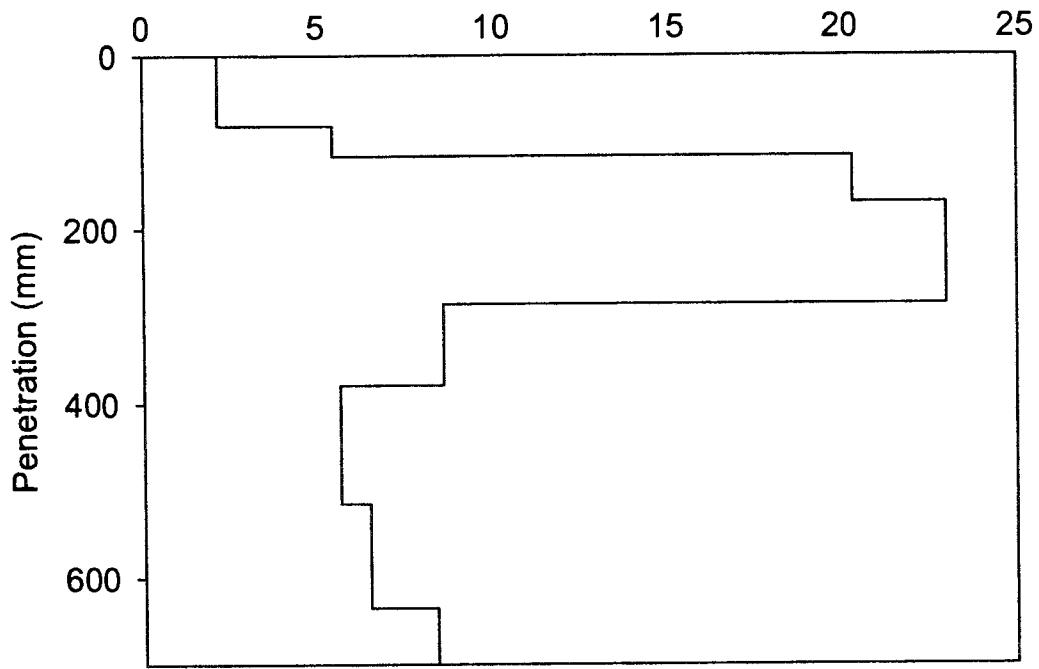


CBR at Location 4 on I235  
CBR%



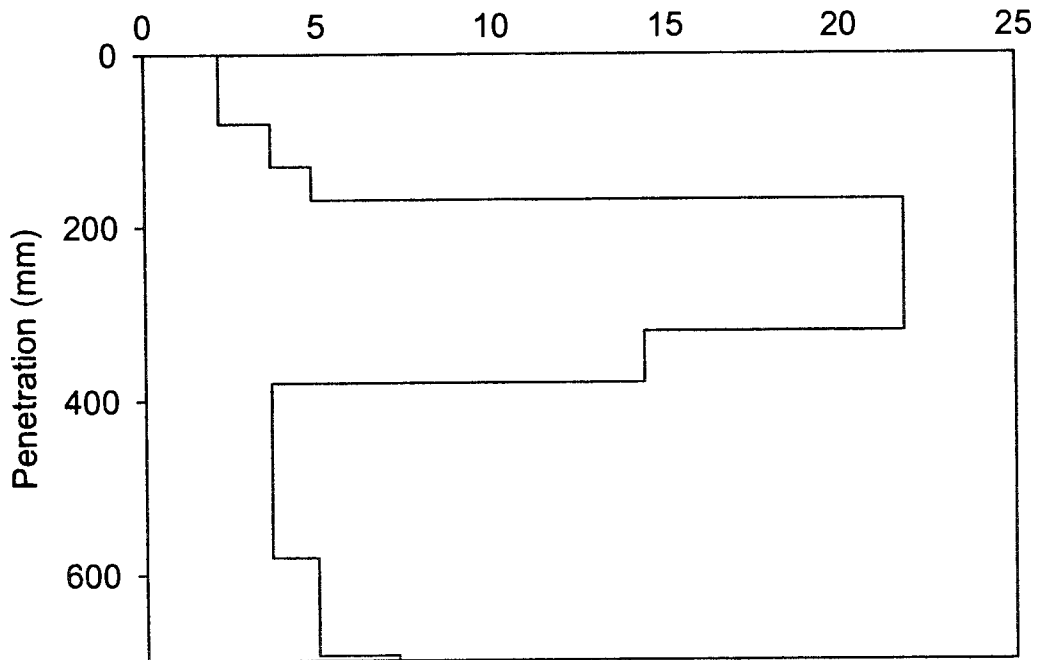
CBR at Location 5 on I235

CBR%

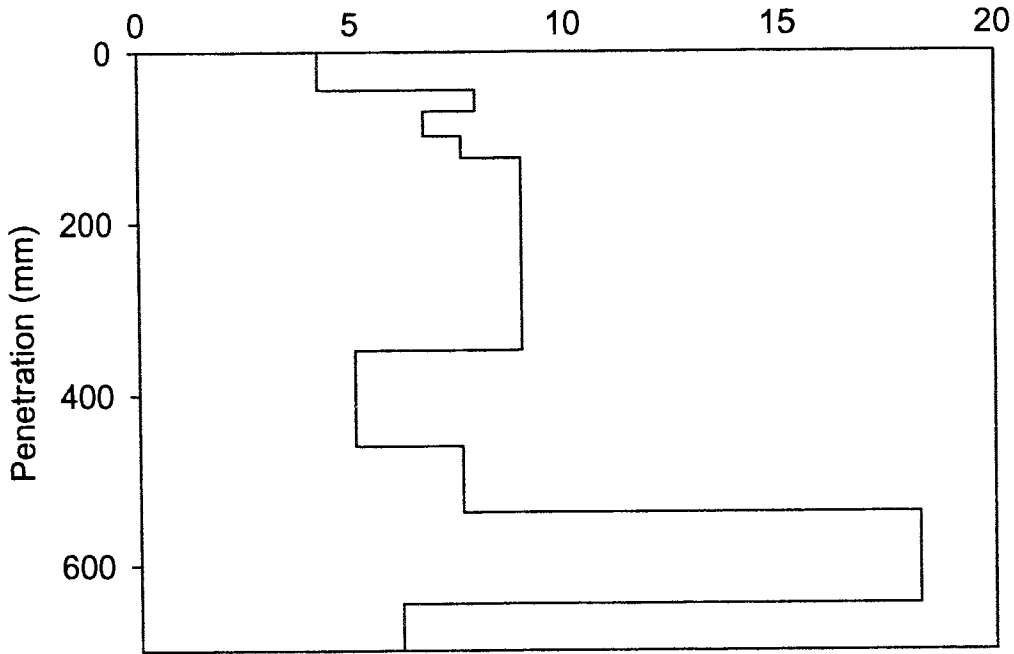


CBR at Location 6 on I235

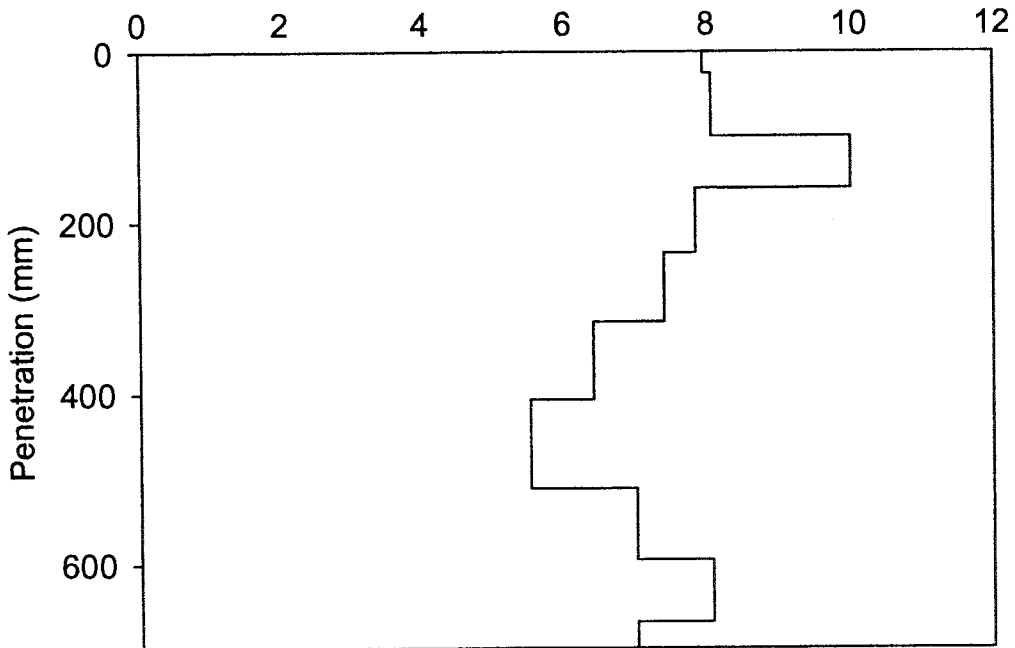
CBR%



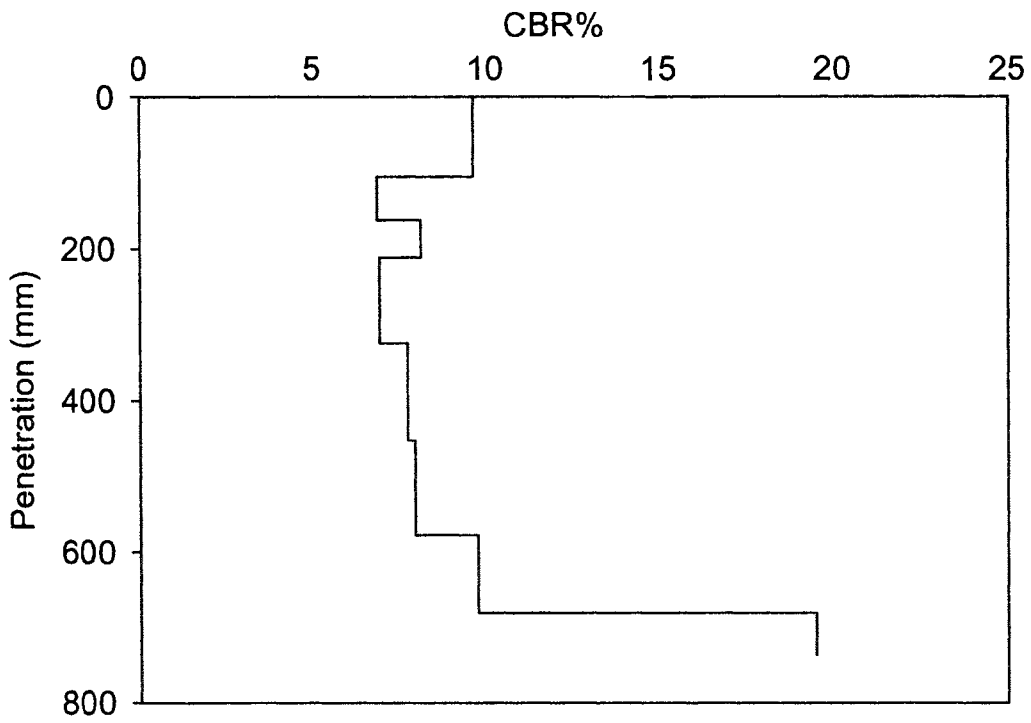
CBR at Location 7 on I235  
CBR%



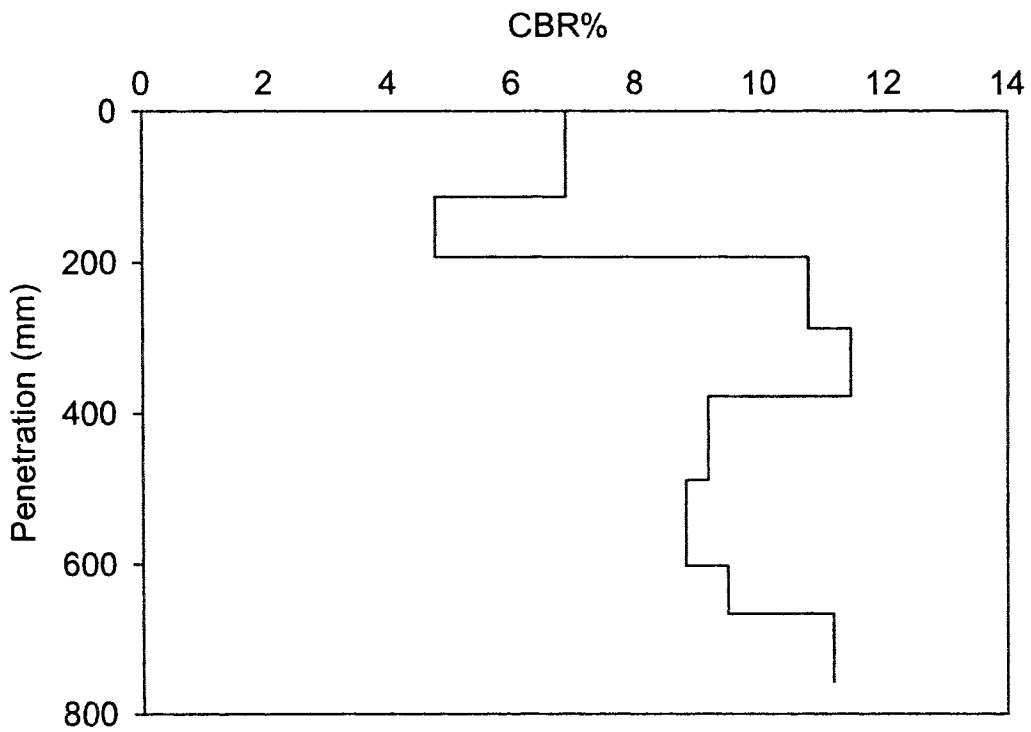
CBR on Right Lane (Top Layer Subgrade)  
CBR%



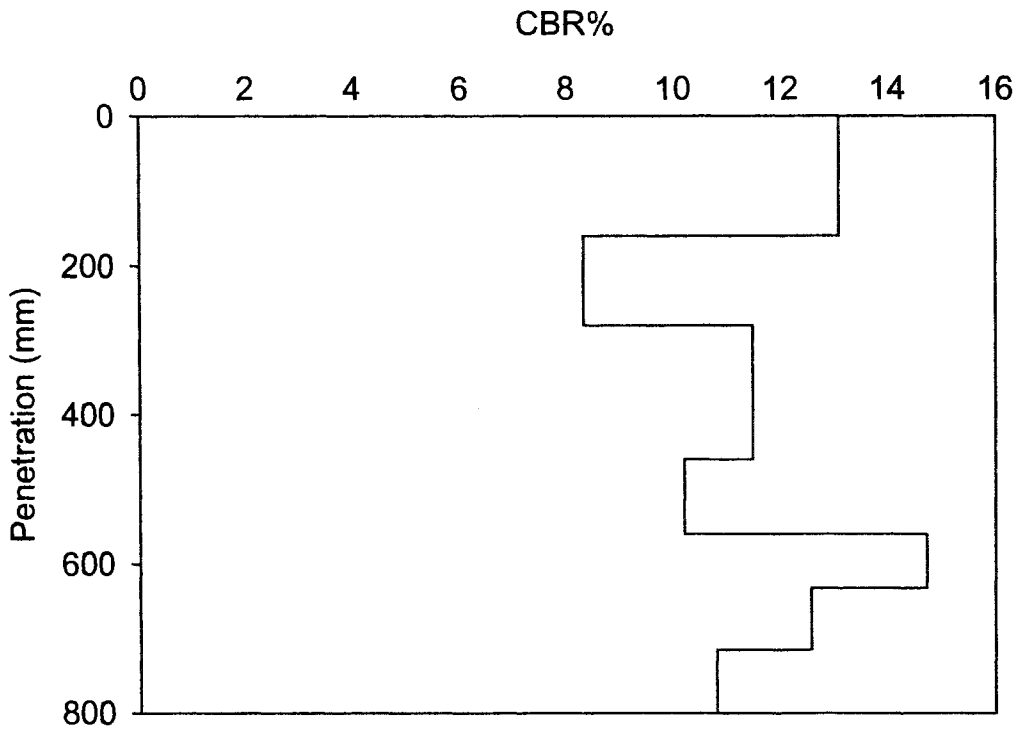
CBR variation at Location 1 on US30 E



CBR Variation at Location 2 on US 30E



CBR Variation at Location 3 on US 30E



CBR Variation at Location 4 on US 30E

